DEVELOPMENT OF NOVEL THERANOSTIC SMALL MOLECULES FOR CANCER TREATMENT

A Dissertation

by

ZHENGYANG JIANG

Submitted to the Office of Graduate and Professional Studies of
Texas A&M University
in partial fulfillment of the requirements for the degree of

DOCTOR OF PHILOSOPHY

Chair of Committee,	Kevin Burgess
Committee Members,	Frank Raushel
	Christian Hilty
	Richard Gomer
Head of Department,	Simon North

August 2019

Major Subject: Chemistry

ABSTRACT

Cancer has become one of the biggest threats to human health. In most cases, cancer cells can be differentiated from normal tissues via the overexpression of certain cellular membrane proteins. Improved therapeutic effects can be achieved by targeting these specific receptors. Compared to antibody targeting, small molecule targeting strategies have the advantages of efficient diffusion and delivery of theranostic agents into tumor tissue. This dissertation focuses on developing novel active targeting small molecule agents for cancer diagnosis and therapy.

The focus of the first study is unique small molecules that bind the TrkC receptor, which is overexpressed in metastatic breast cancer (as well as gliobastoma, neuroblastoma, and melanoma). A conjugate of a TrkC ligand and the highly cytotoxic alkaloid, maytansinoid, was prepared. Cellular studies featuring $TrkC^{+}$ and $TrkC^{-}$ human breast cancer cells indicated this conjugate might have a better therapeutic effect than the maytansinoid alone. It emerged that the conjugate was very efficacious *in vivo*, completely ablating orthotopic 4T1 breast tumor in one case, and dramatically reducing the tumor size in four other mice.

The second study is based on a small sub-set of heptamethine (Cy7) dyes that are preferentially uptaken into tumors, then, in some cases, retained there for extended periods. These dyes absorb in the near infrared (NIR) region

(above 750 nm), and deliver cargoes to various tumor models *in vivo*, offering theranostic effect. This study describes how four heptamethines were synthesized, all having the gemcitabine fragment attached to the *meso*-position of the Cy7 core. One theranostic agent localized in glioblastoma tumor cells with absorption maxima in NIR region and showed similar therapeutic effect to gemcitabine, but at one-third the molar dose.

The third study describes work aimed at discovering a novel targeted small molecule from a one-bead one-compound (OBOC) combinatorial library. Two different screening protocols were established and the on-bead compounds were effectively decoded with an extended linker and step-wise partial capping strategy.

Some other efforts related to developing novel theranostic agents by targeting cancer cell surface receptors are also recorded. These either did not yield promising results, or are a small part of much larger studies in our group.

DEDICATION

To Mom and Dad

ACKNOWLEDGEMENTS

I would like to thank my research advisor Dr. Kevin Burgess, for his guidance, patience and encouragement in my graduate study at Texas A&M University. I've learned immense knowledge and grand passion for the chemistry research from him. It was a great experience to study in his group.

I would also like to thank my committee members, Dr. Frank Raushel, Dr. Christian Hilty, and Dr. Richard Gomer for their support and valuable advice throughout the course of this research.

Thanks to Dr. Anyanee Kamkaew for teaching me all about cell culturing and assays. Thanks to Dr. Dongyue Xin for his advice and help with my projects. Thanks to Mr. Hua Zhou for his help and support throughout my study. Thanks to Dr. Jaru Taechalertpaisarn for his friendship and support with my study. Thanks to Dr. Darrell Pilling for his valuable advice and help with my research. Thanks to Dr. Stan Vitha for teaching me the knowledge and skills about fluorescence confocal imaging. Special Thanks to Dr. Gomika Udugamasooriya for guiding me through the combinatorial library screening experiments. Thanks also go to all current Burgess group members for their friendship and supports.

Thanks to my collaborators, Dr. Zheng Li, Dr. Zhen Yang, Dr. Raquel Sitcheran and Ms. Kathryn Pflug for their efforts and hard work. Thanks to Ms Jill Powers and Ms Andrea Scott for their generous support throughout my study.

Thanks also go to my friends and colleagues and the department faculty and staff for making my time at Texas A&M University a great experience.

Finally, thanks to my mother and father for their love, understanding, patience and support.

CONTRIBUTORS AND FUNDING SOURCES

Contributors

This dissertation was supervised by a committee at Texas A&M University: Professor Kevin Burgess (advisor) of the Department of Chemistry; Professor Frank Raushel (committee member) of the Departments of Chemistry, Biochemistry & Biophysics, and Toxicology; Professor Christian Hilty (committee member) of the Departments of Chemistry, and Biotechnology; Professor Richard Gomer (committee member) of the Department of Biology.

In Chapter II, the *in vivo* studies were performed by Dr. Zhen Yang and Dr. Feng Li under the direction of Dr. Zheng Li. **DM4** was supplied by ImmunoGen (Waltham, MA) with the help of Dr. Nathan Fishkin.

In Chapter III, Ms. Kathryn Pflug conducted the *in vivo* experiments under the direction of Dr. Raquel Sitcheran. Mr. Syed Muhammad Usama provided the dye starting materials and assisted with the confocal imaging experiments. Mr. Dacheng Kuai and Dr. Xin Yan performed the mass spectroscopic analysis to characterize the metabolite **5**.

In Chapter IV, the library **C** was prepared by Dr. Dongyue Xin. Synthesis of library **1** was performed in collaboration with Mr. Jonathan Whisenant. Library screening protocols were modified with the help of Dr. Gomika Udugamasooriya of the College of Pharmacy at University of Houston.

In Appendix A, Dr. Anyanee Kamkaew conducted part of the confocal imaging experiments.

In Appendix B, Dr. Chen-Ming Lin prepared compounds **22**, **23**, and assisted with the compound characterization.

In Appendix C, the plasmid purification and sequencing were performed with the help of Mr. Yu Tang and Dr. Richard Gomer.

All other experiments conducted for the dissertation was completed by the student independently.

Funding Sources

The work in this dissertation was supported by the National Science Foundation (M1603497, CHE1608009), the National Institutes of Health (R01EY029645), the Robert A. Welch Foundation (A-1121), DoD BCRP Breakthrough Award (BC141561), CPRIT (RP150559 and RP170144), George and Angelina Kostas Fund at Houston Methodist Research Institute, and the Texas A&M University T3-Grants Program (246292-00000).

The contents are solely the responsibility of the authors and do not necessarily represent the official views of the National Science Foundation, the National Institutes of Health, the Robert A. Welch Foundation, Department of Defense Breast Cancer Research Program (DoD BCRP), Cancer Prevention and Research Institute of Texas (CPRIT) or Texas A&M University.

TABLE OF CONTENTS

Page

LIST OF FIGURES

Page

LIST OF TABLES

Page

CHAPTER I

INTRODUCTION

1.1 Characterizing, locating, then treating primary and metastatic tumors is crucial in oncology.

Tumors are usually characterized by the overexpression of certain proteins on cancer cell surfaces. One example featured in this dissertation is the tropomyosin receptor kinase (Trk) proteins. There are three main sub-types of Trk proteins (TrkA – C), each having a preferential natural ligand (neurotrophin). TrkA, B and C binds preferably to nerve growth factor (NGF), brain derived neurotrophic factor (BDNF), and neurotrophin-3 (NT-3) respectively.[1-3] Interaction of neurotrophins with cells expressing the Trk receptors is associated with cell proliferation and survival.[4,5]

Targeting probes that specifically recognize and bind to specific cell surface proteins can help with active delivery of diagnostic and therapeutic agents into cancer cells. This active targeting[6] strategy is useful in characterizing, locating and treating cancer. Active targeting can be achieved by small molecules that bind receptors or large molecules (i.e. antibodies).

Monoclonal antibodies (mAbs) are commonly used as targeting probes in cancer diagnosis and treatment, because of their high binding affinity and selectivity to the targeted protein on cancer cell surface. Four antibody-drug conjugates (ADCs) have been approved by the Food and Drug Administration

(FDA) and are commercially available in the US for cancer treatment: brentuximab vedotin (Adcetris®, Seattle Genetics),[7,8] ado-trastuzumab emtansine (Kadcyla®, Genetech/Roche),[9] inotuzumab ozogamicin (Besponsa®, Wyeth Pharmaceuticals),[7,10] and gemtuzumab ozogamicin (Mylotarg®, Wyeth Pharmaceuticals).[10,11] More ADCs are being tested in clinical trials.[12,13]

Active targeting with mAbs has obvious limitations. Solid stress in tumors compresses blood vessels within them, which makes it particularly hard for large biomolecules to permeate.[14] Tumor vasculature tends to be immature, leading to reduced pressure gradients and heterogeneous blood flow[15,16] while tumor hydrostatic pressure is high, disfavoring convective drug transfer from blood vessels. Most mAbs do not penetrate tumors with efficient diffusion. MAbs that do diffuse into tumor tissue tend to be trapped by antigens located on the perivascular tumor cells,[17] an "antigen barrier",[18-20] even around micrometastases.[18] Moreover, slow clearance of mAbs from the body results in high normal tissue exposure[15,16,21] leading to accumulation in the excretory organs; this can lead to toxicity effects and reduces the dose that reaches the target.[22,23] However, small molecules that bind specifically to cell surface receptors can diffuse into tumor tissue easily and have a negligible influence by the antigen barrier.[24] Small molecules are also non-immunogenic, accessible via economical chemical synthesis and have longer shelf lives than mAbs.

1.2 Small molecule therapeutic drugs applied in research and clinical use

Many small molecule compounds have been approved by FDA for chemotherapy of solid tumor and metastasis, and some of them are suitable for conjugation with targeting moieties to act as a therapy "warhead". They possess different mechanisms to inhibit cancer cell proliferation and migration, increasing the diversity of targeted chemotherapy. A few examples are highlighted here (Figure I.1).

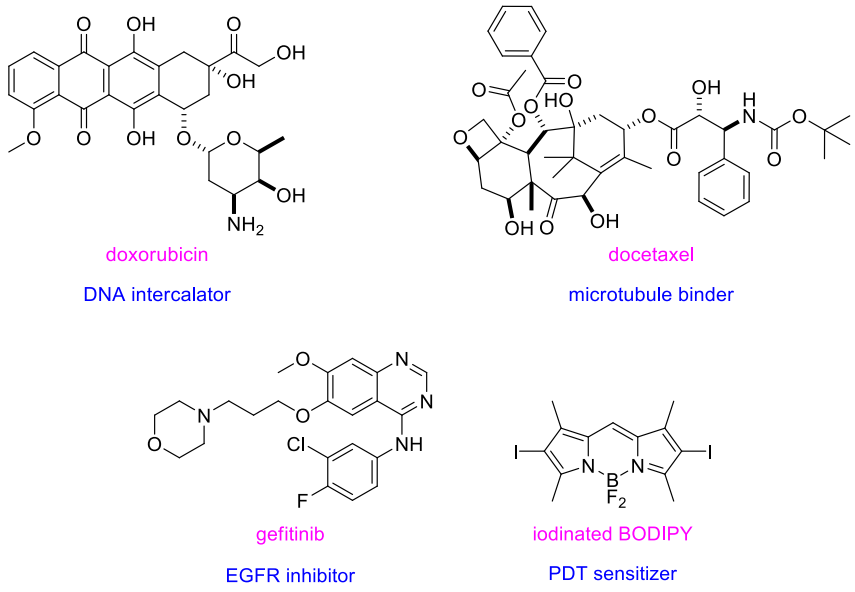

Figure I.1. Chemical structures of illustrative small molecule therapeutic drugs.

Doxorubicin intercalates between two base pairs of the DNA double helix, and inhibits the progression of topoisomerase II, which disrupts DNA replication and transcription.[25-27] Docetaxel is a semi-synthetic analogue of paclitaxel. It binds to microtubules with high affinity, inhibiting their disassembly, thus

preventing mitotic cell division.[28] Gefitinib, trade name Iressa, is an inhibitor of the epidermal growth factor receptor (EGFR), which selectively inhibits its tyrosine kinase domain.[29] EGFR is overexpressed in most human cancers, including lung and breast. Anti-apoptotic pathways are activated by overexpressed EGFR, and induce cell proliferation. Gefitinib can selectively inhibit EGFR, hence cause apoptosis in tumor cells. Other small molecule therapeutic agents are under investigation in clinical trials and research.

Another way to kill cancer cells is by phototherapy that requires light, photosensitizers and singlet oxygen generation. Iodinated BODIPY,[30] a photodynamic therapy (PDT) sensitizer, can generate toxic reactive oxygen species (ROS) and result in cell apoptosis after proper light illumination. It first absorbs light to reach the singlet excited state. Intersystem crossing (ISC) occurs to turn the sensitizer into triplet excited state. Energy transfer (ET) between the PDT sensitizer in triplet state and triplet oxygen produces singlet oxygen, which can oxidize cell components and induce cell death.

1.3 Active targeting molecules for proteins on cancer cell surface

Typical small molecule targeting agents (e.g. androgen,[31] folate,[32-34] and biotin[35]) are of natural origins. Relatively few synthetic small molecules have been discovered for active targeting (Figure I.2). Arginylglycylaspartic acid (**RGD**) peptide analogues recognize various integrins on cancer cell surface.[36-39] Bivalent acetazolamide can selectively deliver toxic compound to cancer cells

overexpressing carbonic anhydrase IX (CAIX).[40] Previous work in our group also revealed a synthetic bivalent small molecule targeting moiety **IY-IY** that selectively binds to TrkC on metastatic breast cancer cells.[41,42]

If we expand the scope to larger peptides and peptidomimetics, some other interesting targeting ligands have been discovered via high throughput screening (HTS) of combinatorial libraries. **AE105**, a selective binder to urokinase receptor (uPAR), was discovered from a phage display peptide combinatorial library. A modified derivative, **AE147**, has improved aqueous solubility but has slightly weaker binding affinity.[43-45] Peptidomimetic **LLP2A** specifically interacts with $\alpha_4\beta_1$ integrin, and accumulates in $\alpha_4\beta_1$ expressing tumors *in vivo*.[46] Peptoids **GU40C** and **GU40E** bind to vascular endothelial growth factor receptor 2 (VEGFR2) with dissociation constants in the low micro molar region.[47]

Most of small molecule targeting fragments have good binding affinity to their protein targets, but compared with mAbs, there are relatively few of them. The diversity of protein expression on cancer cell surface requires more efforts to discover novel small molecules that bind to protein targets with improved affinity and selectivity in expanded chemical space.

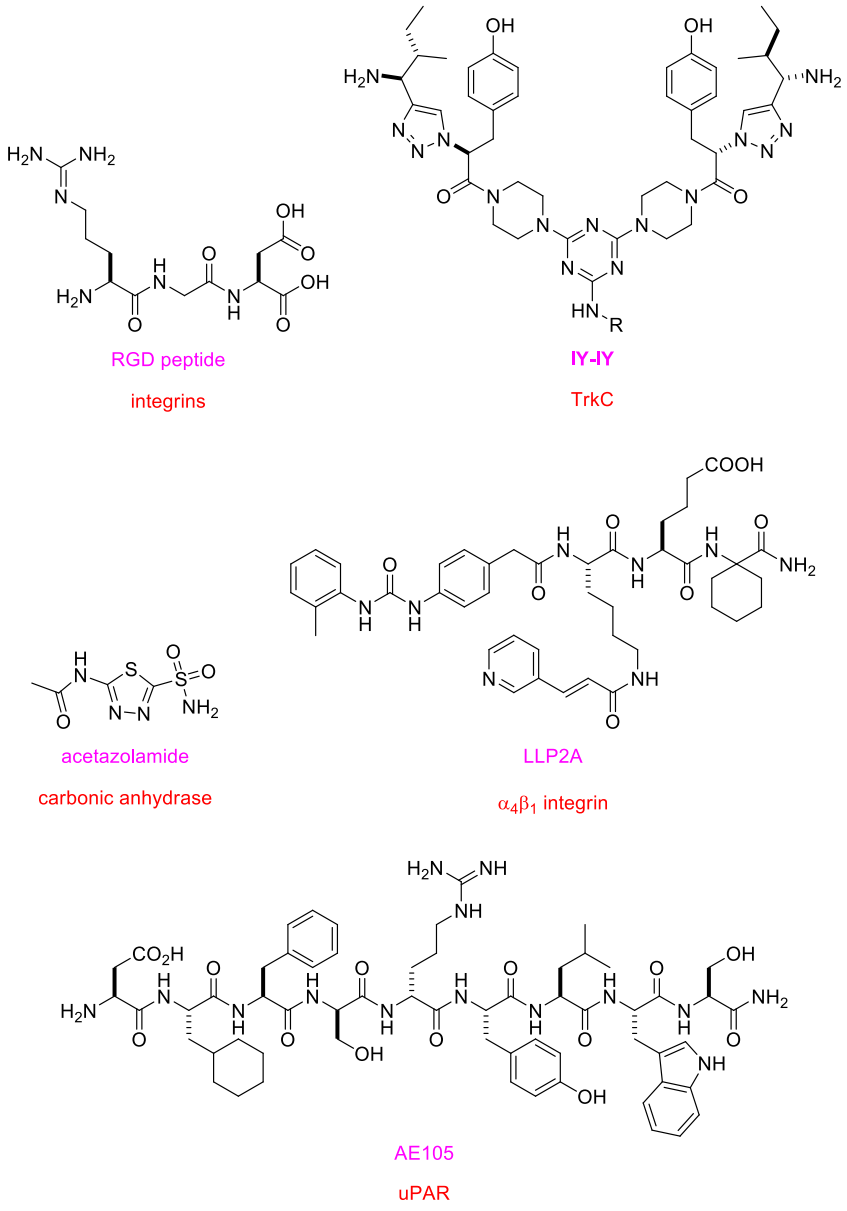

Figure I.2. Chemical structures of featured active targeting molecules and their corresponding protein targets.

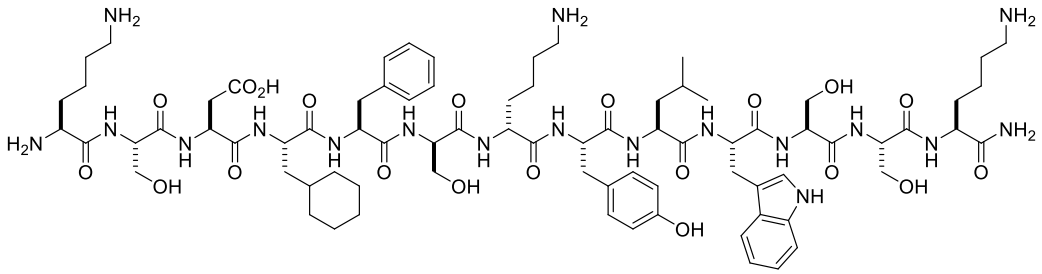

AE147

uPAR

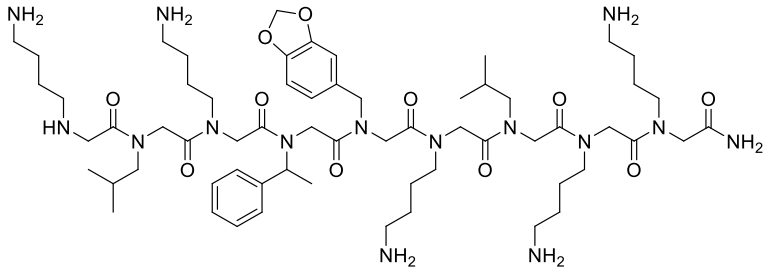

GU40C

VEGFR2

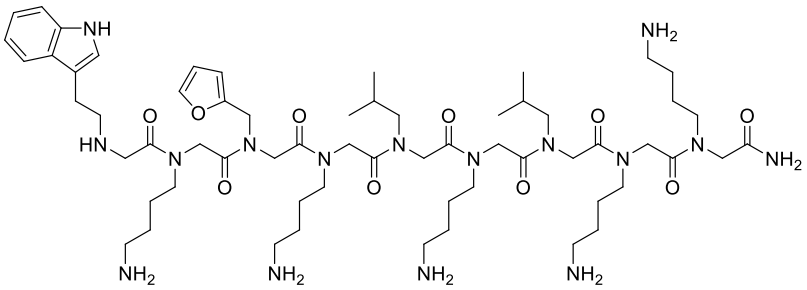

GU40E

VEGFR2

Figure I.2. Continued.

Computational analyses can be useful in designing novel small molecules for active targeting. A computational strategy created by our group, exploring key orientations on secondary structures (EKOS),[48] is developed to compare conformations of semi-rigid peptide mimics with three amino acid residues on

ideal secondary structures. Once a virtual fit is found, Glide and CombiGlide[49-52] can guide the backbone modification and fragment extension in molecule design.

In Chapter II and III of this dissertation, novel targeting small molecule drug conjugates for treatment of metastatic breast cancer and glioblastoma were synthesized. Therapeutic effects have been successfully applied *in vitro* and *in vivo*. Moreover, in Chapter IV, a small molecule combinatorial library has been prepared and screened to discover novel small molecules that selectively bind to proteins overexpressed on cancer cell surface.

CHAPTER II

TARGETED MAYTANSINOID CONJUGATE IMPROVES THERAPEUTIC INDEX FOR METASTATIC BREAST CANCER CELLS*

2.1 Introduction

Cancer is not a single disease. Primary tumors originating from the same organ but in different individuals express different profiles of cell-surface receptors, and those fingerprints indicate prognoses and treatment strategies for personalized care.[53] Breast cancer, for instance, can be classified in terms of expression of the ER, PR, and HER2.[54,55] If all three of these receptors are not expressed (triple negative), the tumor has a high tendency for metastatic spread and the prognoses is relatively poor. It is unlikely that profiling for just these three receptors, however, is optimal for all breast cancer types.

Cell surface receptors overexpressed on breast (and other) types of cancers can be used to favorably skew the pharmacokinetics of drug binding, to increase the local concentration of chemotherapeutics around the tumor, minimize damage to surrounding healthy tissues, and thereby increase therapeutic index (Figure II.1). This is important because therapeutic windows for cytotoxic substances that are not directly targeted to tumor cells are

---

*Reprinted with permission from Jiang, Z.; Yang, Z.; Li, F.; Li, Z.; Fishkin, N.; Burgess, K., Targeted Maytansinoid Conjugate Improves Therapeutic Index for Metastatic Breast Cancer Cells. *Bioconjugate Chem.* **2018,** *29*, 2920-2926.

notoriously narrow, and this severely limits dose levels that can be administered to patients without serious side effects. Directing cytotoxic drugs to cancer cells via cell surface receptors is “active targeting”, which in this article we abbreviate to “targeting”.

Figure II.1. Active targeting can increase therapeutic indices by increasing the potency and decreasing the toxicity of a warhead in a conjugate. Reprinted with permission from [217].

Humanized monoclonal antibodies (humAb) raised to receptors expressed on the surface of cancer cells have proven therapeutic value. For instance, one of the first FDA approved humAb’s for breast cancer, trastuzumab (Herceptin®), binds HER2 extracellular domain and downregulates cell signaling pathways that lead to proliferation.[56,57] This development paved the way to the first mAb-drug conjugates to be FDA approved for solid tumors: ado-trastuzumab emtansine (Kadcyla®) which is typical of a now-broader class of antibody drug conjugates (ADCs) that are used to treat patients today for various forms of cancer.[58] Ado-trastuzumab emtansine has a dual function: the mAb part binds HER2 and inhibits proliferation, while the emtansine cargo (emtansine is a highly cytotoxic derivative of the macrolide maytansine,[59] i.e. a

maytansinoid[13,60]) is preferentially delivered to tumors over healthy tissue.[9,61] Thus ado-trastuzumab emtansine localizes the maytansinoid in tumors, decreasing the therapeutic dose of that cargo relative to the free macrolide, increasing the maximum tolerated dose by suppressing the cytotoxicity of the cargo until it is liberated, thus raising the therapeutic index of the ADC relative to the parent maytansinoid.

There are intrinsic advantages and disadvantages to ADCs. One major attribute is that methods to generate mAbs to cell surface receptors, and others to humanize them, have high success rates.[62] A second advantage is that mAbs have high affinities for the targeted receptors. Paradoxically, those high affinities (and the size of Abs) mean that mAbs tend to accumulate around the surface of tumor cells where they first encountered receptor antigens and compressed vascular structure prevents permeation to the tumor core.[17] Thus solid tumors are said to possess “antigen barriers”.[18-20] Secondly, relatively slow *in vivo* clearances of mAbs mean that ADCs tend to remain in circulation outside tumors where they can damage healthy tissues, decreasing their therapeutic indices.[15,16,21] A third major limitation originates in the difficulties encountered when attempting to obtain batch-to-batch reproducibility with the same Ab to cargo payload.

Maytansine alkaloids (like that in ado-trastuzumab emtansine) are one of the extremely cytotoxic cargoes favored in development of ADCs.[58] In cells, they interact with tubulin preventing its assembly into microtubule fibers, thus

inhibiting cell division.[63] Free maytansinoids tend to be too toxic for chemotherapy; in clinical trials from 1977 to 1984, they were evaluated in 35 different types of tumor in over 800 patients, but complete response was only found in one case and partial response in a few others.[13] Maytansinoids are too destructive to healthy tissue to be used safely without conjugation, but they are ideal for targeted approaches.

Small molecule targeting agents have entirely different, and complementary, disadvantages and advantages relative to ADCs.[64] First, the pool of molecules that bind appropriate cell surface receptors is relatively small, hence the number of appropriate targets is limited.[65,66] Affinities of small molecules for cell surface receptors tend to be lower than mAbs binding the same targets, but this, and the fact that their lower molecular masses lead to more rapid and extensive distribution *in vivo*, and allow them to cross antigen barriers and permeate throughout tumor interiors.[24] Moreover, small molecules having targeting and cytotoxic fragments tend to be more rapidly cleared *in vivo* than ADCs hence minimizing their relative damage to healthy tissues. Other factors that also favor use of small molecule targeting groups include cost, shelf-life, batch-to-batch reproducibility, lack of ambiguity when conjugating cytotoxic cargoes,[67] and the fact that even Abs can cause side-effects related to residual immunogenicity.

Folate,[68] carbonic anhydrase IX,[40,69] and prostate-specific antigen ligands are commonly used for targeting conjugates,[70] and these have been tested with

maytansinoid derivatives. However, for breast cancer, prostate-specific antigen ligands are not applicable, the levels of folate receptor expression tend to be low,[71] and small molecules that target other receptor types may have useful complementary properties.

Some work from our laboratories have focused on using the tropomyosin kinase receptor C (TrkC) to target breast cancer[3,72] (and melanoma[73]).[42,74] More particularly, there is a good correlation between overexpression of TrkC and metastatic breast cancer.[1,75-80] Throughout we have used a bivalent dipeptide mimic designed in these laboratories to bind TrkC; these are the blue parts of structure **1**.[81] An isomer of **1** that has the Ile- and Tyr-like side chains reversed (green fragments in **2**) does not bind TrkC and is therefore a useful control for non-specific binding. All our previous work features photodynamic therapy (PDT).[82,83] Active targeting in PDT involves accumulation of the ligand in tumors, and illumination of those regions; areas that are not illuminated incur less tissue damage, hence there is overall a double targeting effect[74] that increases the therapeutic index.

Research reported in this paper describes, for the first time, use of the TrkC-targeting ligands to deliver a conventional cytotoxic compound *in vivo*, i.e. without PDT. Specifically, the cargo used is the maytansinoid **DM4** (**DM1** and **DM4** differ only in that the thiol is connected directly to a methylene, or an extended CMe2 group, where disulfides from the latter have more favorable rates of cleavage in lysosomes).[84] We hesitated to initiate this work because: (i)

TrkC receptors are found on healthy tissues in the nervous system; (ii) maytansinoids are extremely toxic as discussed above; and, (iii) there would be no double targeting effect (unlike our work on active targeting in PDT). In the worse possible case, TrkC-targeted maytansinoids might negotiate the blood brain barrier and cause catastrophic neurotoxicity issues. In the event, however, the data collected here reveals that was not the case, and a significant reduction in the size of orthotopic TrkC$^+$ tumors was observed in mice treated with agent **1**.

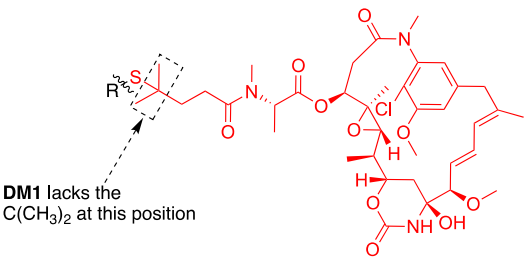

DM4
R = H

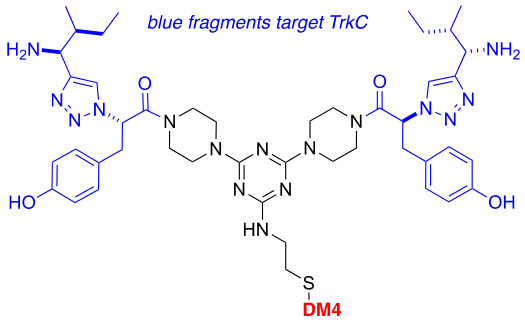

1

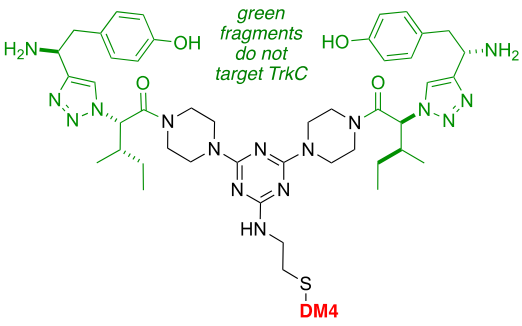

2

2.2 Results and Discussion

Initial experiments were performed to establish the affinity of the TrkC targeting fragment of compound **1**. This was most conveniently achieved using

the fluorescently labeled derivative **A**[3] on live NIH3T3 cells stably transfected with TrkC (Figure II.2). Fluorescence labeling of the cells was measured in the absence (blue line) and presence (red) of a large excess of the unlabeled TrkC-targeting group **B**.[41,81,85] Extent of specific binding in these experiments is revealed by subtraction of fluorescence with the blocking group **B** from the corresponding data without it. Analysis of the data revealed a K_d value of 112 ± 74 nM. A lower K_d value would have been preferable for active targeting, but we decided this affinity was sufficient to justify synthesis of the key compound.

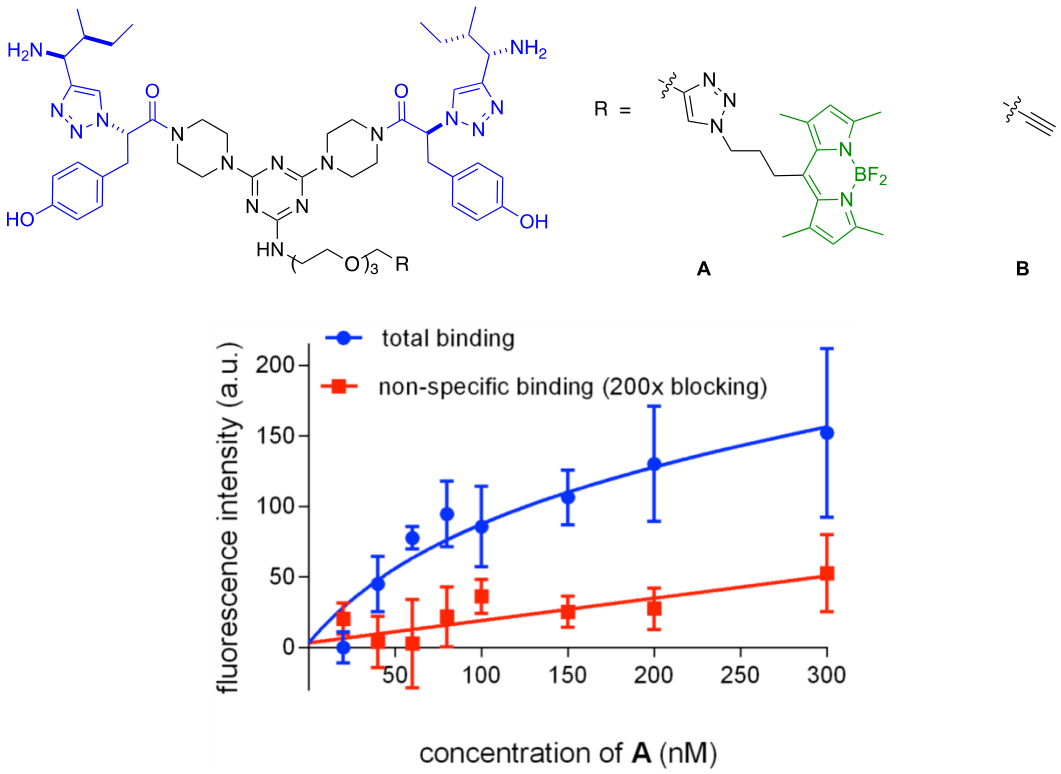

Figure II.2. Cell-based compound dissociation constant measurements indicated K_d = 112 ± 74 nM, based on three parallel experiments, calculated using GraphPad Prism 6. Reprinted with permission from [217].

Scheme II.1 outlines how a known amino disulfide[86] was added to cyanuric chloride in the first of three S_NAr displacements, wherein the last two involved coupling of the TrkC targeting groups **C**.[41] Comparison of NMR data for **DM4** and the conjugate **1** indicated the coupling step had proceeded without perturbation of the **DM4** fragment, as desired (Figure D.1).

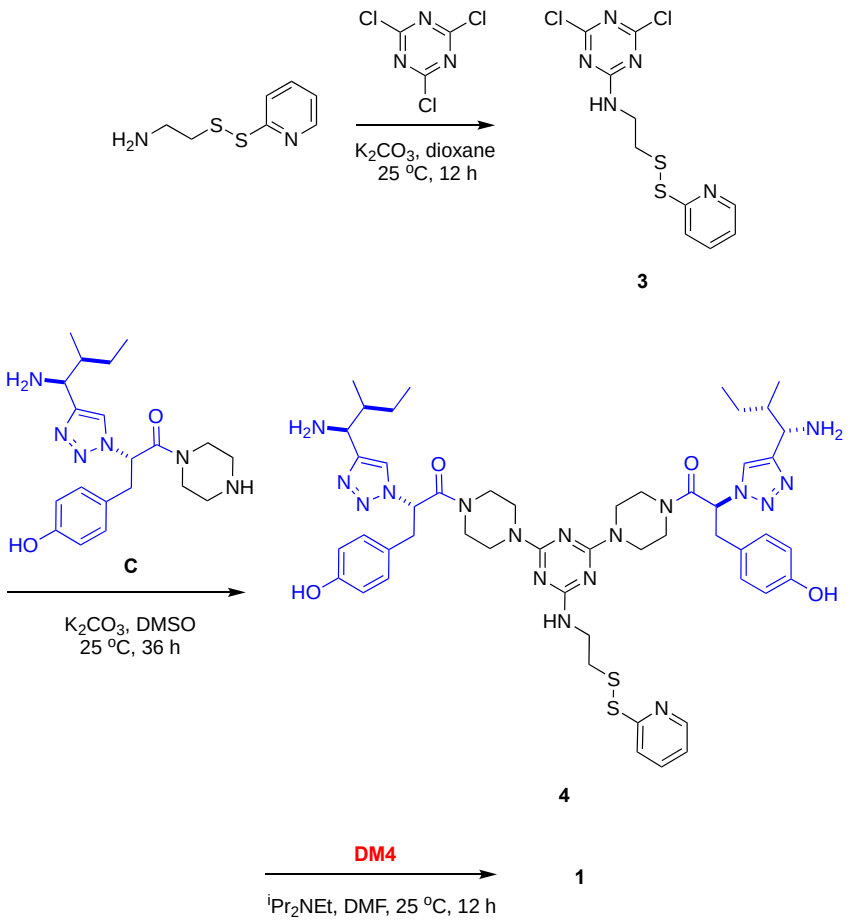

Scheme II.1. Synthesis of the cleavable targeted DM4 conjugate. Reprinted with permission from [217].

Experiments were then performed to assess the solubility and stability of the conjugate **1** in pertinent aqueous media. Maytansinoid **DM4** is hydrophobic hence it was impossible to dissolve **1** in buffer at the required concentrations. Consequently, following literature precedent[87] the solubility of the maytansinoid derivative **1** was measured in pH 7.40 phosphate-buffered saline (PBS) with 9% ethanol, 1% DMSO and 0.5% cremophor EL (CrEL). Thus, using a UV-plate reader assay[88] gave data (Figure II.3a) indicating a solubility of 67 μM. Figure II.3b indicates that conjugate **1** has a half-life of over 40 h in DMEM culture medium or pH 7.40 PBS at 37 °C.

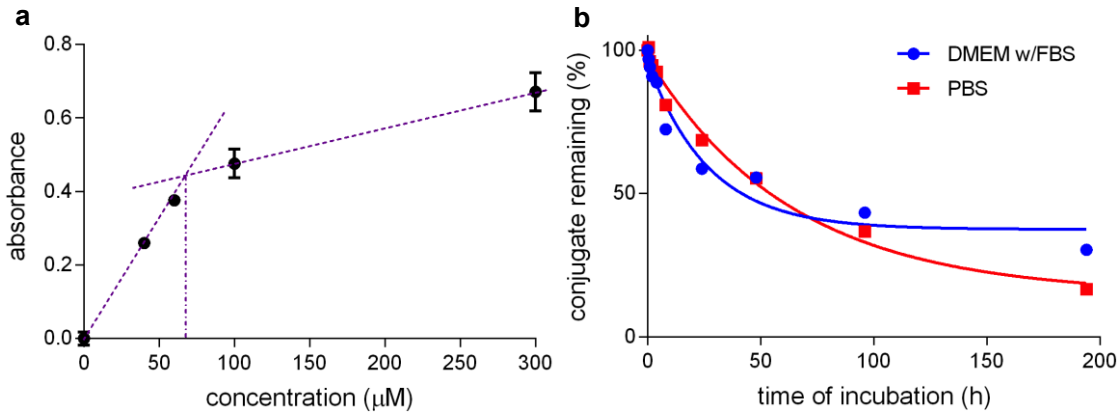

Figure II.3. a Solubility of **1** in pH 7.40 PBS with 9% ethanol, 1% DMSO and 0.5% CrEL. **b** Stability of **1** in either DMEM culture medium or pH 7.40 PBS at 37 °C as evidenced by analytical HPLC (initial concentration 20 μM). Reprinted with permission from [217].

Cell assays were performed on **1** and **2**, to determine if *in vivo* studies were clearly justified. Data collected for these experiments are shown in Figure II.4a for $TrkC^+$ cells, and in Figure II.4b for $TrkC^-$ cells (Hs578t and MCF-7,

respectively). Throughout, **DM4** was the most toxic compound, hence the types of conjugates featured here (**1** and **2**) have reduced cytotoxicity relative to **DM4**. To our surprise, the isomeric control **2** was marginally *more* toxic, even for $TrkC^+$ cells (IC_{50} values for: **1**, 28.1 ± 1.9 nM; and, **2**, 23.0 ± 2.5 nM). However, Figure II.4c shows that the reduction of cytotoxicity for conjugate **1** was sufficient to outweigh its less absolute cytotoxicity affording it a superior therapeutic index in cell assays.

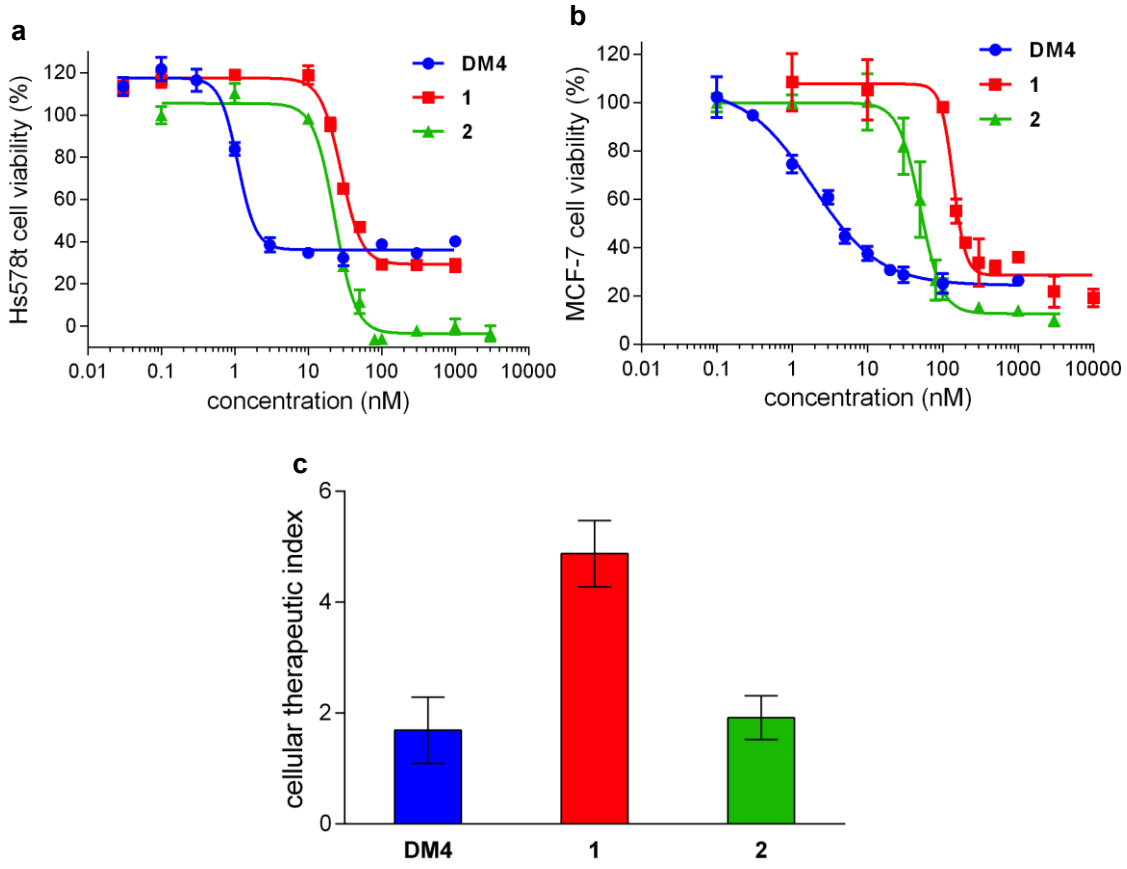

Figure II.4. Cytotoxicity and cellular therapeutic index comparison. **a** and **b** Dose responses of **DM4**, **1** and **2** on human breast cancer cell lines Hs578t ($TrkC^+$) and MCF7 ($TrkC^-$). Calculated IC_{50} values are listed in supporting

material. **c** Calculated *in vitro* therapeutic index based on IC_{50} values {IC_{50} (MCF-7) / IC_{50} (Hs578t)}. Reprinted with permission from [217].

After binding to TrkC proteins on a cell surface, the conjugate **1** is uptaken into lysosomes via endocytosis,[74] then free **DM4** can be released via intracellular reduction of the disulfide bond.[61] Released maytansinoid **DM4** inhibits microtubule function in targeted tumor cells, causes cell cycle arrest, and eventually causes cell death by apoptosis.[89] In any event, cellular therapeutic indices are determined in static systems, whereas pharmacokinetic effects involve dynamic flow of fluids around tumors. In other words, cellular therapeutic indices do not reflect the positive effects active targeting has on pharmacokinetics *in vivo*. For these reasons, an *in vivo* study was initiated.

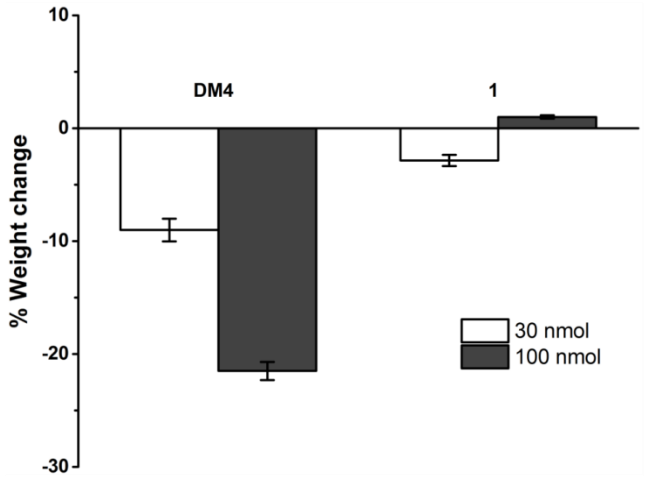

Figure II.5. Body weight changes after single i.v. injection of DM4 and 1 (n = 3). Reprinted with permission from [217].

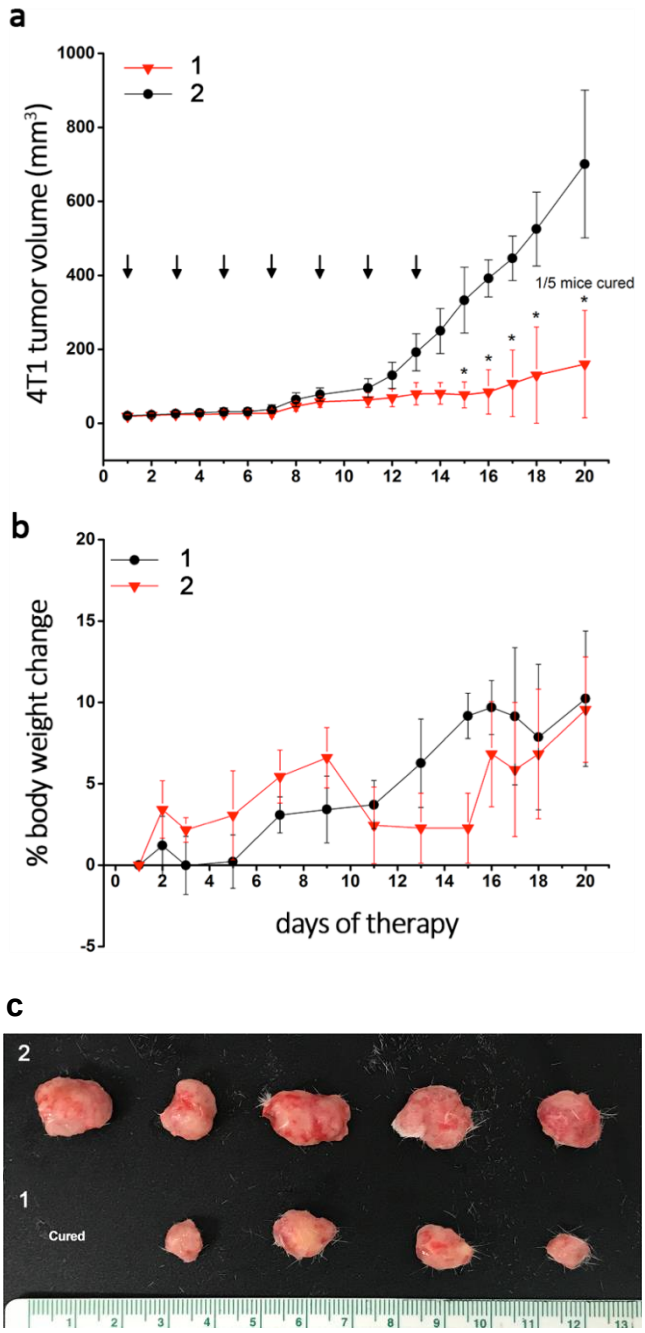

Figure II.6. *In vivo* therapy study of maytansinoid conjugates **1** and **2**. **a** Tumor growth curves of 4T1 xenograft bearing mice injected with 7 x 30 nmol **1** as therapy group and **2** as control group. Data represent mean ± SD (n = 5 per group). * indicates one mice of the five tested was cured of tumor in the therapy group. **b** Weight change of mice shown in **a**. No animals were observed with weight loss >15% throughout the therapy study. **c** Tumors collected from *in vivo* therapeutic studied mice. (Arrows in **a** mark the injection days of therapy. On

each arrow marked injection day, the compounds were reconstituted into PBS buffer and injected into mice via tail vein.) Reprinted with permission from [217].

In vivo toxicity study was carried out using Balb/C mice to compare maytansinoid **DM4** and TrkC targeted maytansinoid conjugate **1** at dose of 30 nmol and 100 nmol per mouse (n = 3) *via* a single intravenous (i.v.) injection. We found that mice lost about 10% of body weight at 30 nmol and over 20% of body weight at 100 nmol in **DM4** group, whereas no significant weight loss in **1** group at both doses was observed (Figure II.5). This result demonstrated that TrkC targeted delivery of toxic compound **DM4** dramatically reduced systemic toxicity as we expected.

Therapeutic efficacy of targeted maytansinoid conjugate **1** was investigated using 4T1 tumor bearing mice. A scrambled non-targeted maytansinoid conjugate **2**, which does not bind to TrkC, was synthesized and used as a control comparison. As shown in Figure II.6a, the administration of **1** efficiently suppressed tumor growth comparing to the control conjugate **2**, which was evidenced by the outcomes that one tumor out of five was cured and the other four were significantly decreased compared with the control group. It strongly supported our hypothesis that conjugating toxic agent such **DM4** with targeting agent IY significantly promoted therapeutic efficacy in tumor targeting therapy. Meanwhile, animal body weight was also monitored throughout the study (Figure II.6b). No animal was observed with weight loss larger than 15%

of its initial weight throughout the study. It suggests that the administration of the therapeutic conjugate **1** was well-tolerated by the animals.

2.3 Conclusions

Expression of ER, PR and HER2 are usually applied to classify breast cancers. This is convenient for predicting prognoses and guiding some treatment strategies. However, that does not mean active targeting of other cell surface receptors in breast cancers is not viable. This work establishes that a TrkC ligand with a modest receptor affinity (~112 nM) can be used to deliver a cytotoxic cargo. Unlike our previous studies featuring PDT, this strategy does not have the advantages of double targeting, but nevertheless it is effective against orthotopic 4T1 tumors in mice. The approach outlined here is complementary to active targeting of ER, PR and/or HER2, and, based on the literature outlined here, probably also to mAb approaches in terms of tumor penetration and residence time *in vivo*.

CHAPTER III

CYANINE-GEMCITABINE CONJUGATES AS TARGETED THERANOSTIC AGENTS FOR GLIOBLASTOMA TUMOR CELLS

3.1 Introduction

Glioblastoma multiforme (GBM) forms aggressive malignant tumors, and patients with this disease have a five-year survival rate of only 5.1%.[90] There are only four FDA approved drugs for brain tumor therapy: temozolomide (TMZ or Temodar®, 2005),[91] lomustine (Gleostine®), carmustine (BiCNU®), and bevacizumab (Avastin®, 2017).[92] Combination of TMZ and radiotherapy is the standard of care for GBM, but more effective therapies need to be established since the median survival is 14.6 months, and this requires new strategies to generate pre-clinical leads.[93,94]

Gemcitabine (dFdC, or **gem**) acts against a wide range of solid tumors (FDA approved for breast, non-small cell lung, ovarian, and pancreatic).[93,95] In cells, a triphosphate is formed from this nucleoside, i.e. dFdCTP; that triphosphate competes with deoxycytidine triphosphate (dCTP) hence acts as a DNA chain-terminator. Simultaneously, the corresponding diphosphate (dFdCDP) inhibits ribonucleotide reductase (RNR) leading to more favorable gemcitabine:dCTP ratios in cells, improving gemcitabine's efficacy. Nevertheless, the efficacy of gemcitabine could be improved, especially for GBM.[95-98] Gemcitabine has been investigated in preclinical and clinical studies

for GBM,[93,98] but the *in vivo* therapeutic response tends to be relatively poor for several reasons.[93] First, penetration through the blood-brain barrier (BBB) is low; even in the brain-tumor-bearing animals where the BBB may be leaky.[99,100] Secondly, gemcitabine has a short half-life due to enzyme metabolism.[95,96] Third, gemcitabine is not actively targeted[101] to tumors versus healthy tissue.

A small set of heptamethine cyanine dyes localize in tumors (MHI-148, **A**; IR-783, **B**; DZ-1, **C**; and, IR-780, **D**).[102-107] The literature on actively targeted[101] small molecule gemcitabine derivatives[108-110] features an example of a conjugate to one of these tumor-seeking fluorophores (**C**) tested on GBM, i.e. NIRG, **E**.[104] In mouse models, both **E** and its parent fluorophore **C** localized in intracranial GBM tissue, and persisted there for over 24 h.

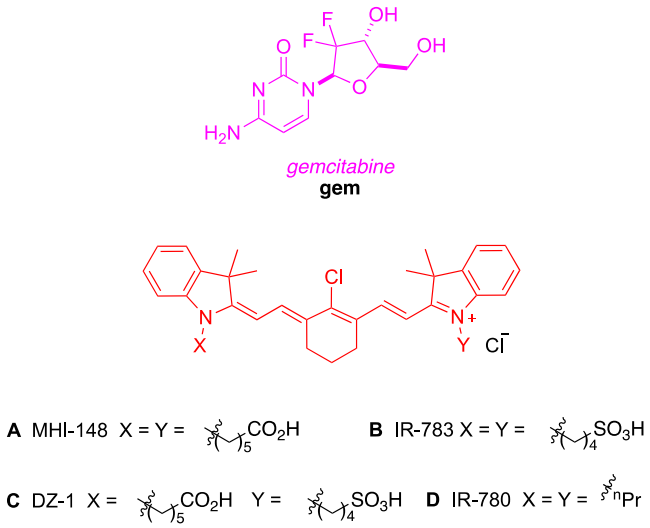

Figure III.1. Background structures and compounds featured in this study.

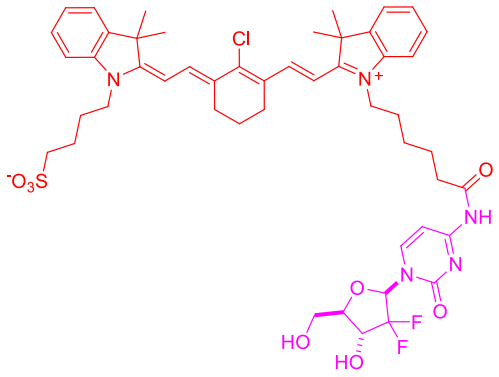

E NIRG

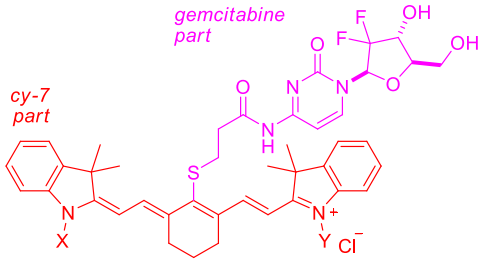

1

a X = Y = $(CH_2)_5CO_2H$ **b** X = Y = $(CH_2)_4SO_3H$

c X = $(CH_2)_5CO_2H$ Y = $(CH_2)_4SO_3H$ **d** X = Y = ^nPr

Figure III.1. Continued.

All four fluorophores **A** – **D** that show the remarkable tumor-seeking effect described above have a *meso*-chloride. This led us to wonder *if a gemcitabine conjugate formed by displacing this chloride thereby rendering the conjugate unable to form a covalent complex with albumin*, *would also localize into tumors in vivo, and, if so, if it would persist there*. To test these ideas, the *meso*-gemcitabine adducts **1** were designed here. We hypothesized these conjugates would localize in cultured glioblastoma cancer cells if the chloride was not

important for short term uptake, but unlike **A**, they would not persist in tumors *in vivo* for long periods because they cannot form covalent adducts with albumin. Consequently, we set out to test if these assertions were true, and to simultaneously probe therapeutic effects of **1** in a mouse subcutaneous xenograft model.

3.2 Results and Discussion

3.2.1 Synthesis, Ex Vivo Stabilities, and Cellular Studies

Conjugates **1a** – **d** were prepared by substitution of the *meso*-Cl in their parent heptamethine cyanine dyes **A** – **D**[111] using the gemcitabine derivative **F**[108] (Scheme III.1 and E.1) as nucleophile. Parent dyes **A** – **D** and their corresponding conjugates **1a** – **d** showed similar fluorescence quantum yield and UV absorption characteristics (Table E.1 and Figure E.1); consequently, they have maximal absorbance at good wavelengths, around 795 nm, and sufficient brightness for *in vivo* diagnostic imaging.

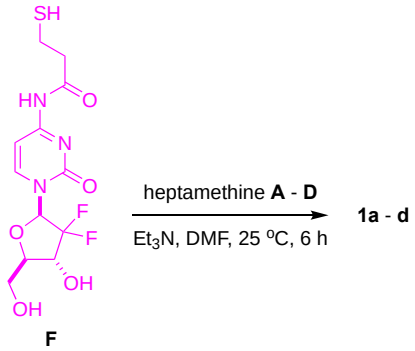

F

Scheme III.1. Synthesis of conjugate **1a** – **d**.

Literature evidence indicates gemcitabine modifications at the exocyclic amine group do not adversely reduce its cytotoxicity.[95,118] To verify this in the current study, we measured the cytotoxicities of gemcitabine and intermediate **F** with respect to U87 glioblastoma cells. The data obtained in these experiments were very similar (IC_{50}: **gem**, 8.2 ± 1.7; **F**, 11.0 ± 1.4 nM; Figure E.7a) indicating formation of the conjugate did not significantly impact the efficacy of the gemcitabine component.

Several experiments were undertaken to test the stabilities of an illustrative conjugate, **1a**, when incubated in physiological media. Thus, U87 tumor tissue from control mice (featured in the *in vivo* experiments described below) was cut into small pieces, homogenized (1 g tumor per mL RIPA buffer) then mixed with **1a**; the stability of **1a** was followed by analytical HPLC using detection at 780 nm corresponding to the fluorophore absorption maxima. Under these conditions the compound had a half-life of around 60 h at 37 °C (Figure III.2a). The half-life of **1a** was even longer when it was incubated with tumor cell lysate (4 million cells lysed with 1 mL RIPA buffer). These data imply **1a** in the tumor may persist in a conjugated form for several hours.

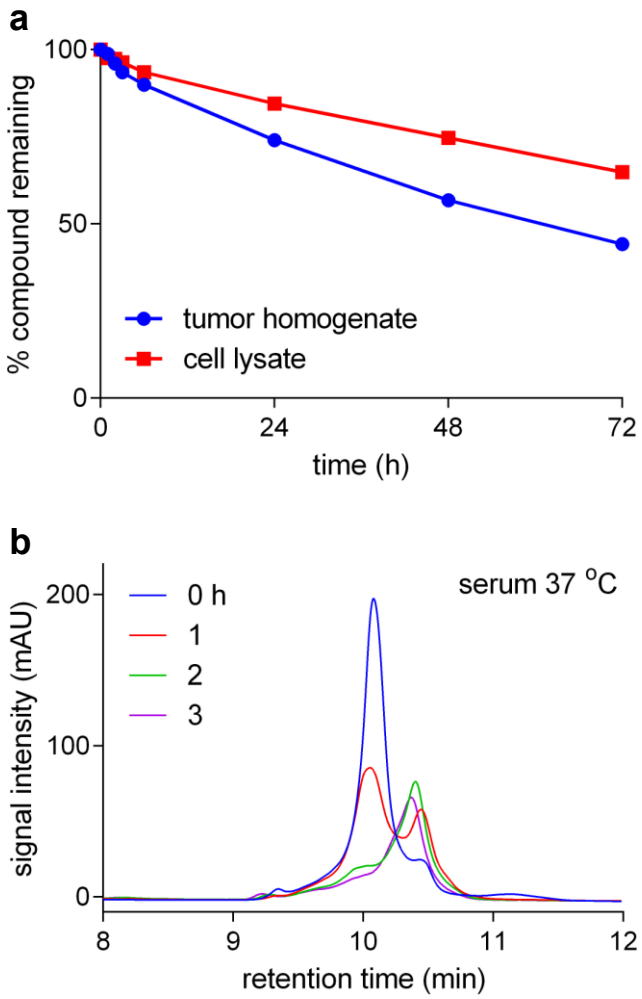

Figure III.2. Conjugate stability of **1a** in physiological conditions. Tumor tissue or cultured U87 cells were homogenized with RIPA buffer on ice before centrifuging down to collect supernatant. Conjugates were incubated at 50 μM at 37 °C for up to 72 h. % Compound remaining was calculated based on area under curve from the analytical HPLC trace through a C4 column (Figure E.4). **a** Conjugate stability of **1a** in U87 tumor homogenate and U87 cell lysate; **b** in serum *in vitro* at 37 °C, conjugate **1a** was metabolized to a new compound in ~3 h; and, **c** half-life of **1a** in mouse serum at 37 °C was determined to be ~1 h. Compound **5** was identified as **1a**-metabolite by mass spectrometry.

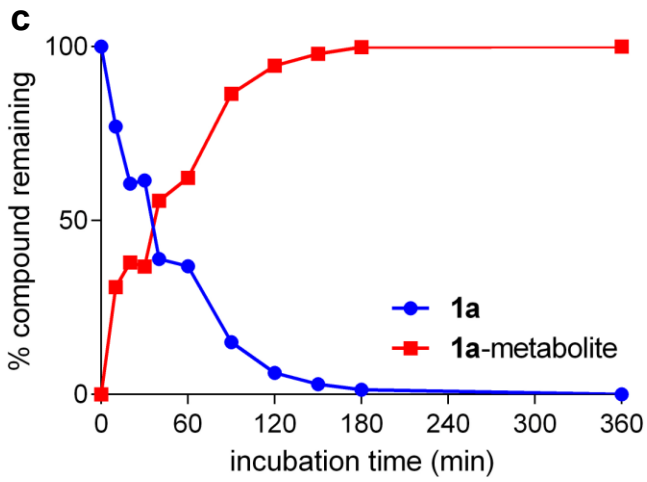

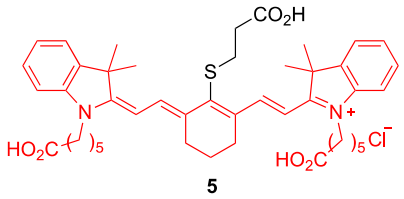

5

Figure III.2. Continued.

The relevance of experiments featuring cell lysates and tumor homogenates to pharmacokinetics is tenuous, but *in vitro* stability tests in serum at 37 °C probably have more physiological relevance. These experiments show the conjugate was metabolized to a new compound in 3 h with relatively high fidelity (Figure III.2b), via a process that was inhibited by a mixture of proteases and phosphatases (Figure E.5b), and was also inhibited at lower temperature (Figure E.5c). Mass spec analyses (Figure E.6b) showed the metabolite had a molecular mass corresponding to the amide hydrolysis product **5**. That assertion was proven by HPLC analyses involving "spiking" the metabolite mixture with synthesized compound **5** and checking co-elution (Figure E.6c).

Thus the amide bond in **1** that connects gemcitabine to the rest of the conjugate is vulnerable to proteolysis in serum *in vitro* giving it a half-life of approximately 1 h at 37 °C (Figure III.2c).

Overall, we concluded that short-term intracellular confocal imaging experiments featuring compounds **1** would be indicative of intracellular localization of the conjugates, and not simply track free fluorophore liberated from the nucleoside.

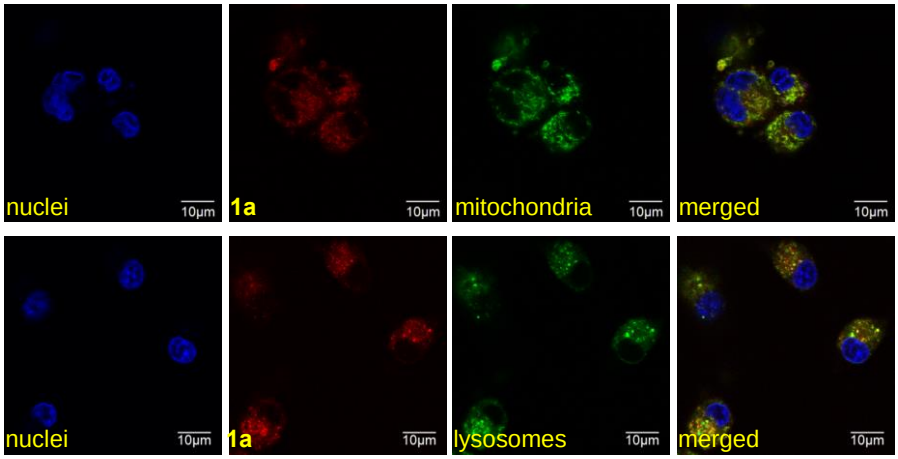

Figure III.3. Conjugate **1a** uptake and subcellular localization in U87 cells at 37 °C. Pearson's correlation coefficient (PCC) for co-localization between red (**1a**) and green (organelle stain) fluorescence was 0.74 with mitochondria, and 0.62 with lysosomes.

Data collected from confocal imaging of **1a** is illustrative of that obtained for all the samples in the series **1a** – **d** (Figures III.3 and E.2). Throughout, colocalization in the lysosome and mitochondria was uniformly observed (just as for the parent dyes **A** – **D**: Figure E.3), except for **1c** which gave no detectable

accumulation in the mitochondria. Mitochondrial localization, and, by inference, escape from the lysosome, is probably favorable with respect to cytotoxicity, so conjugates **1a**, **1b**, and **1d** only were considered beyond this point, and **1c** was excluded because it did not appear to escape from the lysosome.

Cytotoxicity data for **1a**, **1b**, and **1d** were measured, and comparisons made with reference compounds **2** which were specifically prepared for this purpose (Scheme E.2). Conjugates **2** feature the same dye as the key compounds **1**, but the nucleoside cargo, cytidine, is innocuous.

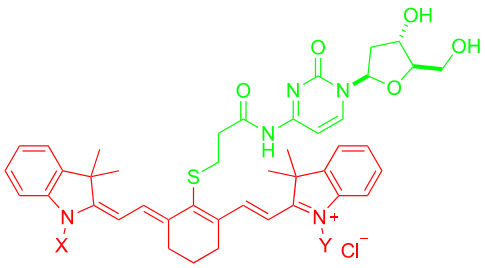

2

a X = Y = $(CH_2)_5CO_2H$ **b** X = Y = $(CH_2)_4SO_3H$ **d** X = Y = ^nPr

Cytotoxicity data for the gemcitabine-derivative **1d** relative to its cytidine control **2d** led us to exclude this compound from further studies, for the following reasons. Both the free dye **D** and the control **2d** are cytotoxic at <10 μM, whereas none of the other dyes **A** – **C** are at these levels (Figures E.7b and III.4a). Moreover, compounds **1a** and **b** proved to be significantly more toxic than their parent dyes **A** and **B**, and their cytidine-based controls **2a** and **b**

(Figures III.4b and c). Conjugates **1a** and **b** were less cytotoxic than gemcitabine, but the difference was not great because all three of those compounds were observed to have IC_{50} values in the 0.01 – 0.02 μM range. The cytotoxicity of gemcitabine on U87 cells has some variance,[119] and often stabilizes at certain values before 100 % apparent cell death;[98] consequently, for the purposes of this study, the IC50 values quoted throughout are calibrated relative to the lowest concentration beyond which no further cell death appears to occur. On the basis of these data either compound **1a** or **b** could have been selected for *in vivo* studies; conjugate 1a was in fact chosen because there is literature[120] that indicates **A** has a superior tumor-to-muscle imaging contrast index relative to **B**.

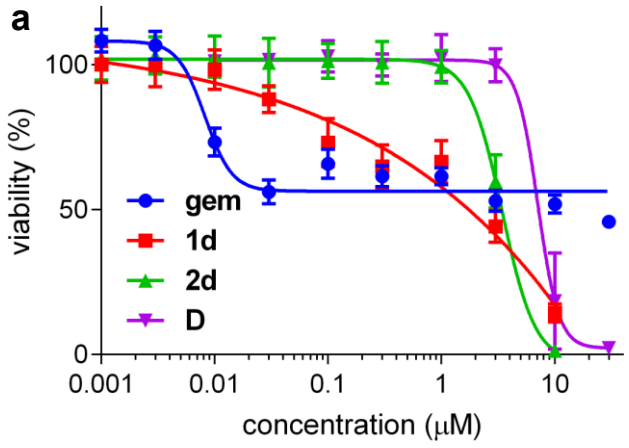

Figure III.4. Cytotoxicity of conjugates **1**, their cytidine analogs **2**, and their parent dyes. **a** Compounds **2d** and **D** were shown to be significantly toxic below 10 μM (IC_{50}: **2d**, 3.4 ± 0.4; **D**, 7.1 ± 1.7 μM). Conversely, in the sets **1a**, **2a**, and **A**, and **1b**, **2b**, and **B**, gemcitabine and compounds **1** are significantly more cytotoxic than the controls **2** and the free dyes (Figure III.4, parts **b** and **c**, respectively. IC_{50} values: **gem**, 8.2 ± 1.7; **1a**, 20.9 ± 5.0; **1b**, 20.7 ± 3.2 nM).

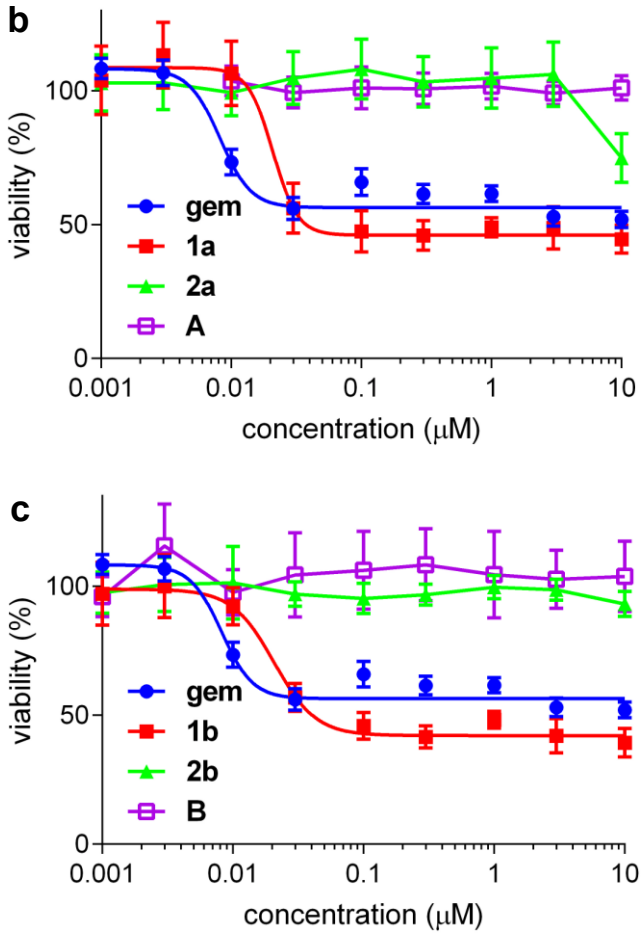

Figure III.4. Continued.

3.2.2 In Vivo Studies

A xenograft mouse model was used to examine the effects of lead compound **1a** on tumor growth *in vivo*. U87 glioma cells stably expressing luciferase and RFP reporters (U87-luc-RFP) were injected subcutaneously into the flanks of Fox1^{nu} mice. In the key experiments, the test compound (**1a** or **gem**, 10 mg/kg) or vehicle control were administered intravenously via retro-orbital vein at day 4 and 8 after tumor inoculation, and then weekly for a total of

6 injections. No significant body weight loss was observed among mice in all treatment groups (Figure E.10). Tumor burden was evaluated using weekly bioluminescent imaging of mice 1 – 5 weeks after drug or vehicle administration. Administration of **1a** or **gem** significantly reduced tumor burden (Figure III.5). There was no significant difference in tumor size in mice injected with **gem** or **1a** on mg/kg basis, but in terms of moles of drugs delivered, **1a** afforded the similar effect at under a third of the dose of **gem** (molecular weight of **1a**, 1034.6, is 3.45 times greater than gemcitabine hydrochloride, 299.66).

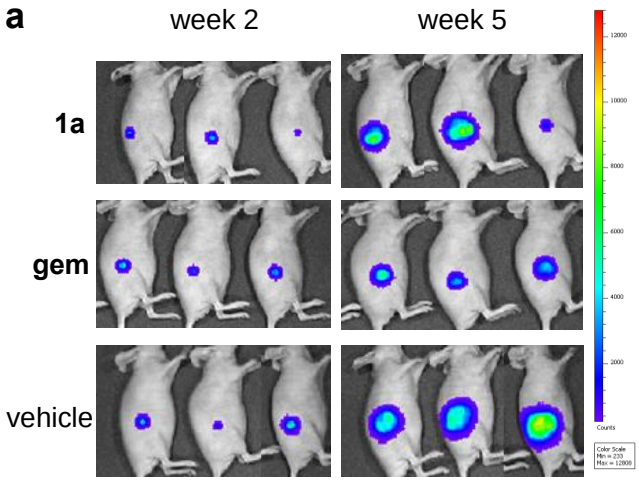

Figure III.5. Therapeutic effect of **1a**. **a** Luminescence images of mice harboring U87-RFP-Luc subcutaneous tumors and treated with indicated compounds were acquired with an IVIS Spectrum *in vivo* imaging system (Perkin Elmer®) at 2 and 5 weeks post drug administration. **b** Mean tumor size (cm^2) with SEM over a 5-week period post drug administration (n = 3). Two-way ANOVA with Bonferroni posttest shows statistically significant differences between **1a** (or **gem**) and vehicle control group at 4 weeks (**p < 0.01) and 5 weeks (***p < 0.001). **c** Mean tumor luminescence (photons per second, p/s) with SEM over a week period (n = 3). Two-way ANOVA with Bonferroni posttest shows statistically significant differences between **1a** or **gem** and the vehicle group at 5 weeks (p < 0.001).

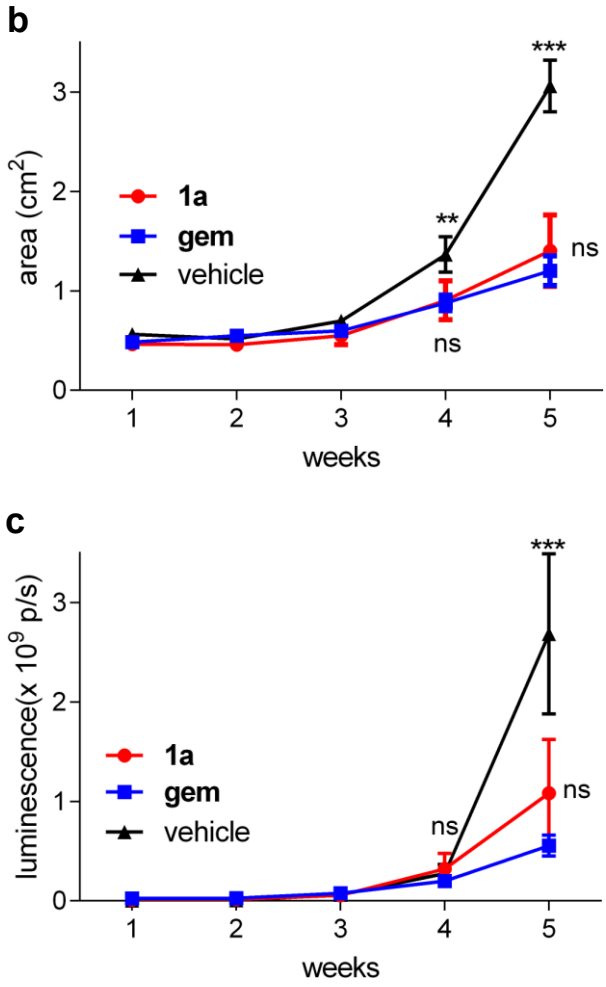

Figure III.5. Continued.

Localization of **1a** *in vivo* was monitored by fluorescence imaging of tumor-bearing mice at different time post-injection. Cyanine fluorescence was observed throughout the mice 30 min after drug injection, with maximal signal in the liver and tumor, and at the site of injection (retro-orbital vein; Figure III.6a, mice 1 – 4). Conjugate **1a** mostly cleared from the mouse after 24 h (Figure III.6a); imaging at 48 h after drug injection revealed residual **1a** fluorescence

signal that was ~10-fold lower than the signal observed at 30 min post-injection and ~100-fold lower at 144 h (Figure III.6b).

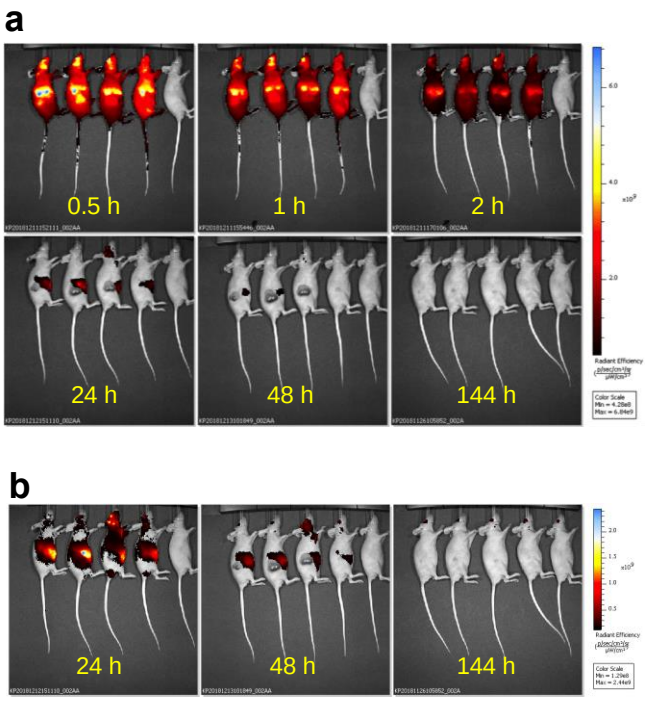

Figure III.6. Localization/clearance of **1a** *in vivo*. **a** Mice were injected with 10 mg/kg **1a** with an uninjected control (last mouse in each view); images were taken at 0.5, 1, 2, 24, 48, and 144 h after intravenous injection, and their fluorescence intensities are normalized to be on the same scale. **b** Images at 10x lower scale show persistence of fluorescence in **1a**-treated mice indicating residual drug localization over extended periods.

Tumor tissue and organs of the mice injected with **1a** were dissected and imaged to further visualize the localization of the drug conjugated to the fluorescent dye. One of the **1a**-treated mice was analyzed 2 h after intravenous injection; the fluorophore had localized to the tumor as well as the intestines, kidneys, liver, and lungs (Figure III.7a). Two days after injecting **1a**, some signal

was still detected in the tumor, and significant signal was also observed in the liver and kidneys (Figures III.7b and E.9c).

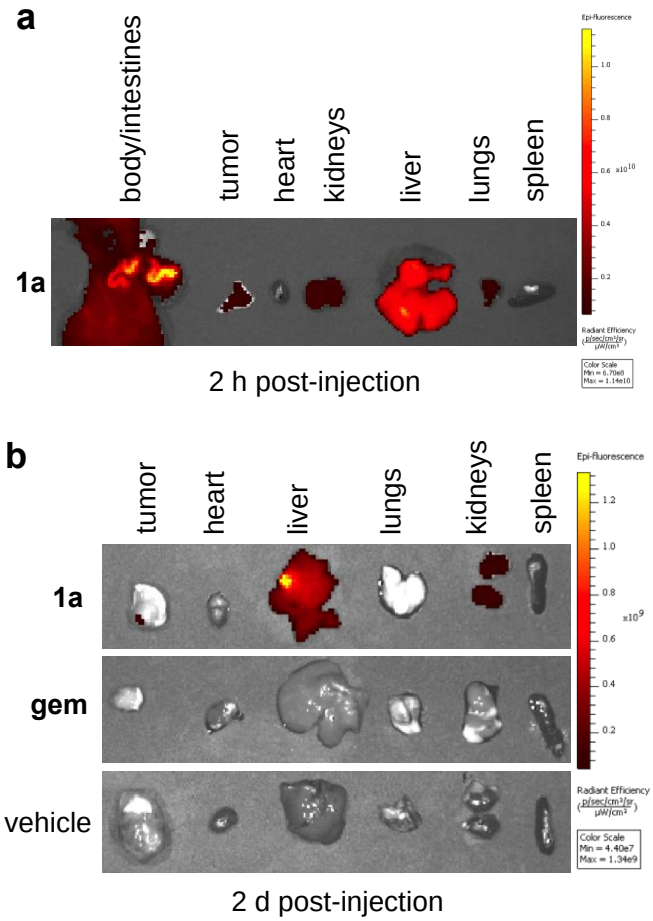

Figure III.7. Localization of **1a** postmortem via fluorescence imaging on tissues: **a** dissected 2 h after intravenous injection of **1a**; and, **b** removed from **1a**-, **gem**- and vehicle-injected mice 2 d after intravenous injection.

3.3 Conclusions

Data presented for above indicate the conjugate **1a** hydrolyzes with a half-life of approximately 1 h in serum at 37 °C, to give free gemcitabine and

fluorophore **5**. However, fluorescence in the tumor implant is near maximal around 30 min after intravenous injection, indicating that some of conjugate **1a** is imported into tumor cells *in vivo*. This assertion is consistent with the observation that the molar efficacy of the conjugate is significantly greater than gemcitabine with respect to reduction of tumor burden in these models. Conjugate **1a** is cleared from the tumor more quickly than the literature conjugate **E**[104] and other fluorophores like MHI-148 that feature a *meso*-Cl,[121] consistent with our original hypothesis.

Conjugate **1a** comprises a Cy7 dye framework; a similar compound, but based on a Cy5 core, has been reported: **G**. Conjugate **G** localized in tumors (from SGC7901 gastric carcinoma cells and decreased their volume), but the decrease does not appear to have been compared to a gemcitabine control.[122] Conjugates such as these based on a Cy5 core ($\lambda_{max\ em}$ ~655 nm) are more difficult to observe *in vivo* than near-IR probes featured in this work.

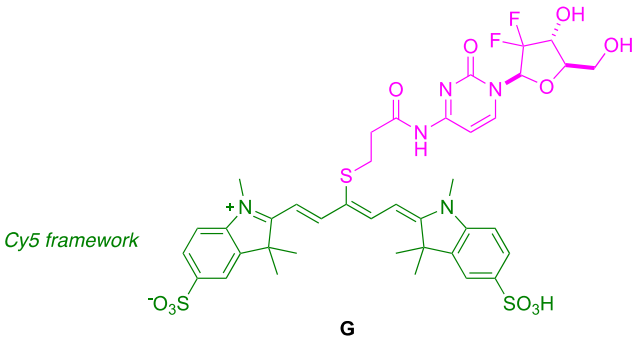

G

In related studies, we[111] and others[117] have found Cy7 dyes with a *meso*-chloride react with albumin ($t_{1/2}$ ~30 min at 37 °C) to give a covalent adduct. Displacement of *meso*-chloride is impossible for conjugates **1** (they do not have a *meso*-Cl) but it can for structure **E**. In previous work we have shown that dyes in this series that have a *meso*-chloride can form conjugates with serum albumin, and the albumin adducts persists in tumors for extended periods.[112,117] Thus the presence of a *meso*-Cl, covalent albumin binding or not, manifests itself in this study by the residence time of the fluorophore in the tumor. Data here also shows that the amide bond connecting the dye and gemcitabine in **1a** are vulnerable to proteolysis in serum. It seems likely that similar amide bonds, as in **E**, are similarly labile. Overall, it is advantageous to conjugate gemcitabine with tumor seeking dyes like **A** at *meso*-position if relatively quick clearance is important to reduce the off-target effect and toxicity to normal organs, and this approach was shown here to give greater molar efficacy of **1a** relative to gemcitabine. Alternatively, if the goal is to increase the residency time in tumors, then a better strategy might be via conjugates like **E** that we strongly suspect form covalent adducts with albumin in serum.

CHAPTER IV

OBOC LIBRARY SCREENING TO DISCOVER NEW TUMOR-TARGETING SMALL MOLECULE AS THERAPEUTIC CANDIDATE

4.1 Introduction

One-bead-one-compound (OBOC) combinatorial libraries, developed by Kit Lam and others,[123,124] has been used for searching oligomers and small molecules with unique biological or medicinal properties.[125,126] Various efforts have been made to expand the accessible chemical space of the library[127,128] and the dimension of its applications[129-132] via high-throughput screening (HTS). Libraries of peptides,[133] peptoids,[134] and small molecules[135,136] can be screened against proteins, intact cells or phage display libraries.[137]

The construction of OBOC libraries follows a “split and combine” strategy in solid-phase synthesis (Figure IV.1). A compound library with enormous combination of building blocks can be obtained easily with less number of steps in synthesis. At the same time, each solid bead contains only one specific fragment combination, which simplifies the characterization (decoding) process of the on-bead compound.

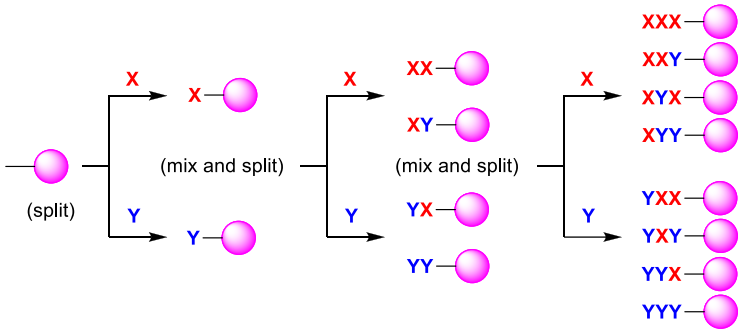

Figure IV.1. Concept scheme of OBOC library construction. Using only two fragment units **X** & **Y**, a library of 2^N molecules with *N* sequential units is obtained with only 2*N* number of synthesis.

Two strategies are commonly used to search OBOC libraries for tumor targeting bio-markers. If the targeted bio-markers are well known and tagged with biotin or fluorescence label, a protein-based assay[124] can be used to identify strong binder. If the bio-markers are unknown, a cell-based assay[138] can be used to select molecules with high binding potential. The latter strategy is potentially useful in cancer research where the pertinent cell surface receptors are uncharacterized.

Screening an OBOC combinatorial library for biological active molecules usually involves three stages: (i) library design and preparation, (ii) library screening, and (iii) active compound decoding.

Library design and preparation is the fundamental stage that directs the later strategies. For a specific target bio-marker, a large and diverse library of molecules based on molecular scaffold of interest is designed. After on-bead hit compounds are found, they need to be cleaved into solution and analyzed,

typically via mass spectrometry (MS). Hence, an optimized cleavable linker has to be added to the design to segregate the molecule core and cleavage spot on bead surface. Various linkers have been developed to serve different cleavage conditions (e.g. nucleophilic, electrophilic, reductive, oxidative or photo-cleavable), while being stable during library construction. [139-144] Encoding systems can be incorporated to the library design as well to characterize the molecule on hit beads.[135,145,146] A topologically segregated bilayer/multilayer bead with test molecule on the surface and coding molecule buried inside (referred as one bead two compound (OB2C) assay[147,148]) is often used for coding various library designs. Partial Alloc-deprotection[149] and partial Fmoc-protection[150] approaches are major techniques for this approach, an enzyme-mediated spatial segregation[151] of bead surface is also feasible. Polymer beads can also be marked with colors or barcodes[126,152,153] to simplify decoding procedure. A halogen tag is also a good marker during MS analysis.[136] Apparently, the synthetic efficiency of the library molecule is also crucial; otherwise, the one-bead-one/two-compound concept is violated.

TentaGel resin, a polystyrene and polyethylene glycol (PEG) crosslinked polymer bead, provides good swelling during organic phase synthesis as well as possibilities for aqueous phase screening.[154] Thus, it is widely applied to OBOC combinatorial library preparation and screening. Yet, the auto-fluorescence of TentaGel beads leads to lower signal-to-noise ratio during screening.[154,155]

Auto-fluorescence of the beads can be reduced by coupling an internal quencher[156] on the bead or by performing image background subtraction.[154,157]

For the ease of observing cells adhered on the bead surface, quantum dots (QDs) are diffused into the cells that show bright color during library screening under fluorescence microscope.[158-161] During the primary screening of the compound library, molecule that binds to the cancer cells may not interact preferably with the targeted cell surface protein. Usually the non-specific binding molecules are eliminated by a secondary screening of the library with a control cell line which does not express the targeted protein. By labeling the targeted and control cells with two different colors of QDs, both types of cells can be screened with the OBOC library at the same time. The beads with single color (targeted) cells adhered are specific for the target protein, and the beads with two colors will be eliminated as non-specific binders.

Decreasing surface ligand density[162] and utilizing redundant libraries[163] (selecting only repeat hits from multiple identical libraries for re-synthesis and re-screening) can also eliminate non-specific (or false positive) binding molecules from library screening.

Manual screening of OBOC combinatorial libraries are time-consuming and laborious due to the large number of molecules in the library, and picking positive beads with micro-pipette is inefficient. This hurdle can be overcome by automated equipment, like Complex Object Parametric Analyzer and Sorter (COPAS)[164,165] and Confocal Nanoscanning (CONA).[166]

Active compound decoding from a single bead is easier as mass spectrometer evolves with lower detection limit and higher resolution. Matrix-assisted laser desorption/ionization (MALDI) mass spectrometry is a prime example of this technological advancement that requires less amount (1 – 2 μL) of test sample. This is extremely helpful in making concentrated samples from one single bead[167] assisting in deciphering the chemical structure of the compound by the mass of coding tag.[168,169] Tandem mass spectrometry (MS/MS) can improve accuracy of decoding.[170,171]

In this chapter, synthetic non-peptide libraries were designed based on the OBOC concept and screened against various types of cells to develop novel tumor-targeting small molecules.

4.2 Results and Discussion

A peptidomimetic **A**-based small molecule was revealed by our group to perturb protein-protein interactions (unpublished results). Both the triazole and hydantoin fragments in **A** showed high potentials in mimicking side chain orientations of peptide secondary structures via computational overlay by exploring key orientations on secondary structures (EKOS) program with low root mean square deviation (RMSD) values.[172] A synthetic combinatorial OBOC library **1** was designed with various amino acid side chains on R^1 – R^3 to explore and expand the application of construct **A**, especially for cancer cell targeting (Figure IV.2a). For ease of synthesis, only seven R^2 groups were included in

this first library design, but it is possible to get more options for R^2 since synthesis of R^2 fragment has been well established.[42]

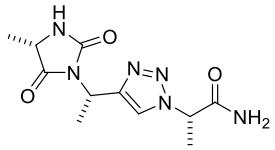

A

*4.2.1 Design and preparation of library **1***

The complex properties of the molecule fragments used for building library **1** required investigation to find an appropriate encoding system (details explained in experimental methods). Eventually, step-wise partial capping[135] (Scheme IV.2) incorporated with bromine isotope label[136] (Scheme IV.1) was applied for efficient synthesis (Figure IV.2a).

In the linker design (Figure IV.2b), methionine served as the cleaving site of the molecule after treating with BrCN solution.[173] Lysine linked with 4-bromobenzoic acid introduced a bromine atom offering a unique MS signal pattern {fragments of (M + 1):(M + 3) = 1:1, where M is the exact mass of the fragment} to assist in compound decoding. Moreover, lysine provided a potential positive charge to ease MALDI-MS detection. The extended linker acted as a spacer between the library molecule and the molecule cleavage site and guaranteed the molecular weight of all library compounds are above 600 to increase signal-to-noise ratio for mass spectrometry analysis.

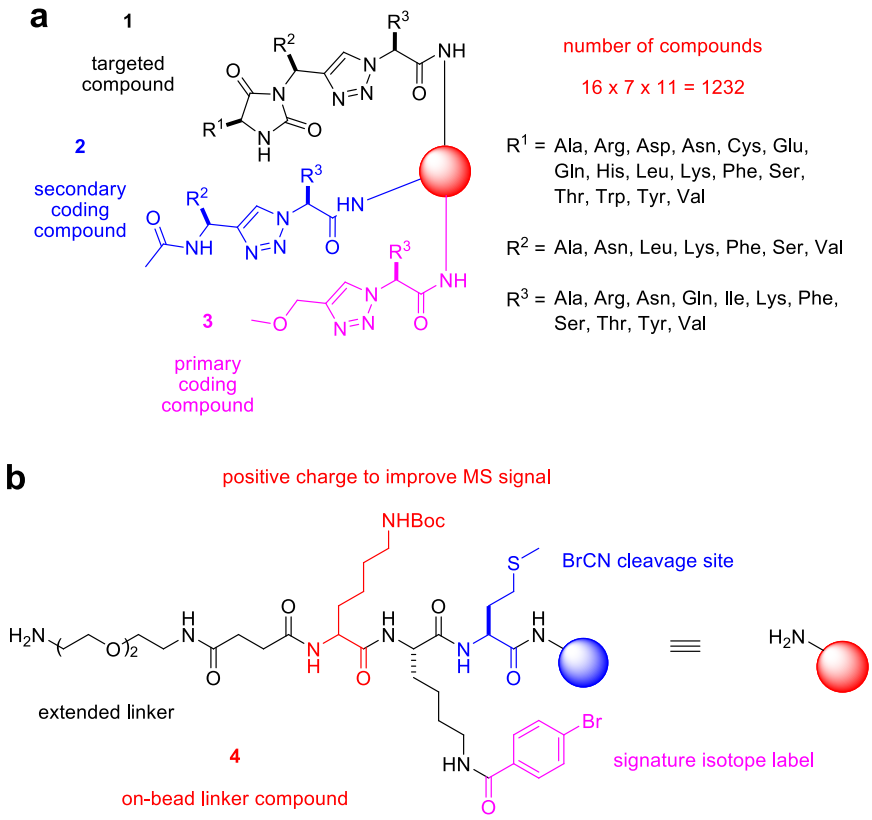

Figure IV.2. Featured structure of OBOC library **1**. **a** Partial capping coding construct of OBOC library **1**; **b** linker structure used in the library **1**.

When constructing the combinatorial library **1**, 20% mole of capping reagent was added together with the defined molecule fragment resulting in a "one-bead-three-compound" library. On the bead, the largest and most abundant molecule is the designed compound that is used to test cell-adherence; the smaller and less abundant molecules are the "codes" for compound characterization after library screening.

4.2.2 Preliminary test with modified screening protocol

While preparing library **1**, a known on-bead cyclic peptide **B**[174] (with sequence of cNGRGEQc, c represent *D*-Cysteine) was used to explore and adjust the screening protocol to fit our instrument settings. **B** was reported to bind the $\alpha_3\beta_1$ integrin expressed on the cellular membrane of A549 cancer cells. Screening of cyclic peptide **B** against A549 cells was performed with modified protocol (details in experimental method section). Significant number of cells adhered on the beads with **B**, while nearly no cells were observed on the surface of blank beads (Figure IV.3).

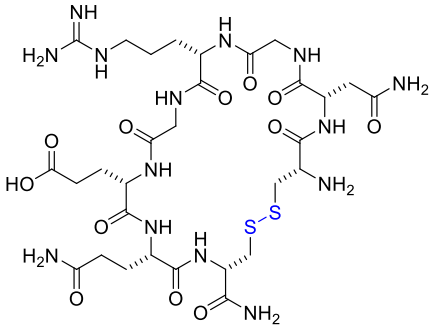

B

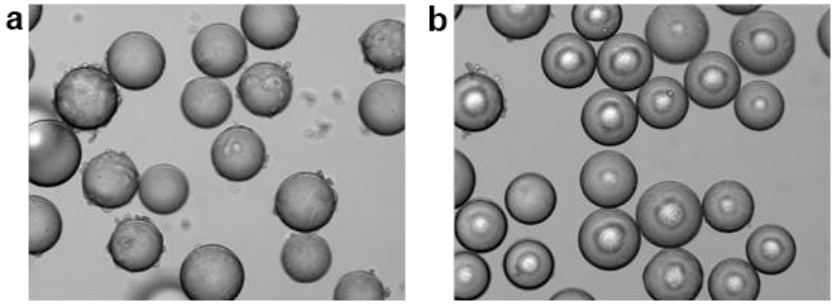

Figure IV.3. TentaGel beads images after equilibrium with A549 cells. **a** Beads loaded with cyclic peptide **B**; **b** blank beads showed minimum binding to cells.

The proper concentration of Bovine Serum Albumin (BSA) in the culture medium during cell-bead equilibrium was proven to be important. With no BSA in the medium, cells do not adhere well to the bead surface. If high concentrations of BSA are used, cells tend to clump together resulting in less cell-to-bead interaction. During trial experiments for **B**, 4% BSA gave the best cell adherence ratio (Figure IV.4).

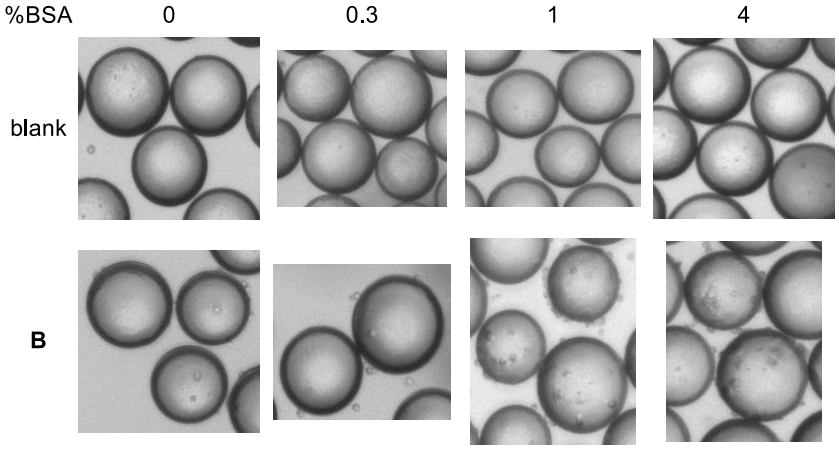

Figure IV.4. Images of cells on beads at different concentrations of BSA in the culture medium.

*4.2.3 Preliminary screening with library **C***

To further validate screening protocol, an OBOC small molecule library **C**[175] prepared by Dr. Dongyue Xin (previous group member) was used to screen against A549 cells. Library **C** possesses three variable arms featuring all natural amino acid side chains (except proline, 19 x 19 x 19 = 6859 compounds). In preliminary results, significant number of cells bound to the surface of 20 beads.

(Figure IV.5) However, without a proper linker segregating the library compound and bead surface, most of the molecules cleaved from bead after screening had low molecular weight (<600, MS background is high[135]) resulting in reduced signal-to-noise ratio in MS signal. Lacking of a proper encoding system also made the compound unable to be characterized by MS.

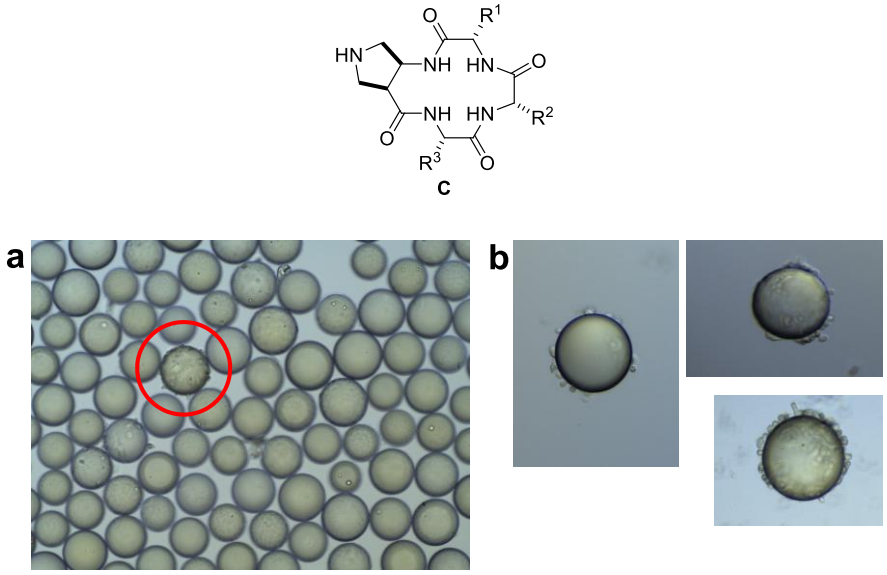

Figure IV.5. Library **C** screening results. **a** One intact view with one bead (in red circle) covered by A549 cells; **b** featured examples of "positive" beads with noticeable number of A549 cells on surface.

*4.2.4 OBOC library **1** screening and analysis based on capping strategy*

Tropomyosin kinase receptor C (TrkC)[1,2,75,80,176] was chosen as the screening target. Wild-type ($TrkC^-$) and TrkC-transfected ($TrkC^+$) NIH3T3 cells formed a perfect pair to eliminate potential nonspecific binding molecules.

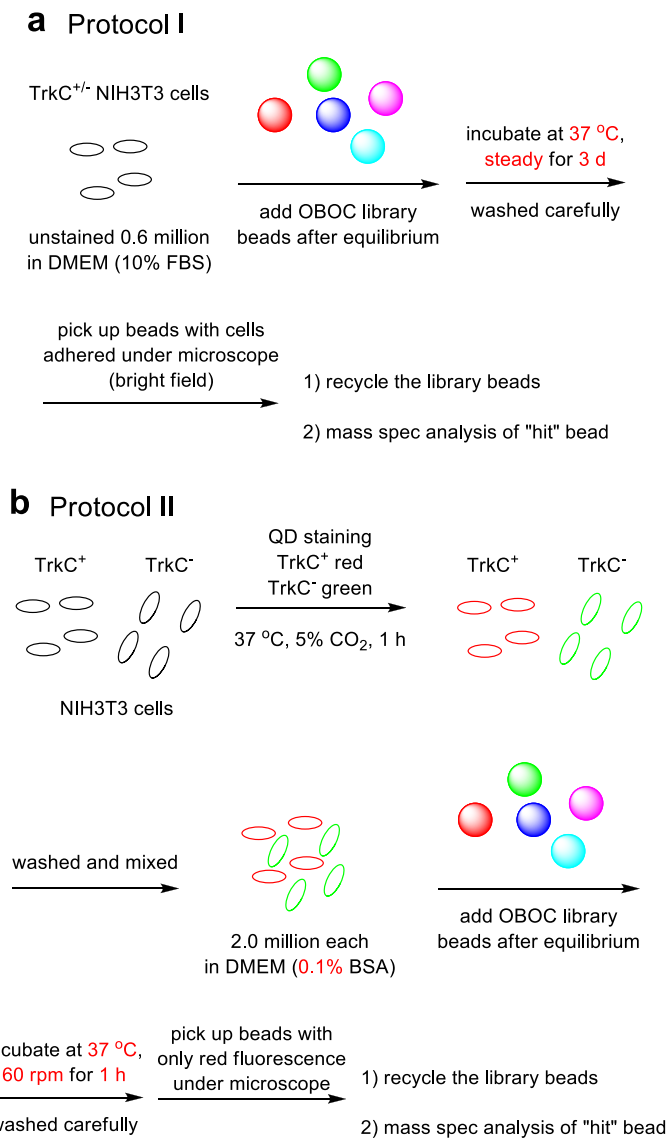

Figure IV.6. Protocols applied for OBOC combinatorial library screening with NIH3T3 cells. **a** Protocol **I** consumes less beads and cells, yet need longer incubation; **b** protocol **II** consumes more beads and cells, but involves much shorter incubation times. Protocol **II** can be applied in single color mode if needed.

There are different ways to perform the library screening against cancer cells. Dr. Lam[174] and Dr. Kodadek[177], pioneers of the field, have reported

different protocols for screening against cancer cells.[47,128,178] Based on this literature we designed and tested several protocols, but only two of them showed promising results. Protocol **I** was directly derived from Dr. Lam's method,[174] screening one cell type at a time. Protocol **II** was based on Dr. Kodadek's procedure[177] in which both $TrkC^+$ and $TrkC^-$ cells can be screened simultaneously using different QD labeling (Figure IV.6).

4.2.5 Compound characterization after screening

Once potential "hit" beads were picked from the library, they were thoroughly washed[177] to remove cells, and each bead was treated with BrCN solution for compound cleavage. Three sequential MS signals (**S1** – **3**, high to low, Figure IV.7b), featuring MS signal of (M + 1):(M + 3) = 1:1, will be detected by MALDI-MS. The molecular weight of the representative amino acids for R^1 – R^3 can be calculated easily by the following equations (*calculated value equal to free amino acid molecular mass):

$$R^3 = \mathbf{S3} - 847.25^*$$

$$R^2 = \mathbf{S2} - \mathbf{S3} + 48.07^*$$

$$R^1 = \mathbf{S1} - \mathbf{S2} + 34.15^*$$

In a preliminary screening, only one "hit" bead resulted in good quality MS signal (**1-vlf**, Figure IV.7a). The low characterization rate indicates towards a low synthesis efficiency of the library. To overcome the synthesis hurdle, the building blocks of the library (azides and alkynes) were re-purified, and the

library (collaborator: Mr. Jonathan Whisenant) was resynthesized on a larger TentaGel resin (300 µm diameter, Rapp Polymere® #300002).

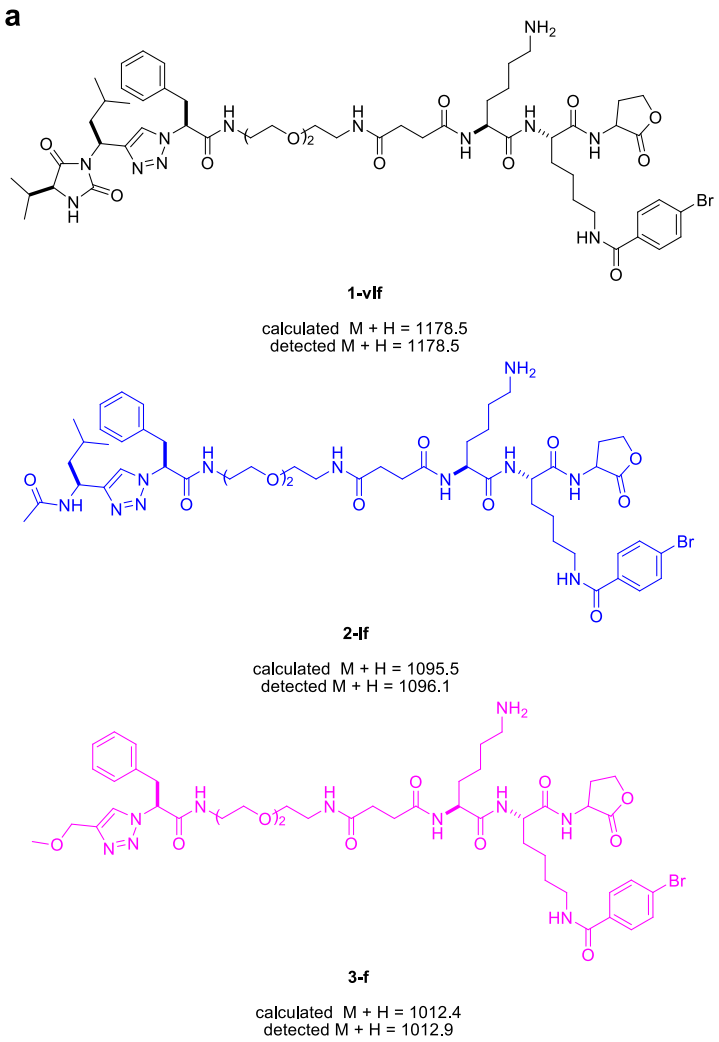

Figure IV.7. Mass spectrometry analysis of the isolated "hit" bead. **a** Chemical structure of the three cleaved compounds, with calculated and detected MS signal; **b** zoom-in MS signal patterns of **S1** – **3** and corresponding amino acid side chains for a "hit" bead. R^3 = 1012.9 (**S3**) – 847.2 = 165.7 (Phe); R^2 = 1096.1 (**S2**) – 1012.9 (**S3**) + 48.1 = 131.3 (Leu); R^1 = 1178.5 (**S1**) – 1096.1 (**S2**) + 34.2 = 116.6 (Val).

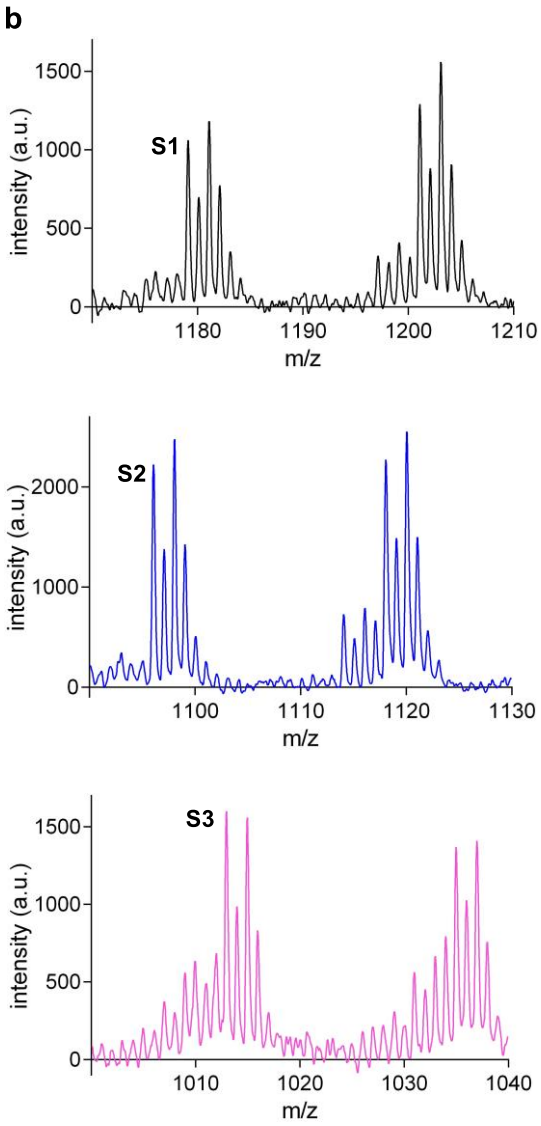

Figure IV.7. Continued.

The new library was screened via protocol **I** to give eight positive beads. Out of these, six beads showed MS ions with the unique isotope pattern in MALDI-MS (data not shown). After much experimentation, we were able to synthesize a combinatorial library **1** that was decodable by MS.

Redundant library screening is crucial to eliminate false positive results.[163] Multiple occurrences of a single molecule signal from repeated screening can significantly increase the possibility of a true "hit" compound that selectively binds to the targeted cells. Unfortunately, no identical hit has been identified from repeated library screenings with TrkC$^{+/-}$ NIH3T3 and A549 cells. This indicates that the library may not contain a molecule with high affinity to the proteins overexpressed on these cell surfaces.

4.3 Conclusions

A peptidomimetic OBOC combinatorial library **1** was established and screened against different types of cells. The screening protocols were adjusted to fit specific needs. Beads picked from library **1** were reliably decodable by MALDI-MS, with the help of a properly designed linker. No repeated sequence was discovered from redundant combinatorial library for either TrkC^{+} NIH3T3 or A549 cells. To overcome the challenge, two parallel strategies will be applied: (i) significantly increasing the number of compounds in the library, and (ii) screening the library against more cancer cell lines. These improvements will increase the chances of finding a strong binding molecule to the cancer cell surface protein.

4.4 Experimental Methods

Computational overlays of hydantoin and triazole dipeptide mimics on common peptide secondary structures (RMSD values included) are in Appendix B.[172] Synthesis of the featured azido acids (with R3) and alkynes (with R2) were previously described.[41]

*4.4.1 Synthesis of **B** on bead and modified screening protocol*

Synthesis of **B** is assisted by Liberty Blue peptide synthesizer following the protocol reported on TentaGel S NH2 resin (130 μm diameter, 0.26 mmol/g, ChemImpex® #04773). **B**-loaded beads as well as blank beads were swelled well in PBS buffer and equilibrated with single suspended A549 cells.

With efforts adapting the reported protocol to the instrument set-up in our lab, a modified screening protocol was finalized with following conditions: 33 mg (~25,000) of either blank beads or **B**-loaded beads were mixed with 0.6 million A549 cells in 2.5 mL DMEM buffer (0 – 4% BSA, in a 30 mm petri dish) on an orbital shaker for 10 min (50 rpm), then steadily set in a CO_2 incubator at 37 ^oC for 3 d. After careful wash with fresh DMEM buffer, beads were transferred to a clean 30 mm petri dish and observed under EVOS2 microscope (10X objective, bright field).

*4.4.2 Preparation of library **1***

Library **1** was prepared via solid-phase synthesis on TentaGel resin beads (Scheme IV.1 and 2). General protocols frequently used during the synthesis are described first as follows.

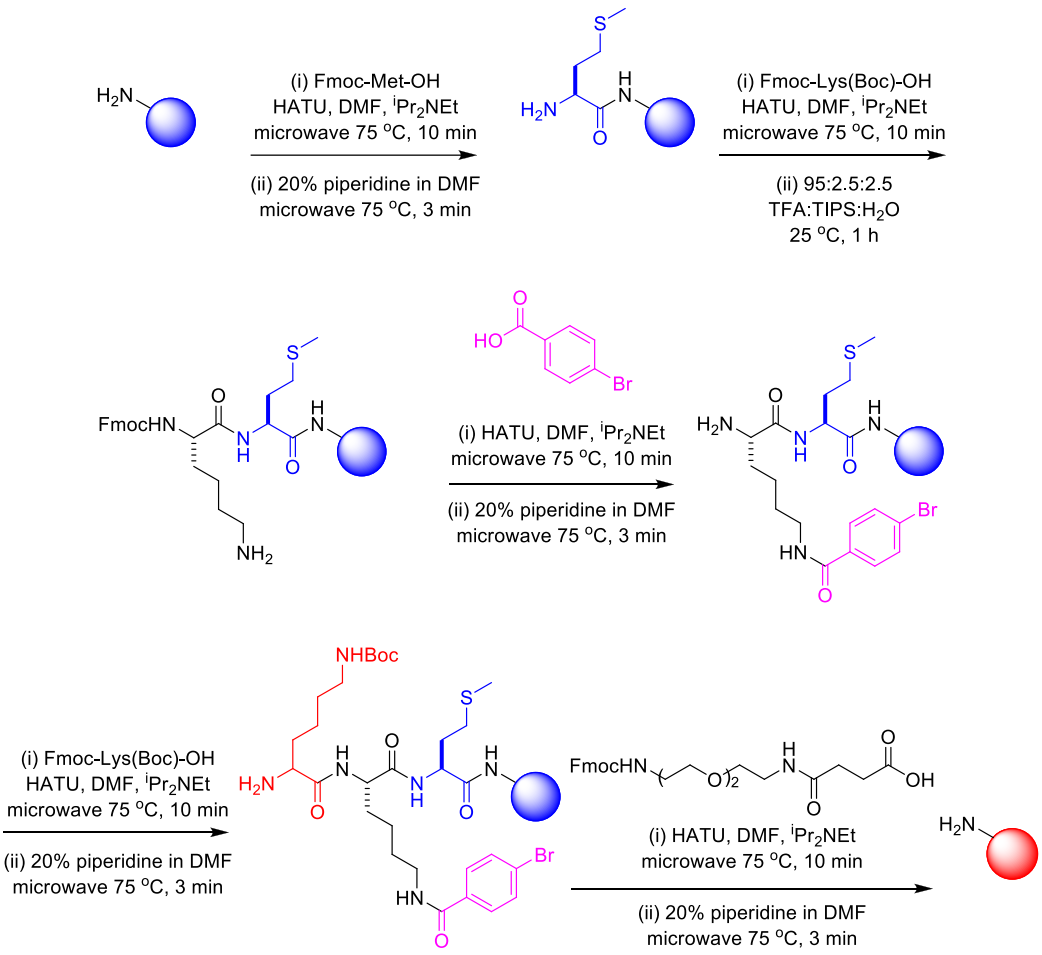

Scheme IV.1. Preparation of the linker on TentaGel resins before library synthesis.

(i) carboxylic acid coupling condition: 4.0 equiv. carboxylic acids, 8.0 equiv. *N,N*-Diisopropylethylamine ($^{i}Pr_2NEt$) and 0.25 M 1-[Bis (dimethylamino) methylene]-1H-1,2,3-triazolo[4,5-b]pyridinium 3-oxid hexafluorophosphate (HATU) in 2.0 mL DMF solution were added to the swelled resin beads and microwaved (400 W) at 75 ^{o}C for 10 min. Solvent was drained and beads were washed with fresh DMF twice.

(ii) Fmoc deprotection: 2.0 mL 20% piperidine in DMF was added to the beads and microwaved (400 W) at 75 ^{o}C for 3 min. Solvent was drained and beads were washed with fresh DMF twice.

(iii) Boc and other acid labile protecting group removal: 2 mL of 95:2.5:2.5 trifluoroacetic acid (TFA):triisopropylsilane (TIPS):H_2O mixture was added to resin and shaken vigorously for 1 h, followed by thorough washing with DMF.

TentaGel S NH_2 resin (600 mg, 130 μm dia.) was swelled well in CH_2Cl_2 and *N*,*N*-dimethylformamide (DMF) in a 5 mL syringe reaction vessel (Torviq® #SF-0500). Fmoc-Met-OH coupling was performed on a bead surface, followed by Fmoc deprotection. After Fmoc-Lys(Boc)-OH coupling, Boc protecting group was removed. 4-bromobenzoic acid coupling added the isotope marker. The Fmoc deprotection led to a second Fmoc-Lys(Boc)-OH coupling. Fmoc deprotection was carried out again and an *N*-Fmoc-protected ethylene glycol linker[168] was coupled.

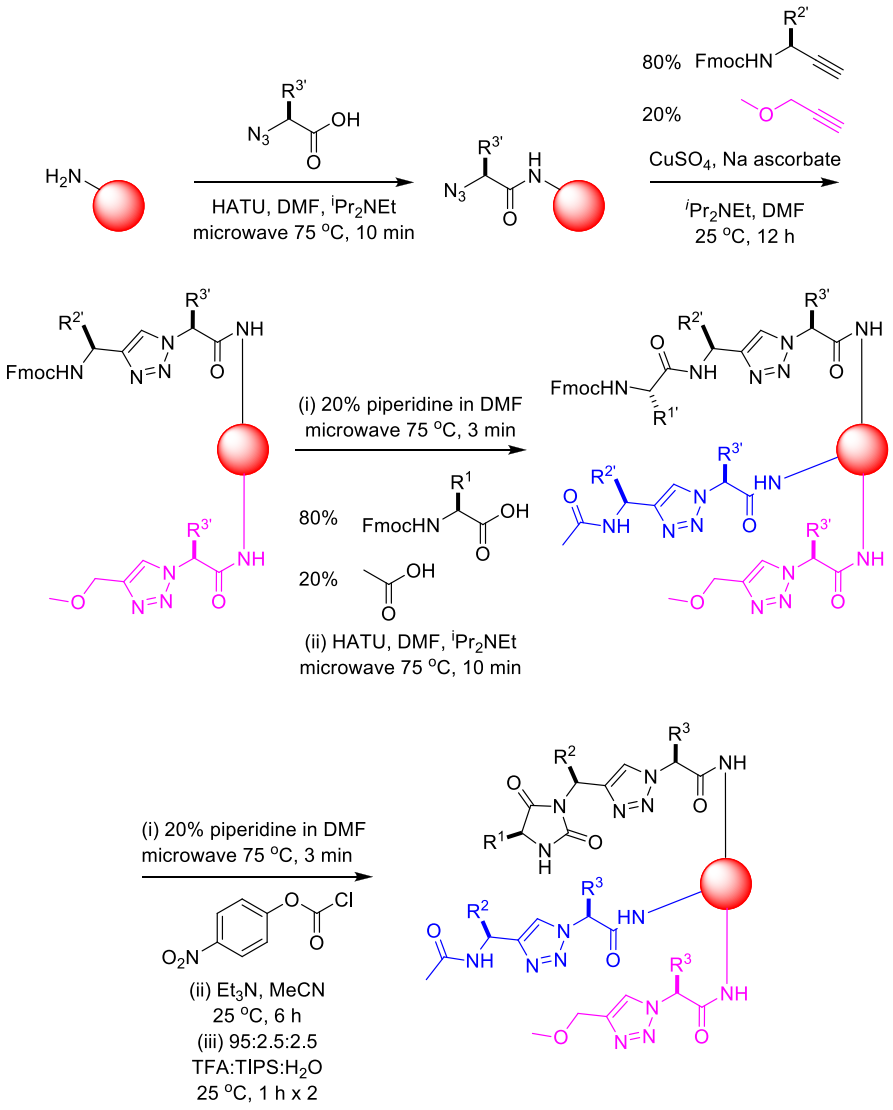

Scheme IV.2. Synthesis of OBOC library **1** with step-wise partial capping.

Following routine Fmoc deprotection, the TentaGel resin was equally separated into 11 fractions. In each fraction, one specific azido acid (with R^3) was coupled to the beads. All fractions were combined and mixed well after a thorough wash with DMF.

The resin was equally separated into seven fractions. In each fraction, 1.6 equiv. Fmoc amino alkyne (with R^2) and 0.4 equiv. methyl propargyl ether was added along with 0.2 equiv. $CuSO_4$, 0.2 equiv. sodium ascorbate, and 8.0 equiv. $^{i}Pr_2NEt$ in 1.0 mL DMF and stirred at 25 ^{o}C for 12 h. After removing reaction solutions, beads were washed with DMF twice. All fractions were combined followed by Fmoc deprotection.

TentaGel resin was then equally separated into 16 fractions. In each fraction, 3.2 equiv. Fmoc amino acid (with R^1) and 0.8 equiv. acetic acid were coupled via carboxylic acid coupling protocol. All fractions were combined followed by Fmoc deprotection, then 3.0 equiv. 4-nitrophenyl chloroformate, and 6.0 equiv. triethylamine (Et_3N) in 2.0 mL acetonitrile (MeCN) were added and stirred at 25 ^{o}C for 6 h to form hydantoin. Protecting groups of R^1 – R^3 (all acid labile) were removed (performed twice to completely remove Pbf protecting group on arginine) in the end to get encoded library **1**.

4.4.3 Cell culture.

A549 (ATCC®) cells were cultured on 75 cm^2 tissue culture flasks in RPMI-1640 medium (ATCC®) with 10% fetal bovine serum (FBS). TrkC transfected NIH3T3 cells were cultured on 75 cm^2 tissue culture flasks in DMEM/F12 supplement with 10% FBS including 400 mg/mL G418 (GIBCO®). All cells were cultured in a humidified incubator at 37 °C with 5% CO_2 and 95% air.

*4.4.4 Screening protocol for library **C***

The OBOC library beads (30 mg, ~24,000 beads with average three copies of each compound in the library) were swelled thoroughly in CH_2Cl_2, and equilibrated in DMF overnight. The next day, the beads were washed in the following sequence: water, PBS buffer and phenol red free DMEM buffer, twice at each step. Beads were kept in equilibrium in DMEM buffer for at least 1 h before mixing them with suspended A549 cells (as described below).

Cultured A549 cells were digested with trypsin solution and resuspended in DMEM buffer with 10% FBS. The suspended cells were filtered through a cell strainer (40 μm pore size, VWR® #10199-654) to get single suspended cells. Filtered cells were prepared in 0.3 million/mL with 2 mL phenol red free DMEM (10% FBS) and mixed with the library beads in a 30 mm diameter petri dish. The mixture was incubated on an orbital shaker at 37 ^{o}C, 60 rpm for 10 min, then steadily in a humidified incubator at 37 °C with 5% CO_2 for 3 d. The beads were then carefully transferred to a 5 mL tube, and gently washed twice with DMEM buffer (no phenol red) to remove the suspended cells. All library beads were observed carefully under microscope (EVOS2 microscope, 10X objective, bright field), and beads with significant number of cells adhered were picked up manually with a micropipette.

Positive hit beads were picked and kept individually in Eppendorf tubes while the rest of library beads collected in a 3 mL syringe with filter. Both sets of beads were thoroughly washed following Kodadek's protocol.[177] Generally,

beads were suspended in 1% sodium dodecyl sulfate (SDS) aqueous buffer and boiled for 1 h, washed with water twice afterwards. Then beads were shaken in enzyme free cell dissociation buffer (Thermo Scientific® #13151-014) for 30 min, and washed with 1:1 MeCN:water, DMF and CH_2Cl_2 twice. Library beads were kept under vacuum for future use, and compounds on the single "hit" bead were cleaved off with 30 mg/mL BrCN in 5:4:1 MeCN:acetic acid:water mixture overnight. After air-drying the cleavage buffer, concentrated sample in 1:1 MeCN:water (5 µL) were sent for MALDI-MS analysis.

*4.4.5 Screening protocol for library **A***

Protocol I:

General protocol is the same as the one for screening library **C**, only difference lies in the density of beads and numbers of NIH3T3 cells. The library beads (30 mg 130 µm dia. or 50 mg 300 µm dia.) were equilibrated with 0.2 million/mL NIH3T3 cells with 2 mL phenol red free DMEM (10% FBS).

Protocol II:

The OBOC library beads (90 mg 130 µm dia. or 120 mg 300 µm dia.) were swelled thoroughly in CH_2Cl_2, and equilibrated in DMF overnight. On the next day, the beads were washed in the following sequence: water, PBS buffer and phenol red free DMEM buffer, twice at each step. Beads were kept in

equilibrium in DMEM buffer for at least 1 h before mixing them with the suspended NIH3T3 TrkC$^{+/-}$ cells.

Cultured NIH3T3 cells were digested with enzyme free cell dissociation buffer and resuspended in DMEM buffer with 10% FBS. The cell density was adjusted to 1.0 million/mL, and TrkC-transfected NIH3T3 cells were stained with red Qdot 655 (Thermo Scientific® #Q25021MP) while wild type NIH3T3 cells were stained with green Qdot 565 (Thermo Scientific® #Q25031MP) in a humidified incubator at 37 °C with 5% CO_2 for 1 h (detailed protocol was same as ref[177]). After washing with DMEM buffer, the suspended cells were filtered through a cell strainer (40 μm pore size) to give single suspended cells.

Each type of filtered cells was prepared in 2.0 million/mL with 1 mL phenol red free DMEM (0.1% BSA) and mixed together with the library beads in a 5 mL tube (Torviq® #SF-0500, 1.0 million/mL red or green cells). The mixture was incubated on an orbital shaker at 37 ^{o}C, 60 rpm for 1 h.

The beads were then gently washed twice with DMEM buffer (no phenol red) to remove the suspended cells. All library beads were observed carefully under microscope (EVOS2 microscope, blue light excitation with long-pass filter, fluorescence under color camera), and beads with only red cells adhered were picked up manually with a micropipette. Bead cleaning and cleavage procedures were same as described in library **C**.

While preparing suspended NIH3T3 cells for library screening in protocol **II**, cell clumps formed quickly (within 30 min). To eliminate cell clump formation,

NIH3T3 cells were digested again with enzyme free cell dissociation buffer right after QD staining before cell strainer filtration.

Original MALDI-MS data of the bead analyzed in Figure IV.7 above is attached here:

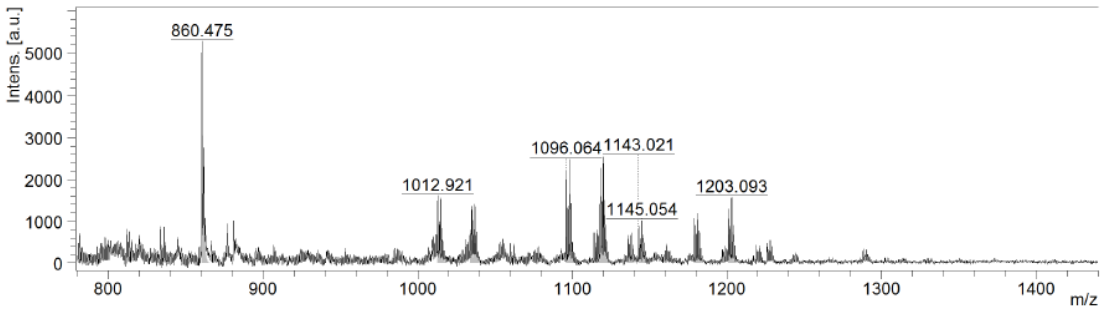

CHAPTER V

CONCLUSIONS

This dissertation explores some potential applications of small molecules in active targeting of cancer cells, especially metastatic breast cancer and glioblastoma.

A TrkC-targeted small molecule with modest binding affinity (~112 nM) was used to deliver maytansinoid, a toxic cargo, to metastatic breast cancer cells. The small molecule conjugate showed improved therapeutic index between $TrkC^+$ and $TrkC^-$ cells *in vitro*. *In vivo*, the targeted conjugate showed better tumor suppression against orthotopic 4T1 tumors in mice than the non-targeted control group. This approach offers an alternative way to actively target breast cancer cells in addition to the commonly used ER, PR and HER2 targeting strategies.

Moreover, four *meso*-substituted heptamethine gemcitabine conjugates were prepared and screened for targeted theranostic effect against glioblastoma cells. These conjugates generally (all except one) had similar organelle localization compared to their parent dyes *in vitro*. One lead compound was tested *in vivo*, and it showed good tumor accumulation and greater molar efficacy in therapy relative to free gemcitabine.

Furthermore, OBOC combinatorial library screening strategy was used to search for novel small molecule as active targeting ligand in cancer therapy.

The screening and coding protocols were successfully established after various attempts. Several modifications, including synthesizing an expanded small molecule library and screening with diverse cancer cell types, are required to discover the targeted synthetic compound with strong affinity to specific protein on cancer cell surface.

Other trials of developing small molecule with active targeting property in cancer characterization and treatment were attempted but the results were negative.

In summary, targeted small molecules have potential advantages in cancer targeting and therapy. Although the process is challenging but the ability to explore diverse synthetic combinatorial libraries to discover high affinity probes with therapeutic applications is promising.

REFERENCES

1. Stephens, P.; Edkins, S.; Davies, H.; Greenman, C.; Cox, C.*, et al.*, A screen of the complete protein kinase gene family identifies diverse patterns of somatic mutations in human breast cancer. *Nat. Genet.* **2005,** *37* (6), 590-592.

2. Ivanov, S. V.; Panaccione, A.; Brown, B.; Guo, Y.; Moskaluk, C. A.*, et al.*, TrkC signaling is activated in adenoid cystic carcinoma and requires NT-3 to stimulate invasive behavior. *Oncogene* **2013,** *32* (32), 3698-3710.

3. Kue, S. C., Anyanee Kamkaew, Hong Boon Lee, Lip Long Chung, Lik Voon Kiew, and Kevin Burgess, Targeted PDT Agent Eradicates TrkC Expressing Tumors Via Photodynamic Therapy (PDT). *Mol. Pharmacetics* **2015,** *12*, 212-222.

4. Huang, E. J.; Reichardt, L. F., Trk receptors: roles in neuronal signal transduction. *Annu. Rev. Biochem.* **2003,** *72*, 609-642.

5. Chao, M. V., Neurotrophins and their receptors: A convergence point for many signalling pathways. *Nat. Rev. Neurosci.* **2003,** *4* (4), 299-309.

6. Torchilin Vladimir, P., Passive and active drug targeting: drug delivery to tumors as an example. *Handb. Exp. Pharmacol.* **2010,** *197*, 3-53.

7. Alley, S. C.; Okeley, N. M.; Senter, P. D., Antibody-drug conjugates: Targeted drug delivery for cancer. *Curr. Opin. Chem. Biol.* **2010,** *14* (4), 529-537.

8. Katz, J.; Janik, J. E.; Younes, A., Brentuximab Vedotin (SGN-35). *Clin. Cancer Res.* **2011,** *17*, 6428-6436.

9. Lambert, J. M.; Chari, R. V. J., Ado-trastuzumab Emtansine (T-DM1): An Antibody-Drug Conjugate (ADC) for HER2-Positive Breast Cancer. *J. Med. Chem.* **2014,** *57*, 6949-6964.

10. Ricart, A. D., Antibody-Drug Conjugates of Calicheamicin Derivative: Gemtuzumab Ozogamicin and Inotuzumab Ozogamicin. *Clin. Cancer Res.* **2011,** *17*, 6417-6427.

11. Wu, A. M.; Senter, P. D., Arming antibodies: prospects and challenges for immunoconjugates. *Nat. Biotechnol.* **2005,** *23* (9), 1137-1146.

12. Chari, R. V. J.; Miller, M. L.; Widdison, W. C., Antibody-Drug Conjugates: An Emerging Concept in Cancer Therapy. *Angew. Chem., Int. Ed.* **2014,** *53*, 3796-3827.

13. Cassady, J. M.; Chan, K. K.; Floss, H. G.; Leistner, E., Recent developments in the maytansinoid antitumor agents. *Chem. Pharm. Bull.* **2004,** *52*, 1-26.

14. Chauhan, V. P.; Stylianopoulos, T.; Boucher, Y.; Jain, R. K., Delivery of molecular and nanoscale medicine to tumors: transport barriers and strategies. *Annu. Rev. Chem. Biomol. Eng.* **2011,** *2*, 281-298.

15. di Tomaso, E.; Capen, D.; Haskell, A.; Hart, J.; Logie, J. J.*, et al.*, Mosaic Tumor Vessels: Cellular Basis and Ultrastructure of Focal Regions Lacking Endothelial Cell Markers. *Cancer Res.* **2005,** *65* (13), 5740-5749.

16. Baluk, P.; Morikawa, S.; Haskell, A.; Mancuso, M.; McDonald Donald, M., Abnormalities of basement membrane on blood vessels and endothelial sprouts in tumors. *Am. J. Pathol.* **2003,** *163* (5), 1801-1815.

17. Dennis, M. S.; Jin, H.; Dugger, D.; Yang, R.; McFarland, L.*, et al.*, Imaging Tumors with an Albumin-Binding Fab, a Novel Tumor-Targeting Agent. *Cancer Res.* **2007,** *67* (1), 254-261.

18. Saga, T.; Neumann, R. D.; Heya, T.; Sato, J.; Kinuya, S.*, et al.*, Targeting cancer micrometastases with monoclonal antibodies: a binding-site barrier. *Proc. Natl. Acad. Sci.* **1995,** *92* (19), 8999-9003.

19. Adams, G. P.; Schier, R.; McCall, A. M.; Simmons, H. H.; Horak, E. M.*, et al.*, High affinity restricts the localization and tumor penetration of single-chain Fv antibody molecules. *Cancer Res.* **2001,** *61* (12), 4750-4755.

20. Rudnick, S. I.; Lou, J.; Shaller, C. C.; Tang, Y.; Klein-Szanto, A. J. P.*, et al.*, Influence of Affinity and Antigen Internalization on the Uptake and Penetration of Anti-HER2 Antibodies in Solid Tumors. *Cancer Res.* **2011,** *71* (6), 2250-2259.

21. O'Connor, R., The pharmacology of cancer resistance. *Anticancer Res.* **2007,** *27* (3A), 1267-1272.

22. Borsi, L.; Balza, E.; Bestagno, M.; Castellani, P.; Carnemolla, B.*, et al.*, Selective targeting of tumoral vasculature: comparison of different formats of an antibody (L19) to the ED-B domain of fibronectin. *Int. J. Cancer* **2002,** *102* (1), 75-85.

23. Carrasco-Triguero, M.; Yi, J.-H.; Dere, R.; Qiu, Z. J.; Lei, C.*, et al.*, Immunogenicity assays for antibody-drug conjugates: case study with ado-trastuzumab emtansine. *Bioanalysis* **2013,** *5* (9), 1007-1023.

24. Vlashi, E.; Sturgis, J. E.; Thomas, M.; Low, P. S., Real Time, Noninvasive Imaging and Quantitation of the Accumulation of Ligand-Targeted Drugs into Receptor-Expressing Solid Tumors. *Mol. Pharmaceutics* **2009,** *6* (6), 1868-1875.

25. Yang, H. M.; Reisfeld, R. A., Doxorubicin conjugated with a monoclonal antibody directed to a human melanoma-associated proteoglycan suppresses the growth of established tumor xenografts in nude mice. *Proc. Natl. Acad. Sci.* **1988,** *85* (4), 1189-1193.

26. Primeau, A. J.; Rendon, A.; Hedley, D.; Lilge, L.; Tannock, I. F., The Distribution of the Anticancer Drug Doxorubicin in Relation to Blood Vessels in Solid Tumors. *Clin. Cancer Res.* **2005,** *11* (24, Pt. 1), 8782-8788.

27. Aubel-Sadron, G.; Londos-Gagliardi, D., Daunorubicin and doxorubicin, anthracycline antibiotics, a physicochemical and biological review. *Biochimie* **1984,** *66*, 333-52.

28. Takeda, Y.; Yoshizaki, I.; Nonaka, Y.; Yanagie, H.; Matsuzawa, A.; Eriguchi, M., Docetaxel alone or orally combined with 5-fluorouracil and its derivatives: effects on mouse mammary tumor cell line MM2 in vitro and in vivo. *Anti-Cancer Drugs* **2001,** *12* (8), 691-698.

29. Lurje, G.; Lenz, H.-J., EGFR Signaling and Drug Discovery. *Oncology* **2009,** *77* (6), 400-410.

30. Kamkaew, A.; Lim Siang, H.; Lee Hong, B.; Kiew Lik, V.; Chung Lip, Y.; Burgess, K., BODIPY dyes in photodynamic therapy. *Chem. Soc. Rev.* **2012,** *42*, 77-88.

31. Ravindranathan, P.; Lee, T.-K.; Yang, L.; Centenera, M. M.; Butler, L.*, et al.*, Peptidomimetic targeting of critical androgen receptor-coregulator interactions in prostate cancer. *Nat. Commun.* **2013,** *4*, 1-11.

32. Lu, Y.; Low Philip, S., Folate-mediated delivery of macromolecular anticancer therapeutic agents. *Adv. Drug Deliv. Rev.* **2012,** *64*, 342-352.

33. Walters, C. L.; Arend, R. C.; Armstrong, D. K.; Naumann, R. W.; Alvarez, R. D., Folate and folate receptor alpha antagonists mechanism of action in ovarian cancer. *Gynecol. Oncol.* **2013,** *131* (2), 493-498.

34. Xia, W.; Low, P. S., Folate-Targeted Therapies for Cancer. *J. Med. Chem.* **2010,** *53* (19), 6811-6824.

35. Ojima, I., Guided molecular missiles for tumor-targeting chemotherapy-case studies using the second-generation taxoids as warheads. *Acc. Chem. Res.* **2008,** *41* (1), 108-119.

36. Ruoslahti, E.; Pierschbacher, M. D., New perspectives in cell adhesion: RGD and integrins. *Science* **1987,** *238* (4826), 491-497.

37. Pfaff, M.; Tangemann, K.; Müller, B.; Gurrath, M.; Müller, G.*, et al.*, Selective Recognition of Cyclic RGD Peptides of NMR Defined Conformation by αIIbβ3, αVβ3, and α5β1 Integrins. *J. Biol. Chem.* **1994,** *269*, 20233-20238.

38. Dubey, P. K.; Mishra, V.; Jain, S.; Mahor, S.; Vyas, S. P., Liposomes modified with cyclic RGD peptide for tumor targeting. *J. Drug Targeting* **2004,** *12* (5), 257-264.

39. Kapp, T. G.; Rechenmacher, F.; Neubauer, S.; Maltsev, O. V.; Cavalcanti-Adam, E. A.*, et al.*, A Comprehensive Evaluation of the Activity and Selectivity Profile of Ligands for RGD-binding Integrins. *Sci. Rep.* **2017,** *7*, 39805.

40. Krall, N.; Pretto, F.; Neri, D., A bivalent small molecule-drug conjugate directed against carbonic anhydrase IX can elicit complete tumour regression in mice. *Chem. Sci.* **2014,** *5*, 3640-3644.

41. Chen, D.; Brahimi, F.; Angell, Y.; Li, Y.-C.; Moscowicz, J.; Saragovi, H. U.; Burgess, K., Bivalent Peptidomimetic Ligands of TrkC are Biased Agonists, Selectively Induce Neuritogenesis, or Potentiate Neurotrophin-3 Trophic Signals. *ACS Chem. Biol.* **2009,** *4* (9), 769-781

42. Ko, E.; Kamkaew, A.; Burgess, K., Small Molecules Ligands for Active Targeting of TrkC-expressing Tumor Cells. *ACS Med. Chem. Lett.* **2012,** *3*, 1008-1012.

43. Jorgensen, T. J. D.; Gaardsvoll, H.; Dano, K.; Roepstorff, P.; Ploug, M., Dynamics of Urokinase Receptor Interaction with Peptide Antagonists Studied by Amide Hydrogen Exchange and Mass Spectrometry. *Biochemistry* **2004,** *43* (47), 15044-15057.

44. Mani, T.; Liu, D.; Zhou, D.; Li, L.; Knabe, W. E.*, et al.*, Probing Binding and Cellular Activity of Pyrrolidinone and Piperidinone Small Molecules Targeting the Urokinase Receptor. *ChemMedChem* **2013,** *8* (12), 1963-1977.

45. Liu, D.; Zhou, D.; Wang, B.; Knabe, W. E.; Meroueh, S. O., A New Class of Orthosteric uPAR•uPA Small-Molecule Antagonists Are Allosteric Inhibitors of the uPAR•Vitronectin Interaction. *ACS Chem. Biol.* **2015,** *10* (6), 1521-1534.

46. Peng, L.; Liu, R.; Marik, J.; Wang, X.; Takada, Y.; Lam, K. S., Combinatorial chemistry identifies high-affinity peptidomimetics against α4β1 integrin for in vivo tumor imaging. *Nat. Chem. Biol.* **2006,** *2* (7), 381-389.

47. Udugamasooriya, D. G.; Dineen, S. P.; Brekken, R. A.; Kodadek, T., A Peptoid "Antibody Surrogate" That Antagonizes VEGF Receptor 2 Activity. *J. Am. Chem. Soc.* **2008,** *130* (17), 5744-5752.

48. Xin, D.; Ko, E.; Perez, L. M.; Ioerger, T. R.; Burgess, K., Evaluating Minimalist Mimics by Exploring Key Orientations on Secondary Structures (EKOS). *Org. Biomol. Chem.* **2013,** *11*, 7789-7801.

49. Friesner, R. A.; Banks, J. L.; Murphy, R. B.; Halgren, T. A.; Klicic, J. J.*, et al.*, Glide: A new approach for rapid, accurate docking and scoring. 1. method and assessment of docking accuracy. *J. Med. Chem.* **2004,** *47* (7), 1739-1749.

50. Friesner, R. A.; Murphy, R. B.; Repasky, M. P.; Frye, L. L.; Greenwood, J. R.*, et al.*, Extra Precision Glide: Docking and Scoring Incorporating a Model of Hydrophobic Enclosure for Protein-Ligand Complexes. *J. Med. Chem.* **2006,** *49* (21), 6177-6196.

51. Halgren, T. A.; Murphy, R. B.; Friesner, R. A.; Beard, H. S.; Frye, L. L.; Pollard, W. T.; Banks, J. L., Glide: A new approach for rapid, accurate docking and scoring. 2. Enrichment factors in database screening. *J. Med. Chem.* **2004,** *47* (7), 1750-1759.

52. Kaminski, G. A.; Friesner, R. A.; Tirado-Rives, J.; Jorgensen, W. L., Evaluation and Reparametrization of the OPLS-AA Force Field for Proteins via Comparison with Accurate Quantum Chemical Calculations on Peptides. *J. Phys. Chem. B* **2001,** *105* (28), 6474-6487.

53. van 't Veer, L. J.; Bernards, R., Enabling personalized cancer medicine through analysis of gene-expression patterns. *Nature* **2008,** *452*, 564-570.

54. Reis-Filho, J. S.; Tutt, A. N. J., Triple negative tumours: a critical review. *Histopathology* **2008,** *52*, 108-118.

55. Vici, P.; Pizzuti, L.; Natoli, C.; Gamucci, T.; Di Lauro, L.*, et al.*, Triple positive breast cancer: A distinct subtype? *Cancer Treat. Rev.* **2015,** *41*, 69-76.

56. Goldenberg, M. M., Trastuzumab, a recombinant DNA-derived humanized monoclonal antibody, a novel agent for the treatment of metastatic breast cancer. *Clin. Ther.* **1999,** *21*, 309-318.

57. Hudis, C. A., Trastuzumab - mechanism of action and use in clinical practice. *N. Engl. J. Med.* **2007,** *357*, 39-51.

58. Chari Ravi, V. J.; Miller Michael, L.; Widdison Wayne, C., Antibody-drug conjugates: an emerging concept in cancer therapy. *Angew. Chem. Int. Ed. Engl.* **2014,** *53*, 3796-3827.

59. Kupchan, S. M.; Komoda, Y.; Court, W. A.; Thomas, G. J.; Smith, R. M.*, et al.*, Tumor inhibitors. LXXIII. Maytansine, a novel antileukemic ansa macrolide from Maytenus ovatus. *J. Amer. Chem. Soc.* **1972,** *94*, 1354-1356.

60. Widdison, W. C.; Wilhelm, S. D.; Cavanagh, E. E.; Whiteman, K. R.; Leece, B. A.*, et al.*, Semisynthetic Maytansine Analogs for the Targeted Treatment of Cancer. *J. Med. Chem.* **2006,** *49*, 4392-4408.

61. Lewis Phillips, G. D.; Li, G.; Dugger, D. L.; Crocker, L. M.; Parsons, K. L.*, et al.*, Targeting HER2-Positive Breast Cancer with Trastuzumab-DM1, an Antibody-Cytotoxic Drug Conjugate. *Cancer Res.* **2008,** *68* (22), 9280-9290.

62. Li, J.; Chen, F.; Cona Marlein, M.; Feng, Y.; Himmelreich, U.*, et al.*, A review on various targeted anticancer therapies. *Target Oncol.* **2012,** *7* (1), 69-85.

63. Fellous, A.; Luduena, R. F.; Prasad, V.; Jordan, M. A.; Anderson, W.; Ohayon, R.; Smith, P. T., Effects of Tau and MAP2 on the interaction of maytansine with tubulin: inhibitory effect of maytansine on vinblastine-induced aggregation of tubulin. *Cancer Res.* **1985,** *45*, 5004-5010.

64. Srinivasarao, M.; Galliford, C. V.; Low, P. S., Principles in the design of ligand-targeted cancer therapeutics and imaging agents. *Nat. Rev. Drug Discovery* **2015,** *14* (3), 203-219.

65. Srinivasarao, M.; Low, P. S., Ligand-Targeted Drug Delivery. *Chem. Rev.* **2017,** *117*, 12133-12164.

66. Kue, C. S.; Kamkaew, A.; Burgess, K.; Kiew, L. V.; Chung, L. Y.; Lee, H. B., Small Molecules for Active Targeting in Cancer. *Med. Res. Rev.* **2016,** *36*, 494-575.

67. Firer, M. A.; Gellerman, G., Targeted drug delivery for cancer therapy: the other side of antibodies. *J. Hematol. Oncol.* **2012,** *5*, 70.

68. Reddy, J. A.; Westrick, E.; Santhapuram, H. K. R.; Howard, S. J.; Miller, M. L.*, et al.*, Folate Receptor-Specific Antitumor Activity of EC131, a Folate-Maytansinoid Conjugate. *Cancer Res.* **2007,** *67* (13), 6376-6382.

69. Krall, N.; Pretto, F.; Decurtins, W.; Bernardes, G. J. L.; Supuran, C. T.; Neri, D., A small-molecule drug conjugate for the treatment of carbonic anhydrase IX expressing tumors. *Angew. Chem., Int. Ed.* **2014,** *53* (16), 4231-4235.

70. Kumar, A.; Mastren, T.; Wang, B.; Hsieh, J.-T.; Hao, G.; Sun, X., Design of a Small-Molecule Drug Conjugate for Prostate Cancer Targeted Theranostics. *Bioconjugate Chem.* **2016,** *27* (7), 1681-1689.

71. Necela, B. M.; Crozier, J. A.; Andorfer, C. A.; Lewis-Tuffin, L.; Kachergus, J. M.*, et al.*, Folate receptor-α (FOLR1) expression and function in triple negative tumors [Erratum to document cited in CA163:716888]. *PLoS One* **2015,** *10*, e0127133/1.

72. Kamkaew, A.; Li, F.; Li, Z.; Burgess, K., An agent for optical imaging of TrkC-expressing, breast cancer. *MedChemComm* **2017,** *8*, 1946-1952.

73. Kamkaew, A.; Fu, N.; Cai, W.; Burgess, K., Novel Small Molecule Probes for Metastic Melanoma. *ACS Med. Chem. Lett.* **2017,** *8* (2), 179-184.

74. Kamkaew, A.; Burgess, K., Double-targeting Using a TrkC-Ligand Conjugated to Dipyrrometheneboron Difluoride (BODIPY) Based Photodynamic Therapy (PDT) Agent. *J. Med. Chem.* **2013,** *56*, 7608-7614.

75. Jin, W.; Kim, G.-M.; Kim, M.-S.; Lim, M.-H.; Yun, C.-H.*, et al.*, TrkC plays an essential role in breast tumor growth and metastasis. *Carcinogenesis* **2010,** *31* (11), 1939-1947.

76. Jin, W.; Yun, C.; Jeong, J.; Park, Y.; Lee, H.-D.; Kim, S.-J., c-Src Is Required for Tropomyosin Receptor Kinase C (TrkC)-induced Activation of the Phosphatidylinositol 3-Kinase (PI3K)-AKT Pathway. *J. Biol. Chem.* **2008,** *283*, 1391-1400.

77. Jin, W.; Yun, C.; Kwak, M. K.; Kim, T. A.; Kim, S. J., TrkC binds to the type II TGF-β receptor to suppress TGF-β signaling. *Oncogene* **2007,** *26* (55), 7684-7691.

78. Blasco-Gutierrez, M. J.; San Jose-Crespo, I. J.; Zozaya-Alvarez, E.; Ramos-Sanchez, R.; Garcia-Atares, N., TrkC: a new predictive marker in breast cancer? *Cancer Invest.* **2007,** *25* (6), 405-410.

79. Louie, E.; Chen, X. F.; Coomes, A.; Ji, K.; Tsirka, S.; Chen, E. I., Neurotrophin-3 modulates breast cancer cells and the microenvironment to promote the growth of breast cancer brain metastasis. *Oncogene* **2012,** *32* (35), 4064-4077.

80. Kim, M. S.; Jeong, J.; Seo, J.; Kim, H.-S.; Kim, S.-J.; Jin, W., Dysregulated JAK2 expression by TrkC promotes metastasis potential, and EMT program of metastatic breast cancer. *Sci. Rep.* **2016,** *6*, 33899.

81. Angell, Y.; Chen, D.; Brahimi, F.; Saragovi, H. U.; Burgess, K., A Combinatorial Method for Solution-Phase Synthesis of Labeled Bivalent β-Turn Mimics. *J. Am. Chem. Soc.* **2008,** *130* (2), 556-565.

82. van Straten, D.; Mashayekhi, V.; Oliveira, S.; de Bruijn Henriette, S.; Robinson Dominic, J.; Oliveira, S., Oncologic Photodynamic Therapy: Basic Principles, Current Clinical Status and Future Directions. *Cancers* **2017,** *9*, 19-63.

83. Fan, W.; Huang, P.; Chen, X., Overcoming the Achilles' heel of photodynamic therapy. *Chem. Soc. Rev.* **2016,** *45* (23), 6488-6519.

84. Erickson, H. K.; Park, P. U.; Widdison, W. C.; Kovtun, Y. V.; Garrett, L. M.*, et al.*, Antibody-Maytansinoid Conjugates Are Activated in Targeted Cancer Cells by Lysosomal Degradation and Linker-Dependent Intracellular Processing. *Cancer Res.* **2006,** *66*, 4426-4433.

85. Wayua, C.; Low, P. S., Evaluation of a Cholecystokinin 2 Receptor-Targeted Near-Infrared Dye for Fluorescence-Guided Surgery of Cancer. *Mol. Pharmaceutics* **2014,** *11*, 468-476.

86. Johnson, R. J.; Chenoweth, D. E., Labeling the granulocyte C5a receptor with a unique photoreactive probe. *J. Biol. Chem.* **1985,** *260*, 7161-7164

87. Kalepu, S.; Nekkanti, V., Insoluble drug delivery strategies: review of recent advances and business prospects. *Acta. Pharm. Sin. B* **2015,** *5*, 442-453.

88. Bharate, S. S.; Vishwakarma, R. A., Thermodynamic equilibrium solubility measurements in simulated fluids by 96-well plate method in early drug discovery. *Bioorg. Med. Chem. Lett.* **2015,** *25* (7), 1561-1567.

89. Blanc, V.; Bousseau, A.; Caron, A.; Carrez, C.; Lutz, R. J.; Lambert, J. M., SAR3419: An Anti-CD19-Maytansinoid Immunoconjugate for the Treatment of B-Cell Malignancies. *Clin. Cancer Res.* **2011,** *17*, 6448-6458.

90. Zhu, P.; Du Xianglin, L.; Zhu, P.; Lu, G.; Zhu, J.-J., Survival benefit of glioblastoma patients after FDA approval of temozolomide concomitant with

radiation and bevacizumab: A population-based study. *Oncotarget* **2017,** *8*, 44015-44031.

91. Cohen, M. H.; Johnson, J. R.; Pazdur, R., Food and Drug Administration Drug Approval Summary: Temozolomide Plus Radiation Therapy for the Treatment of Newly Diagnosed Glioblastoma Multiforme. *Clin. Cancer Res.* **2005,** *11*, 6767-6771.

92. Davis Mary, E., Glioblastoma: Overview of Disease and Treatment. *Clin. J. Oncol. Nurs.* **2016,** *20*, S2-S8.

93. Bastiancich, C.; Bastiat, G.; Lagarce, F., Gemcitabine and glioblastoma: challenges and current perspectives. *Drug Discovery Today* **2018,** *23*, 416-423.

94. Stupp, R.; Hegi, M. E.; Mason, W. P.; van den Bent, M. J.; Taphoorn, M. J. B.*, et al.*, Effects of radiotherapy with concomitant and adjuvant temozolomide versus radiotherapy alone on survival in glioblastoma in a randomised phase III study: 5-year analysis of the EORTC-NCIC trial. *Lancet Oncol.* **2009,** *10*, 459-466.

95. Moysan, E.; Bastiat, G.; Benoit, J.-P., Gemcitabine versus Modified Gemcitabine: A Review of Several Promising Chemical Modifications. *Mol. Pharmaceutics* **2013,** *10*, 430-444.

96. Plunkett, W.; Huang, P.; Xu, Y.-Z.; Heinemann, V.; Grunewald, R.; Gandhi, V., Gemcitabine: metabolism, mechanisms of action, and self-potentiation. *Semin. Oncol.* **1995,** *22*, 3-10.

97. Pulido, J.; Sobczak, A. J.; Balzarini, J.; Wnuk, S. F., Synthesis and Cytostatic Evaluation of 4-N-Alkanoyl and 4-N-Alkyl Gemcitabine Analogs. *J. Med. Chem.* **2014,** *57*, 191-203.

98. Rieger, J.; Durka, S.; Streffer, J.; Dichgans, J.; Weller, M., Gemcitabine cytotoxicity of human malignant glioma cells: modulation by antioxidants, BCL-2 and dexamethasone. *Eur. J. Pharmacol.* **1999,** *365*, 301-308.

99. Kerr, J. Z.; Berg, S. L.; Dauser, R.; Nuchtern, J.; Egorin, M. J.*, et al.*, Plasma and cerebrospinal fluid pharmacokinetics of gemcitabine after intravenous administration in nonhuman primates. *Cancer Chemother. Pharmacol.* **2001,** *47*, 411-414.

100. Apparaju, S. K.; Gudelsky, G. A.; Desai, P. B., Pharmacokinetics of gemcitabine in tumor and non-tumor extracellular fluid of brain: an in vivo assessment in rats employing intracerebral microdialysis. *Cancer Chemother. Pharmacol.* **2008,** *61*, 223-229.

101. Peer, D.; Karp, J. M.; Hong, S.; Farokhzad, O. C.; Margalit, R.; Langer, R., Nanocarriers as an emerging platform for cancer therapy. *Nat. Nanotechnol.* **2007,** *2* (12), 751-760.

102. Yang, X.; Shi, C.; Tong, R.; Qian, W.; Zhau, H. E.*, et al.*, Near IR Heptamethine Cyanine Dye-Mediated Cancer Imaging. *Clin. Cancer Res.* **2010,** *16*, 2833-2844.

103. Zhang, C.; Liu, T.; Su, Y.; Luo, S.; Zhu, Y.*, et al.*, A near-infrared fluorescent heptamethine indocyanine dye with preferential tumor accumulation for in vivo imaging. *Biomaterials* **2010,** *31*, 6612-6617.

104. Wu, J. B.; Shi, C.; Chu, G. C.-Y.; Xu, Q.; Zhang, Y.*, et al.*, Near-Infrared Fluorescence Heptamethine Carbocyanine Dyes Mediate Imaging and Targeted Drug Delivery for Human Brain Tumor. *Biomaterials* **2015,** *67*, 1-10.

105. Shi, C.; Wu Jason, B.; Pan, D., Review on near-infrared heptamethine cyanine dyes as theranostic agents for tumor imaging, targeting, and photodynamic therapy. *J. Biomed. Opt.* **2016,** *21*, 50901:1 - 50901:11.

106. Zhang, E.; Luo, S.; Tan, X.; Shi, C., Mechanistic study of IR-780 dye as a potential tumor targeting and drug delivery agent. *Biomaterials* **2014,** *35*, 771-778.

107. Kushal, S.; Wang, W.; Vaikari, V. P.; Kota, R.; Chen, K.*, et al.*, Monoamine oxidase A (MAO A) inhibitors decrease glioma progression. *Oncotarget* **2016,** *7*, 13842-13853.

108. Dasari, M.; Acharya, A. P.; Kim, D.; Lee, S.; Lee, S.*, et al.*, H-Gemcitabine: A New Gemcitabine Prodrug for Treating Cancer. *Bioconjugate Chem.* **2013,** *24* (1), 4-8.

109. Yang, Z.; Lee Jae, H.; Jeon Hyun, M.; Han Ji, H.; Park, N.*, et al.*, Folate-based Near-infrared Fluorescent Theranostic Gemcitabine Delivery. *J. Am. Chem. Soc.* **2013,** *135*, 11657-11662.

110. Quinn, B. A.; Wang, S.; Barile, E.; Das, S. K.; Emdad, L.*, et al.*, Therapy of pancreatic cancer via an EphA2 receptor-targeted delivery of gemcitabine. *Oncotarget* **2016,** *7*, 17103-17110.

111. Lin, C.-M.; Usama, S. M.; Burgess, K., Site-Specific Labeling of Proteins With Near-IR Dyes. *Molecules* **2018,** *23*, 2900.

112. Usama, S. M.; Lin, C.-M.; Burgess, K., On the Mechanisms of Update of Tumor-Seeking Cyanine Dyes. *Bioconjugate Chem.* **2018,** *29*, 3886-3895.

113. Levitt, D. G.; Levitt, M. D., Human serum albumin homeostasis: a new look at the roles of synthesis, catabolism, renal and gastrointestinal excretion, and the clinical value of serum albumin measurements. *Int. J. Gen. Med.* **2016,** *9*, 229-255.

114. Liu, Z.; Chen, X., Simple bioconjugate chemistry serves great clinical advances: albumin as a versatile platform for diagnosis and precision therapy. *Chem. Soc. Rev.* **2016,** *45*, 1432-1456.

115. Frei, E., Albumin binding ligands and albumin conjugate uptake by cancer cells. *Diabetol. Metab. Syndr.* **2011,** *3*, 11.

116. Stehle, G.; Sinn, H.; Wunder, A.; Schrenk, H. H.; Schutt, S.; Maier-Borst, W.; Heene, D. L., The loading rate determines tumor targeting properties of methotrexate-albumin conjugates in rats. *Anti-Cancer Drugs* **1997,** *8*, 677-685.

117. Canovas, C.; Bellaye, P.-S.; Moreau, M.; Romieu, A.; Denat, F.; Goncalves, V., Site-specific near-infrared fluorescent labelling of proteins on cysteine residues with meso-chloro-substituted heptamethine cyanine dyes. *Org. Biomol. Chem.* **2018,** *16*, 8831-8836.

118. Koolen, S. L. W.; Witteveen, P. O.; Jansen, R. S.; Langenberg, M. H. G.; Kronemeijer, R. H.*, et al.*, Phase I Study of Oral Gemcitabine Prodrug (LY2334737) Alone and in Combination with Erlotinib in Patients with Advanced Solid Tumors. *Clin. Cancer Res.* **2011,** (18), 6071-6082.

119. Shin, D. H.; Xuan, S.; Kim, W.-Y.; Bae, G.-U.; Kim, J.-S., CD133 antibody-conjugated immunoliposomes encapsulating gemcitabine for targeting glioblastoma stem cells. *J. Mater. Chem. B* **2014,** *2*, 3771-3781.

120. Luo, S.; Tan, X.; Fang, S.; Wang, Y.; Liu, T.*, et al.*, Mitochondria-Targeted Small-Molecule Fluorophores for Dual Modal Cancer Phototherapy. *Adv. Funct. Mater.* **2016,** *26*, 2826-2835.

121. Lv, Q.; Wang, D.; Yang, Z.; Yang, J.; Zhang, R.*, et al.*, Repurposing antitubercular agent isoniazid for treatment of prostate cancer. *Biomater. Sci.* **2019,** *7*, 296-306.

122. Zhang, X.; Zhao, N.; Wang, B.; Tian, Z.; Dai, Y.; Ning, P.; Chen, D., Structure-inherent near-infrared fluorescent probe mediates apoptosis imaging and targeted drug delivery in vivo. *Dyes Pigm.* **2017,** *138*, 204-212.

123. Lam, K. S.; Salmon, S. E.; Hersh, E. M.; Hruby, V. J.; Kazmierski, W. M.; Knapp, R. J., A new type of synthetic peptide library for identifying ligand-binding activity. *Nature* **1991,** *354*, 82-84.

124. Lam, K. S.; Lebl, M.; Krchnak, V., The "One-Bead-One-Compound" Combinatorial Library Method. *Chem. Rev.* **1997,** *97*, 411-448.

125. Townsend, J. B.; Shaheen, F.; Liu, R.; Lam, K. S., Jeffamine Derivatized TentaGel Beads and Poly(dimethylsiloxane) Microbead Cassettes for Ultrahigh-Throughput in Situ Releasable Solution-Phase Cell-Based Screening of One-Bead-One-Compound Combinatorial Small Molecule Libraries. *J. Comb. Chem.* **2010,** *12* (5), 700-712.

126. Komnatnyy, V. V.; Nielsen, T. E.; Qvortrup, K., Bead-based screening in chemical biology and drug discovery. *Chem. Commun.* **2018,** *54*, 6759-6771.

127. Sun, Y.-S.; Fei, Y.; Luo, J.; Dixon, S.; Landry, J. P.; Lam, K. S.; Zhu, X., Generating Encoded Compound Libraries for Fabricating Microarrays as a High-Throughput Protein Ligand Discovery Platform. *Synth. Commun.* **2014,** *44*, 987-1001.

128. Matharage Jaya, M.; Minna John, D.; Brekken Rolf, A.; Udugamasooriya, D. G., Unbiased Selection of Peptide-Peptoid Hybrids Specific for Lung Cancer Compared to Normal Lung Epithelial Cells. *ACS Chem. Biol.* **2015,** *10* (12), 2891-2899.

129. Aina, O. H.; Sroka, T. C.; Chen, M.-L.; Lam, K. S., Therapeutic cancer targeting peptides. *Biopolymers* **2002,** *66* (3), 184-199.

130. Lam, K. S.; Liu, R.; Miyamoto, S.; Lehman, A. L.; Tuscano, J. M., Applications of one-bead one-compound combinatorial libraries and chemical microarrays in signal transduction research. *Acc. Chem. Res.* **2003,** *36*, 370-377.

131. Park, S.-H.; Wang, X.; Liu, R.; Lam, K. S.; Weiss, R. H., High throughput screening of a small molecule one-bead-one-compound combinatorial library to identify attenuators of p21 as chemotherapy sensitizers. *Cancer Biol. Ther.* **2008,** *7*, 2015-2022.

132. Miyamoto, S.; Liu, R.; Hung, S.; Wang, X.; Lam, K. S., Screening of a one bead-one compound combinatorial library for β-actin identifies molecules active toward Ramos B-lymphoma cells. *Anal. Biochem.* **2008,** *374*, 112-120.

133. Pennington, M. E.; Lam, K. S.; Cress, A. E., The use of a combinatorial library method to isolate human tumor cell adhesion peptides. *Mol. Diversity* **1996,** *2* (1/2), 19-28.

134. Chen, L.; Long, C.; Youn, J.; Lee, J., A Phenotypic Cell-Binding Screen Identifies a Novel Compound Targeting Triple-Negative Breast Cancer. *ACS Comb. Sci.* **2018,** *20*, 330-334.

135. Wang, X.; Zhang, J.; Song, A.; Lebrilla, C. B.; Lam, K. S., Encoding method for OBOC small molecule libraries using a biphasic approach for ladder-synthesis of coding tags. *J. Am. Chem. Soc.* **2004,** *126*, 5740-5749.

136. Hwang, S. H.; Lehman, A.; Cong, X.; Olmstead, M. M.; Lam, K. S.; Lebrilla, C. B.; Kurth, M. J., OBOC Small-Molecule Combinatorial Library Encoded by Halogenated Mass-Tags. *Org. Lett.* **2004,** *6*, 3829-3832.

137. Wu, C.-Y.; Wang, D.-H.; Wang, X.; Dixon, S. M.; Meng, L.*, et al.*, Rapid Discovery of Functional Small Molecule Ligands against Proteomic Targets through Library-Against-Library Screening. *ACS Comb. Sci.* **2016,** *18*, 320-329.

138. Aina, O. H.; Marik, J.; Liu, R.; Lau, D. H.; Lam, K. S., Identification of novel targeting peptides for human ovarian cancer cells using "one-bead one-compound" combinatorial libraries. *Mol. Cancer Ther.* **2005,** *4* (5), 806-813.

139. Guillier, F.; Orain, D.; Bradley, M., Linkers and Cleavage Strategies in Solid-Phase Organic Synthesis and Combinatorial Chemistry. *Chem. Rev.* **2000,** *100*, 2091-2157.

140. Paulick, M. G.; Hart, K. M.; Brinner, K. M.; Tjandra, M.; Charych, D. H.; Zuckermann, R. N., Cleavable Hydrophilic Linker for One-Bead-One-Compound Sequencing of Oligomer Libraries by Tandem Mass Spectrometry. *J. Comb. Chem.* **2006,** *8*, 417-426.

141. Patek, M.; Lebl, M., Safety-catch and multiply cleavable linkers in solid-phase synthesis. *Biopolymers* **1999,** *47*, 353-363.

142. Mikkelsen, R. J. T.; Grier, K. E.; Mortensen, K. T.; Nielsen, T. E.; Qvortrup, K., Photolabile Linkers for Solid-Phase Synthesis. *ACS Comb. Sci.* **2018,** *20*, 377-399.

143. Millington, C. R.; Quarrell, R.; Lowe, G., Aryl hydrazides as linkers for solid phase synthesis which are cleavable under mild oxidative conditions. *Tetrahedron Lett.* **1998,** *39*, 7201-7204.

144. Woo, Y.-H.; Mitchell, A. R.; Camarero, J. A., The use of aryl hydrazide linkers for the solid phase synthesis of chemically modified peptides. *Int. J. Pept. Res. Ther.* **2007,** *13*, 181-190.

145. Yao, N.; Xiao, W.; Wang, X.; Marik, J.; Park, S. H.; Takada, Y.; Lam, K. S., Discovery of Targeting Ligands for Breast Cancer Cells Using the One-Bead One-Compound Combinatorial Method. *J. Med. Chem.* **2009,** *52* (1), 126-133.

146. Baek, H. G.; Liu, R.; Lam, K. S., Development of Hydrogel TentaGel Shell-Core Beads for Ultrahigh Throughput Solution-Phase Screening of Encoded OBOC Combinatorial Small Molecule Libraries. *J. Comb. Chem.* **2009,** *11*, 91-102.

147. Meldal, M., The one-bead two-compound assay for solid phase screening of combinatorial libraries. *Biopolymers* **2002,** *66*, 93-100.

148. Meldal, M., One bead two compound libraries' for detecting chemical and biochemical conversions. *Curr. Opin. Chem. Biol.* **2004,** *8*, 238-244.

149. Wang, X.; Peng, L.; Liu, R.; Gill, S. S.; Lam, K. S., Partial Alloc-Deprotection Approach for Ladder Synthesis of "One-Bead One-Compound" Combinatorial Libraries. *J. Comb. Chem.* **2005,** *7*, 197-209.

150. Liu, R.; Marik, J.; Lam, K. S., A Novel Peptide-Based Encoding System for "One-Bead One-Compound" Peptidomimetic and Small Molecule Combinatorial Libraries. *J. Am. Chem. Soc.* **2002,** *124*, 7678-7680.

151. Vagner, J.; Barany, G.; Lam, K. S.; Krchnak, V.; Sepetov, N. F.*, et al.*, Enzyme-mediated spatial segregation on individual polymeric support beads: application to generation and screening of encoded combinatorial libraries. *Proc. Natl. Acad. Sci. U. S. A.* **1996,** *93*, 8194-8199.

152. Luo, J.; Zhang, H.; Xiao, W.; Kumaresan, P. R.; Shi, C.*, et al.*, Rainbow Beads: A Color Coding Method to Facilitate High-Throughput Screening and Optimization of One-Bead One-Compound Combinatorial Libraries. *J. Comb. Chem.* **2008,** *10* (4), 599-604.

153. Liu, T.; Qian, Z.; Xiao, Q.; Pei, D., High-Throughput Screening of One-Bead-One-Compound Libraries: Identification of Cyclic Peptidyl Inhibitors against Calcineurin/NFAT Interaction. *ACS Comb. Sci.* **2011,** *13*, 537-546.

154. Helmer, D.; Brahm, K.; Helmer, C.; Wack, J. S.; Brenner-Weiss, G.; Schmitz, K., Two-channel image analysis method for the screening of OBOC libraries. *Anal. Methods* **2016,** *8*, 4142-4152.

155. Ding, H.; Prodinger, W. M.; Kopecek, J., Two-Step Fluorescence Screening of CD21-Binding Peptides with One-Bead One-Compound Library and Investigation of Binding Properties of N-(2-Hydroxypropyl)methacrylamide Copolymer-Peptide Conjugates. *Biomacromolecules* **2006,** *7*, 3037-3046.

156. Townsend, J.; Do, A.; Lehman, A.; Dixon, S.; Sanii, B.; Lam, K. S., 3-nitro-tyrosine as an internal quencher of autofluorescence enhances the

compatibility of fluorescence based screening of OBOC combinatorial libraries. *Comb. Chem. High Throughput Screening* **2010,** *13*, 422-429.

157. Heusermann, W.; Ludin, B.; Pham, N. T.; Auer, M.; Weidemann, T.; Hintersteiner, M., A Wide-Field Fluorescence Microscope Extension for Ultrafast Screening of One-Bead One-Compound Libraries Using a Spectral Image Subtraction Approach. *ACS Comb. Sci.* **2016,** *18*, 209-219.

158. Kelf, T. A.; Sreenivasan, V. K. A.; Sun, J.; Kim, E. J.; Goldys, E. M.; Zvyagin, A. V., Non-specific cellular uptake of surface-functionalized quantum dots. *Nanotechnology* **2010,** *21*, 285105/1-285105/8.

159. Olivos, H. J.; Bachhawat-sikder, K.; Kodadek, T., Quantum dots as a visual aid for screening bead-bound combinatorial libraries. *ChemBioChem* **2003,** *4*, 1242-1245.

160. Resch-Genger, U.; Grabolle, M.; Cavaliere-Jaricot, S.; Nitschke, R.; Nann, T., Quantum dots versus organic dyes as fluorescent labels. *Nat. Methods* **2008,** *5*, 763-775.

161. Jaiswall, J. K.; Goldman, E. R.; Mattoussi, H.; Simon, S. M., Use of quantum dots for live cell imaging. *Nat. Methods* **2004,** *1*, 73-78.

162. Chen, X.; Tan, P. H.; Zhang, Y.; Pei, D., On-Bead Screening of Combinatorial Libraries: Reduction of Nonspecific Binding by Decreasing Surface Ligand Density. *J. Comb. Chem.* **2009,** *11* (4), 604-611.

163. Doran, T. M.; Gao, Y.; Mendes, K.; Dean, S.; Simanski, S.; Kodadek, T., Utility of Redundant Combinatorial Libraries in Distinguishing High and Low Quality Screening Hits. *ACS Comb. Sci.* **2014,** *16* (6), 259-270.

164. Cho, C.-F.; Behnam Azad, B.; Luyt, L. G.; Lewis, J. D., High-Throughput Screening of One-Bead-One-Compound Peptide Libraries Using Intact Cells. *ACS Comb. Sci.* **2013,** *15* (8), 393-400.

165. Hintersteiner, M.; Auer, M., A two-channel detection method for autofluorescence correction and efficient on-bead screening of one-bead one-compound combinatorial libraries using the COPAS fluorescence activated bead sorting system. *Methods Appl. Fluoresc.* **2013,** *1*, 017001.

166. Hintersteiner, M.; Buehler, C.; Uhl, V.; Schmied, M.; Muller, J.; Kottig, K.; Auer, M., Confocal Nanoscanning, Bead Picking (CONA): PickoScreen Microscopes for Automated and Quantitative Screening of One-Bead One-Compound Libraries. *J. Comb. Chem.* **2009,** *11* (5), 886-894.

167. Franz, A. H.; Liu, R.; Song, A.; Lam, K. S.; Lebrilla, C. B., High-Throughput One-Bead-One-Compound Approach to Peptide-Encoded Combinatorial Libraries: MALDI-MS Analysis of Single TentaGel Beads. *J. Comb. Chem.* **2003,** *5*, 125-137.

168. Song, A.; Zhang, J.; Lebrilla, C. B.; Lam, K. S., A Novel and Rapid Encoding Method Based on Mass Spectrometry for "One-Bead-One-Compound" Small Molecule Combinatorial Libraries. *J. Am. Chem. Soc.* **2003,** *125*, 6180-6188.

169. Steen, H.; Mann, M., The abc's (and xyz's) of peptide sequencing. *Nat. Rev. Mol. Cell Biol.* **2004,** *5*, 699-711.

170. Sarkar, M.; Pascal, B. D.; Steckler, C.; Aquino, C.; Micalizio, G. C.; Kodadek, T.; Chalmers, M. J., Decoding Split and Pool Combinatorial Libraries with Electron-Transfer Dissociation Tandem Mass Spectrometry. *J. Am. Soc. Mass Spectrom.* **2013,** *24*, 1026-1036.

171. Lee, S. S.; Lim, J.; Tan, S.; Cha, J.; Yeo, S. Y.; Agnew, H. D.; Heath, J. R., Accurate MALDI-TOF/TOF Sequencing of One-Bead-One-Compound Peptide Libraries with Application to the Identification of Multiligand Protein Affinity Agents Using in Situ Click Chemistry Screening. *Anal. Chem.* **2010,** *82*, 672-679.

172. Taechalertpaisarn, J.; Lyu, R.-L.; Arancillo, M.; Lin, C.-M.; Jiang, Z.*, et al.*, Design Criteria for Minimalist Mimics of Protein-protein Interface Segments. *Org. Biomol. Chem.* **2019,** *17*, 908-915.

173. Macmillan, D.; Arham, L., Cyanogen Bromide Cleavage Generates Fragments Suitable for Expressed Protein and Glycoprotein Ligation. *J. Am. Chem. Soc.* **2004,** *126*, 9530-9531.

174. Lau, D. H.; Guo, L.; Liu, R.; Song, A.; Shao, C.; Lam, K. S., Identifying peptide ligands for cell surface receptors using cell-growth-on-bead assay and one-bead one-compound combinatorial library. *Biotechnol. Lett.* **2002,** *24* (6), 497-500.

175. Xin, D.; Jeffries, A.; Burgess, K., Interplay of Stereochemisty, Conformational Rigidity, and East of Synthesis for 13-Membered Cyclic Peptidomimetics Containing APC Residues. *ACS Combi. Chem.* **2017**, 414-421.

176. Butte, M. J.; Hwang, P. K.; Mobley, W. C.; Fletterick, R. J., Crystal Structure of Neurotrophin-3 Homodimer Shows Distinct Regions Are Used To Bind Its Receptors. *Biochem.* **1998,** *37*, 16846-16852.

177. Udugamasooriya, D. G.; Kodadek, T., On-Bead Two-Color (OBTC) Cell Screen for Direct Identification of Highly Selective Cell Surface Receptor Ligands. *Curr. Protoc. Chem. Biol.* **2012,** *4*, 35-48.

178. Kumaresan, P. R.; Wang, Y.; Saunders, M.; Maeda, Y.; Liu, R.; Wang, X.; Lam, K. S., Rapid Discovery of Death Ligands with One-Bead-Two-Compound Combinatorial Library Methods. *ACS Comb. Sci.* **2011,** *13*, 259-264.

179. Garrido-Laguna, I.; Hidalgo, M., Pancreatic cancer: from state-of-the-art treatments to promising novel therapies. *Nat. Rev. Clin. Oncol.* **2015,** *12*, 319-334.

180. Kamisawa, T.; Wood, L. D.; Itoi, T.; Takaori, K., Pancreatic cancer. *Lancet* **2016,** *388*, 73-85.

181. Yabar, C. S.; Winter, J. M., Pancreatic Cancer: A Review. *Gastroenterol Clin North Am* **2016,** *45*, 429-445.

182. Siegel, R. L.; Miller, K. D.; Jemal, A., Cancer statistics, 2018. *CA Cancer J Clin* **2018,** *68*, 7-30.

183. Ying, H.; Dey, P.; Yao, W.; Kimmelman, A. C.; Draetta, G. F.; Maitra, A.; DePinho, R. A., Genetics and biology of pancreatic ductal adenocarcinoma. *Genes Dev.* **2016,** *30*, 355-385.

184. Rahib, L.; Smith, B. D.; Aizenberg, R.; Rosenzweig, A. B.; Fleshman, J. M.; Matrisian, L. M., Projecting Cancer Incidence and Deaths to 2030: The Unexpected Burden of Thyroid, Liver, and Pancreas Cancers in the United States. *Cancer Res.* **2014,** *74*, 2913-2921.

185. Arlt, A.; Mueerkoester, S. S.; Schaefer, H., Targeting apoptosis pathways in pancreatic cancer. *Cancer Lett.* **2013,** *332*, 346-358.

186. Silvestris, N.; Gnoni, A.; Brunetti, A. E.; Vincenti, L.; Santini, D.*, et al.*, Target Therapies in Pancreatic Carcinoma. *Curr. Med. Chem.* **2014,** *21*, 948-965.

187. Javadinia Seyed, A.; Shahidsales, S.; Fanipakdel, A.; Joudi-Mashhad, M.; Talebian, S.*, et al.*, Therapeutic potential of targeting the Wnt/β-catenin pathway in the treatment of pancreatic cancer. *J. Cell. Biochem.* **2018**, 1-8.

188. Neuzillet, C.; Hammel, P.; Tijeras-Raballand, A.; Couvelard, A.; Raymond, E., Targeting the Ras-ERK pathway in pancreatic adenocarcinoma. *Cancer Metastasis Rev.* **2013,** *32*, 147-162.

189. Feldmann, G.; Fendrich, V.; McGovern, K.; Bedja, D.; Bisht, S.*, et al.*, An orally bioavailable small-molecule inhibitor of Hedgehog signaling inhibits tumor initiation and metastasis in pancreatic cancer. *Mol. Cancer Ther.* **2008,** *7*, 2725-2735.

190. Vogler, M.; Walczak, H.; Stadel, D.; Haas, T. L.; Genze, F.*, et al.*, Small Molecule XIAP Inhibitors Enhance TRAIL-Induced Apoptosis and Antitumor Activity in Preclinical Models of Pancreatic Carcinoma. *Cancer Res.* **2009,** *69*, 2425-2434.

191. Zhang, J.; He, D.-H.; Zajac-Kaye, M.; Hochwald, S. N., A small molecule FAK kinase inhibitor, GSK2256098, inhibits growth and survival of pancreatic ductal adenocarcinoma cells. *Cell Cycle* **2014,** *13*, 3143-3149.

192. Abulwerdi, F.; Liao, C.; Liu, M.; Azmi, A. S.; Aboukameel, A.*, et al.*, A Novel Small-Molecule Inhibitor of Mcl-1 Blocks Pancreatic Cancer Growth In Vitro and In Vivo. *Mol. Cancer Ther.* **2014,** *13*, 565-575.

193. Eck, W.; Craig, G.; Sigdel, A.; Ritter, G.; Old, L. J.*, et al.*, PEGylated Gold Nanoparticles Conjugated to Monoclonal F19 Antibodies as Targeted Labeling Agents for Human Pancreatic Carcinoma Tissue. *ACS Nano* **2008,** *2*, 2263-2272.

194. Yang, F.; Jin, C.; Subedi, S.; Lee, C. L.; Wang, Q.*, et al.*, Emerging inorganic nanomaterials for pancreatic cancer diagnosis and treatment. *Cancer Treat. Rev.* **2012,** *38*, 566-579.

195. Lee, G. Y.; Qian, W. P.; Wang, L.; Wang, Y. A.; Staley, C. A.*, et al.*, Theranostic Nanoparticles with Controlled Release of Gemcitabine for Targeted Therapy and MRI of Pancreatic Cancer. *ACS Nano* **2013,** *7*, 2078-2089.

196. Aghevlian, S.; Lu, Y.; Winnik, M. A.; Hedley, D. W.; Reilly, R. M., Panitumumab Modified with Metal-Chelating Polymers (MCP) Complexed to 111In and 177Lu-An EGFR-Targeted Theranostic for Pancreatic Cancer. *Mol. Pharmaceutics* **2018,** *15*, 1150-1159.

197. Lee, S.; Xie, J.; Chen, X., Peptides and Peptide Hormones for Molecular Imaging and Disease Diagnosis. *Chem. Rev.* **2010,** *110*, 3087-3111.

198. Henne, W. A.; Kularatne, S. A.; Ayala-Lopez, W.; Doorneweerd, D. D.; Stinnette, T. W.; Lu, Y.; Low, P. S., Synthesis and activity of folate conjugated didemnin B for potential treatment of inflammatory diseases. *Bioorg. Med. Chem. Lett.* **2012,** *22* (1), 709-712.

199. Ko, E.; Liu, J.; Burgess, K., Minimalist and Universal Peptidomimetics. *Chem. Soc. Rev.* **2011,** *40*, 4411-4421.

200. Ko, E.; Liu, J.; Perez, L. M.; Lu, G.; Schaefer, A.; Burgess, K., Universal Peptidomimetics. *J. Am. Chem. Soc.* **2011,** *133*, 462-477.

201. Conte, L. L.; Chothia, C.; Janin, J., The Atomic Structure of Protein-Protein Recognition Sites. *J. Mol. Biol.* **1999,** *285*, 2177-2198.

202. Shi, Q.; Nguyen, A. T.; Angell, Y.; Deng, D.; Na, C.-R*., et al.*, A Combinatorial Approach for Targeted Delivery using Small Molecules and Reversible Masking to Bypass Non-Specific Uptake In Vivo. *Gene Ther.* **2010,** *17*, 1085-1097.

203. Yogo, T.; Urano, Y.; Ishitsuka, Y.; Maniwa, F.; Nagano, T., Highly efficient and photostable photosensitizer based on BODIPY chromophore. *J. Am. Chem. Soc.* **2005,** *127*, 12162-12163.

204. Lim, S. H.; Thivierge, C.; Nowak-Sliwinska, P.; Han, J.; Van den Bergh, H*., et al.*, In vitro and in vivo photo-cytotoxicity of boron dipyrromethene derivatives for photodynamic therapy. *J. Med. Chem.* **2010,** *53* (7), 2865-2874.

205. Agostinis, P.; Berg, K.; Cengel Keith, A.; Foster Thomas, H.; Girotti Albert, W*., et al.*, Photodynamic Therapy of Cancer: An Update. *CA Cancer J Clin* **2011,** *61*, 250-281.

206. Dolmans, D. E. J. G. J.; Fukumura, D.; Jain, R. K., TIMELINE: Photodynamic therapy for cancer. *Nat. Rev. Cancer* **2003,** *3* (5), 380-387.

207. Juarranz, A.; Jaen, P.; Sanz-Rodriguez, F.; Cuevas, J.; Gonzalez, S., Photodynamic therapy of cancer. Basic principles and applications. *Clin. Transl. Oncol.* **2008,** *10* (3), 148-154.

208. Kochevar, I. E.; Redmond, R. W., Photosensitized production of singlet oxygen. *Methods Enzymol.* **2000,** *319*, 20-28.

209. Kamkaew, A.; Burgess, K., Aza-BODIPY Dyes with Enhanced Hydrophilicity. *Chem. Comm.* **2015,** *51*, 10664-10667.

210. Crider, A. M.; Tita, T. T.; Wood, J. D.; Hinko, C. N., Esters of nipecotic and isonipecotic acids as potential anticonvulsants. *J. Pharm. Sci.* **1982,** *71*, 1214-1219

211. Mosmann, T., Rapid colorimetric assay for cellular growth and survival: application to proliferation and cytotoxicity assays. *J. Immunol. Meth.* **1983,** *65*, 55-63.

212. Shao, W.; Brown, M., Advances in estrogen receptor biology: prospects for improvements in targeted breast cancer therapy. *Breast Cancer Res.* **2004,** *6* (1), 39-52.

213. Obr, A. E.; Edwards, D. P., The biology of progesterone receptor in the normal mammary gland and in breast cancer. *Mol. Cell. Endocrinol.* **2012,** *357*, 4-17.

214. Chavez Kathryn, J.; Garimella Sireesha, V.; Lipkowitz, S., Triple negative breast cancer cell lines: one tool in the search for better treatment of triple negative breast cancer. *Breast Dis.* **2010,** *32* (1-2), 35-48.

215. Matutino, A.; Amaro, C.; Verma, S., CDK4/6 inhibitors in breast cancer: beyond hormone receptor-positive HER2-negative disease. *Ther. Adv. Med. Oncol.* **2018,** *10*, 1-13

216. Rinnerthaler, G.; Gampenrieder, S. P.; Greil, R., ASCO 2018 highlights: metastatic breast cancer. *Memo* **2018,** *11*, 276-279.

217. Jiang, Z.; Yang, Z.; Li, F.; Li, Z.; Fishkin, N.; Burgess, K., Targeted Maytansinoid Conjugate Improves Therapeutic Index for Metastatic Breast Cancer Cells. *Bioconjugate Chem.* **2018,** *29*, 2920-2926.

218. Tian, J.; Zhou, J.; Shen, Z.; Ding, L.; Yu, J.-S.; Ju, H., A pH-activatable and aniline-substituted photosensitizer for near-infrared cancer theranostics. *Chem. Sci.* **2015,** *6* (10), 5969-5977.

219. Tanaka, K.; Okugawa, Y.; Toiyama, Y.; Inoue, Y.; Saigusa, S.*, et al.*, Brain-derived neurotrophic factor (BDNF)-induced tropomyosin-related kinase B (Trk B) signaling is a potential therapeutic target for peritoneal carcinomatosis arising from colorectal cancer. *PLoS One* **2014,** *9*, e96410/1-e96410/12.

220. Mauri, G.; Valtorta, E.; Cerea, G.; Amatu, A.; Schirru, M.*, et al.*, TRKA expression and NTRK1 gene copy number across solid tumours. *J. Clin. Pathol.* **2018,** *71*, 926-931.

221. Lawn, S.; Chan Jennifer, A.; Krishna, N.; Pisklakova, A.; Qu, X.*, et al.*, Neurotrophin signaling via TrkB and TrkC Receptors promote the growth of Brain Tumor Initiating Cells. *J. Biol. Chem.* **2014,** *290*, 3814-3824.

222. Vaishnavi, A.; Le Anh, T.; Doebele Robert, C., TRKing Down an Old Oncogene in a New Era of Targeted Therapy. *Cancer Discov.* **2015,** *5*, 25-34.

223. Weeraratna, A. T.; Dalrymple, S. L.; Lamb, J. C.; Denmeade, S. R.; Miknyoczki, S.; Dionne, C. A.; Isaacs, J. T., Pan-trk inhibition decreases metastasis and enhances host survival in experimental models as a result of its selective induction of apoptosis of prostate cancer cells. *Clin. Cancer Res.* **2001,** *7*, 2237-2245.

224. Yano, H.; Lee, F. S.; Kong, H.; Chuang, J.-Z.; Arevalo, J. C.*, et al.*, Association of Trk neurotrophin receptors with components of the cytoplasmic dynein motor. *J. Neurosci.* **2001,** *21*, RC125/1-RC125/7.

225. Kaufman, R. J., Overview of vector design for mammalian gene expression. *Mol. Biotechnol.* **2000,** *16*, 151-160.

226. Colosimo, A.; Goncz, K. K.; Holmes, A. R.; Kunzelmann, K.; Novelli, G.*, et al.*, Transfer and expression of foreign genes in mammalian cells. *BioTechniques* **2000,** *29*, 314-331.

227. Zaccaro, M. C.; Lee, B. H.; Pattarawarapan, M.; Xia, Z.; Caron, A.*, et al.*, Selective Small Molecule Peptidomimetic Ligands of TrkC and of TrkA Receptors Afford Discrete or Complete Neurotrophic Activities. *Chem. Biol.* **2005,** *12*, 1015-1028.

228. Kim, T. K.; Eberwine, J. H., Mammalian cell transfection: the present and the future. *Anal. Bioanal. Chem.* **2010,** *397*, 3173-3178.

229. Dyson Michael, R., Fundamentals of Expression in Mammalian Cells. In *Adv Exp Med Biol*, Vega, M. C., Ed. Switzerland, 2016; Vol. 896, pp 217-224.

230. Graf, L. H., Jr., Gene transformation. *Am. Sci.* **1982,** *70*, 496-505.

231. Potter, H., Transfection by electroporation. *Curr Protoc Mol Biol* **2003,** *Chapter 9*, Unit 9 3.

232. Longo, P. A.; Kavran, J. M.; Kim, M.-S.; Leahy, D. J., Generating mammalian stable cell lines by electroporation. *Methods Enzymol.* **2013,** *529* (Laboratory Methods in Enzymology: DNA), 209-226.

233. Ye, J.; Coulouris, G.; Zaretskaya, I.; Cutcutache, I.; Rozen, S.; Madden, T. L., Primer-BLAST: a tool to design target-specific primers for polymerase chain reaction. *BMC Bioinf.* **2012,** *13*, 134.

234. Bustin, S.; Huggett, J., qPCR primer design revisited. *Biomol. Detect. Quantif.* **2017,** *14*, 19-28.

235. Usama, S. M.; Thavornpradit, S.; Burgess, K., Optimized Heptamethine Cyanines for Photodynamic Therapy. *ACS Appl. Bio Mater.* **2018,** *1*, 1195-1205.

236. Mottram, L. F.; Maddox, E.; Schwab, M.; Beaufils, F.; Peterson, B. R., A Concise Synthesis of the Pennsylvania Green Fluorophore and Labeling of Intracellular Targets with O6-Benzylguanine Derivatives. *Org. Lett.* **2007,** *9*, 3741-3744.

237. Adler, J.; Parmryd, I., Quantifying colocalization by correlation: the Pearson correlation coefficient is superior to the Mander's overlap coefficient. *Cytometry A* **2010,** *77*, 733-742.

238. Dunn, K. W.; Kamocka, M. M.; McDonald, J. H., A practical guide to evaluating colocalization in biological microscopy. *Am. J. Physiol.* **2011,** *300*, C723-C742.

239. Wang, Y.; Liu, T.; Zhang, E.; Luo, S.; Tan, X.; Shi, C., Preferential accumulation of the near infrared heptamethine dye IR-780 in the mitochondria of drug-resistant lung cancer cells. *Biomaterials* **2014,** *35*, 4116-4124.

APPENDIX A

POTENTIAL THERANOSTIC SMALL MOLECULE DESIGNED AND TESTED AGAINST PANCREATIC CANCER CELLS

A.1 Introduction

Pancreatic ductal adenocarcinoma (PDAC) is one of the most deadly types of cancer that has threatened human health for years. It is the 12th most commonly diagnosed cancer and 4th leading cause of cancer related death among all types of cancers in the United States.[179-181] The overall 5-year survival rate for PDAC is less than 8%, with more than 50% of the patients diagnosed in the late stage of disease,[182] due to its varied or even asymptomatic early stage.[179,180] In the last few decades, although death rates associated with many major types of cancer has reduced, mortality by pancreatic cancer has increased.[182] Moreover, PDAC is predicted to be one of the top 3 life-threatening types of cancer by 2030.[183,184]

Surgery is considered to be the best strategy to treat PDAC. There are a few FDA approved drugs available to inhibit the progress of PDAC (as listed in Figure A.1), but they showed insignificant increase of the five-year survival rate of the patients.[179,185] Several proteins involved in the signaling pathways of PDAC have been considered as therapeutic targets, such as epidermal growth factor receptor (EGFR), mammalian target of rapamycin (mTOR), cyclooxygenase-2 (COX-2), etc.[185-188] In order to develop more promising

therapeutic agents against PDAC, numerous small-molecule inhibitors[189-192] as well as therapeutic nanoparticles[193-196] have been developed and tested in various *in vitro* and *in vivo* models.

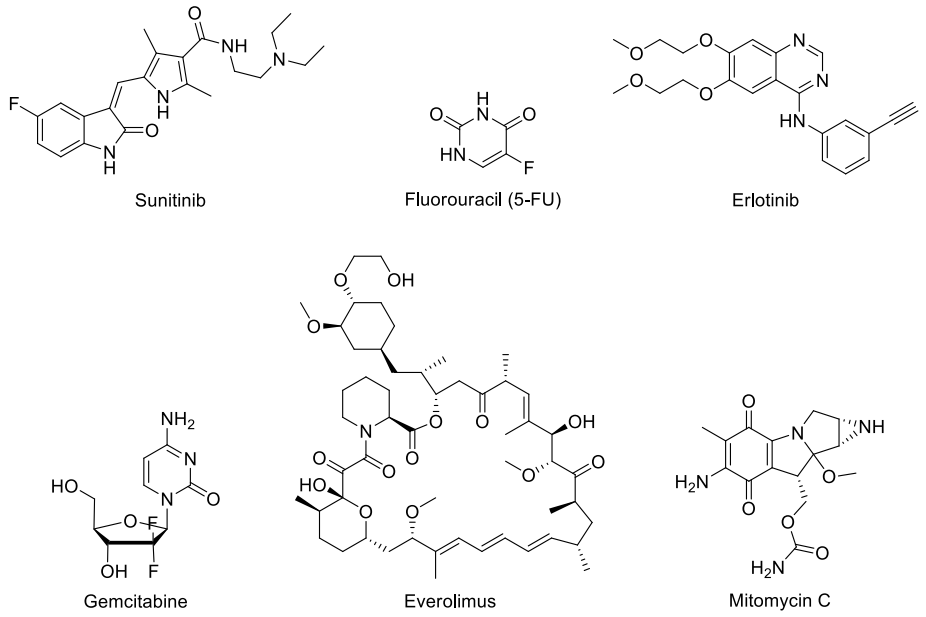

Figure A.1. FDA approved drugs for treatment of pancreatic cancer.

Most of the chemotherapeutic agents in clinical use are non-specific to cancer cells and have potentially high risk of side effects to normal tissue and organs. A specific strategy that enables selective interaction between the chemical agent and the receptors on the cancer cell surfaces, or “active targeting”, will be beneficial.[6] Naturally occurring small molecules (e.g. biotin, folate, androgen)[32,35] and monoclonal antibodies (mAbs)[193,196] are commonly conjugated with the chemotherapeutic cargo to perform active targeting to tumor

tissue. Relatively few synthetic small molecules have been reported for active targeting compared with mAbs.[40,197,198]

To develop novel small molecules with active targeting properties, our group developed a combinatorial solution-phase synthesis of a small molecule library mimicking bivalent β-turn structures.[41,81,199,200] The library contained commonly found amino acid side chains at protein-protein interfaces;[201] it was hypothesized that these would have a higher chance of interaction with the cell surface proteins. Two compounds based on this strategy have been applied in active targeting and agent delivery to metastatic breast and melanoma tissues.[73,74] These successes inspired a further investigation of other outstanding compounds from the library. Compound **A** (**KB1005**) was identified as a specific probe that binds unknown cell surface receptors on PANC-1 cells via a high throughput luciferase assay against various types of cancer cell lines.[202]

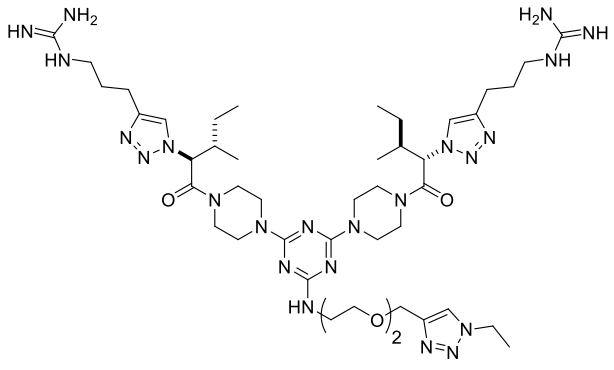

A

A dipyrrometheneboron difluoride (BODIPY) dye was conjugated with the targeting moiety of compound **A**, that has two symmetric dipeptide mimics with isoleucine (I) and arginine (R) (abbreviated as **IR-IR**), to form the "first generation" targeted compound **1-F**. The tumor accumulation was checked via optical imaging to confirm its potential in labeling pancreatic cancer cells as diagnostic probe. A simple derivative **1-PDT** was generated with similar strategy by conjugating the **IR-IR** targeting moiety with a BODIPY-based photodynamic therapy (PDT) sensitizer;[203,204] and its toxicity on pancreatic cancer cells (PANC-1) was tested to evaluate the targeted therapeutic potency.

In PDT, cells are damaged when the sensitizer is irradiated at specific wavelength of light (~530 nm for diiodo-BODIPY applied in this case).[30] Briefly, the PDT sensitizer transfers energy to $^3O_2$ generating $^1O_2$ (singlet oxygen) through a series of photochemical reactions.[205,206] Singlet oxygen damages tumor tissue and the microenvironment around it, promoting immune response.[207] Since singlet oxygen has very limited half-life,[208] the PDT effect is highly localized, and can be applied as a highly focused therapy to the targeted and photon-ignited region.

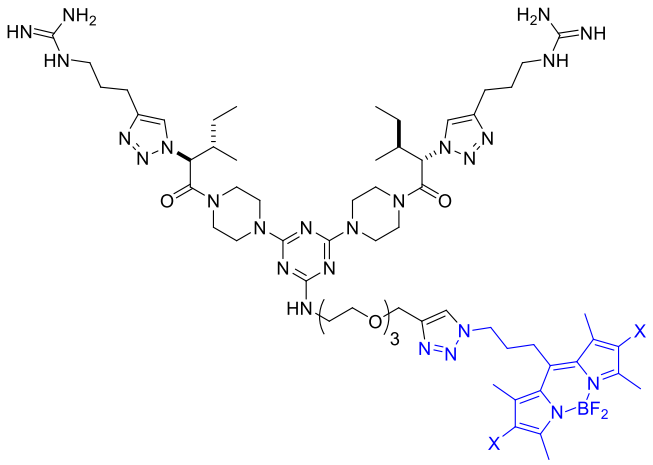

1-F or **IR-IR-F**, X = H
1-PDT or **IR-IR-PDT**, X = I

A.2 Results and Discussion

*A.2.1 In vitro cytotoxicity of "first generation" targeted probes **1-F** and **1-PDT***

Compound **1-F** and **1-PDT** were prepared by the protocol described below. (Scheme A.1) General cytotoxicity and PDT effect of compound **1-PDT** was tested against PANC-1 cells *in vitro*. (Figure A.2) The results unambiguously showed that compound **1-PDT** was uptaken by the PANC-1 cells, and was only toxic to the cells when exposed to light. It can suppress the cell proliferation efficiently at sub-micromolar level *in vitro*, that implied its potential therapeutic effect.

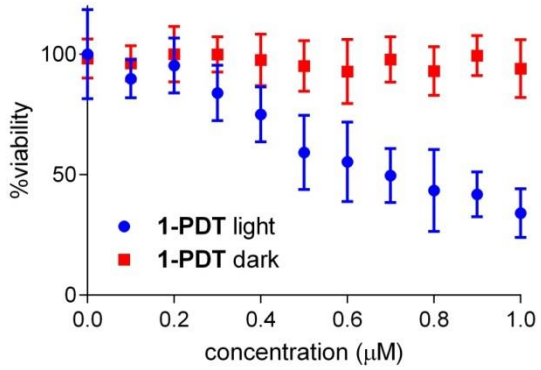

Figure A.2. Light and dark cytotoxicity of compound 1-**PDT**. Data was averaged from 12 independent parallel experiments. (n = 12, mean ± SD)

*A.2.2 Preparation and cytotoxicity check of gemcitabine conjugate **22***

To further investigate the potential of targeted delivery via the **IR-IR** fragment, gemcitabine, an FDA approved drug for pancreatic cancer, was chosen as the therapeutic cargo. After modification of the linker between the targeting moiety and gemcitabine, compound **22** was prepared. (Scheme A.2) A pair of targeted and non-targeted probe with a different linker was also prepared as back-up. (Scheme A.8 and 9)

The cytotoxicity test of **22** on PANC-1 cells was carried out in a similar procedure with two modifications: (i) a larger dose range was used and (ii) no light treatment involved. Free gemcitabine was used as a positive control to measure the efficiency of the conjugated drug. Interestingly, compound **22** seemed to be as effective as the free gemcitabine on the PANC-1 cells as tested, yet the cells showed general resistance to therapy in both cases. (Figure A.3)

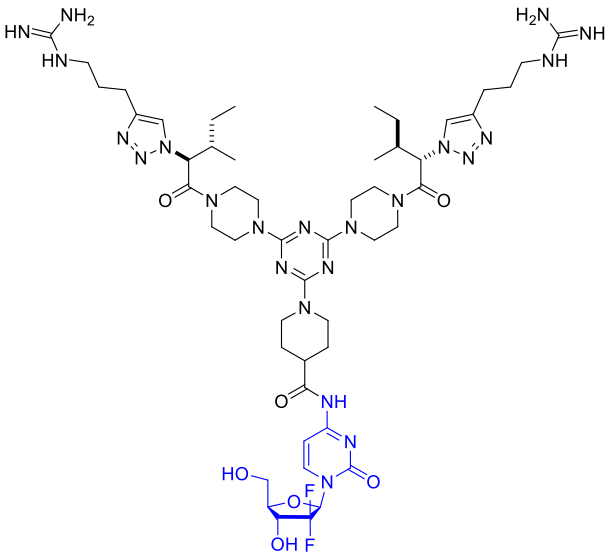

22

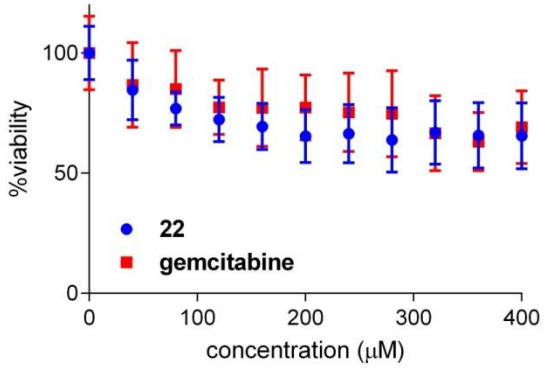

Figure A.3. Cytotoxicity comparison between compound **22** and gemcitabine. Data was averaged from 12 independent parallel experiments. (n = 12, mean ± SD)

*A.2.3 Fluorescence tissue histology of compound **1-F** and **1-R***

The selectivity of the designed molecule **1** can be determined in three ways: (i) comparison of the cytotoxicity between targeted the control (non-targeted) compound in parallel on PANC-1 cells; (ii) comparison of the

cytotoxicity of the targeted compound on PANC-1 versus normal pancreas cells; (iii) comparison of the fluorescence intensity of tumor and normal pancreas tissues sampled from patients. Compared to the first two methods, the third method offered an inexpensive way to exam more diverse cases, and also may provide some hints for the cell surface target the designed molecule possibly bound to.

The fixed tumor and adjacent normal tissues sampled from PDAC patients were stained with 2 μM **1-F** for 1 h, and confocal images were taken after a thorough wash. (Figure A.4) To our surprise, **1-F** did not show any fluorescence contrast on staining the tumor against adjacent normal tissues. Instead, in some cases, the normal tissues were stained brighter than the tumor.

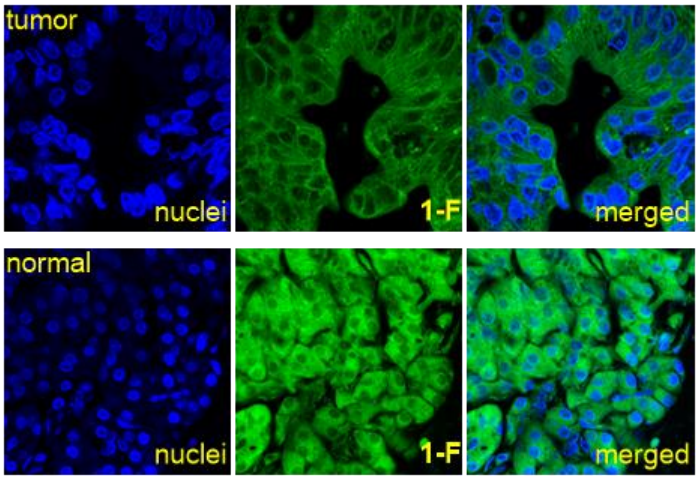

Figure A.4. Featured confocal fluorescence images of **1-F** on fixed tumorous and normal pancreas tissues. DAPI stained the nuclei of pancreas cells with blue fluorescence, and **1-F** stained cells with green fluorescence.

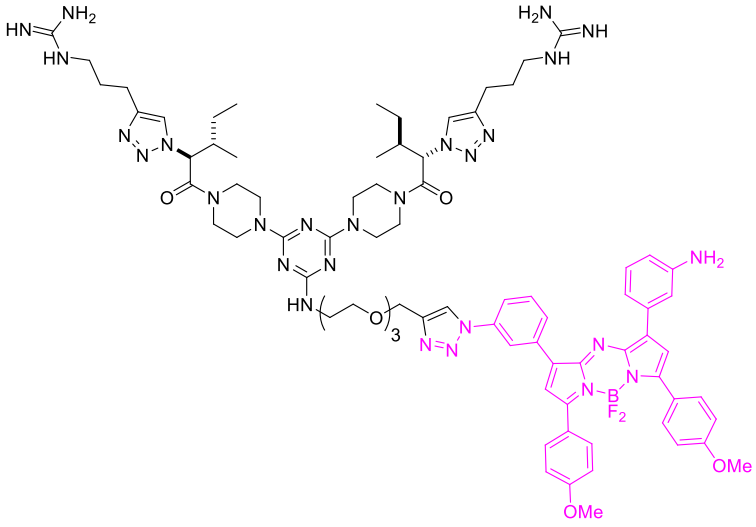

1-R

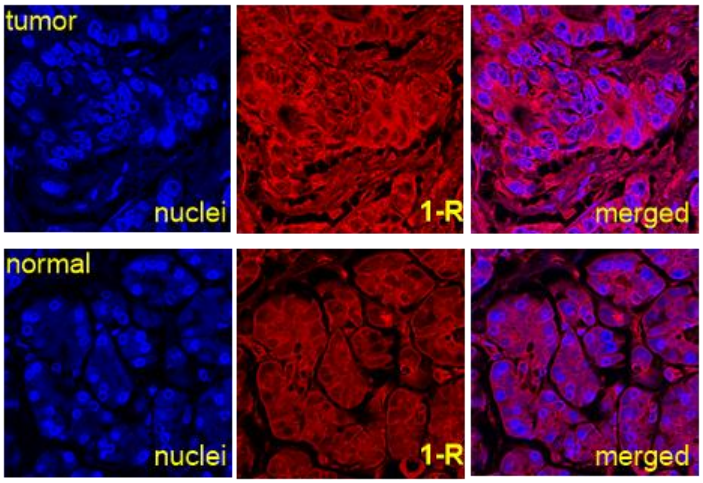

Figure A.5. Featured confocal fluorescence images of **1-R** on fixed tumorous and normal pancreas tissue. **1-R** stained cells with red fluorescence.

To further confirm that the results were not biased because of the auto-fluorescence from the tissue (cellular components are also fluorescent in green light region), a red fluorescence probe **1-R** was prepared. (Scheme A.3) Unfortunately, the red fluorescence signals from **1-R** did not distinguish between tumor and normal tissues (Figure A.5). This indicated that the targeting moiety

of compound **1-F** and **1-PDT** was not selective in patient tissues, thus the investigation of their application came to a dead end.

*A.2.4 Design and preparation of "second generation" targeted probe **17-F** and **17-PDT***

Although BODIPY is photostable and provides bright fluorescence, and its iodinated derivatives serves as a good PDT agent, the absorbance spectrum lies in green to yellow region (A_{max} ~530 nm). Light in red to near-infrared (NIR) region can penetrate deeper through the tissues than the green light. The low absorbance wavelength significantly restricted its potential as *in vivo* imaging and PDT agent for tumors buried deep inside the body.[205]

The huge opportunity of NIR light for diagnostic and therapeutic applications inspired us to develop a new generation of targeted fluorescence molecule based on the core structure of aza-BODIPY (like compound **G**[209] in Scheme A.4). By eliminating the extended linker between the targeted moiety and the fluorescent dye, compound **17-F** and **17-PDT** were prepared as the "second generation"[72] targeted probe. Compound **18-F** and **18-PDT** were designed to be the non-targeted control. Control compound synthesis was terminated after preparation of the non-targeted ligand **16**. (Scheme A.5) Due to the non-selective tissue histology results, no biological experiments were performed on these compounds.

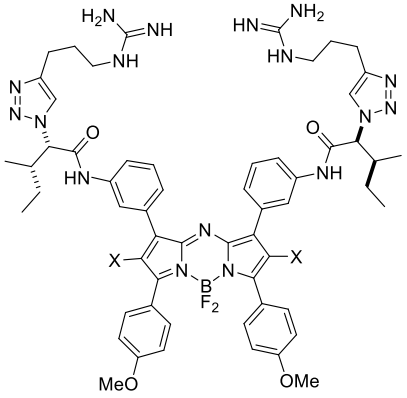

17-F or **IR-IR-azaBODIPY**, X = H
17-PDT or **IR-IR-I2-azaBODIPY**, X = I

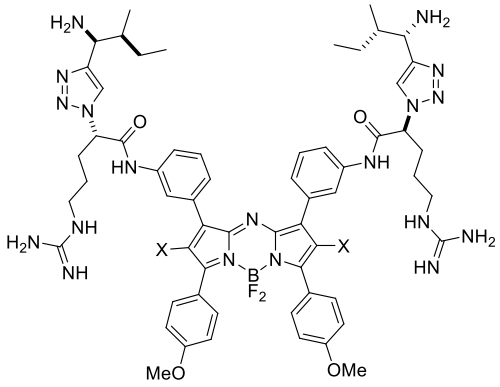

18-F or **RI-RI-azaBODIPY**, X = H
18-PDT or **RI-RI-I2-azaBODIPY**, X = I

*A.2.5 Design of "first generation" control compound **2-F** and **2-PDT***

Along with the targeted molecule design, a set of non-targeted compound **2-F** and **2-PDT** with reversed sequence of isoleucine and arginine was proposed as negative control. The very original design of the non-targeted fragment was shown as molecule **C** in Figure A.6. Since the accessibility of the chiral alkyne (red fragment in **C**) was really poor, an isoleucine alkyne derivative was used to replace the original design to ease synthesis, while keeping the chemical features in the original design. The synthesis of **2-F** and **2-PDT** was halted half way because of the non-selectivity of **1-F** in tissue histology, only the non-targeted fragment **3** was prepared. (Scheme A.6)

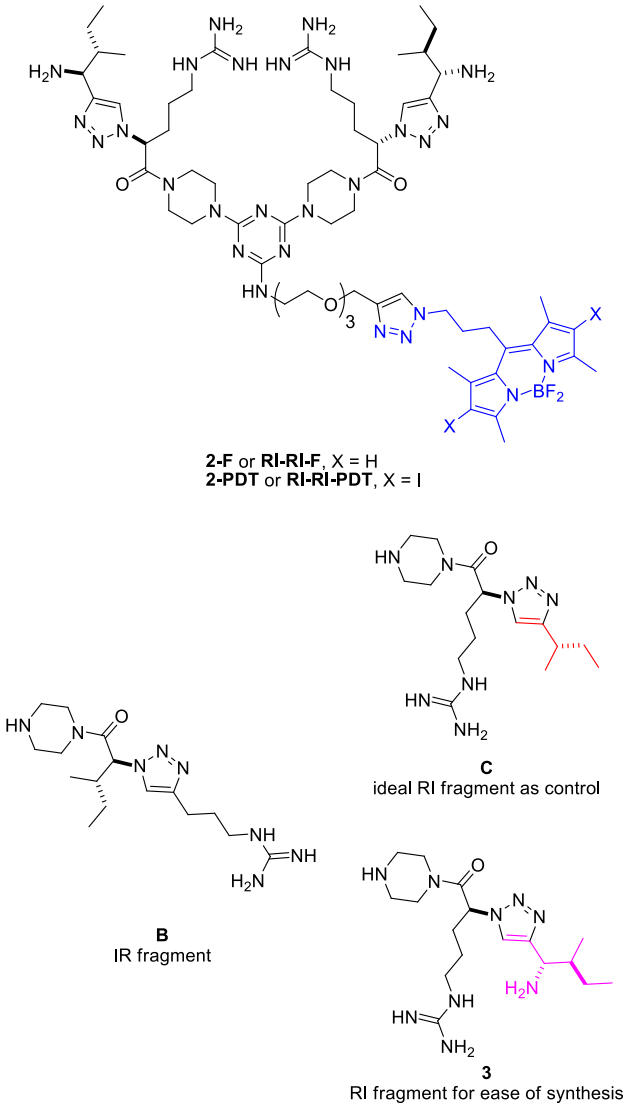

Figure A.6. Alternated design for the original non-targeted fragment **C**.

A.3 Conclusions

A few targeted molecules emerged from our previous studies were synthesized, and their theranostic potential was tested on PANC-1 cell line as well as tissue histology from pancreatic cancer patients. Although cytotoxicity of compounds **1-PDT** and **22** was observed, non-selectivity in staining of **1-F**

between tumor and normal pancreas tissues proved the targeting moiety in **1-F** and **1-PDT** was not suitable for targeted drug delivery to pancreatic cancer tissues.

A.4 Experimental Methods

A.4.1 Synthesis of the featured compounds

Synthesis of compound 1-F and 1-PDT

Compound **B**, **D** as well as the BODIPYs were prepared as described in previous publications.[74,81] The key synthetic step was carried out by mixing 1.0 equiv. **D** with 1.0 equiv. cyanuric chloride in acetonitrile (MeCN) on ice, followed by adding 1.5 equiv. *N,N*-diisopropylethylamine ($^{i}Pr_2NEt$). The cooled reaction mixture was kept and stirred at 25 ^{o}C for 30 min to acquire compound **4** after removing the solvent. Purity of **4** was confirmed via the absorbance trace at 254 nm on a reverse-phase analytical HPLC column. Without further purification, 1.0 equiv. **4** and 3.0 equiv. **B** was dissolved in DMSO and 5.0 equiv. K_2CO_3 added. The mixture was stirred at 25 ^{o}C for 3 d to get targeting moiety **5**. Compound **5** was purified through a preparative reverse-phase C18 HPLC column with water/acetonitrile (MeCN) system (10 – 90% MeCN in 30 min), and lyophilized. A simple Cu(I)-based “click” reaction was then applied to conjugate the targeting moiety **5** and imaging/ therapeutic probe to eventually achieve **1-F** and **1-PDT**.

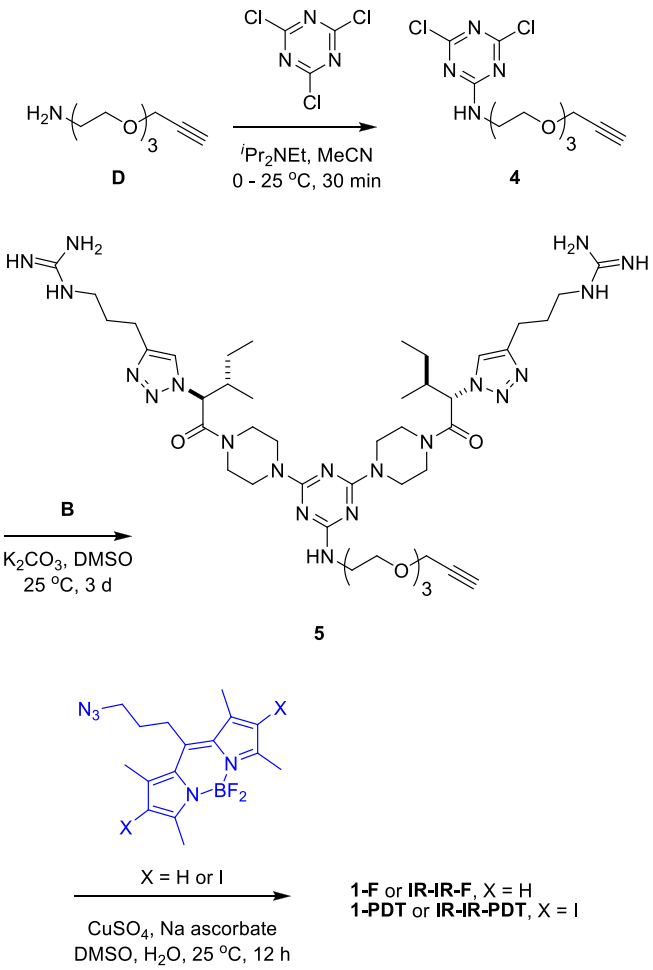

Scheme A.1. Synthesis of compound **1-F** and **1-PDT**.

Synthesis of compound 22

Compound **E** was prepared as previously described.[210] Equal moles of gemcitabine hydrochloride and **E** were dissolved in dichloromethane on ice. The mixture was kept cold on ice, and HOBt, EDCI, NMM were then added in that order. The reaction mixture was stirred at 25 °C for 12 h, and compound **23** was isolated via flash chromatography (5% MeOH in CH_2Cl_2). After Boc deprotection of **23**, the product was dissolved in MeCN on ice, cyanuric chloride and $^{i}Pr_2NEt$

were added and the reaction mixture was stirred for one hour at 25 ^{o}C to give compound **24**. Without further purification, 2.0 equiv. fragment **B** was added to a DMSO solution of **24** with 5.0 equiv. K_2CO_3. After 2 d of reaction, compound **22** was isolated through a preparative reverse-phase C18 HPLC column with water/acetonitrile (MeCN) system (10 – 90% MeCN in 30 min).

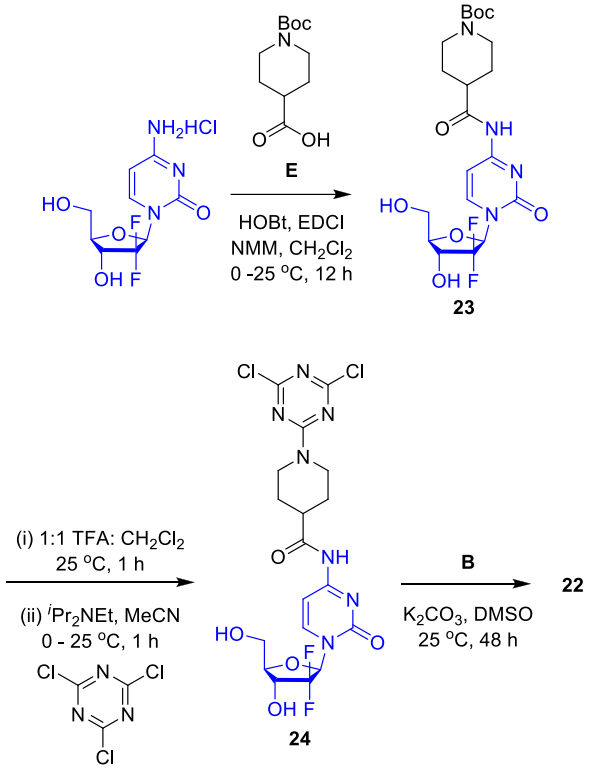

Scheme A.2. Synthesis of compound **22**.

Synthesis of compound 1-R

Compound **F**, a gift from Dr. Anyanee Kamkaew (a former graduate student in our group), was conjugated to **5** via Cu(I)-based “click” reaction to

give **1-R**. The crude compound was purified through a reverse phase preparative HPLC column with water/acetonitrile (MeCN) system (10 – 90% MeCN in 30 min).

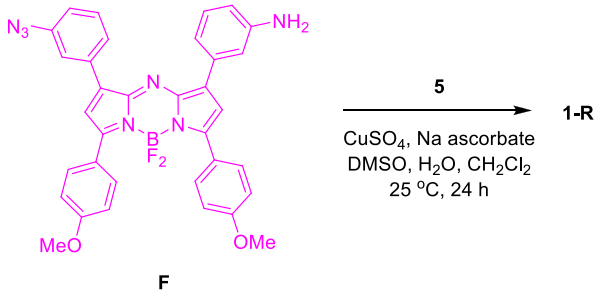

Scheme A.3. Synthesis of compound **1-R**.

Synthesis of compound 17-F and 17-PDT

Synthesis of aza-BODIPY **G** was repeated according to the synthetic protocol previously published.[209] Isoleucine azide was dissolved in cold *N,N*-dimethyl-formamide (DMF) on ice, and HOAt, EDCI were added in sequence. The solution was stirred gently and mixed with compound **G** and $^{i}Pr_2NEt$. Amide coupling reaction was carried out at 25 ^{o}C for 12 h before removing the solvent. Compound **19** was purified with flash chromatography (1:1 EtOAc:hexane). A Cu(I)-based "click" reaction was applied to conjugate **19** with **12** (synthesis described in later section) to acquire compound **20-F**.

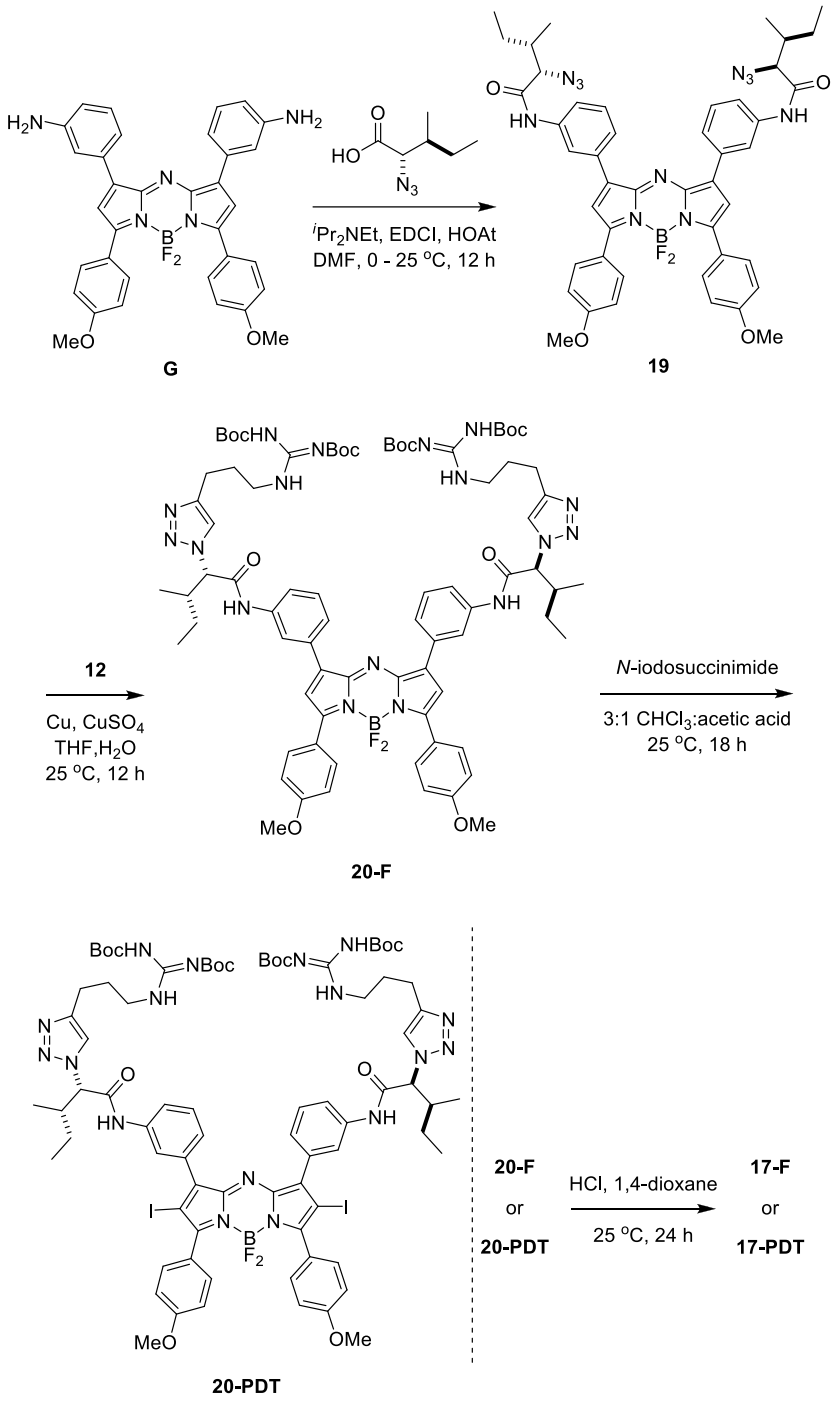

Scheme A.4. Synthesis of compound **17-F** and **17-PDT**.

Flash chromatography purified (2% MeOH in CH_2Cl_2) **20-F** was solubilized in 3:1 $CHCl_3$:acetic acid with 2.5 equiv. *N*-iodosuccinimide. The reaction took 18 h at 25 ^oC to acquire **20-PDT**. Boc deprotection (1 d) with hydrochloride in 1,4-dioxane will eventually get compound **17-F** and **17-PDT** without further purification.

Synthesis of non-targeted fragment 16

A Cu(I)-based "click" reaction was applied to conjugate **6** with **H** to get **14** via flash chromatography (5% MeOH in CH_2Cl_2). After removal of Cbz protecting group, the ornithine residue was converted to Boc-protected arginine to form compound **16**.

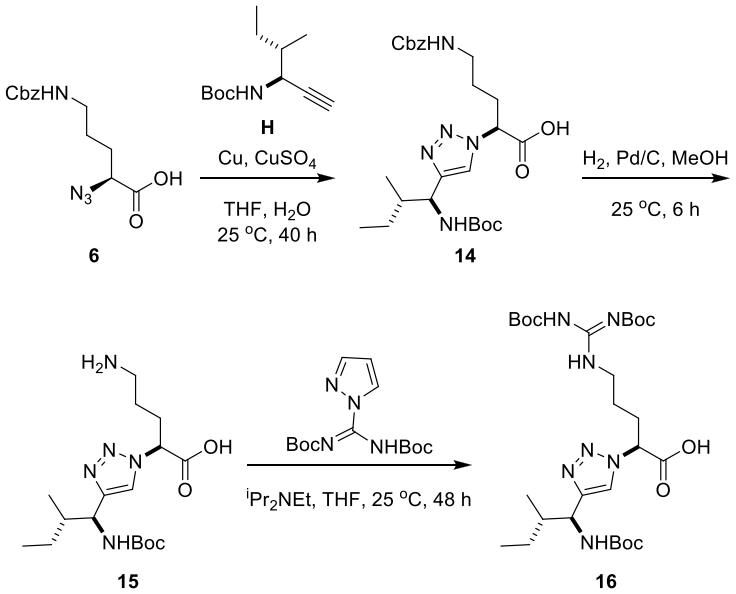

Scheme A.5. Synthesis of compound **16**.

Synthesis of scrambled non-targeted fragment 3

L-Orn(Z)-OH were converted to its azide derivative **6** followed by the similar protocol.[81] Compound **7** was acquired by amide coupling between **6** and Boc-piperazine. After a simple 10% citric acid wash followed by a saturated $NaHCO_3$ base wash to get pure compound **7** in organic layer, a Cu(I)-based "click" reaction was applied to conjugate **7** with **H**.[41] Compound **8** was purified via flash chromatography, and the Cbz protecting group was removed by common hydrogenation condition to form **9** in quantitative yield. A simple substitute reaction then converted the ornithine residue to Boc-protected arginine in compound **10**. The scrambled non-targeted fragment **3** was achieved by routine Boc deprotection without further purification.

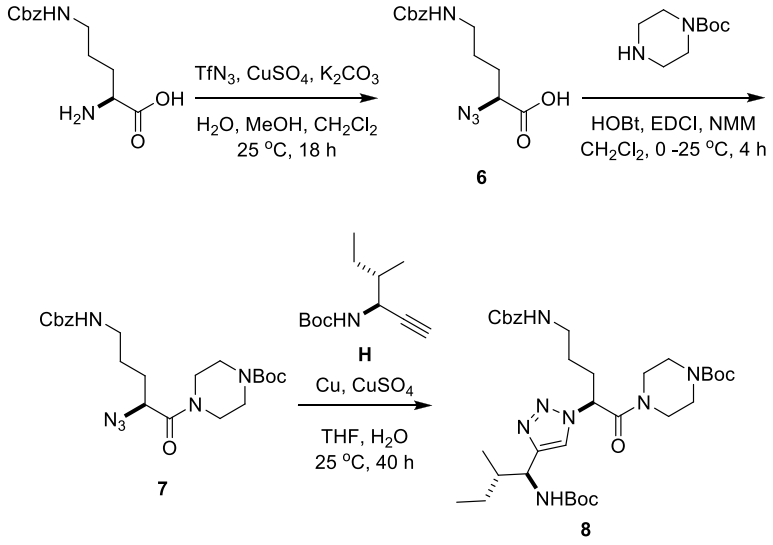

Scheme A.6. Synthesis of compound **3**.

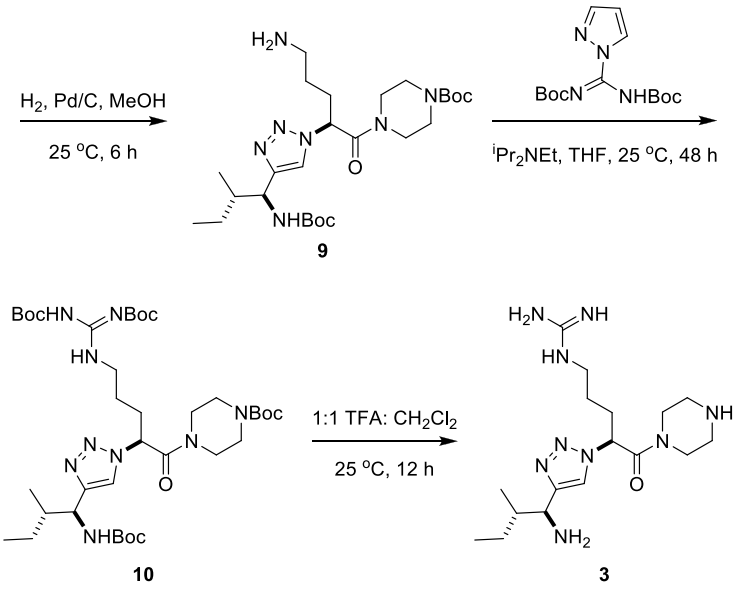

Scheme A.6. Continued.

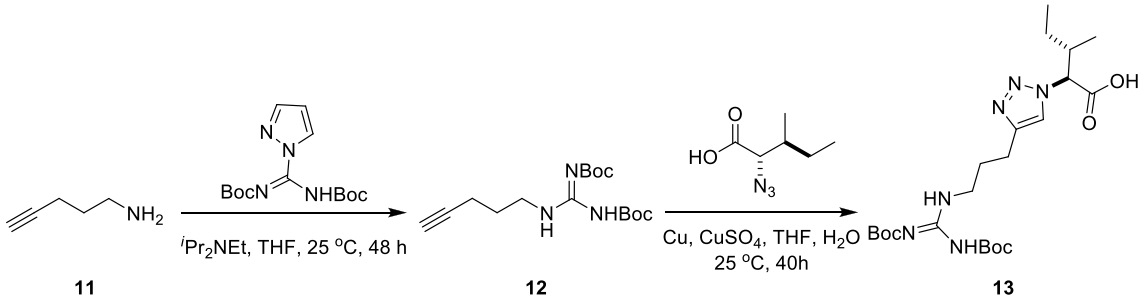

Scheme A.7. Synthesis of compound **12** and **13**.

Synthesis of compound 12 and targeted fragment 13

Alternative synthetic route to get targeted fragment for **17-F** and **17-PDT** was proven success (Scheme A-7). Compound **11** was converted to **12** using the same protocol to convert **9** to **10**. And a Cu(I)-based "click" reaction was applied to conjugate **12** with isoleucine azide to form **13**.

Synthesis of the alternative design of IR-IR targeted fragment 28

Isoleucine azide **J** was coupled with Cbz-protected piperazine **K** to form compound **25**. After routine "click" reaction with compound **12**, the Cbz group was removed to form fragment **26**. Simple substitution reaction between **K** and cyanuric chloride (1:1 ratio) resulted in **27**. Without further purification, 2.0 equiv. **26** was coupled to **27** to achieve the IR-IR targeted fragment **28**.

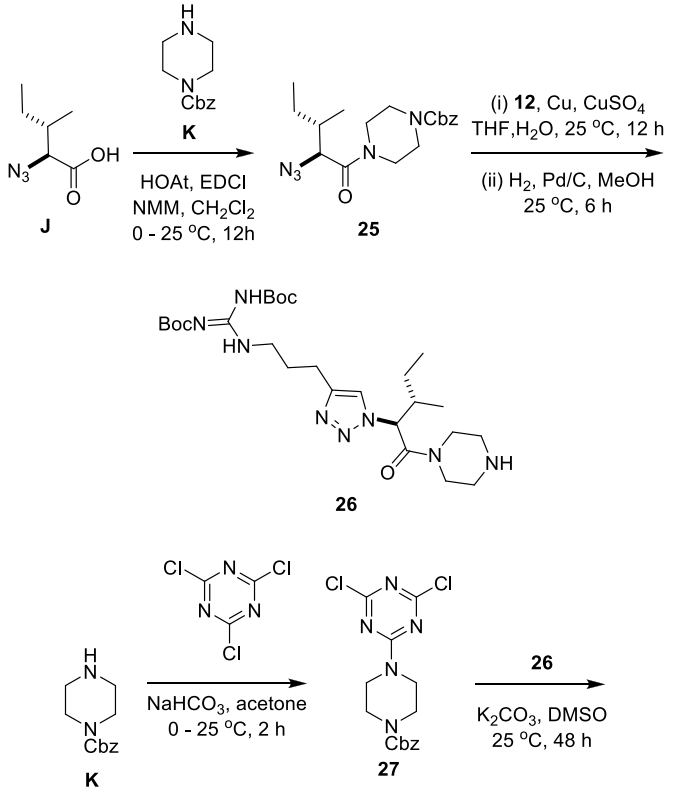

Scheme A.8. Synthesis of compound **28**.

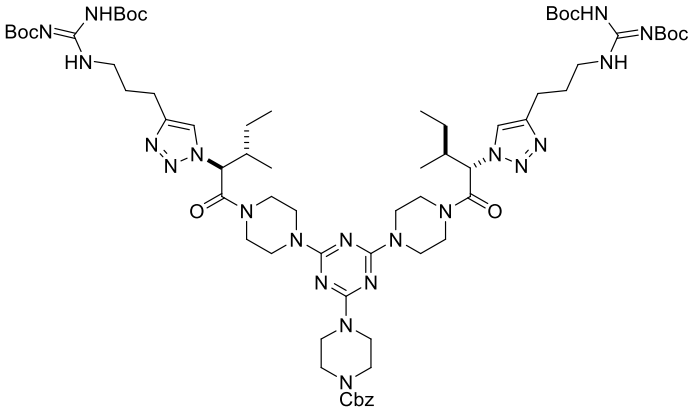

28

Scheme A.8. Continued.

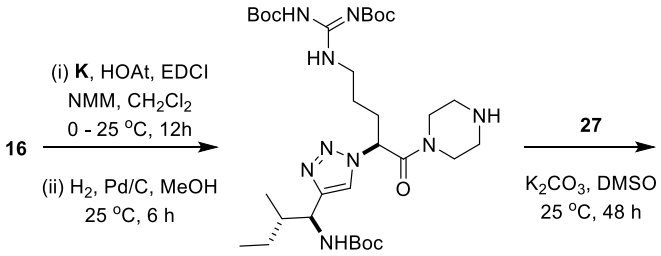

29

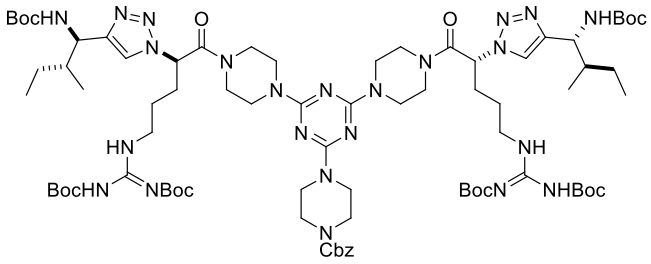

30

Scheme A.9. Synthesis of compound **30**.

Synthesis of the alternative design of RI-RI non-targeted fragment 30

Amide coupling between **16** and **K** was followed by a hydrogenation to remove Cbz protecting group to form compound **29**. A simple substitution

reaction between 2.0 equiv. **29** and 1.0 equiv. **27** resulted in compound **30** (**RI-RI**, the non-targeted fragment).

A.4.2 Photocytotoxicity test on PANC-1 cells in vitro

PANC-1 cells were cultured on 75 cm^2 tissue culture flasks in Dulbecco's Modified Eagle Medium/nutrient mixture F-12 Ham (DMEM/F12, Millipore Sigma) supplement with 10% fetal bovine serum (FBS) in a 37 ^oC incubator with full humidity and 5% CO_2.

To test the PDT effect of **1-PDT**, PANC-1 cells were seeded on 96-well plates as 5000 cells/well (50 μL) and incubated overnight. Various concentrations of **1-PDT** were prepared in 50 μL protein-free hybridoma medium (PFHM II) and added to cells to make final concentrations from 0 to 1.0 μM. For the light treatment (PDT) group, cells were illuminated (>480 nm source with fluence rate of 12.2 mW/cm^2 for 10 min) after **1-PDT** was added to induce singlet oxygen generation; for dark treatment (control) group, the cells were put back to incubator right after adding **1-PDT** without light interference. All plates were incubated for 72 h, and cell viability was tested with MTT assay.[211] Briefly, 20 μL of 3-(4,5-dimethylthiazol-2-yl)-2,5-diphenyltetrazolium bromide (MTT, as 5 mg/mL in Hank's balanced salt solution) was added to each well, and incubated for 3 h in 37 ^oC incubator with full humidity and 5% CO_2. The medium was then removed, and 100 μL of DMSO was added to dissolve the formazan product. The solution absorbance (570 nm) of each sample was measured with BioTek®

Synergy 4 Microplate Reader. Viability data were processed through GraphPad Prism® 6.0 software (Figure A.2).

A.4.3 Fluorescence tissue histology

Tissue slices (Biomax® #PA241b, 6 cases) were incubated with 2 μM **1-F** for 1 h after removal of parafilm. After thorough washing with phosphate saline buffers, the tissue was mounted with Vectashield® mounting medium (with DAPI) under cover glass. Confocal fluorescence imaging was taken with Olympus® FV-1000 microscope in the Microscopy and Imaging Center in Texas A&M University.

A.5 Compound Characterization

1-F

$C_{60}H_{94}BF_2N_{25}O_5$

^{1}H NMR (500 MHz, DMSO-d6) δ 8.08 (s, 1H), 7.83 (s, 2H), 7.58 (s, 1H), 7.27 – 7.14 (m, 2H), 6.72 (s, 2H), 6.05 (s, 2H), 5.52 (s, 1H), 5.50 (s, 1H), 4.42 (t, J = 6.1 Hz, 2H), 4.39 (s, 2H), 3.71 – 3.60 (m, 2H), 3.55 – 3.45 (m, 8H), 3.43 – 3.28 (m, 18H), 3.26 – 3.18 (m, 2H), 2.99 (dd, J = 12.7, 6.4 Hz, 4H), 2.76 (dd, J = 10.8, 6.3 Hz, 2H), 2.35 (dd, J = 3.4, 1.7 Hz, 4H), 2.23 (s, 6H), 2.18 – 2.09 (m, 2H), 2.03 (s, 6H), 1.95 – 1.86 (m, 2H), 1.70 – 1.58 (m, 4H), 0.87 – 0.70 (m, 10H), 0.62 (t, J = 7.3 Hz, 6H).

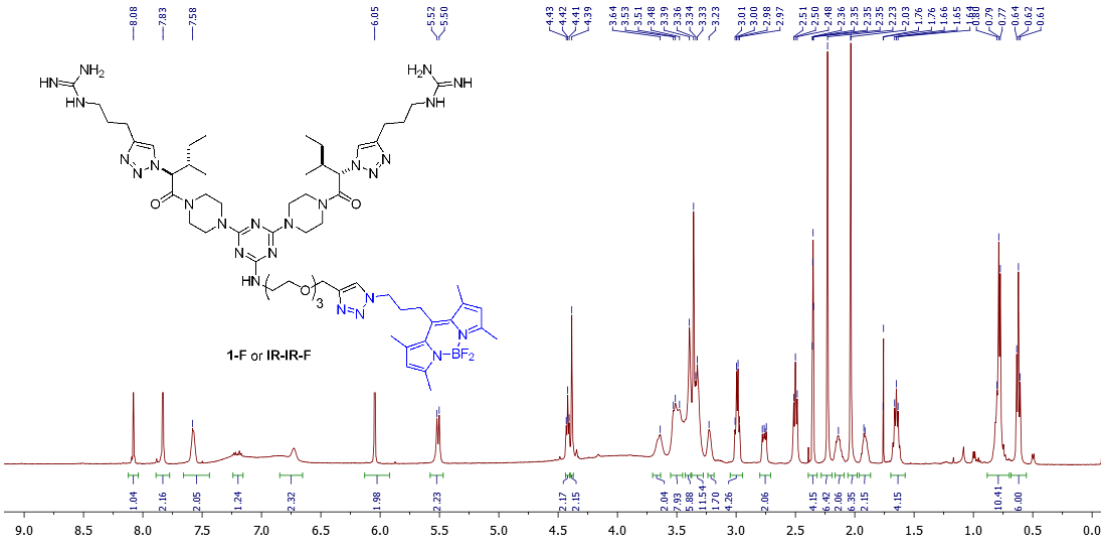

^{13}C NMR (126 MHz, DMSO-d6) δ 166.31, 158.45, 158.27, 158.18, 156.83, 156.78, 153.40, 146.19, 145.03, 144.05, 140.89, 130.63, 124.55, 121.82, 121.01, 69.79, 69.73, 69.53, 68.96, 68.85, 63.42, 62.32, 49.31, 45.26, 44.58, 43.05, 42.39, 41.72, 40.23, 37.17, 31.78, 28.25, 25.11, 24.09, 22.13, 21.09, 15.54, 15.07, 14.10, 10.56

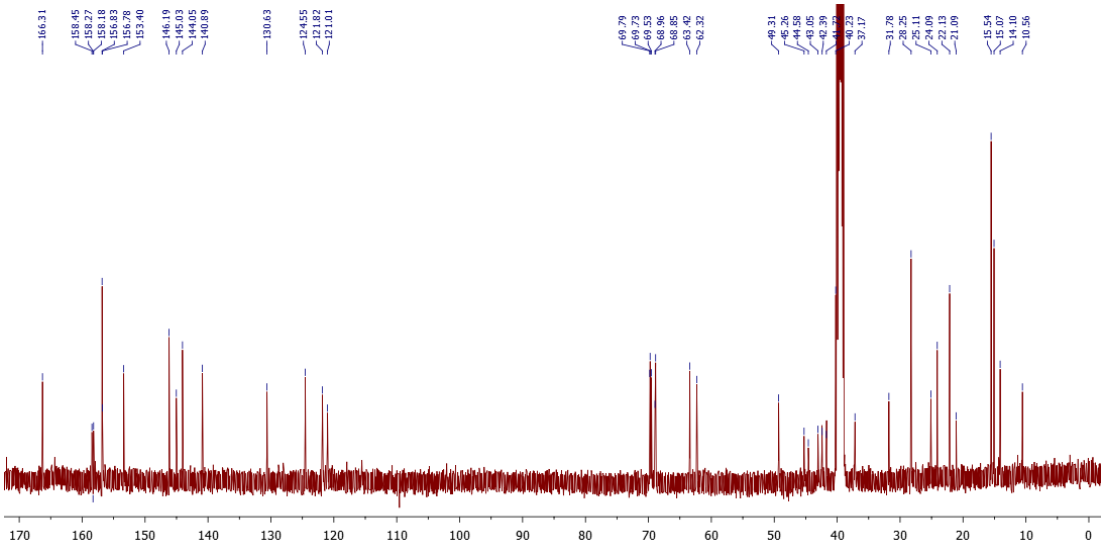

2-PDT

$C_{60}H_{92}BF_2I_2N_{25}O_5$

^{1}H NMR (400 MHz, DMSO-d6) δ 8.44 – 8.29 (m, 4H), 8.28 – 8.20 (m, 2H), 7.64 – 7.57 (m, 2H), 7.20 (s, 1H), 7.07 (s, 1H), 6.94 (s, 1H), 6.75 – 6.69 (m, 1H), 6.06 – 5.97 (m, 2H), 4.61 – 4.56 (m, 2H), 4.56 – 4.51 (m, 2H), 4.46 – 4.39 (m, 2H), 3.84 – 3.39 (m, 28H), 3.18 – 3.09 (m, 3H), 3.06 – 2.99 (m, 2H), 2.71 – 2.62 (m, 2H), 2.54 (s, 3H), 2.36 – 2.30 (m, 2H), 2.25 (s, 3H), 2.14 – 1.87 (m, 9H), 1.56 – 1.35 (m, 6H), 1.33 – 1.16 (m, 7H), 1.14 – 0.97 (m, 4H), 0.88 (dt, J = 14.2, 8.5 Hz, 6H), 0.77 (d, J = 6.7 Hz, 3H).

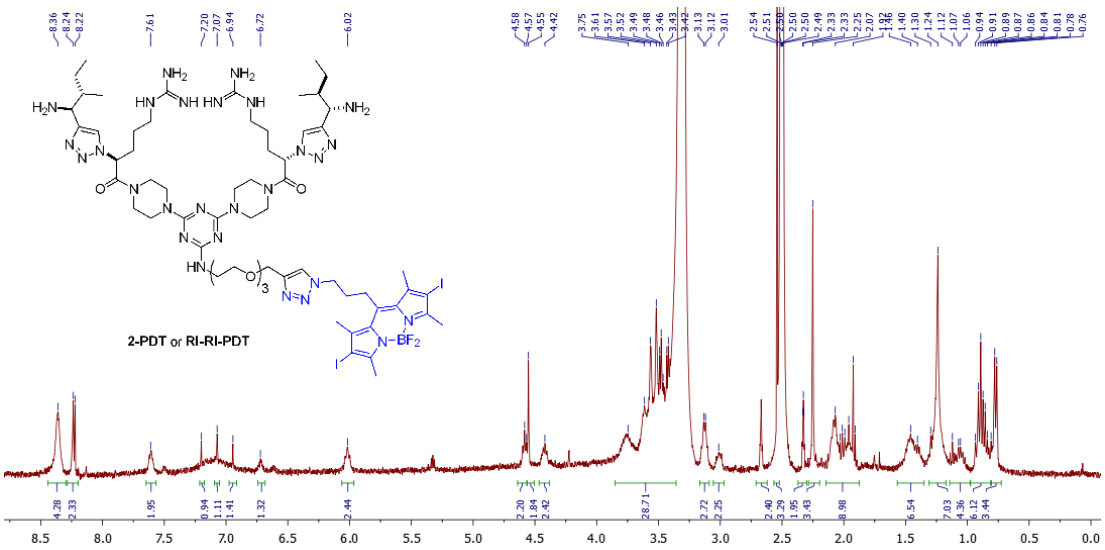

3

$C_{17}H_{33}N_9O$

^{1}H NMR (400 MHz, MeOD) δ 8.15 (s, 1H), 5.91 (t, J = 7.4 Hz, 1H), 4.38 (d, J = 6.4 Hz, 1H), 3.92 – 3.62 (m, 4H), 3.13 (td, J = 14.6, 7.3 Hz, 4H), 2.19 – 2.09 (m,

2H), 2.06 – 1.94 (m, 1H), 1.60 – 1.49 (m, 1H), 1.48 – 1.40 (m, 1H), 1.38 – 1.24 (m, 2H), 1.20 – 1.07 (m, 2H), 0.91 (t, J = 7.4 Hz, 3H), 0.80 (d, J = 6.8 Hz, 3H).

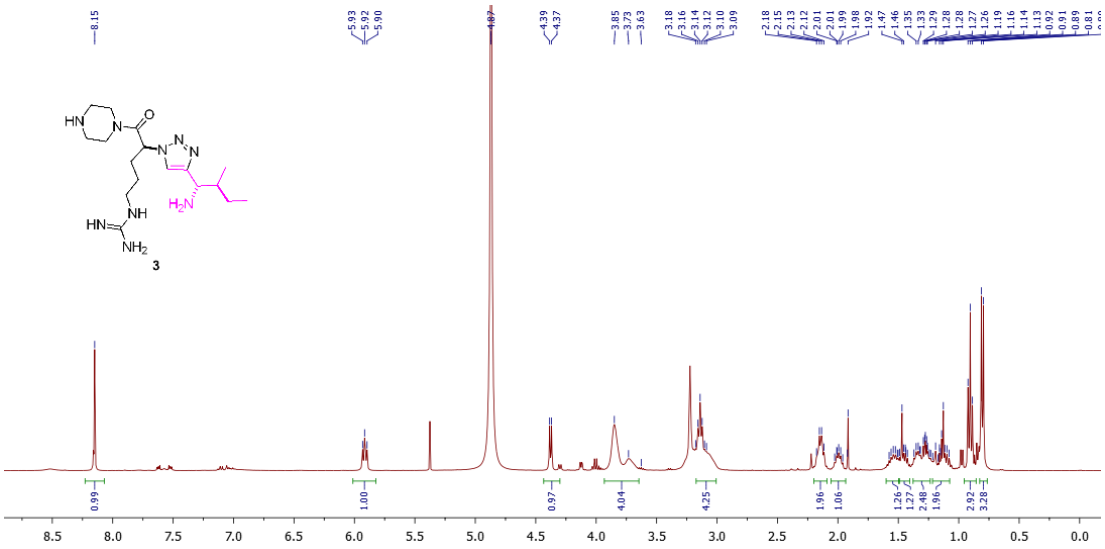

6

$C_{13}H_{16}N_4O_4$

^{1}H NMR (400 MHz, $CDCl_3$) δ 10.30 (s, 1H), 7.43 – 7.11 (m, 5H), 5.21 – 5.02 (m, 2H), 4.97 (s, 1H), 3.98 – 3.73 (m, 1H), 3.22 (s, 2H), 1.88 (ddd, J = 13.8, 7.0, 4.0 Hz, 1H), 1.83 – 1.69 (m, 1H), 1.65 (dt, J = 9.2, 6.5 Hz, 2H).

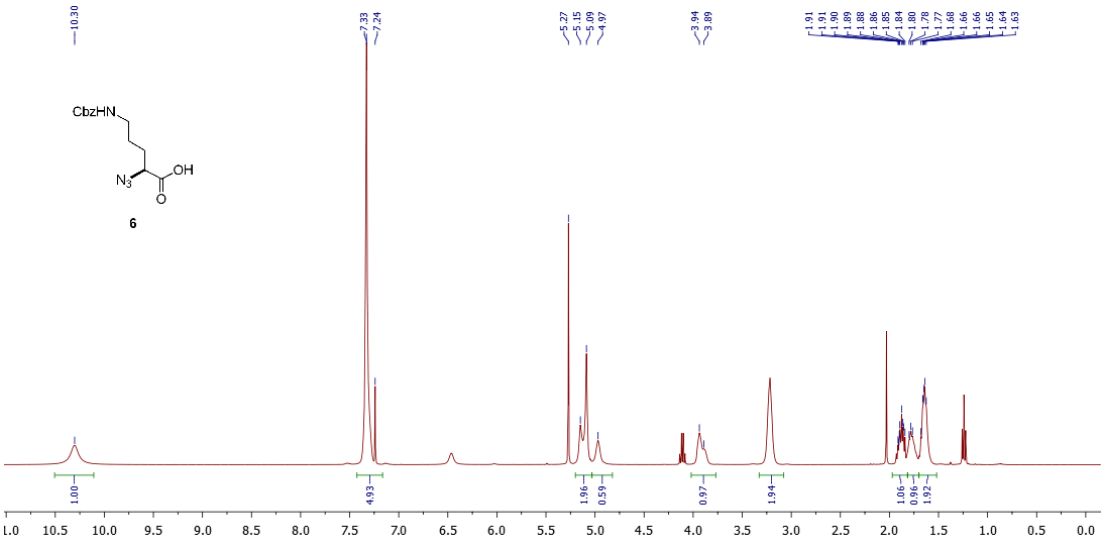

7

$C_{22}H_{32}N_6O_5$

^{1}H NMR (400 MHz, MeOD) δ 7.58 – 7.29 (m, 5H), 5.19 (s, 2H), 4.35 (t, J = 6.7 Hz, 1H), 3.82 – 3.49 (m, 8H), 3.30 (td, J = 6.6, 4.0 Hz, 2H), 1.99 – 1.86 (m, 2H), 1.86 – 1.67 (m, 2H), 1.60 (s, 9H).

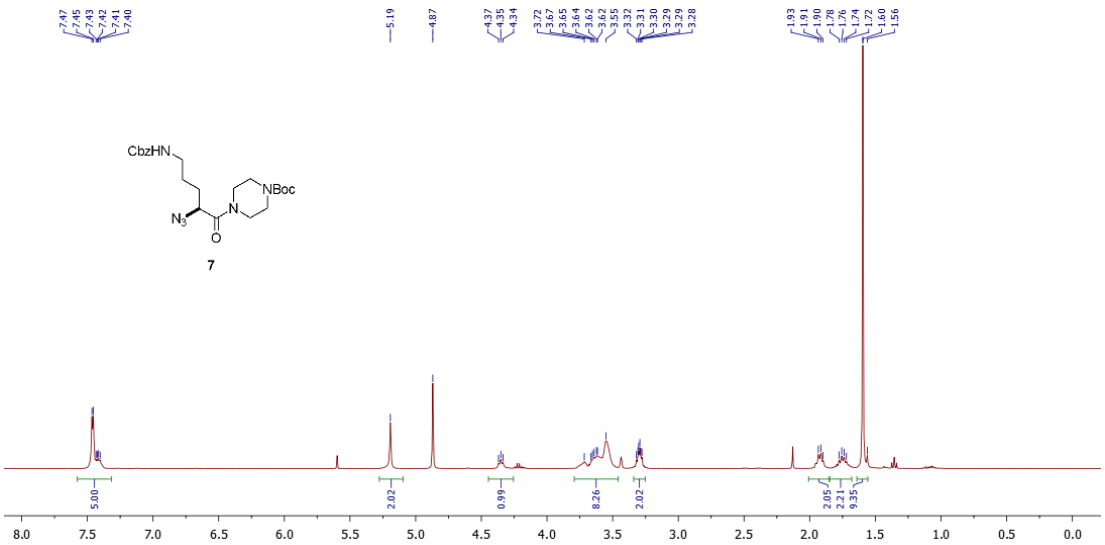

8

$C_{34}H_{53}N_7O_7$

^{1}H NMR (400 MHz, $CDCl_3$) δ 7.59 (s, 1H), 7.38 – 7.26 (m, 5H), 5.79 – 5.66 (m, 1H), 5.36 – 5.20 (m, 1H), 5.07 (s, 2H), 4.85 (s, 1H), 4.76 – 4.63 (m, 1H), 3.75 – 3.34 (m, 6H), 3.31 – 2.92 (m, 4H), 2.19 – 1.99 (m, 2H), 1.96 – 1.85 (m, 1H), 1.43 (s, 9H), 1.39 (s, 9H), 1.36 – 1.16 (m, 3H), 1.13 – 1.00 (m, 1H), 0.88 (t, J = 7.4 Hz, 3H), 0.78 (d, J = 6.8 Hz, 3H).

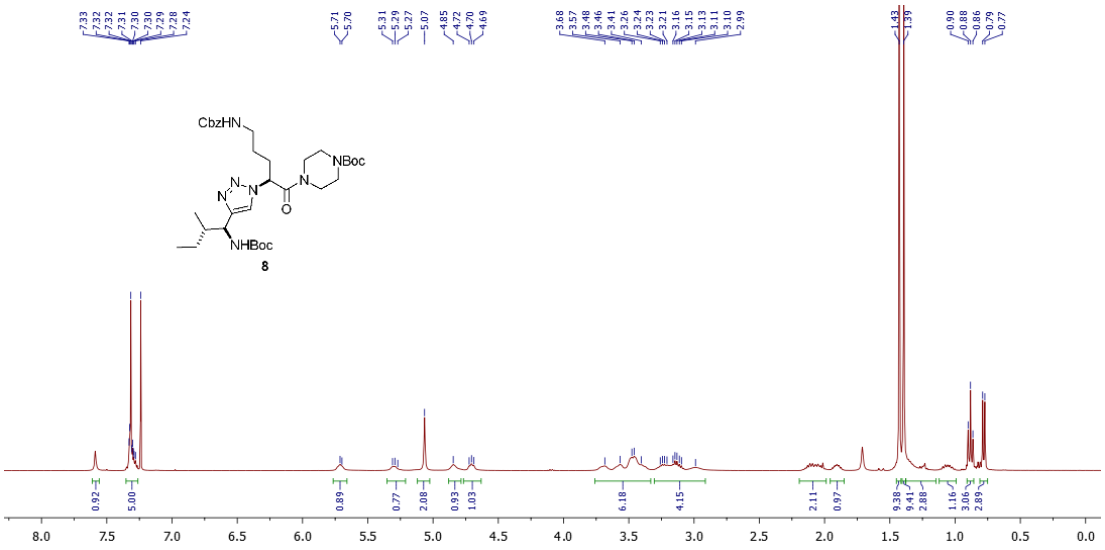

9

$C_{26}H_{47}N_7O_5$

^{1}H NMR (400 MHz, $CDCl_3$) δ 7.71 (s, 1H), 5.88 – 5.67 (m, 1H), 5.50 – 5.25 (m, 1H), 4.81 – 4.59 (m, 1H), 3.60 – 3.40 (m, 6H), 3.22 – 2.82 (m, 4H), 2.31 – 2.08 (m, 2H), 1.96 – 1.80 (m, 1H), 1.69 – 1.49 (m, 1H), 1.42 (s, 9H), 1.34 (s, 9H),

1.31 – 1.17 (m, 3H), 1.14 – j0.97 (m, 2H), 0.89 (td, J = 7.5, 4.8 Hz, 3H), 0.79 (d, J = 6.6 Hz, 3H).

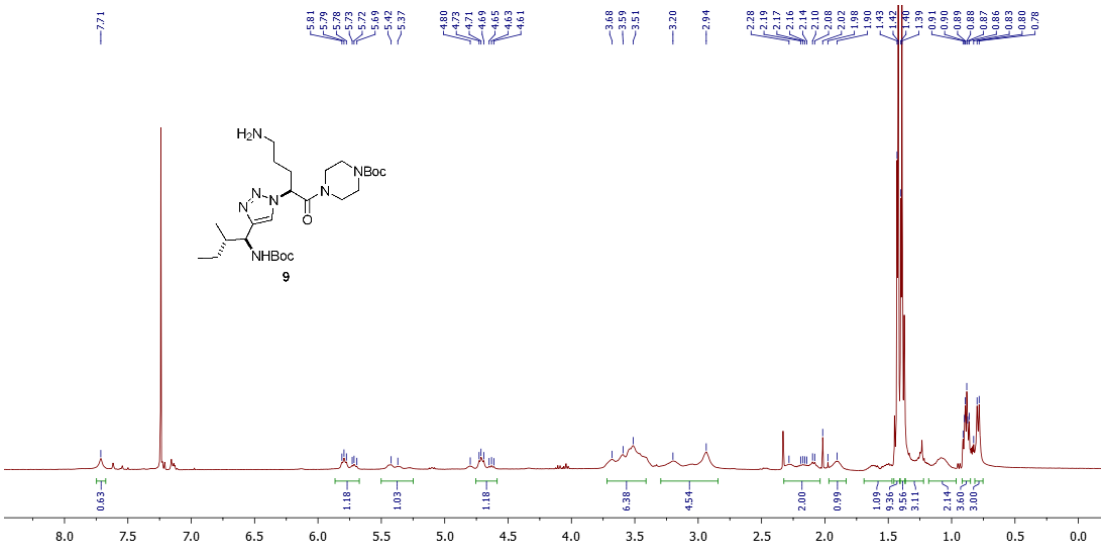

10

$C_{37}H_{65}N_9O_9$

^{1}H NMR (400 MHz, $CDCl_3$) δ 8.50 (s, 1H), 7.61 (s, 1H), 5.79 (t, J = 7.3 Hz, 1H), 5.29 (s, 1H), 4.73 (s, 1H), 3.85 – 3.32 (m, 8H), 3.32 – 2.83 (m, 2H), 2.28 – 2.13 (m, 1H), 2.13 – 2.02 (m, 1H), 2.00 – 1.84 (m, 1H), 1.69 – 1.52 (m, 3H), 1.49 (s, 9H), 1.48 (s, 9H), 1.43 (s, 9H), 1.40 (s, 9H), 1.34 – 1.19 (m, 1H), 1.06 (tt, J = 15.6, 7.9 Hz, 1H), 0.89 (t, J = 7.4 Hz, 3H), 0.79 (d, J = 6.8 Hz, 3H).

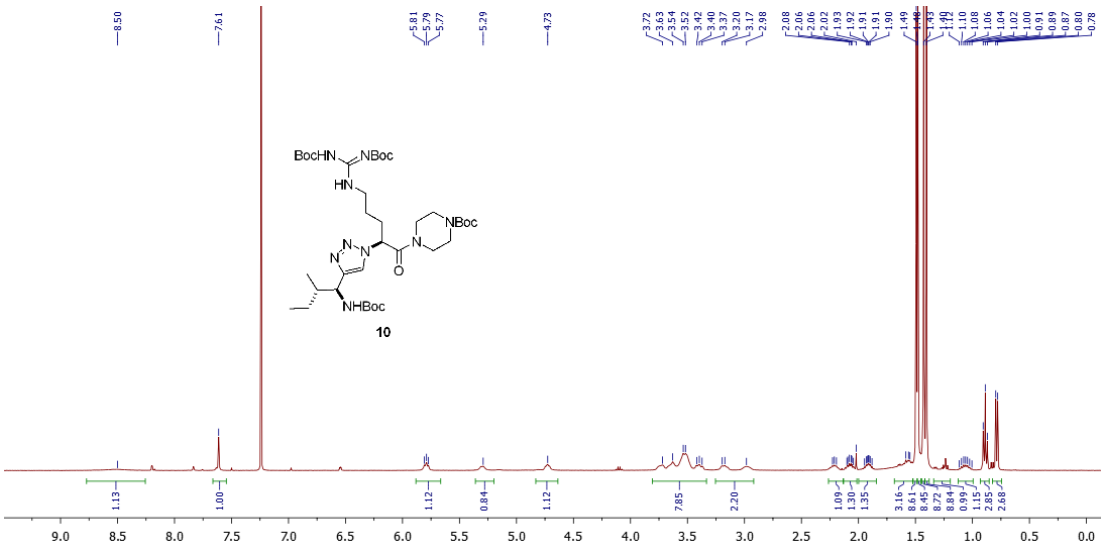

12

$C_{16}H_{27}N_3O_4$

^{1}H NMR (400 MHz, $CDCl_3$) δ 8.35 (s, 1H), 3.51 (dd, J = 12.6, 6.9 Hz, 2H), 2.25 (td, J = 7.1, 2.6 Hz, 2H), 1.95 (t, J = 2.6 Hz, 1H), 1.80 (p, J = 7.1 Hz, 2H), 1.48 (s, 9H), 1.47 (s, 9H).

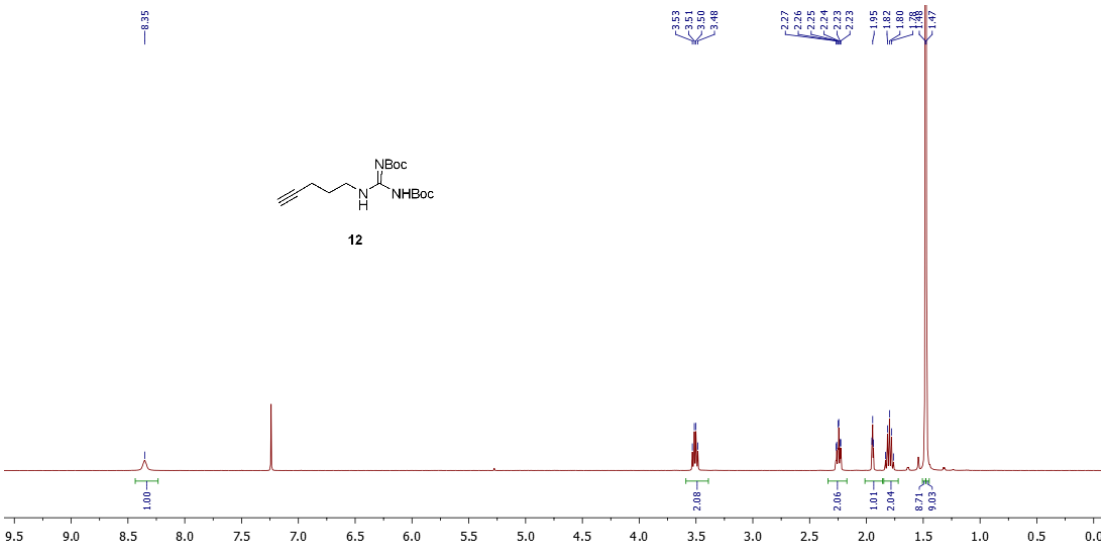

13

$C_{22}H_{38}N_6O_6$

^{1}H NMR (400 MHz, $CDCl_3$) δ 7.78 (s, 1H), 5.24 – 4.96 (m, 1H), 3.62 – 3.34 (m, 2H), 2.85 – 2.58 (m, 2H), 2.36 – 2.17 (m, 1H), 2.09 – 1.91 (m, 2H), 1.50 (s, 9H), 1.49 (s, 9H), 1.28 (dt, J = 14.3, 5.2 Hz, 2H), 1.01 (d, J = 6.6 Hz, 3H), 1.00 – 0.87 (m, 2H), 0.84 (t, J = 7.2 Hz, 3H).

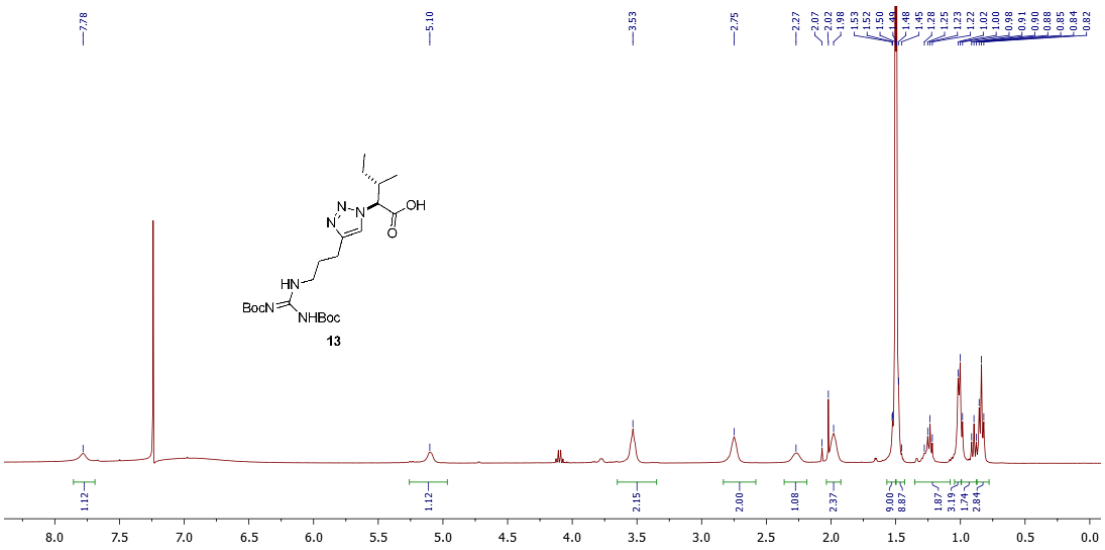

14

$C_{25}H_{37}N_5O_6$

^{1}H NMR (400 MHz, $CDCl_3$) δ 7.80 (s, 1H), 7.65 (s, 1H), 7.30 (s, 5H), 5.79 – 5.54 (m, 1H), 5.44 – 5.24 (m, 1H), 5.18 – 5.10 (m, 1H), 5.05 (s, 2H), 4.93 – 4.55 (m, 1H), 3.28 – 3.05 (m, 2H), 2.41 – 1.77 (m, 3H), 1.57 – 1.44 (m, 3H), 1.38 (s, 9H), 1.17 – 0.98 (m, 1H), 0.93 – 0.80 (m, 3H), 0.80 – 0.66 (m, 3H).

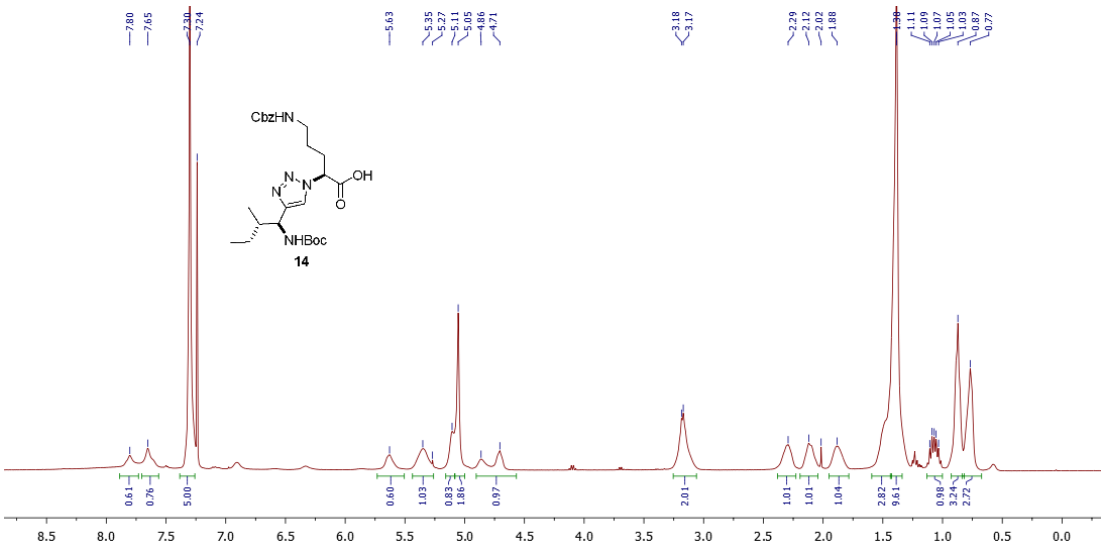

^{13}C NMR (101 MHz, $CDCl_3$) δ 171.72, 156.91, 156.03, 147.55, 136.55, 128.68, 128.31, 128.22, 121.72, 120.97, 79.93, 66.97, 62.62, 51.61, 40.14, 39.36, 29.93, 28.47, 26.33, 25.47, 15.41, 11.50.

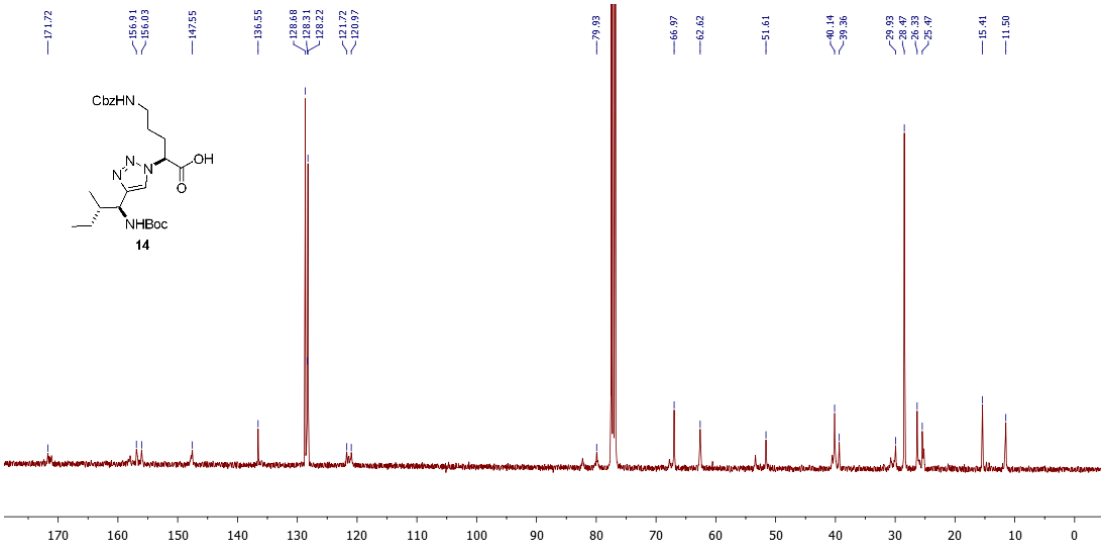

15

$C_{17}H_{31}N_5O_4$

^{1}H NMR (400 MHz, MeOD) δ 7.92 (s, 1H), 5.22 (dd, J = 8.9, 5.4 Hz, 1H), 4.69 (d, J = 6.6 Hz, 1H), 2.96 (td, J = 8.2, 3.4 Hz, 2H), 2.44 – 2.15 (m, 2H), 1.96 – 1.80 (m, 1H), 1.77 – 1.63 (m, 1H), 1.61 – 1.47 (m, 2H), 1.43 (s, 9H), 1.23 – 1.08 (m, 1H), 0.93 (t, J = 7.4 Hz, 3H), 0.83 (d, J = 6.8 Hz, 3H).

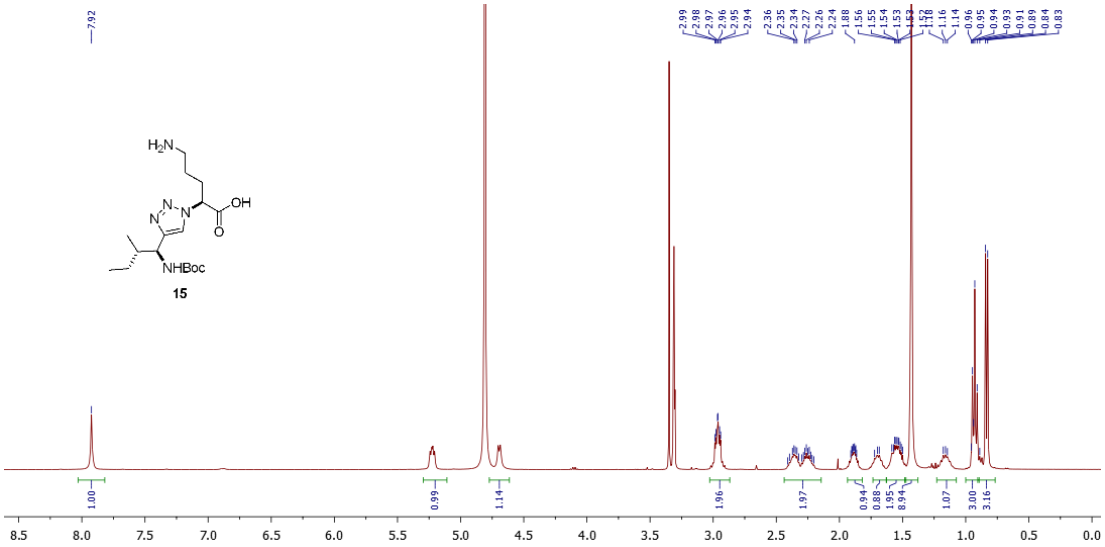

^{13}C NMR (101 MHz, MeOD) δ 173.66, 157.79, 149.27, 123.42, 80.28, 66.01, 53.27, 40.63, 40.01, 30.68, 28.77, 26.31, 25.36, 16.00, 11.65.

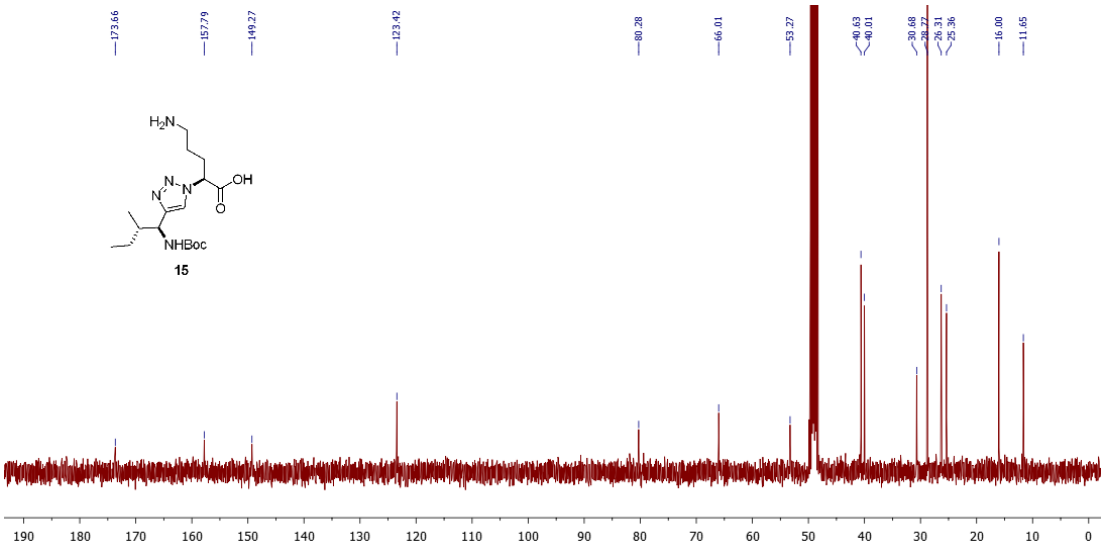

16

$C_{28}H_{49}N_7O_8$

^{1}H NMR (400 MHz, MeOD) δ 7.90 (s, 1H), 7.84 (s, 1H), 5.46 (dd, J = 9.4, 4.3 Hz, 1H), 4.66 (d, J = 5.5 Hz, 1H), 3.45 – 3.31 (m, 2H), 2.40 – 2.15 (m, 2H), 1.94 – 1.80 (m, 1H), 1.48 (s, 9H), 1.44 (s, 9H), 1.52 – 1.36 (m, 4H), 1.38 (s, 9H), 1.21 – 1.06 (m, 1H), 0.88 (t, J = 7.4 Hz, 3H), 0.79 (d, J = 6.8 Hz, 3H).

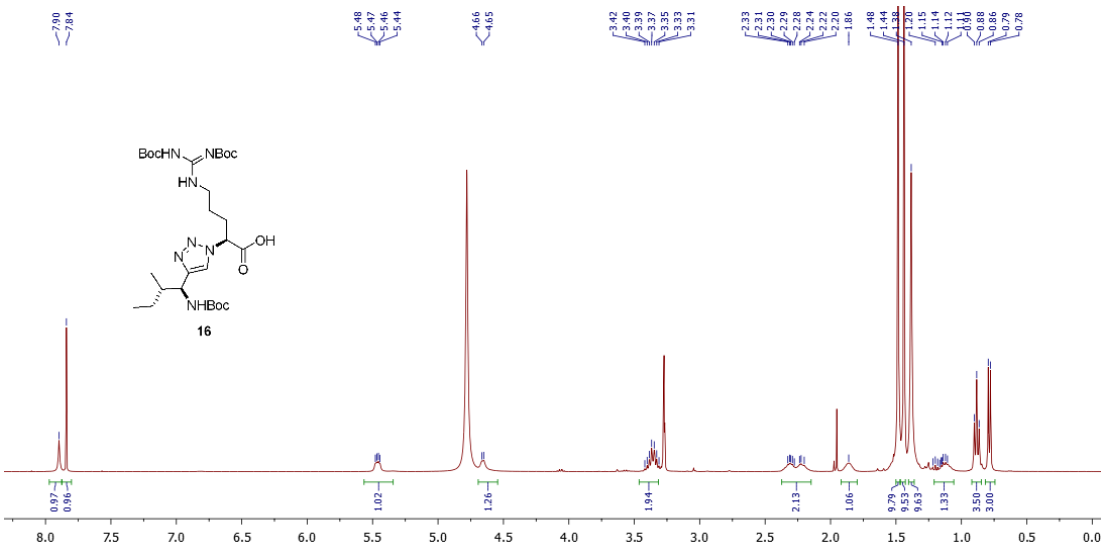

17-F

$C_{58}H_{68}BF_2N_{17}O_4$

^{1}H NMR (400 MHz, MeOD) δ 8.39 (s, 2H), 8.06 (s, 2H), 7.99 (d, J = 7.5 Hz, 4H), 7.76 (d, J = 6.7 Hz, 2H), 7.53 (d, J = 5.6 Hz, 2H), 7.18 – 7.08 (m, 2H), 7.04 (s, 2H), 6.88 (d, J = 7.5 Hz, 4H), 5.41 (d, J = 9.1 Hz, 2H), 3.80 (s, 6H), 3.77 – 3.53

(m, 10H), 3.30 – 3.23 (m, 4H), 2.96 – 2.83 (m, 4H), 2.55 – 2.41 (m, 2H), 2.08 – 1.95 (m, 4H), 1.33 – 1.25 (m, 2H), 1.12 – 1.08 (m, 6H), 0.93 – 0.87 (m, 6H).

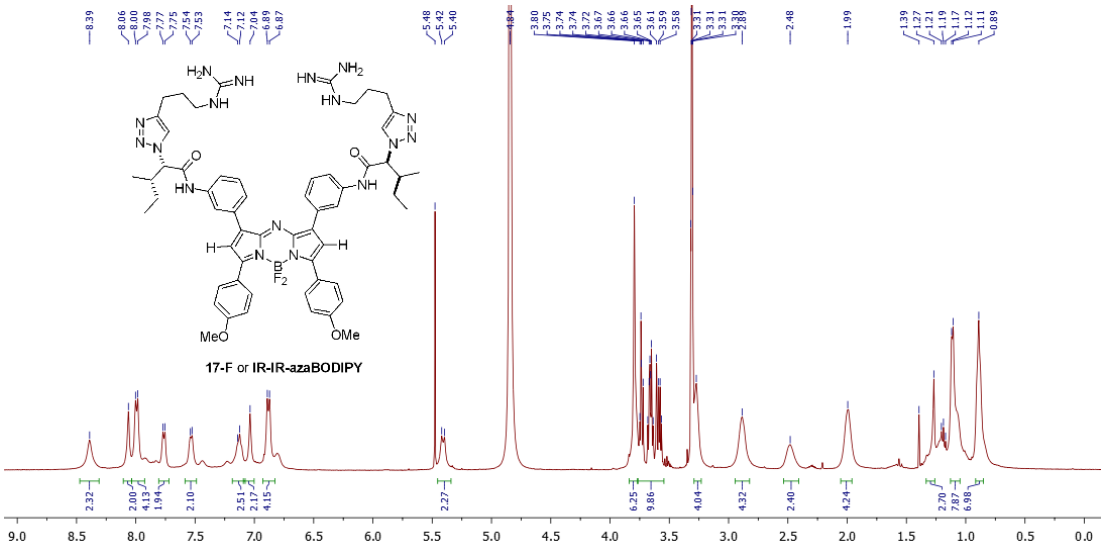

17-PDT

$C_{58}H_{66}BF_2I_2N_{17}O_4$

^{1}H NMR (400 MHz, MeOD) δ 8.41 (s, 2H), 8.15 (s, 2H), 8.07 – 7.85 (m, 2H), 7.82 – 7.59 (m, 4H), 7.42 – 7.22 (m, 2H), 7.21 – 6.90 (m, 4H), 5.47 – 5.30 (m, 2H), 4.31 – 4.18 (m, 4H), 3.92 – 3.74 (m, 8H), 3.68 (s, 6H), 3.03 – 2.85 (m, 2H), 2.61 – 2.40 (m, 2H), 2.14 – 1.88 (m, 4H), 1.42 – 1.25 (m, 4H), 1.22 – 1.07 (m, 6H), 1.00 – 0.84 (m, 6H).

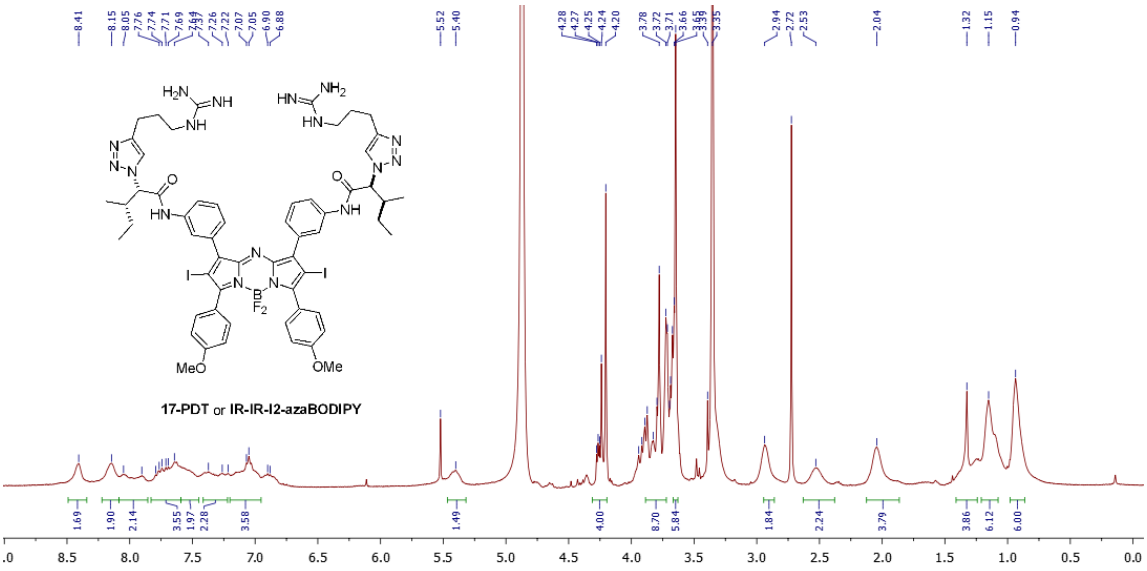

19

$C_{46}H_{46}BF_2N_{11}O_4$

^{1}H NMR (400 MHz, $CDCl_3$) δ 8.07 – 8.01 (m, 4H), 8.00 (s, 2H), 7.93 (s, 2H), 7.80 (d, J = 7.7 Hz, 2H), 7.74 (d, J = 7.7 Hz, 2H), 7.38 (t, J = 7.3 Hz, 2H), 7.04 (s, 2H), 6.96 (d, J = 7.5 Hz, 4H), 3.95 – 3.88 (m, 2H), 3.84 (s, 6H), 2.03 – 1.89 (m, 2H), 1.55 – 1.45 (m, 2H), 1.31 – 1.25 (m, 2H), 1.09 – 1.01 (m, 6H), 0.98 – 0.90 (m, 6H).

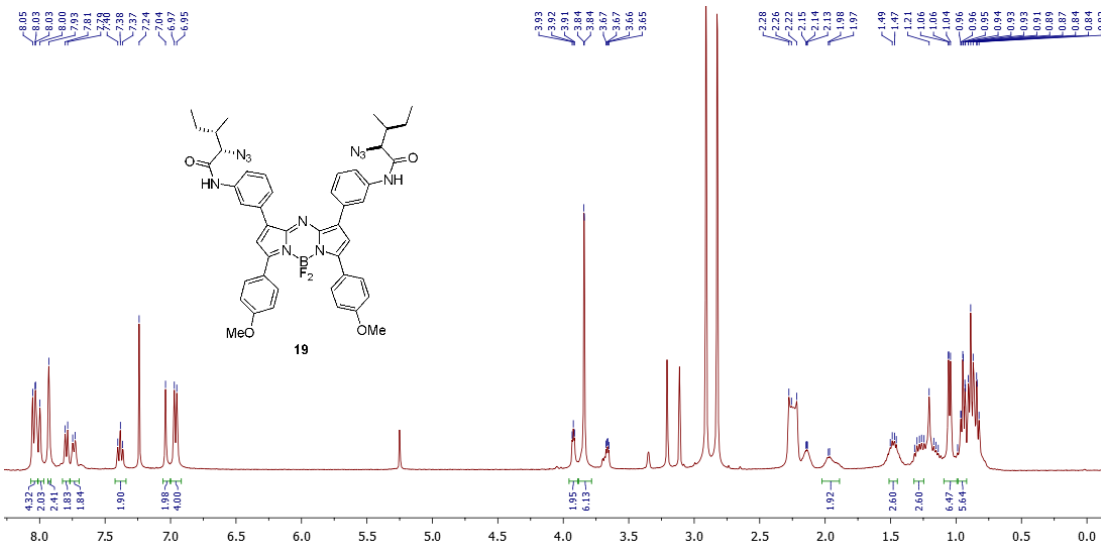

^{19}F NMR (376 MHz, $CDCl_3$) δ -78.61, -78.62, -79.38.

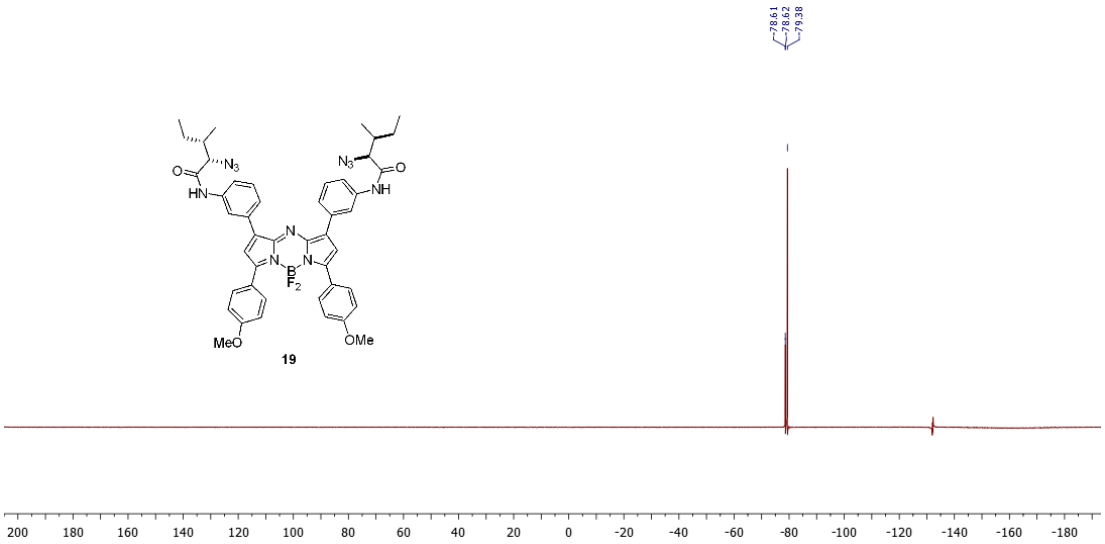

20-F

$C_{78}H_{100}BF_2N_{17}O_{12}$

^{1}H NMR (400 MHz, $CDCl_3$) δ 9.07 (s, 2H), 8.39 (t, J = 5.1 Hz, 2H), 8.03 (d, J = 8.5 Hz, 5H), 7.77 (s, 2H), 7.68 (d, J = 7.8 Hz, 2H), 7.55 (d, J = 8.0 Hz, 2H), 7.28

(t, J = 7.9 Hz, 2H), 6.96 (d, J = 9.1 Hz, 5H), 5.09 (d, J = 10.1 Hz, 2H), 3.83 (s, 6H), 3.45 (dd, J = 12.7, 6.5 Hz, 4H), 2.76 (t, J = 7.5 Hz, 4H), 2.46 – 2.31 (m, 2H), 1.95 (dt, J = 14.5, 7.3 Hz, 4H), 1.47 (s, 18H), 1.46 (s, 18H), 1.30 – 1.12 (m, 4H), 1.05 (d, J = 6.6 Hz, 6H), 1.00 – 0.90 (m, 4H), 0.82 (t, J = 7.3 Hz, 6H).

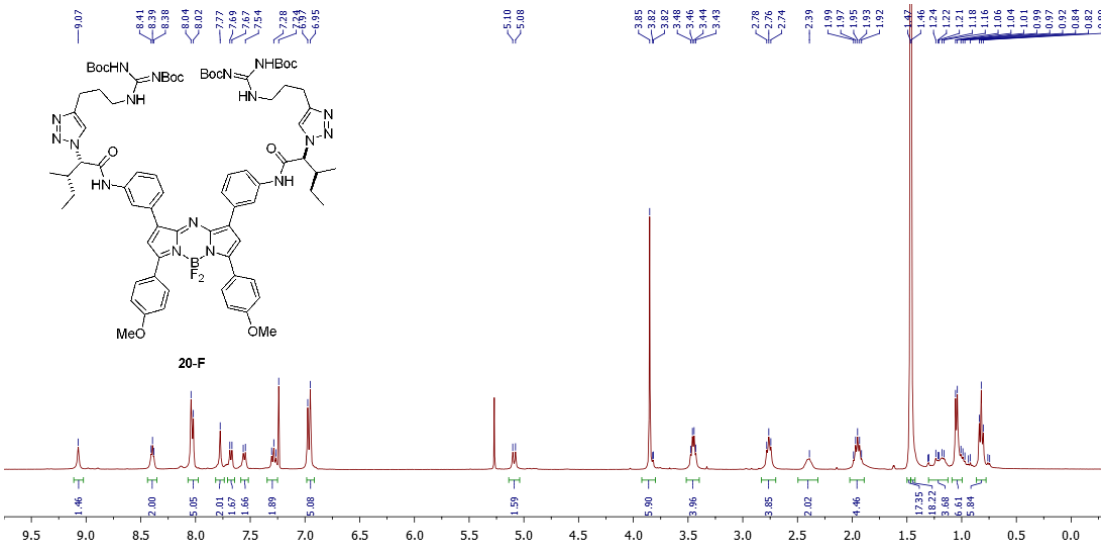

^{13}C NMR (101 MHz, $CDCl_3$) δ 166.66, 163.75, 162.19, 158.30, 156.45, 153.44, 147.57, 145.46, 142.90, 137.31, 133.57, 131.91, 131.86, 129.20, 126.26, 124.14, 121.80, 121.67, 119.57, 114.41, 83.28, 79.44, 70.19, 55.56, 40.32, 38.49, 28.82, 28.48, 28.22, 25.07, 23.19, 15.63, 10.53.

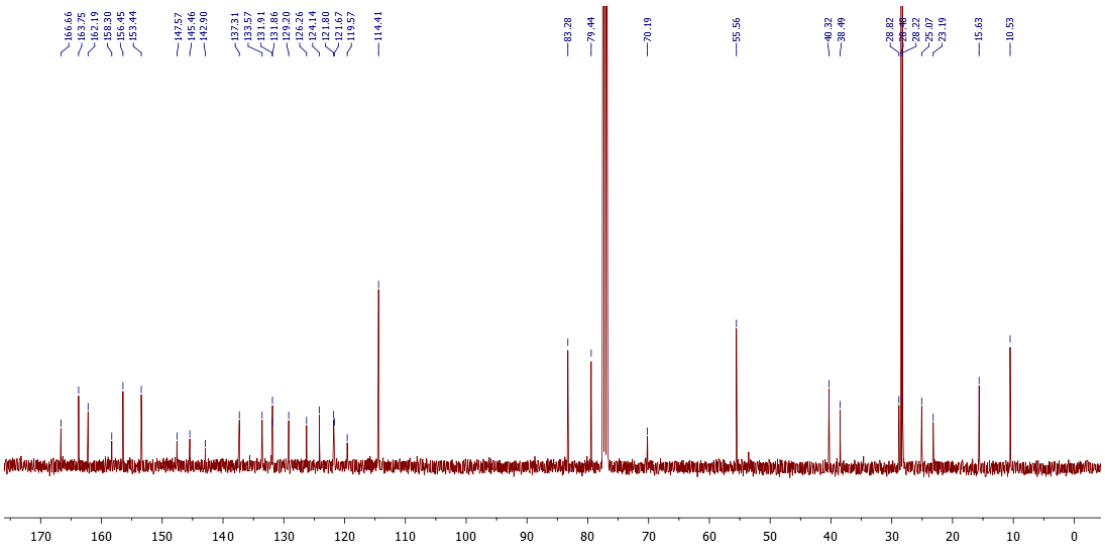

^{11}B NMR (128 MHz, $CDCl_3$) δ 1.14, 0.90, 0.65.

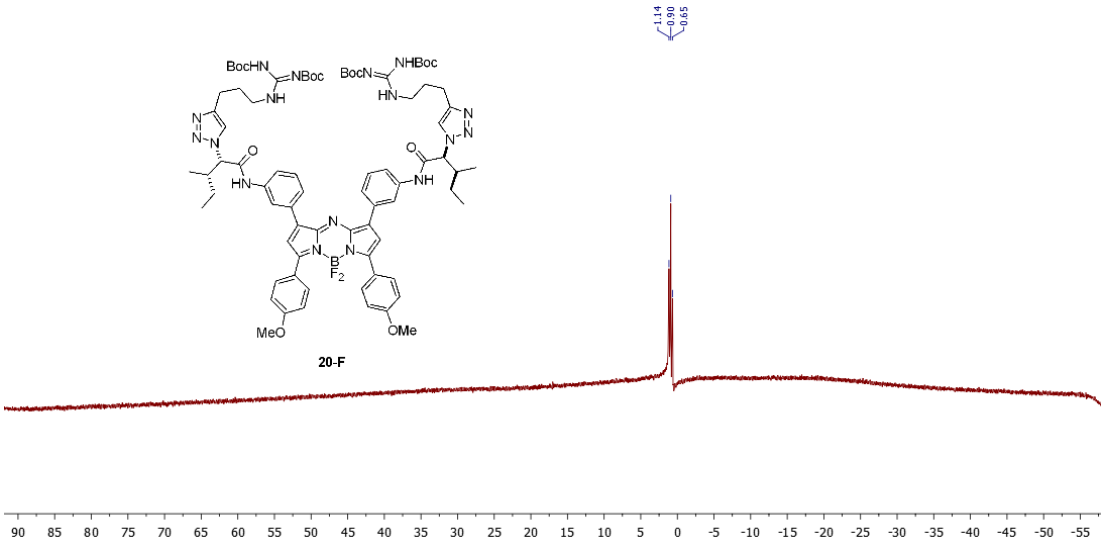

20-PDT

$C_{78}H_{98}BF_2I_2N_{17}O_{12}$

^{1}H NMR (400 MHz, MeOD) δ 8.06 (s, 2H), 8.01 (s, 2H), 7.62 (d, J = 8.7 Hz, 4H), 7.57 (d, J = 8.1 Hz, 2H), 7.46 (d, J = 7.9 Hz, 2H), 7.12 (t, J = 8.0 Hz, 2H), 6.97 (d,

J = 8.9 Hz, 4H), 5.19 (d, J = 10.7 Hz, 2H), 3.84 (s, 6H), 3.43 – 3.36 (m, 4H), 2.77 (t, J = 7.5 Hz, 4H), 2.46 – 2.35 (m, 2H), 1.96 – 1.89 (m, 4H), 1.49 (s, 18H), 1.43 (s, 18H), 1.25 – 1.12 (m, 4H), 1.07 (d, J = 6.7 Hz, 6H), 0.86 (t, J = 7.4 Hz, 6H).

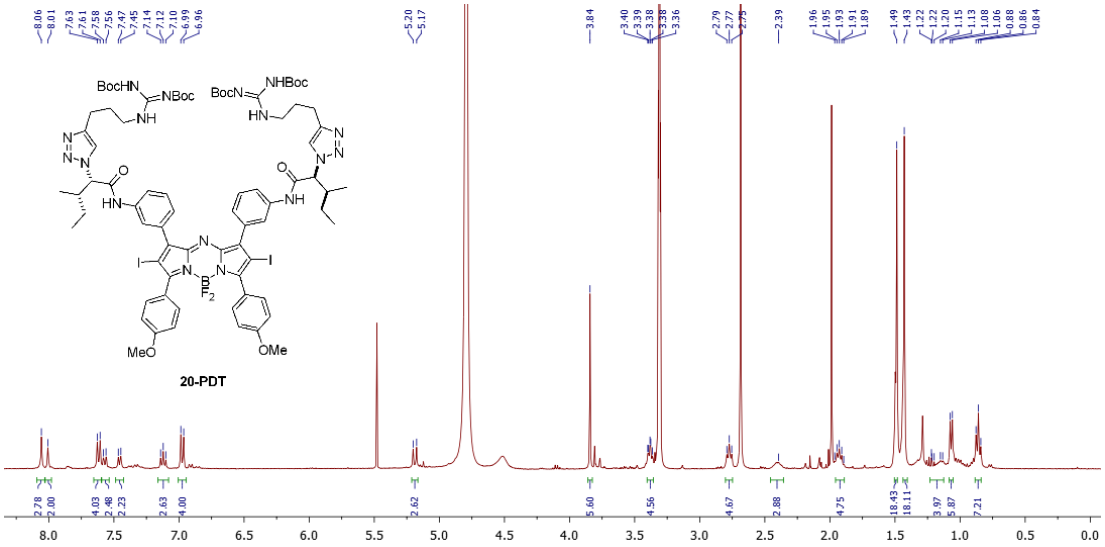

^{11}B NMR (128 MHz, MeOD) δ 0.32, 0.07, -0.13.

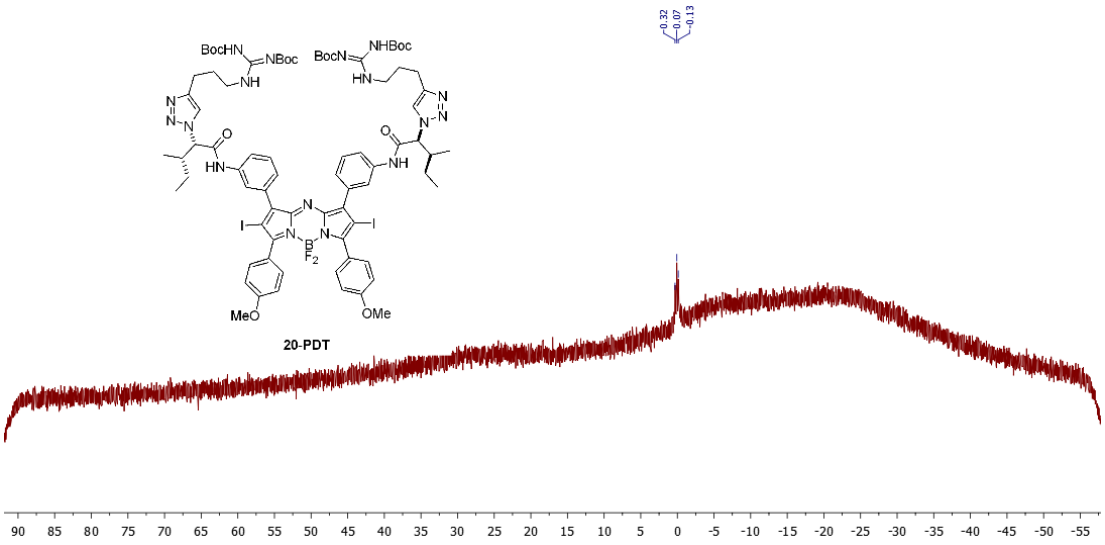

21-F

$C_{90}H_{122}BF_2N_{19}O_{16}$

^{1}H NMR (400 MHz, $CDCl_3$) δ 8.09 – 7.97 (m, 2H), 7.93 (d, J = 8.2 Hz, 2H), 7.84 (d, J = 13.4 Hz, 2H), 7.74 – 7.60 (m, 2H), 7.59 – 7.44 (m, 6H), 7.20 – 7.11 (m, 2H), 6.97 – 6.78 (m, 4H), 6.76 – 6.48 (m, 2H), 5.55 – 5.30 (m, 2H), 4.89 – 4.66 (m, 4H), 3.80 (s, 6H), 2.21 – 2.04 (m, 2H), 1.98 – 1.78 (m, 4H), 1.62 – 1.16 (m, 54H), 1.16 – 1.03 (m, 4H), 0.89 (t, J = 7.2 Hz, 6H), 0.80 (d, J = 6.4 Hz, 6H). 0.89 – 0.75 (m, 12H).

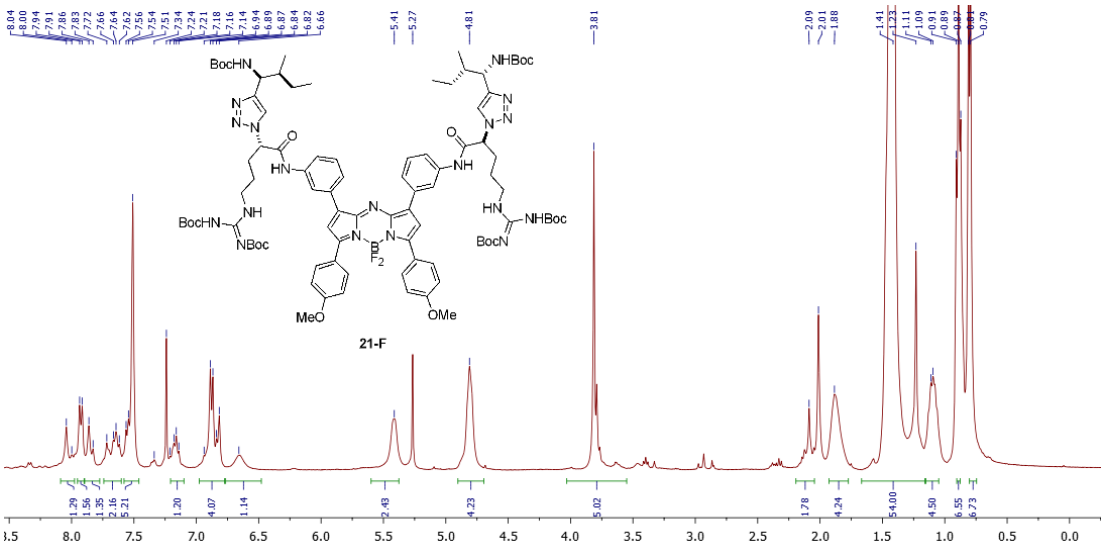

^{11}B NMR (128 MHz, $CDCl_3$) δ 1.06, 0.81, 0.56.

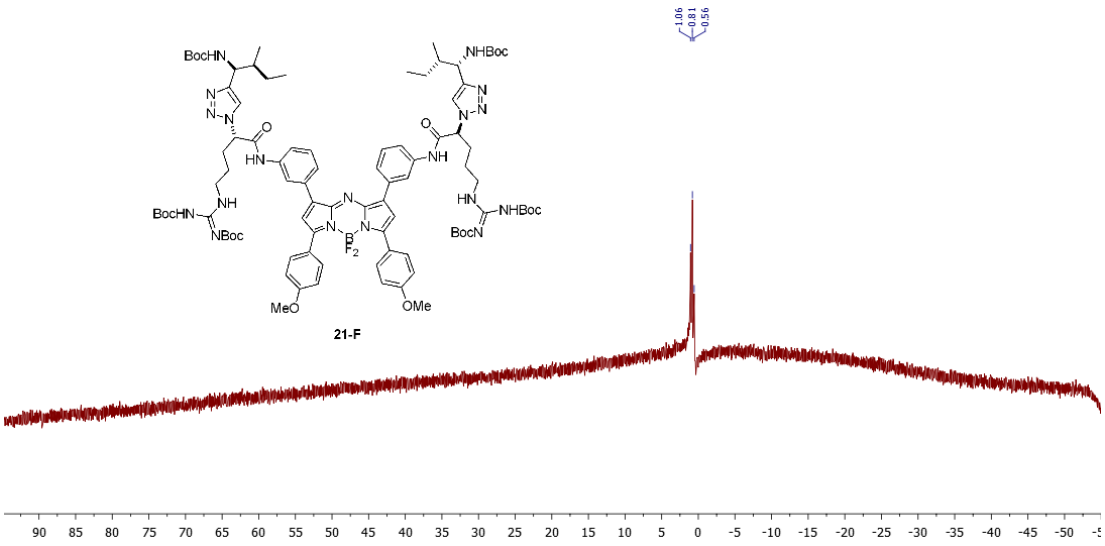

^{19}F NMR (376 MHz, $CDCl_3$) δ -131.01.

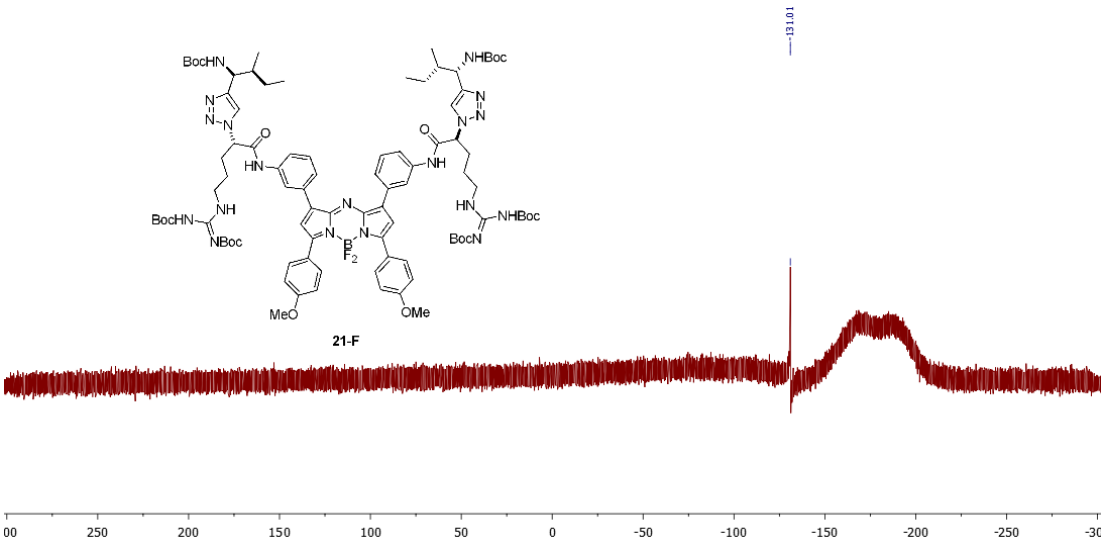

22

$C_{50}H_{77}F_2N_{23}O_7$

^1H NMR (400 MHz, MeOD) δ 8.33 (d, J = 7.6 Hz, 1H), 7.94 (s, 2H), 7.46 (d, J = 7.6 Hz, 1H), 6.31 – 6.20 (m, 1H), 5.67 (d, J = 10.3 Hz, 2H), 4.65 – 4.52 (m, 1H),

4.48 – 4.23 (m, 1H), 4.06 – 3.35 (m, 18H), 3.24 (t, J = 7.0 Hz, 4H), 3.04 – 2.85 (m, 2H), 2.77 (dd, J = 17.4, 9.8 Hz, 4H), 2.62 – 2.50 (m, 2H), 2.48 – 2.33 (m, 2H), 2.06 – 1.81 (m, 6H), 1.69 – 1.51 (m, 2H), 1.16 – 1.07 (m, 4H), 1.04 (d, J = 6.7 Hz, 6H), 0.86 (t, J = 7.4 Hz, 6H).

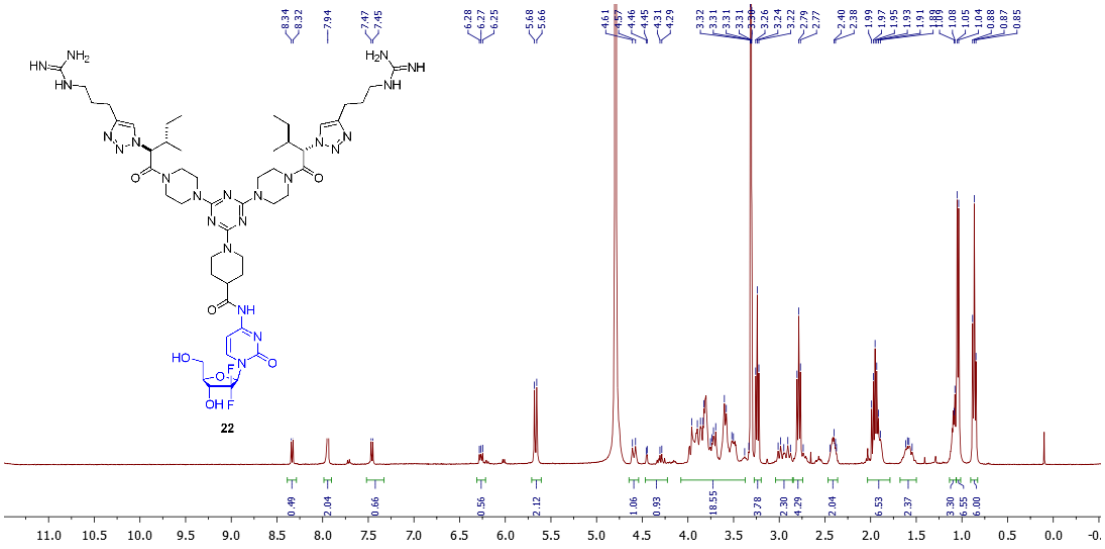

^{13}C NMR (101 MHz, MeOD) δ 178.57, 178.46, 177.49, 168.50, 166.71, 166.33, 158.81, 157.61, 148.26, 146.07, 122.39, 98.29, 64.87, 60.31, 47.26, 44.54, 43.89, 43.71, 43.59, 42.46, 41.77, 39.10, 29.52, 29.25, 29.16, 25.72, 23.26, 15.76, 10.90.

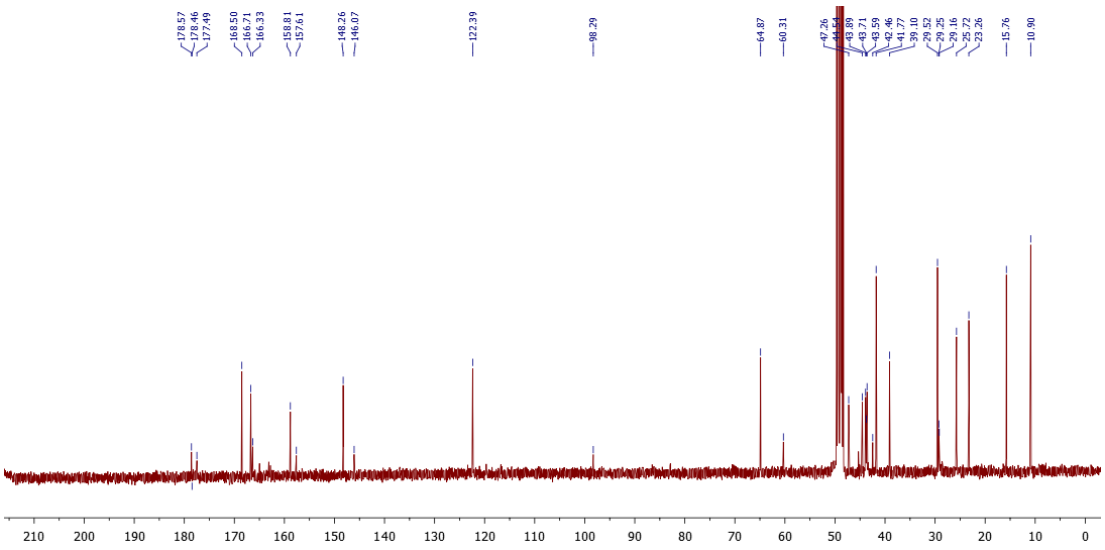

23

$C_{20}H_{28}F_2N_4O_7$

^{1}H NMR (400 MHz, MeOD) δ 8.34 (d, J = 7.6 Hz, 1H), 7.48 (d, J = 7.5 Hz, 1H), 6.34 – 6.14 (m, 1H), 4.59 – 4.43 (m, 2H), 4.30 (td, J = 12.1, 8.2 Hz, 1H), 4.17 – 4.06 (m, 2H), 4.02 – 3.92 (m, 2H), 3.81 (dd, J = 13.2, 3.6 Hz, 1H), 2.95 – 2.79 (m, 2H), 2.65 (ddd, J = 14.9, 7.4, 3.8 Hz, 1H), 1.93 – 1.80 (m, 2H), 1.62 (td, J = 12.3, 4.1 Hz, 2H), 1.47 (s, 9H).

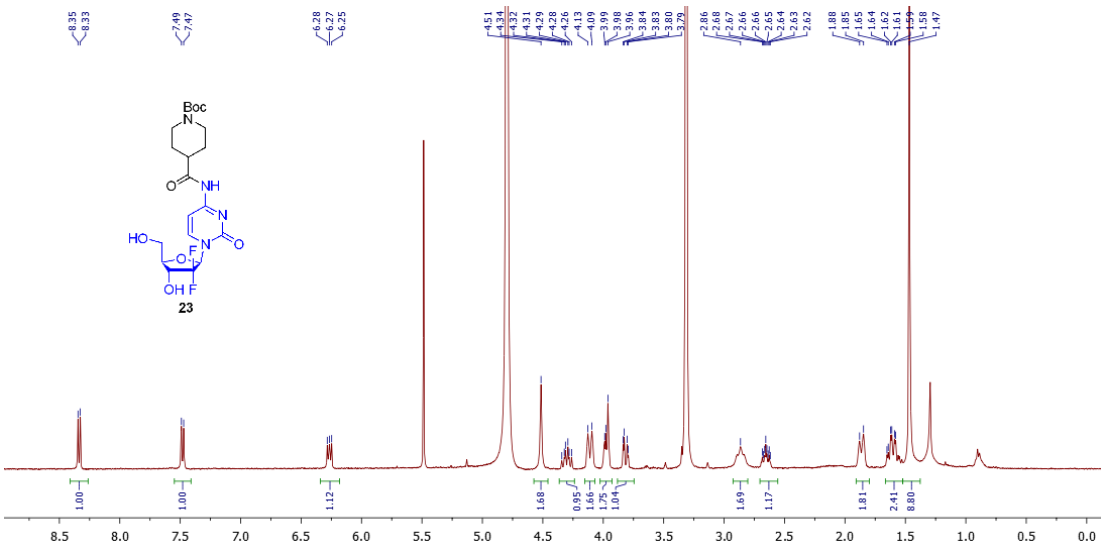

^{13}C NMR (101 MHz, MeOD) δ 177.24, 165.00, 157.63, 156.47, 156.43, 146.06, 98.31, 82.95, 81.23, 70.48, 70.03, 60.31, 54.77, 44.75, 29.18, 28.67.

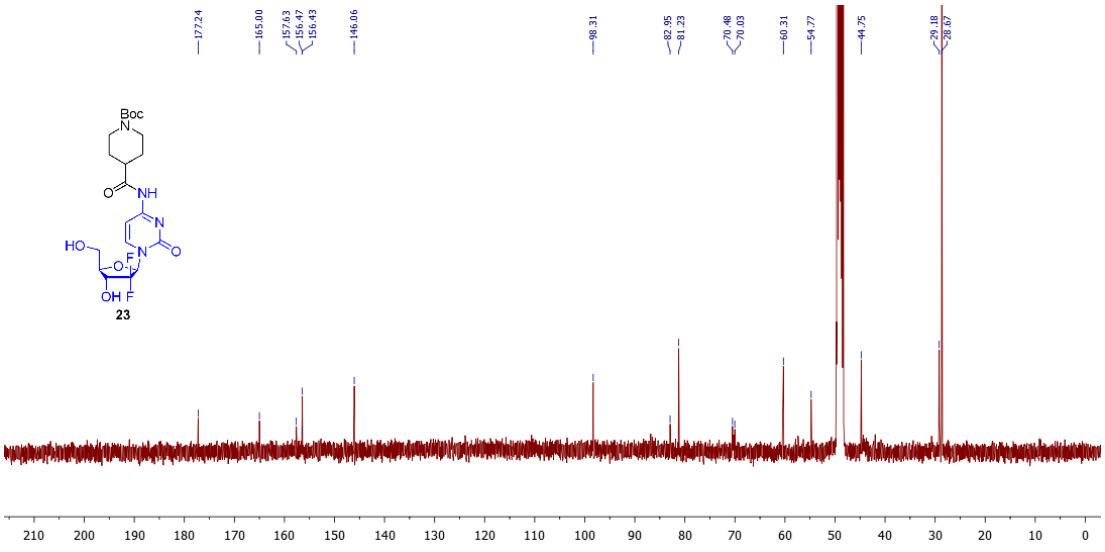

25

$C_{18}H_{25}N_5O_3$

^{1}H NMR (400 MHz, $CDCl_3$) δ 7.39 – 7.28 (m, 5H), 5.13 (s, 2H), 3.77 – 3.65 (m, 1H), 3.62 – 3.43 (m, 8H), 2.08 – 1.97 (m, 1H), 1.77 – 1.67 (m, 1H), 1.24 (ddq, J = 14.5, 11.0, 7.3 Hz, 1H), 0.92 (t, J = 7.4 Hz, 3H), 0.89 (d, J = 6.7 Hz, 3H).

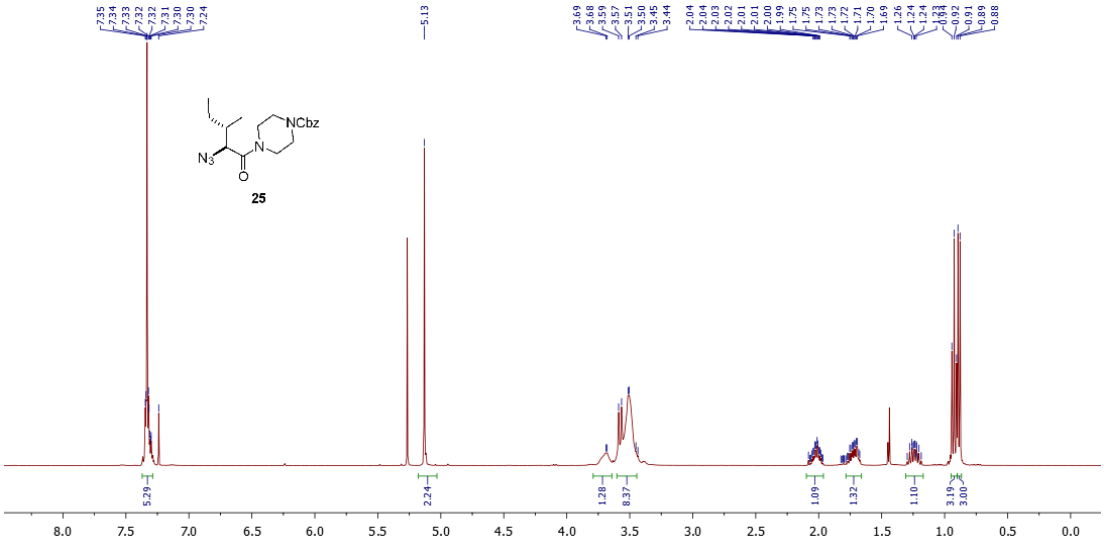

26

$C_{26}H_{46}N_8O_5$

^{1}H NMR (400 MHz, MeOD) δ 7.92 (s, 1H), 5.57 (d, J = 10.3 Hz, 1H), 3.83 – 3.60 (m, 3H), 3.49 (ddd, J = 13.1, 7.5, 3.3 Hz, 1H), 3.41 (t, J = 7.0 Hz, 2H), 2.86 – 2.74 (m, 4H), 2.73 – 2.63 (m, 1H), 2.60 – 2.51 (m, 1H), 2.45 – 2.34 (m, 1H), 2.01 – 1.89 (m, 2H), 1.53 (s, 9H), 1.47 (s, 9H), 1.10 – 1.03 (m, 2H), 1.02 (d, J = 6.7 Hz, 3H), 0.85 (t, J = 7.4 Hz, 3H).

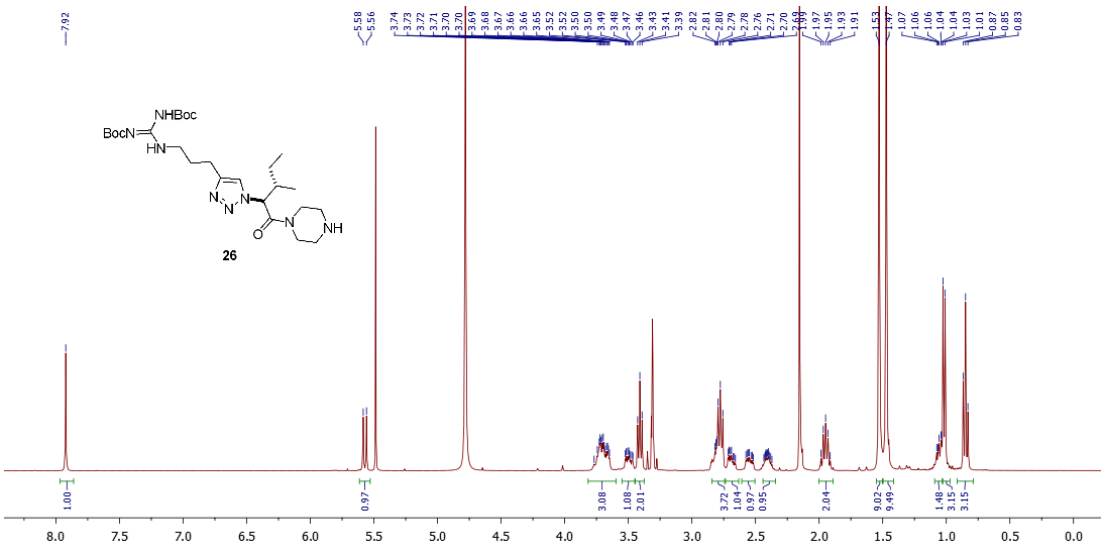

28

$C_{67}H_{105}N_{21}O_{12}$

^{1}H NMR (400 MHz, $CDCl_3$) δ 8.53 (s, 2H), 7.67 (s, 2H), 7.42 – 7.28 (m, 5H), 5.41 (d, J = 10.5 Hz, 2H), 5.16 (s, 2H), 3.96 – 3.34 (m, 30H), 2.78 (t, J = 7.7 Hz, 4H), 2.45 – 2.30 (m, 2H), 2.07 – 1.91 (m, 4H), 1.50 (s, 18H), 1.49 (s, 18H), 1.13 – 1.02 (m, 4H), 1.01 (d, J = 6.6 Hz, 6H), 0.84 (t, J = 7.2 Hz, 6H).

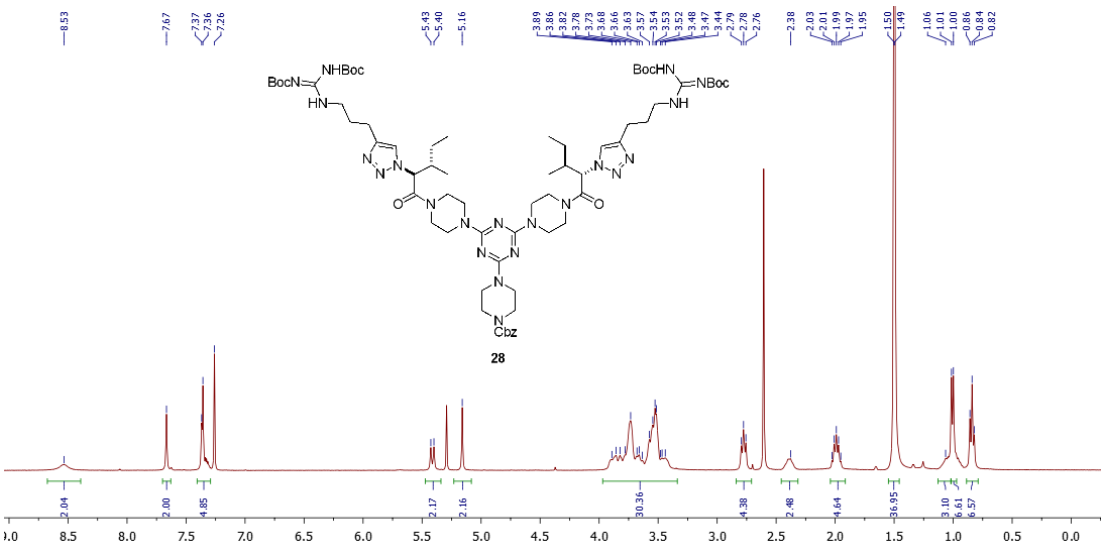

^{13}C NMR (101 MHz, $CDCl_3$) δ 166.97, 165.15, 155.98, 155.46, 153.27, 147.56, 136.75, 128.68, 128.25, 128.07, 119.88, 67.47, 63.55, 46.28, 43.81, 43.53, 43.19, 43.10, 42.44, 41.21, 38.01, 28.77, 28.41, 28.21, 24.72, 23.24, 15.92, 10.57.

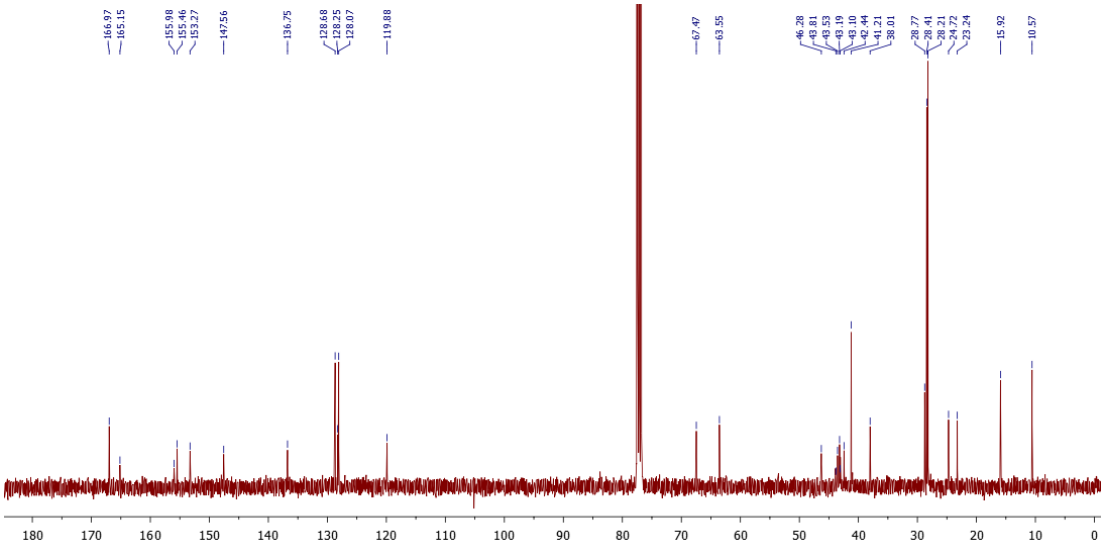

30

$C_{79}H_{127}N_{23}O_{16}$

^{1}H NMR (400 MHz, $CDCl_3$) δ 8.32 (s, 2H), 7.59 (s, 2H), 7.38 – 7.25 (m, 5H), 5.87 – 5.65 (m, 2H), 5.12 (s, 2H), 4.86 – 4.61 (m, 2H), 3.92 – 3.16 (m, 34H), 2.31 – 1.77 (m, 10H), 1.45 (s, 36H), 1.38 (s, 18H), 1.12 – 0.95 (m, 2H), 0.91 – 0.81 (m, 6H), 0.77 (dd, J = 16.7, 6.9 Hz, 6H).

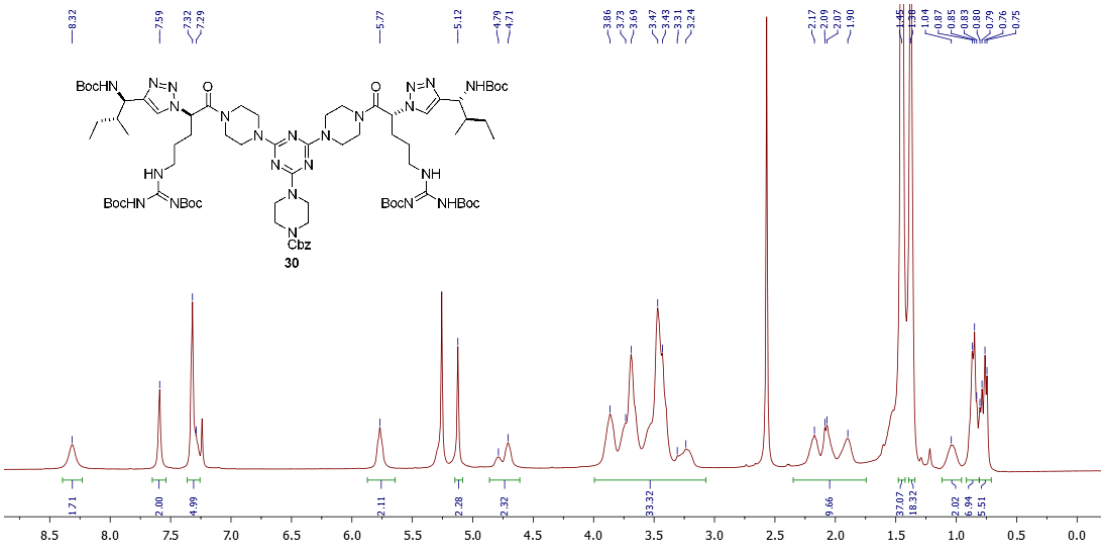

^{13}C NMR (101 MHz, $CDCl_3$) δ 166.15, 165.24, 156.31, 155.49, 155.41, 153.33, 136.71, 128.62, 128.19, 128.00, 119.97, 119.80, 83.57, 79.50, 67.39, 58.96, 53.51, 51.76, 45.93, 43.82, 43.36, 43.06, 42.82, 42.58, 41.14, 39.76, 39.60, 39.47, 30.11, 28.47, 28.38, 28.16, 26.06, 25.43, 15.31, 14.58, 11.62.

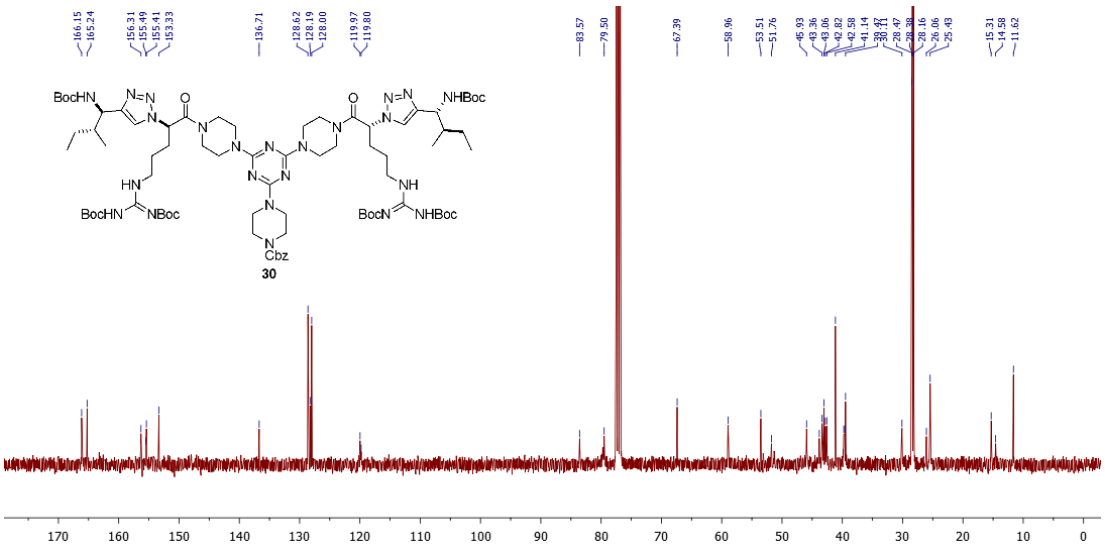
166.15
165.24
156.31
155.49
155.41
153.33
136.71
128.62
128.19
128.00
119.97
119.80
83.57
79.50
67.39
58.96
53.51
51.76
45.93
43.36
43.06
42.82
42.58
41.14
28.47
28.38
28.16
26.06
25.43
15.31
14.58
11.62
BocHN
NHBoc
HN
BocHN
NBoc
NH
BocN
NHBoc
N
Cbz
30
170
160
150
140
130
120
110
100
90
80
70
60
50
40
30
20
10
0

APPENDIX B

DESIGN AND MODIFICATION OF ACTIVELY TARGETED, NEAR-IR ABSORBING, THERANOSTIC AGENTS FOR METASTATIC BREAST CANCER

B.1 Introduction

Breast cancer is one of the most commonly diagnosed cancers in US,[182] and targeted therapies have been established based on selective binding with several different cell surface receptors {(estrogen receptor (ER), progesterone receptor (PR) and human epidermal growth factor receptor 2 (HER2)}.[61,212,213] Metastatic breast cancer, a more aggressive form with poor prognoses, does not always have these biomarkers. If none of the three are present on cell surface then it is called “triple negative” [54,214]).

Several inhibitors of kinases involved in the cellular signaling pathways have been actively studied e.g. Cyclin-dependent kinase (CDK) 4/6, Phosphoinositide 3-kinase (PI3K).[215,216] Yet, these compounds are not designed for active targeting to cancer cells via cell surface receptors. Tropomyosin kinase receptor C (TrkC), a member of the receptor tyrosine kinase family, along with its selective natural ligand neurotrophin-3 (NT-3) are proven to be essential for proliferation and metastasis of metastatic breast and other types of cancer.[1,2,75,80,176] This provides potential in developing novel targeting strategies for diagnosis and treatment of metastatic breast cancer.

As discussed in previous chapters, small molecule targeting agents have several advantages over mAbs in tumor targeting.[217] Previous work in our group revealed a synthetic small molecule targeting moiety that preferably binds to TrkC on metastatic breast cancer cells.[41] A library of 152 fluorescein-labeled peptidomimetics was screened through a FACS-based binding assay via flow cytometer on cells that were transformed to stably express TrkA, TrkC, or p75. Only 10 out of 152 compounds bound significantly and selectively to $TrkC^+$ cells. Selected probes were then equipped with biotin tags and subjected to a second binding assay. This screening method narrowed the positive hit compounds to 8 that were tested in further cell-based assay. Finally, a bivalent **IY-IY** moiety (I stands for isoleucine or Ile, Y for tyrosine or Tyr) gave best binding affinity and internalized in $TrkC^+$ cells.[41,42]

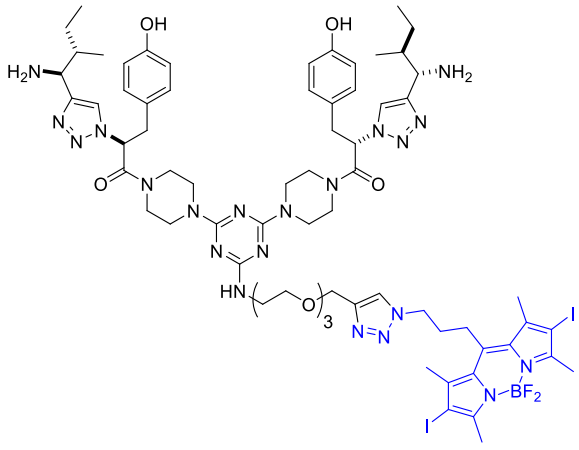

A

A “first generation” targeted therapeutic agent **A** based on the screening result showed enhanced killing of TrkC$^+$ cells *in vitro*, and ablated metastatic breast tumors completely *in vivo* after one dose (10 mg/kg) and one illumination.[3] The outstanding results encouraged us to develop theranostic agents with advance design. Therefore, a “second generation” targeted agent **B** and **C** were accomplished by fusing the targeting moiety with a near-IR absorbing aza-BODIPY.[72,209] These imaging agents had a much longer absorbance wavelength and were more compact, thus giving a better chance of non-invasive photodynamic therapy with near-IR light ignition.[205] Aza-BODIPYs can absorb light around 700 nm, but tend to be hydrophobic. Coupling with a pair of cysteic acid significantly increased the hydrophilicity of the probe.[209] Histochemistry of agent **C** on human breast tissue array showed that the agent stained on breast cancer tissue brighter than normal breast tissue, and *in vivo* imaging presented enhanced tumor staining compared to its scrambled control.[72]

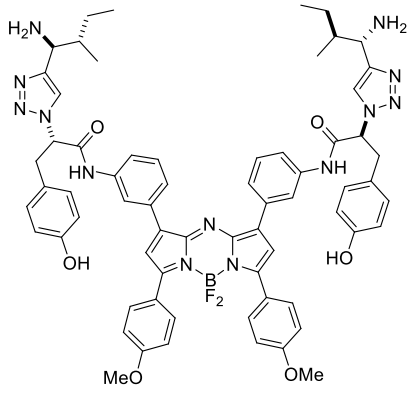

B

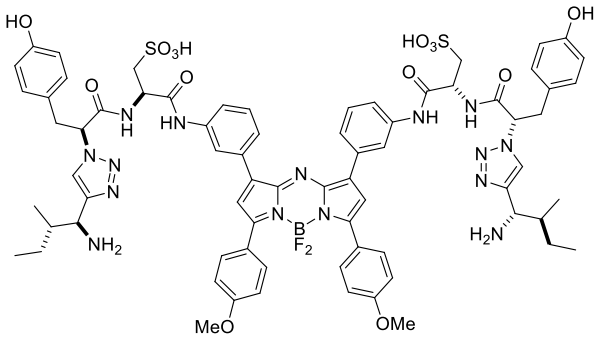

C

Previous protocol[72] was unable to generate the second-generation photosensitizers due to problems with incorporation of iodine. Specifically, iodination reagents react with tyrosine phenol, so iodination must precede incorporation of that residue, but the C-I bond in the product was cleaved by copper in the “click” reaction (Dr. Kamkaew, Thesis). Thus, forming the proposed second-generation targeting agent **1** and its control **2** was an unsolved challenge. If success, the second-generation agent **1** will have improved ability to treat tumors buried in deep tissues, give high signal-to-noise ratio in imaging, while retaining the theranostic properties for TrkC^{+} metastatic breast cancer.

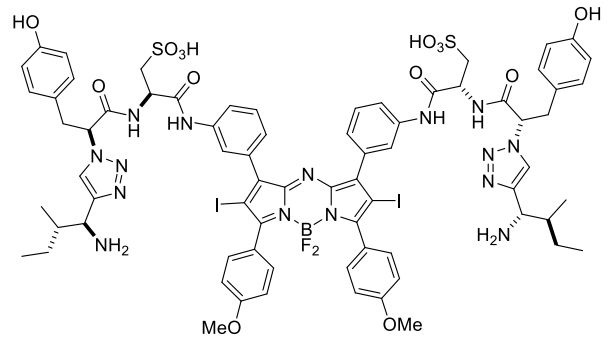

1

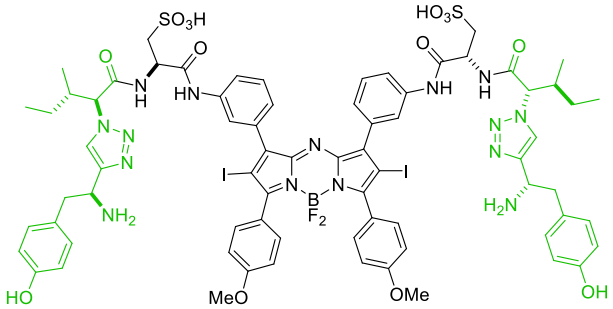

2

Evolving the conformational design of the original targeting moiety can potentially enhance the affinity of the theranostic agent to the target TrkC protein. In this work, a computational strategy created by our group and collaborator, exploring key orientations on secondary structures (EKOS),[48] was used to develop better backbone scaffolds for bivalent peptidomimetic ligands.

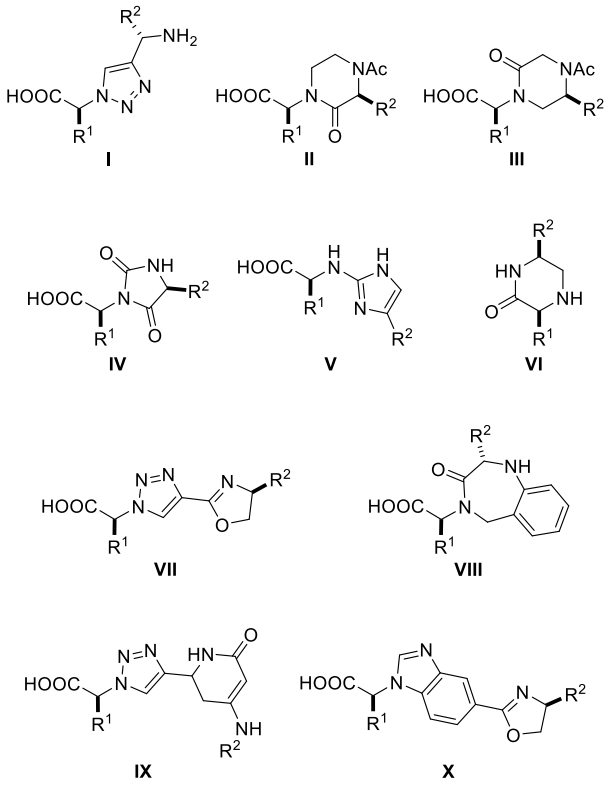

Figure B.1. Molecular structures of all dipeptide mimics evaluated by EKOS.

EKOS was developed to explore the potential semi-rigid peptide mimics with three amino acid residues on ideal secondary structures. The Cα and Cβ coordinates of each residue within the molecule is overlaid on corresponding

coordinates within the peptide secondary structures. The level of fit is quantified in terms of root mean squared deviation (RMSD, Å) for each overlay. This computational approach can guide the development and synthesis of dipeptide mimetics by highlighting proposed structures that cannot achieve the desired conformations to bind.

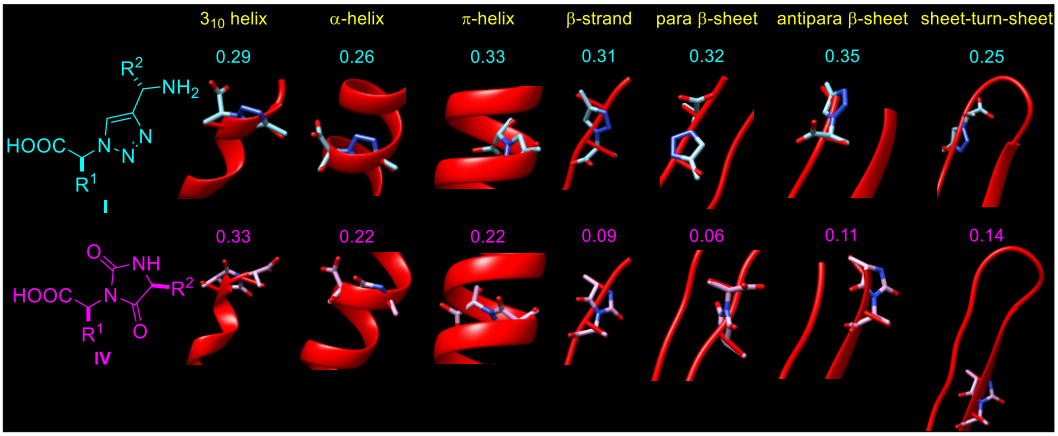

Figure B.2. List of the overlay RMSD values (Å) of R^1 and R^2 arms in triazole and hydantoin on seven common types of ideal protein secondary structures. Average RMSD for triazole **I** (0.30) was much bigger than that of hydantoin **IV** (0.17), indicating hydantoin backbone was a better fit in mimicking secondary structure side chain orientations in general.

Several compact dipeptide mimics (including the triazole core that has been used in our actively targeted agent **A**[3]), were evaluated by EKOS (Figure B-1). Surprisingly, a simple hydantoin-based dipeptide mimic fit on the secondary structures better than the triazole core applied in our actively targeted probe (calculation results shown in Figure B-2). This inspired us to design new potential dipeptide targeting probes by switching the triazole core to hydantoin.

First generation imaging agents, **3-G** and **3-R**, were synthesized and their binding potential to TrkC^{+} cells was tested *in vitro*.

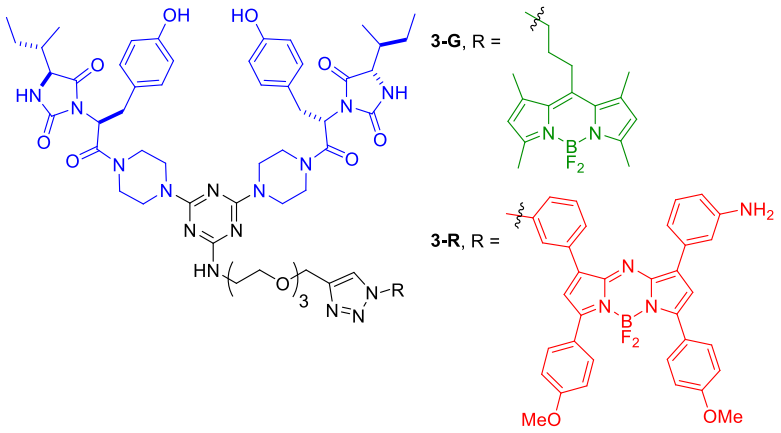

Furthermore, while searching for optimal photosensitizers to incorporate with our bivalent TrkC-targeted ligand, we became aware that a pH-activatable photosensitizer **D** was reported to show unique properties and high potential for modification.[218] In the original reference, **D** was wrapped inside nanoparticles for delivery. The acidic environment of lysosomes in cancer cells activated the probe that acted as a theranostic agent with near-IR illumination. With regional modifications, a novel second generation targeted agent **4** was proposed as a substitute to agent **1** in treatment of metastatic breast cancer. Cysteic acid was introduced to improve the hydrophilicity of the probe.

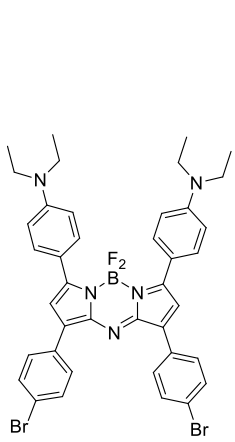

D

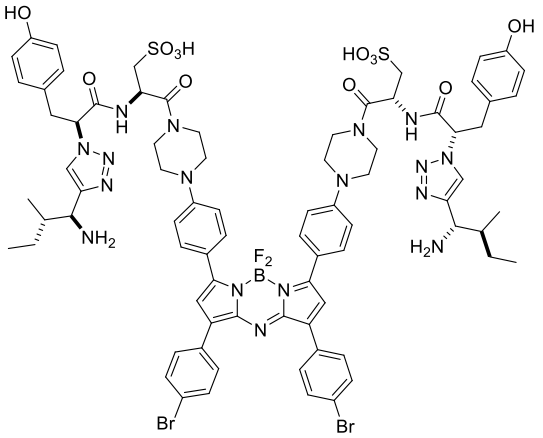

4

B.2 Results and discussion

*B.2.1 Second generation agent **1** preparation and cytotoxicity behavior*

Based on preliminary results of iodination and its failure to incorporate in the aza-BODIPY core with “click” reaction, the targeted agent **1** was obtained via the route shown in Scheme B.1. The iodination was carried out directly after the generation of aza-BODIPY. A mild condition was used to remove the Boc protecting group throughout the procedure to protect iodine from falling off. Afterwards, a targeting ligand **8**, prepared in advance, was coupled with PDT sensitizer to obtain the target molecule **1**.

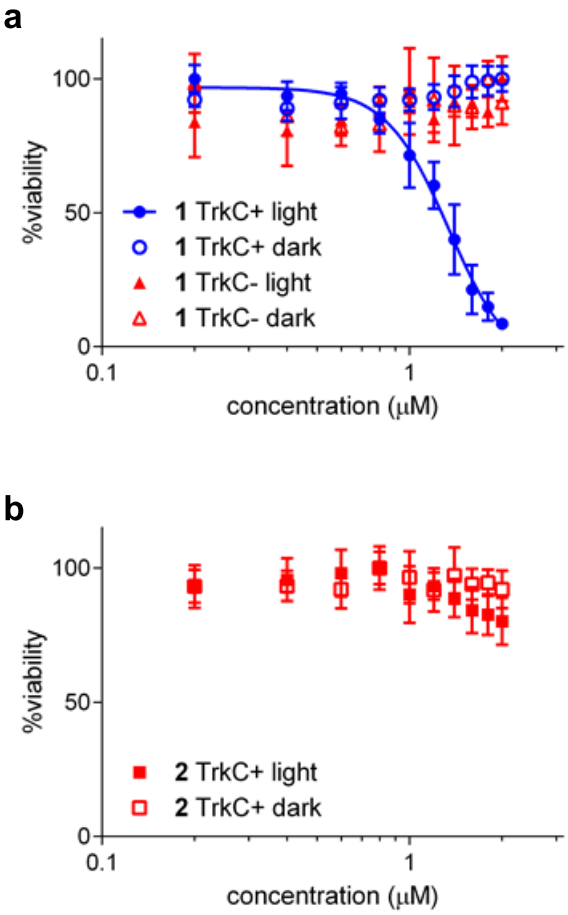

Figure B.3. Light and dark cytotoxicity of targeting (**1**, **a**) and non-targeting (**2**, **b**) agent on $TrkC^+$ or $TrkC^-$ cells *in vitro*. IC_{50} (**1**) = 1.34 ± 0.10 μM. (n = 8, mean ± SD)

Cytotoxicity of the targeting agent **1** and the control compound **2** (Scheme B-2) was tested with TrkC transfected ($TrkC^+$) and wild-type ($TrkC^-$) NIH3T3 cells with and without illumination *in vitro* for PDT effect and general toxicity respectively. The results (Figure B.3a) showed that **1** was selectively uptaken to $TrkC^+$ cells compared with $TrkC^-$ cells, and only toxic when illuminated with light. The low cytotoxicity output from compound **2** (Figure B.3b) further supports the

argument that targeting effect only exists when the targeting moiety was assembled in the correct position.

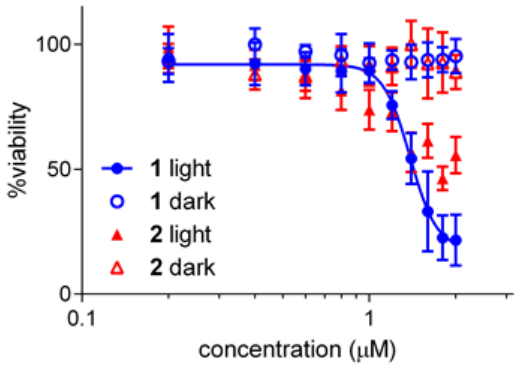

Figure B.4. Light and dark cytotoxicity of targeting (**1**) and non-targeting (**2**) agent on 4T1 cells *in vitro*. IC_{50} (**1**) = 1.39 ± 0.05 μM. (n = 8, mean ± SD)

In vitro cytotoxicity tests were then performed on a metastatic breast cancer cell line 4T1 (TrkC expression confirmed by literature[75]) prior to *in vivo* study to check the selectivity of the cell line as tumor model. The control compound **2** also exposed weak light toxicity to 4T1 cells (Figure B.4).

Furthermore, while exploring the potential to increase reaction yields and product purities, compound **5** was found to be unstable in aqueous solution. Compound stability in water/acetonitrile was compared between compound **5** (iodinated) and compound **F** (non-iodinated). Although all vials were kept in dark, **5** lost its color and decomposed quickly (by 12 h) while solution of **F** was unchanged up to 36 h end point (Figure B.5). The unexpected short compound half-life in aqueous solution of iodine incorporated with sulfonic acid caused the

termination of further study on this compound pair, and one of the opportunities to develop the near-IR absorbing therapeutic probe was lost.

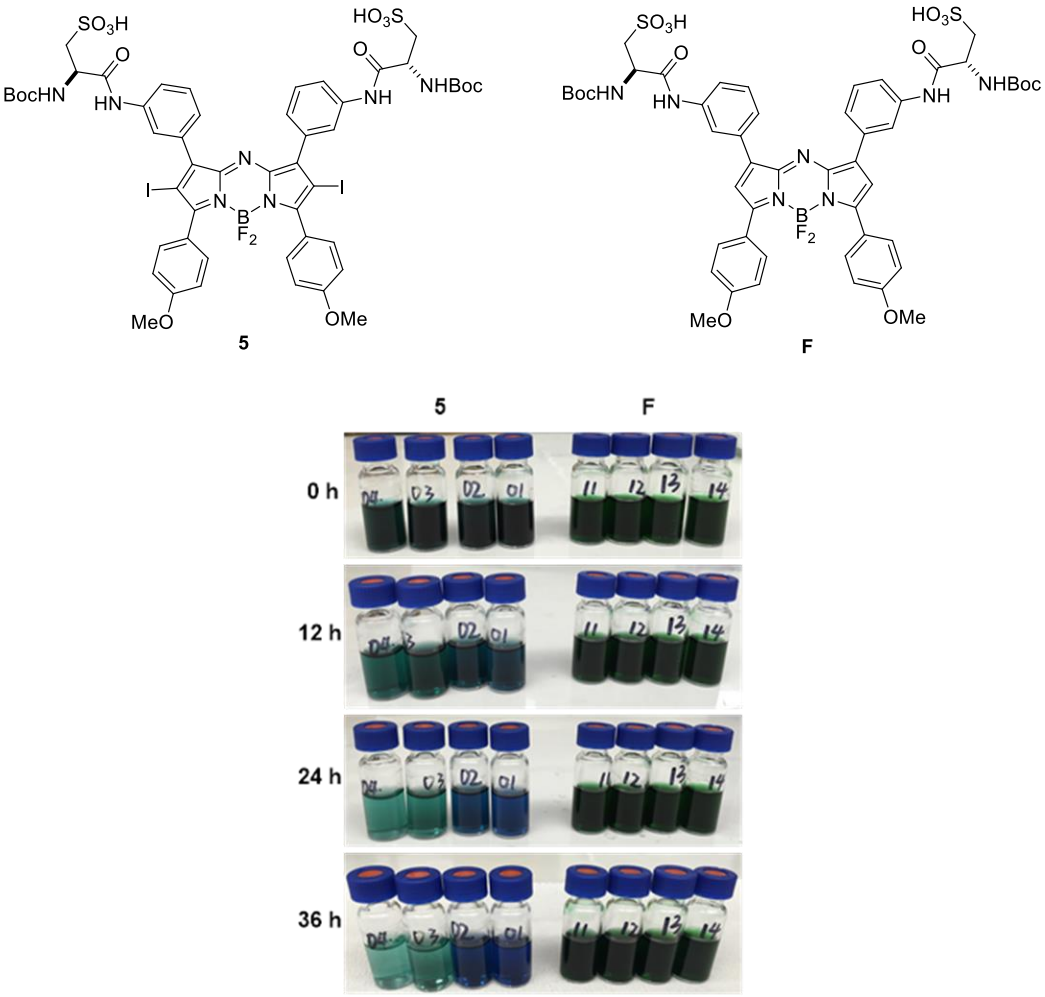

Figure B.5. Stability comparison between **5** (vials 01 – 04) and **F** (vials 11 – 14). Both compounds were prepared as 1 mg/mL at the beginning. Conditions tested in each vial: 01 & 11, pure water/acetonitrile 1:1 mixture; 02 & 12, 0.1% acetic acid in water/acetonitrile; 03 & 13, 0.1% TFA in water/acetonitrile; 04 & 14, 0.1% TFA in water/CAN with C18 silica gel. All vials were kept in dark except when photos were taken. Compound **5** was not stable in both neutral and weak acidic environment.

B.2.2 Hydantoin replacing first generation targeting agent preparation and biological affinity check

Both green and red fluorescence dye were tagged with hydantoin "IY-IY" targeting moiety **15** through simple "click" reaction (Scheme B.4). Other synthetic route for the hydantoin fragment synthesis was also successful (Scheme B.5). Non-targeting control fragment was synthesized at the same time (Scheme B.6 and 7).

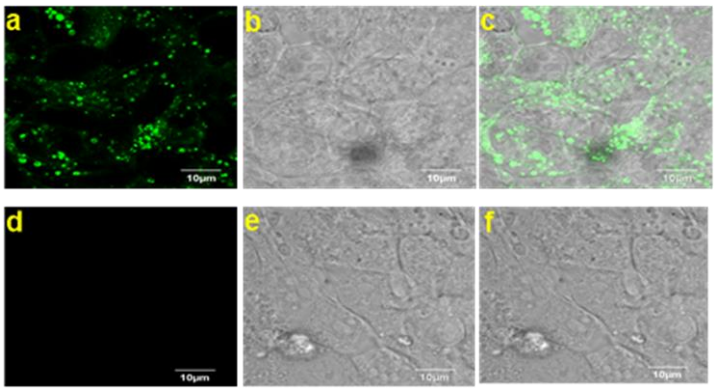

Figure B.6. Live cell imaging of **3-G** on 4T1 cells. Top: 2 μM **3-G** stained for 1 h followed by washing, **a** fluorescence channel; **b** bright field; **c** merged. Bottom: blank control with washing, **d** fluorescence channel; **e** bright field; **f** merged.

Live cell imaging with 4T1 breast cancer cells indicated compound **3-G** was uptaken into the cells within 1 h (Figure B.6), but histochemical staining with breast cancer and normal tissues showed contradictory results. As shown in Figure B.7, **3-G** stained brighter on malignant cells than normal cells in general, yet in rare cases, the normal tissues also showed strong fluorescence. However,

3-R did not provide any observable red fluorescence signal for either tumor or normal tissue (Figure B.8a, c). Antibody staining (Figure B.8b, d) indicated that tumor cells expressed more TrkC on cell surface. Furthermore, the K_d value could not be obtained using Low's method (detected cell associated fluorescence on NIH3T3-TrkC$^+$ cells, excitation/emission at 485/528 nm).[85]

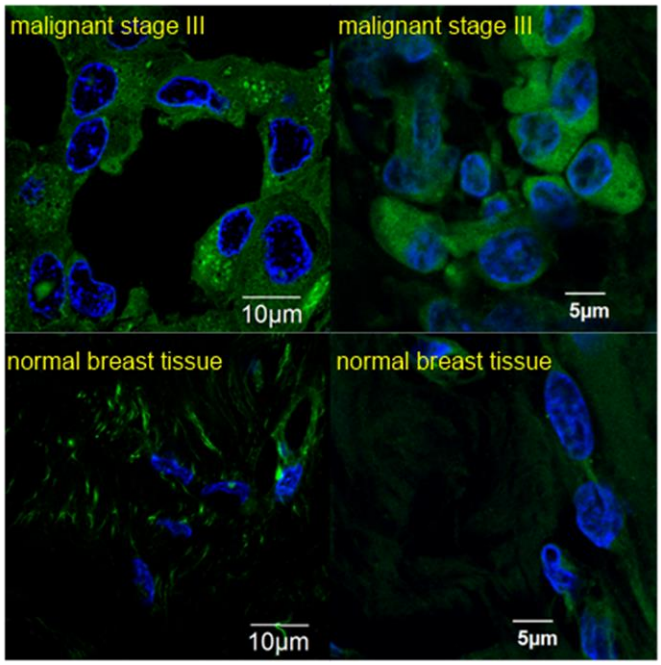

Figure B.7. Histochemical staining of **3-G** on tumor (malignant stage III) and normal tissues.

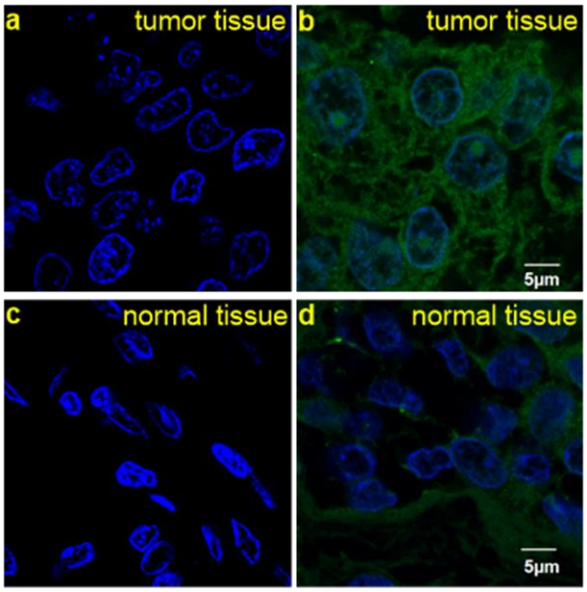

Figure B.8. 3-R (**a**, **c**) and TrkC antibody (**b**, **d**) staining on tumor and normal tissues (same magnification scale).

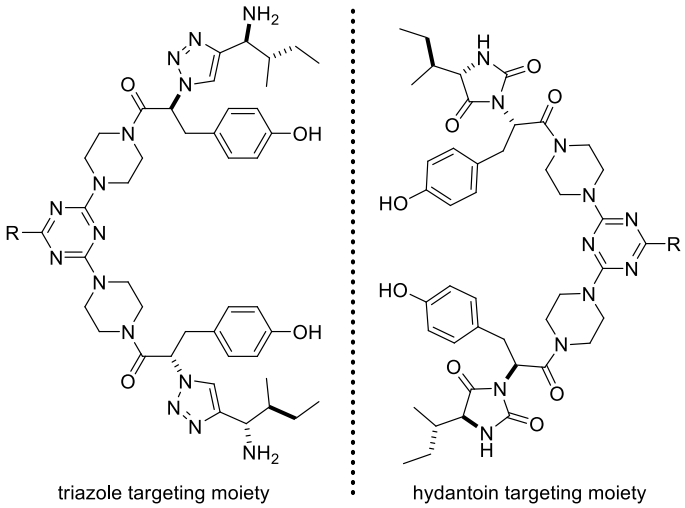

Figure B.9. Structural comparison between targeting moieties in **A** (left) and **3** (right).

When comparing the original triazole targeting moiety and the replaced hydantoin moiety (Figure B.9), atom distance between Tyr Cα and Ile Cα in triazole was one bond extra (four *vs*. three). Triazole contains a free primary amine in its structure that can be protonated and interact in biological environment while hydantoin used the amine during cyclization reaction. These unique structural properties of the original targeting design are critical for the binding affinity to TrkC protein.

B.2.3 Preparation and photo-physical property of new aza-BODIPY based photosensitizer

Heavy atom bromine was anchored in the aza-BODIPY core structure at the beginning of the scheme (Scheme B.3). The intermediates were easy to purify without flash chromatography till compound **20**. Compound **20** showed promising photo-physical property with maximum emission at 829 nm (Figure B.10). Yet, its Boc deprotection product showed poor water solubility. Coupling cysteic acid to the dye core did not make the compound soluble enough in aqueous solution for biological assays. Further attempts, including anchoring fixed cation charges in the molecule and coupling with ethylene glycols, did not help in increasing the water solubility.

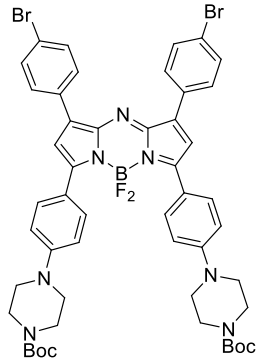

20

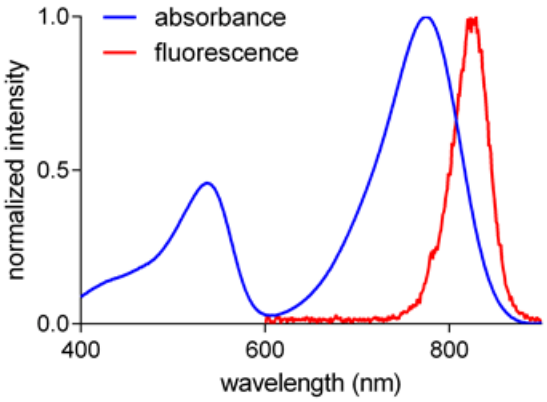

Figure B.10. Normalized absorbance and fluorescence spectrum of **20**. Ex_{max}/Em_{max} = 774/829 nm. ε = 5.21×10^4 $M^{-1}cm^{-1}$ in $CHCl_3$.

B.3 Conclusions

Although near-IR imaging agent **C** showed possibility in tumor diagnosis with TrkC expressing metastatic breast cancer,[72] the iodinated therapeutic probe **1** was extremely hard to obtain. Although the targeted compound showed therapeutic potential with TrkC-transfected NIH3T3 cells, but not with 4T1 breast cancer cell line. Furthermore, the photosensitizer core was not stable in aqueous solution. Moreover, the use of hydantoin, as a better dipeptide mimic, did not help in improving the binding affinity of the original TrkC-targeting moiety, with an unmeasurable cell-based K_d value. Attempts to synthesize a novel near-IR photosensitizer dye was also hit a dead end. Even though the new photosensitizer core was stable and easy to synthesize in a large scale, the poor solubility reduced its opportunity. Unfortunately, the attempts to obtain a targeted, near-IR absorbing theranositc agent ended up with failure.

B.4 Experimental methods

B.4.1 Synthesis of the featured compounds

Synthesis of 1 and 2

Compounds **E** and **F** were synthesized following the protocol in our previous publication,[209] with minor modifications: (i) **E** was obtained by precipitation instead of time-consuming flash chromatography after aqueous phase washing. Briefly, reaction mixture was dissolved in CH_2Cl_2 and filtered through cotton to remove insoluble particles, then 4X volume of hexanes was dropwise added to filtered solution with gentle stirring to get **E** as dark green powder (1.72 g, 46% yield). (ii) 3.0 equiv. N^{α}-Boc-Cysteic acid triethyl amine salt and corresponding coupling reagents, instead of 5.0 equiv., were used to synthesize **F** with similar yield (1.39 g, 75%). Iodination was performed before Boc deprotection to obtain **5** after reverse phase C18 flash chromatography with water-acetonitrile mixture (0.60 g, 45%). Since BF_2 complex can be easily damaged under common Boc deprotection conditions (TFA or HCl), a mild condition with 10 equiv. $^{i}Pr_2NEt$ and 15 equiv. BF_3OEt_2 was applied to get **6** (180 mg, 90% yield). Targeting ligand **8** was then coupled to the free amines in **6** followed by the same mild Boc deprotection to finally acquire **1** (5 mg, 30% yield from **6**, Scheme B.1). Compound **8** was prepared separately to avoid C-I bond cleavage during “click” reaction.

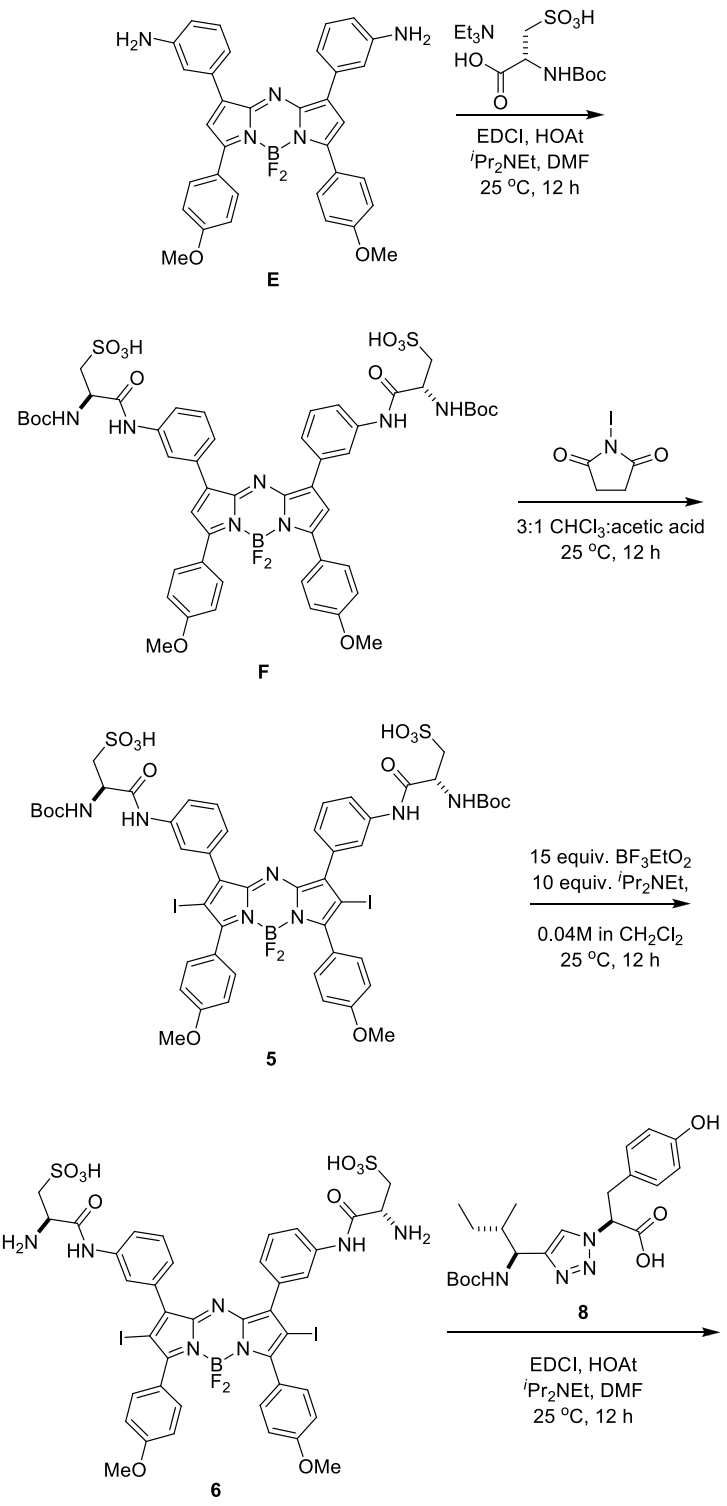

Scheme B.1. Synthesis of second generation targeted therapeutic agent **1**.

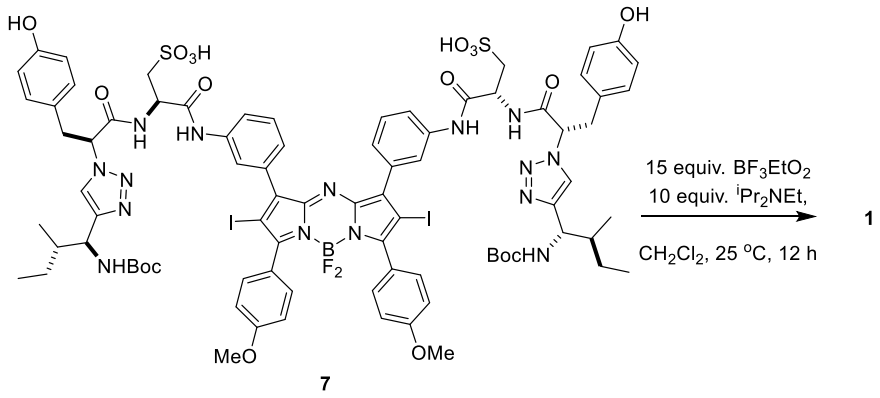

Scheme B.1. Continued.

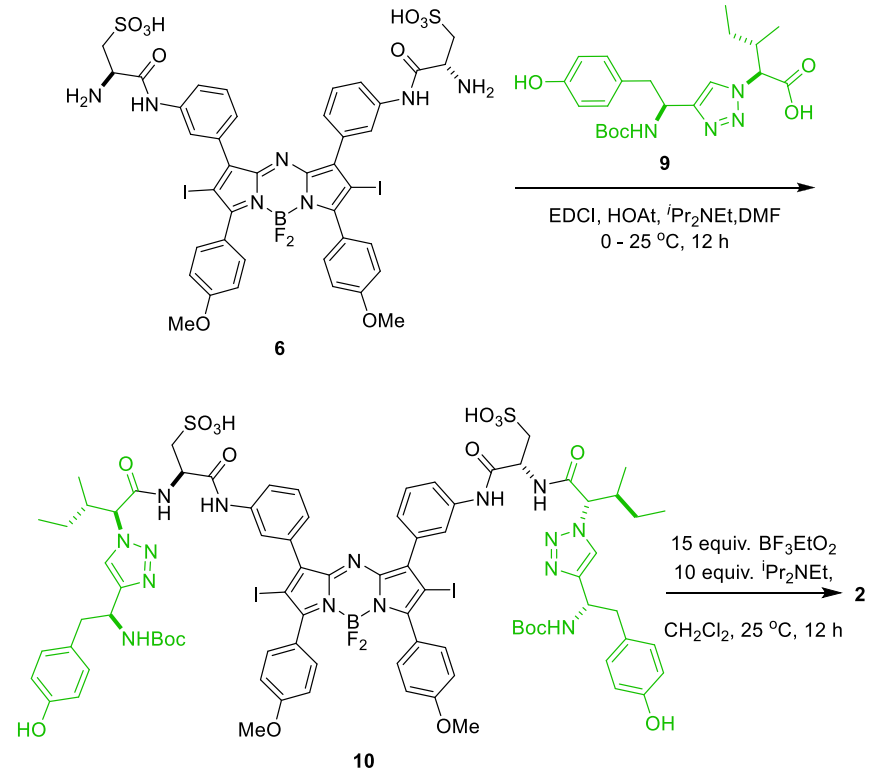

Scheme B.2. Synthesis of second-generation non-targeting control compound **2**.

The scrambled control compound **2** was synthesized in a similar way from compound **6** by using a non-targeting ligand **9** (21% yield from **6**, Scheme B.2).

Synthesis of new photosensitizer core 20 and 23

4'-(1-Piperazinyl) acetophenone (**J**, 12.3 g, 60 mmol) was dissolved in 200 mL CH_2Cl_2 and cooled down to 0 ^oC on ice. 3.0 equiv. Et_3N and 1.0 equiv. Boc_2O was added to reaction solution and mixed well. Removed ice bath and stirred for 6 h, followed by 150 mL 1M HCl wash, *sat*. NaHCO3 and brine wash. After removing the solvents on rotavapor, a light yellow powder was obtained as **16** (17.9 g, 98% yield). 1.0 equiv. 4-bromobenzaldehyde was then mixed with **16** and dissolved in 120 mL MeOH. Nine pellets of KOH was added to the solution and stirred vigorously at 25 ^oC for 12 h. Solid precipitate was filtered out and washed with cold MeOH 200 mL five times to yield **17** as yellow powder (12.73 g, 46%). 80 mL MeOH was used to dissolve **17**, and 1.2 equiv. KOH and 20 equiv. nitromethane were added followed by 20 mL of MeOH. The solution was refluxed in 80 ^oC oil bath for 24 h. After removal of solvent on rotavapor, 200 mL EtOAc was used to re-dissolve the solid and washed with 200 mL water. Crude compound was extracted from aqueous layer by extra $_{100}$ mL EtOAc. Combined EtOAc solution was dried to give 12.5 g (87% yield) **18** as sticky brownish solid. Together with 20 equiv. NH_4OAc, **18** was dissolved in 200 mL *n*-BuOH and refluxed at 120 ^oC for 24 h. Reaction mixture was cooled to 0 ^oC on ice and filtered to collect the precipitate. After cold MeOH wash, 6.16 g (54%

yield) dark green powder **19** was obtained. 0.3 mmol **19** was then dissolved in 6 mL CH_2Cl_2 with 10 equiv. BF_3OEt_2 and 20 equiv. $^{i}Pr_2NEt$ and stirred at 25 ^{o}C for 24 h to yield 170 mg (55%) dark pink powder **20** via flash chromatography (3% EtOAc in CH_2Cl_2). Several Boc deprotection conditions were attempted until the 3rd one (same for deprotection of **5** and **7**) gave quantitative yield of **21**. 5.0 equiv. Boc-cysteic acid, 5.5 equiv. EDCI, 5.5 equiv. HOAt and 10 equiv. $^{i}Pr_2NEt$ were mixed with **21** in DMF and stirred for 12 h to obtain 95 mg **22** with 59% yield after reverse phase C18 flash chromatography. Compound **23** was obtained with a quick Boc deprotection quantitatively with no further purification needed (Scheme B.3).

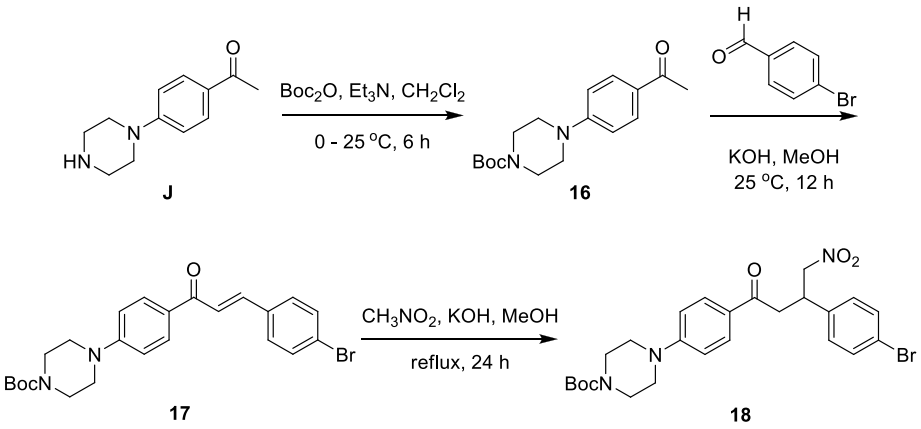

Scheme B.3. Synthesis of new photosensitizer core **20** and **23**.

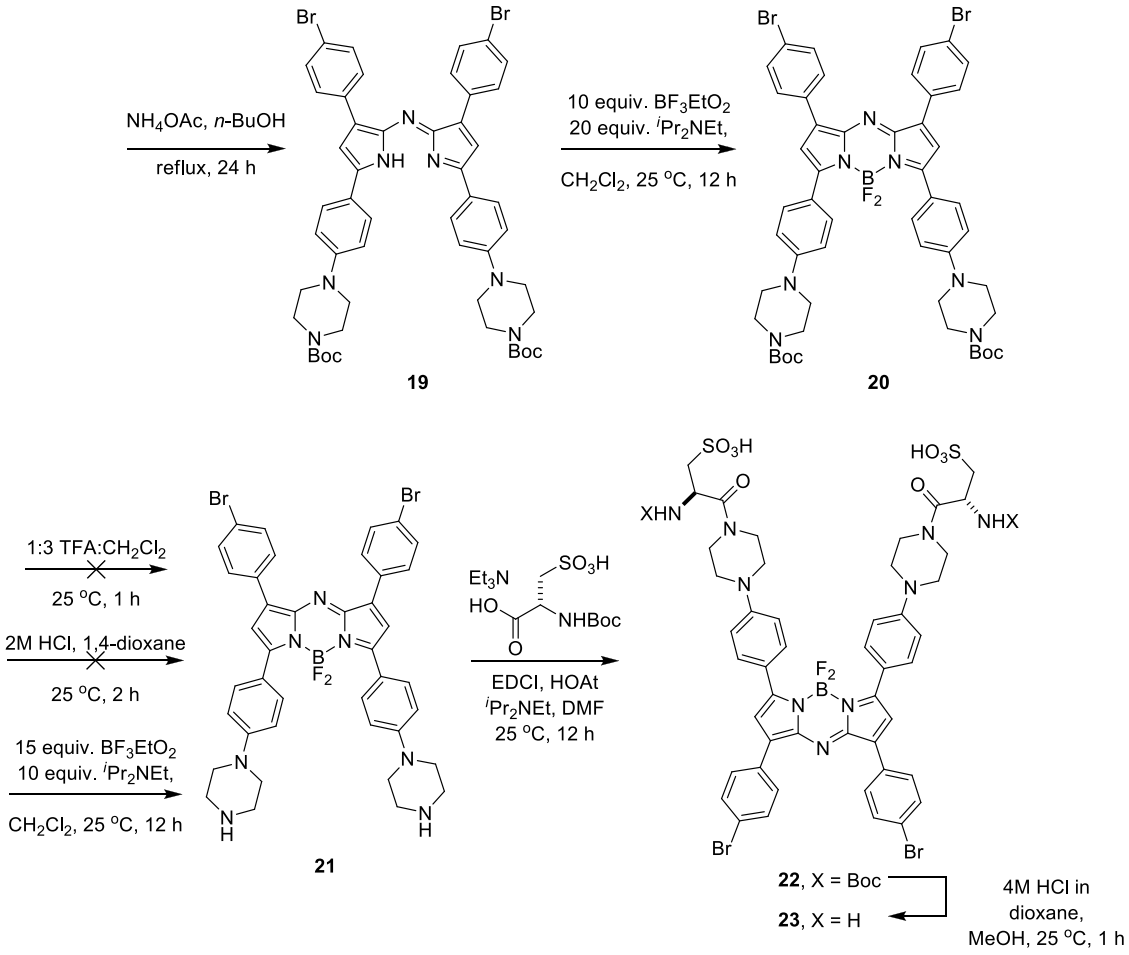

Scheme B.3. Continued.

Synthesis of 3-G and 3-R

N$^{\alpha}$-Boc-Tyr(OBn)-OH (20 mmol) was dissolved in 80 mL CH_2Cl_2 and cooled down to 0 ^{o}C. 1.1 equiv. HOBt and 1.15 equiv. EDCI was then added in sequence and gently stirred for 20 min at 0 ^{o}C. 20 mL CH_2Cl_2 solution of 1.1 equiv. Cbz-piperazine was poured into the reaction mixture followed by NMM. The reaction was finished in 12 h, and washed with 30 mL 2M HCl aqueous solution. Aqueous solution was further extracted with 3 X 100 mL EtOAc, and all

organic fractions were combined and dried with $MgSO_4$ to yield **11** (10.6 g, 92%). Compound **11** was then dissolved in 60 mL TFA:CH_2Cl_2 (1:1) and stirred for 1 h to remove Boc protecting group. After removal of solvents and washing with *sat*. $NaHCO_3$, the compound was coupled with N^{α}-Boc-Ile-OH that gave **12** (7.17 g, 57%) as a white powder **12**. Boc deprotection followed by hydantoin formation led to formation of compound **13** (2.20 g, 35%). Briefly, Boc deprotected **12** (4.17 g, 7.1 mmol) was dissolved in acetonitrile (MeCN), then 1.2 equiv. $NaHCO_3$ and 1.3 equiv. 4-nitrophenyl chloroformate were mixed in the solution under argon atmosphere. The reaction was stirred at 25 ^{o}C for 6 h (negative ninhydrin test) before 1.0 equiv. of Et_3N was added. The white sticky mixture turned to bright yellow and reacted 10 h more followed by solvent removal. **13** was purified through flash chromatography with 1% MeOH in CH_2Cl_2. To completely remove Bn and Cbz protecting group to get **14** (0.713 g, 91%), 1.23 g compound **13** was dissolved in 20 mL EtOH mixed with 0.13 equiv. Pd/C under H_2 atmosphere. IY-IY-hydantoin targeting moiety **15** (173 mg, 28%) was then obtained by substitute reaction between 1.2 mmol **14** and 0.6 mmol **N** (synthesis described in Appendix A) followed by reverse phase HPLC purification with water/MeCN system. **3-G** (1.7 mg, 13%) and **3-R** (1.2 mg, 8%) were then synthesized by “click” **15** with either the green fluorescence dye **G** or the red fluorescence dye **H** and purified by reverse phase HPLC purification with water/MeCN system.

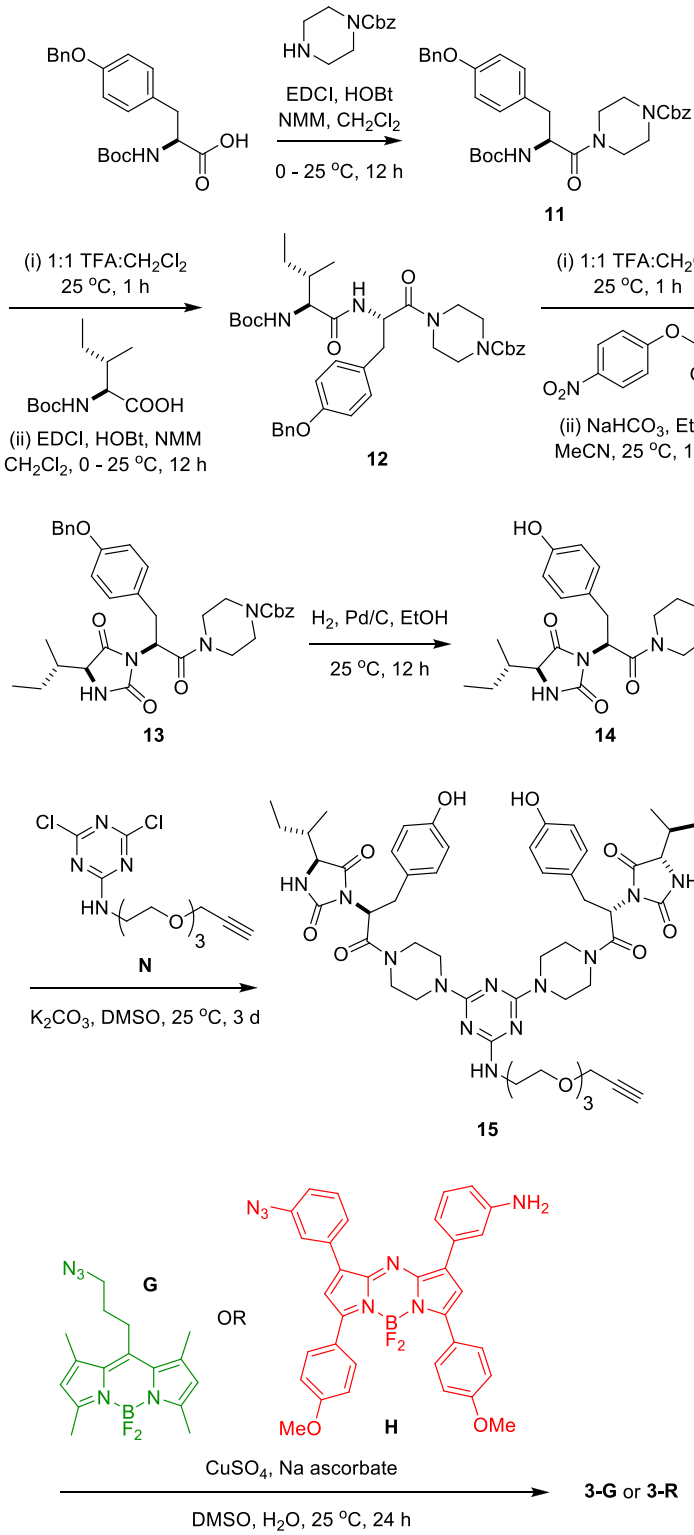

Scheme B.4. Synthesis of hydantoin replacing targeting agent **3-G** and **3-R**.

Synthesis of targeting (8) and non-targeting (9) ligands

Synthesis of **K** and **L** were described in our previous publication.[41] The targeting ligand **8** was obtained through a Cu(I) based "click" reaction (1.0 equiv. copper powder, 0.1 equiv. $CuSO_4 5H_2O$ in 6:1 THF:H2O) followed by flash chromatography purification.(3.04 g, 30%, Scheme B.5)

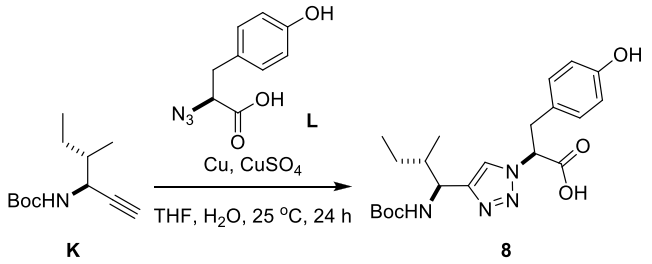

Scheme B.5. Synthesis of the targeting ligand **8**.

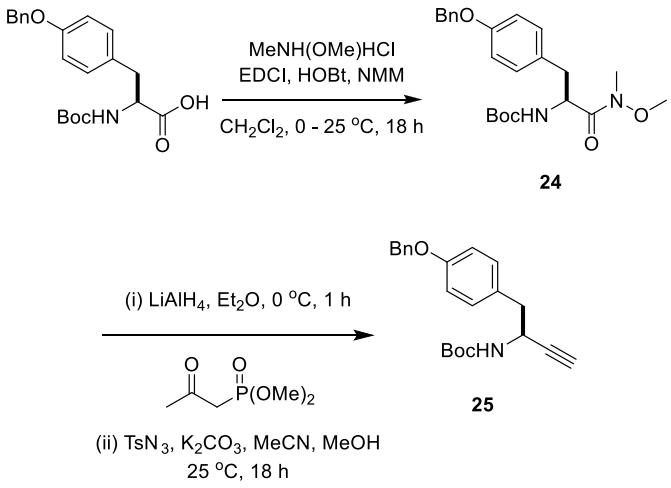

Scheme B.6. Synthesis of the non-targeting ligand **9**.

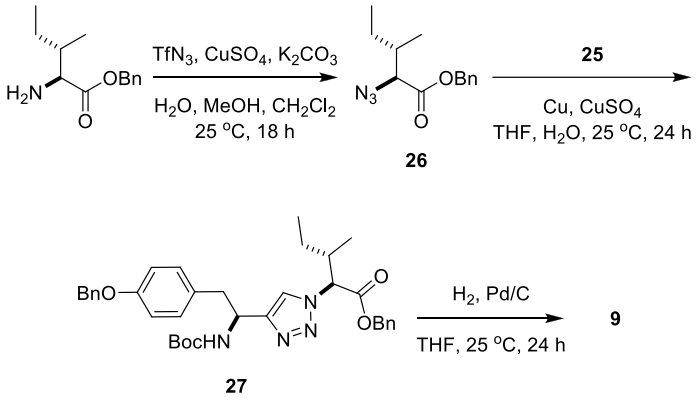

Scheme B.6. Continued.

The non-targeting ligand **9** was synthesized in a similar way. Compound **24** (17.2 g, 82%) was converted from N^{α}-Boc-Tyr(OBn)-OH after coupling with *N,O*-dimethylhydroxylamine. Compounds **25** (5.55 g, 38%) and **26** (5.01 g, 100%) were obtained following similar protocol as reported earlier.[41] A "click" reaction followed by general hydrogenation resulted in **9** (2.43 g, 100%) through **27** (7.22 g, 77%, Scheme B.6).

Attempted synthesis of non-targeting hydantoin ligand 31

To improve the overall synthesis yield in making the non-targeting hydantoin probe **31**, benzyl protecting group was added to N^{α}-Boc-Tyr(OBn)-OH at the start of the synthetic route by mixing with 1.0 equiv. benzyl bromide and 3.0 equiv. K_2CO_3 in DMF solution to get compound **28** (14.4 g, 63%). The following protocol was similar to the one used for synthesis of **14**. The synthesis was halted after compound **30** characterization (2.31 g, 75% yield from **28**),

because no selectivity was observed with the targeting hydantoin probes (Scheme B.7).

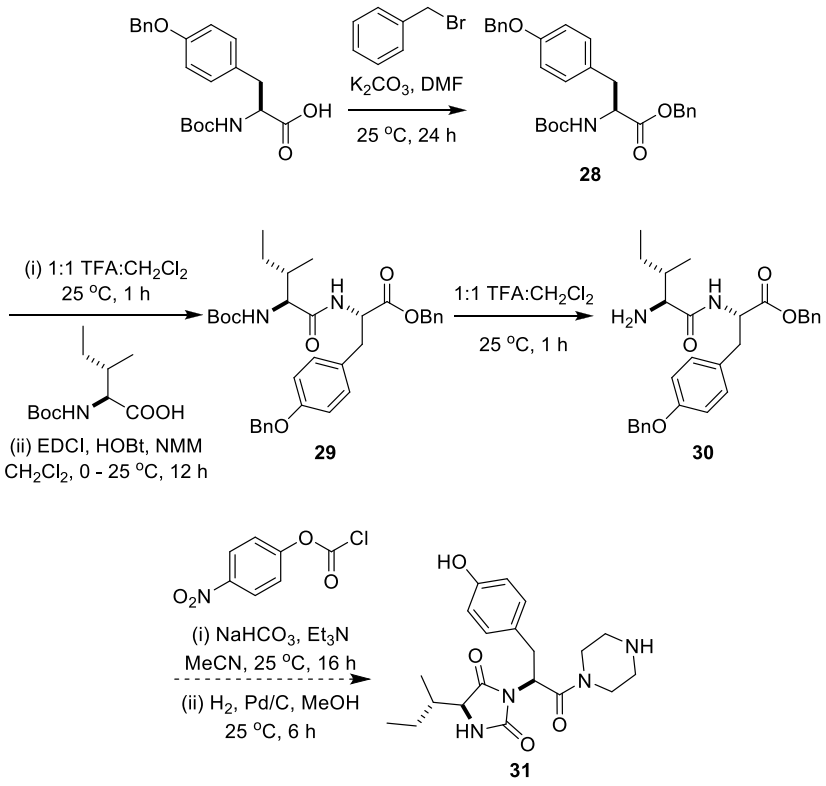

Scheme B.7. Attempted synthesis of non-targeting hydantoin ligand **31**.

Improved synthesis of targeting agent C

Large scale synthesis of compound **C** is hampered by the purification of the intermediates. Introduction of side chain protected tyrosine azide **M** to the synthetic route paved way to easier purification of the coupling product **32** (161 mg, 75%) and the “click” product **33** (63 mg, 70%) by reverse phase C18 flash chromatography. After final Boc removal with HCl, the solvent was removed and

solid was washed thoroughly with MeCN (remove yellow filtrate) to get **C** without further purification (85% yield, Scheme B.8).

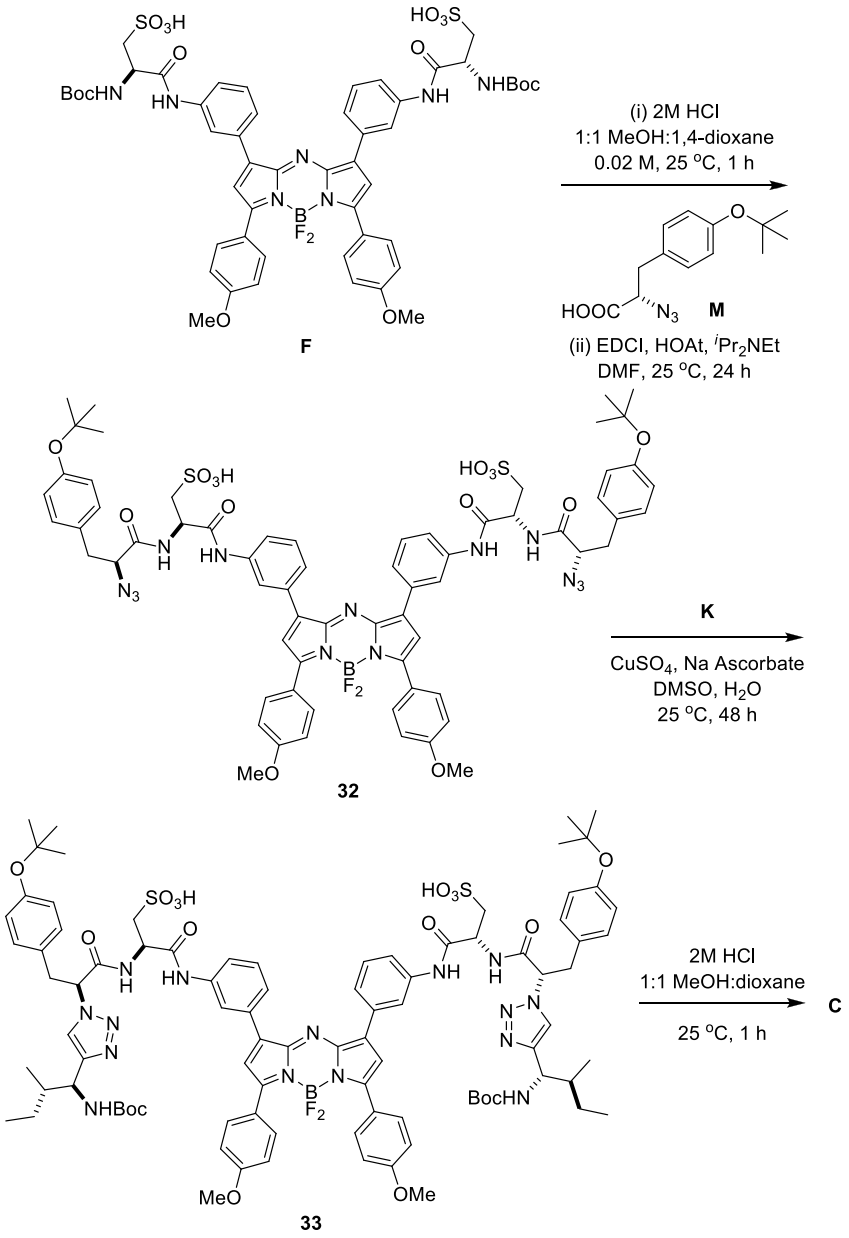

Scheme B.8. Improved synthesis of targeting agent **C**.

B.4.2 Light and dark cytotoxicity assay settings

4T1 and wild-type NIH3T3 cells were cultured with full culture medium (DMEM/F12 medium supplied with 10% FBS), and TrkC-transfected NIH3T3 cells were cultured with full culture medium containing 0.4 g/L G418 adduct. Each type of cells were seeded in a 96-well plate as 5000 cell per well the day before the experiment to get cells adhered to plate surface in a single layer. At the beginning of the test, various concentrations of compounds (0 – 2 μM final concentration) were added to each well. Dark control plates were transferred to CO_2 incubator directly, and light illumination plates were exposed to halogen lamp for 10 min before transferring to incubator. Cell viability in each well was tested by a simple MTT assay. Data was processed with Graph Prism® 6.0 software.

B.4.3 Live cell imaging protocol

4T1 cells were (50,000) seeded in one of the 4-well imaging chamber (Thermo Scientific® #155383) the day before imaging. Adhered cells were incubated with 2 μM **3-G** or protein free medium (as blank control) for 1 h at 37 ^{o}C in a CO_2 incubator followed by thorough washing with culture medium without phenol red. Confocal fluorescence images were taken under 20X objective with GFP emission filter using Olympus® FV1000 microscope at Microscopy and Imaging Center (MIC) in Texas A&M University.

B.4.4 Tissue histology staining and imaging protocol

Breast cancer tissue array with matched adjacent healthy breast tissue (BR243n, US Biomax) was washed sequentially with xylene, EtOH X 2, 90% EtOH, 70% EtOH, pure water, and PBS buffer X 2, 5 min each. Carefully remove the liquid covered on the tissue samples and equilibrate the tissue with 2 μM fluorescent compound (**3-G**, **3-R**) or TrkC Rabbit monoclonal antibody (1:1000 dilution, Cell Signaling Technology® #3376) followed by Alexa Fluor 488 tagged goat anti-rabbit secondary mAb (1:500 dilution, Jackson ImmunoResearch® #111-545-144) for 40 min. After thorough washing with PBS buffer, the tissue array was mounted with Vectashield® medium (with DAPI) with cover glass. Confocal fluorescence images were taken under 20X objective with corresponding emission filter (DAPI, GFP, CY5.5) using Olympus® FV1000 microscope at MIC at Texas A&M University.

B.5 Compound Characterization

1

$C_{72}H_{76}BF_2I_2N_{15}O_{14}S_2$

^{1}H NMR (400 MHz, DMSO) δ 10.35 (s, 2H), 8.86 (s, 2H), 8.56 – 8.23 (m, 8H), 8.22 – 8.09 (m, 4H), 7.97 – 7.84 (m, 1H), 7.77 – 7.56 (m, 2H), 7.47 (dd, J = 19.4, 8.0 Hz, 2H), 7.40 – 7.27 (m, 2H), 7.20 (d, J = 8.3 Hz, 1H), 7.12 (d, J = 8.4 Hz, 2H), 6.91 (d, J = 7.1 Hz, 4H), 6.53 (d, J = 7.9 Hz, 4H), 5.68 (d, J = 8.8 Hz, 2H),

4.86 – 4.60 (m, 2H), 4.44 – 4.23 (m, 2H), 3.87 (s, 6H), 3.72 – 3.55 (m, 4H), 3.23 – 2.86 (m, 6H), 2.00 – 1.81 (m, 2H), 1.43 – 1.18 (m, 6H), 1.01 – 0.65 (m, 12H).

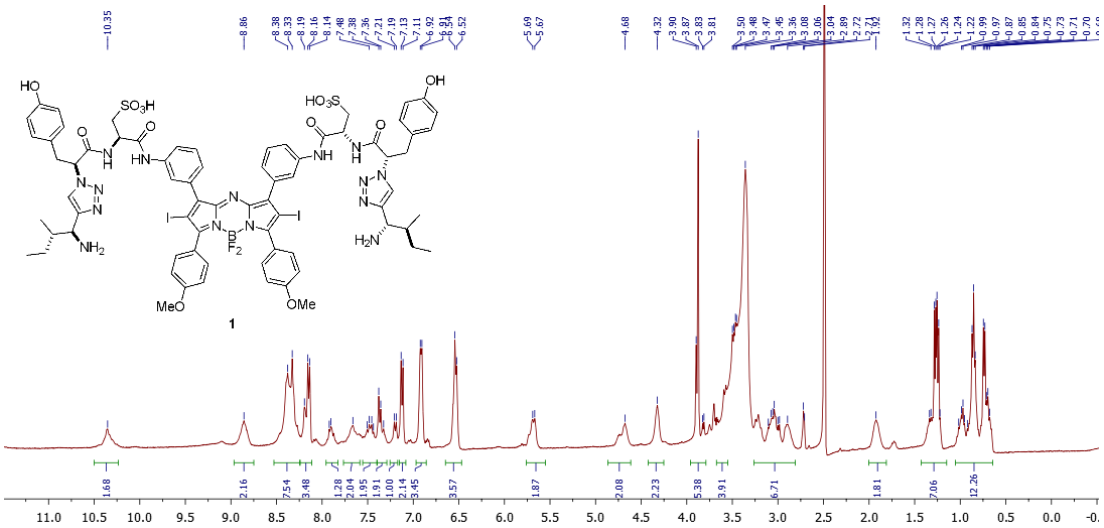

^{13}C NMR (101 MHz, DMSO) δ 168.90, 167.20, 161.97, 157.26, 156.05, 144.45, 142.56, 141.84, 139.36, 132.03, 131.73, 129.83, 126.09, 125.98, 123.12, 119.64, 119.58, 115.08, 115.01, 114.94, 114.88, 114.45, 64.34, 55.57, 53.37, 51.92, 50.98, 37.07, 25.05, 17.97, 13.74, 13.64, 11.02, 1.09.

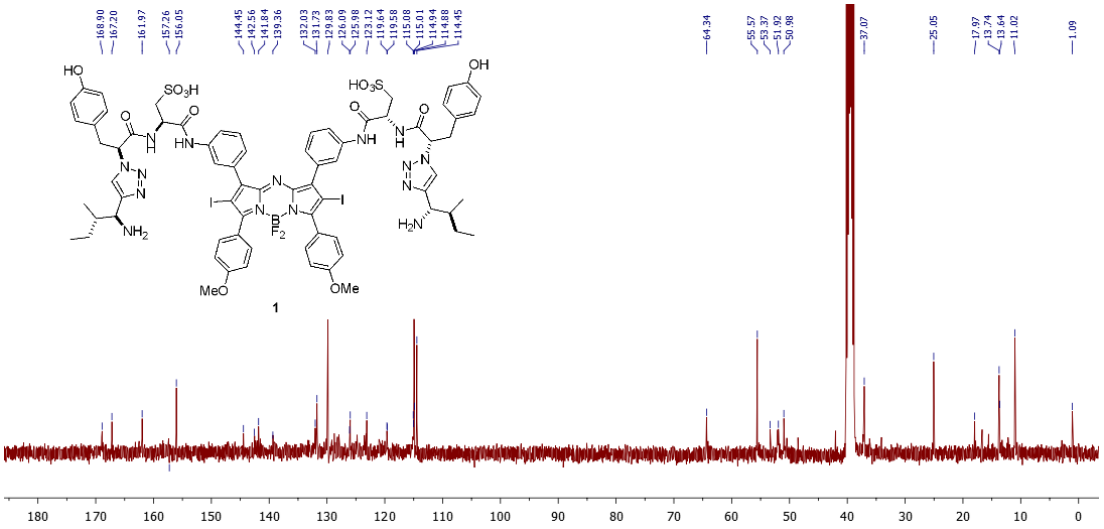

^{11}B NMR (128 MHz, DMSO) δ 1.12, 0.87, 0.62.

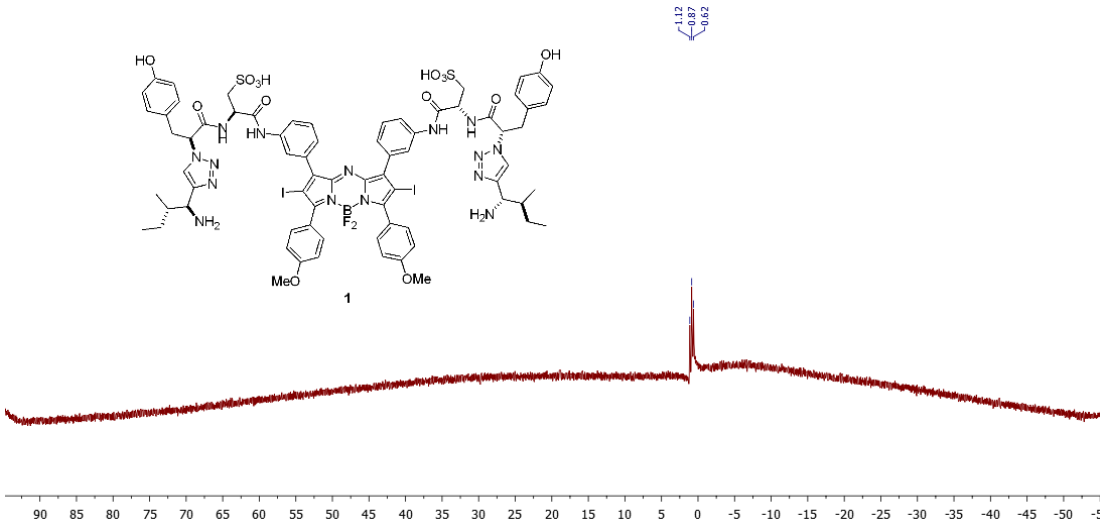

^{19}F NMR (376 MHz, DMSO) δ -130.34, -130.42, -130.51, -130.61.

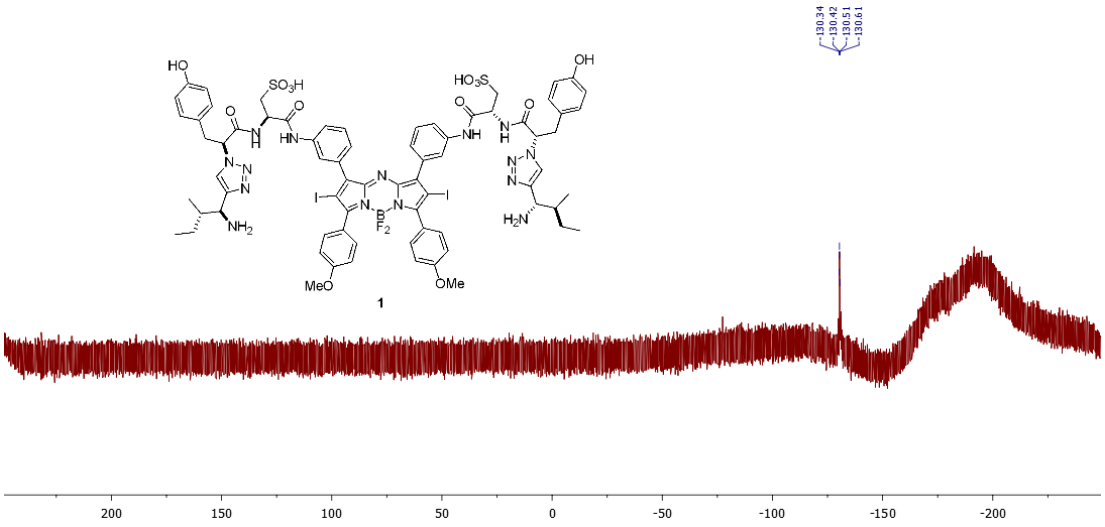

2

$C_{72}H_{76}BF_2I_2N_{15}O_{14}S_2$

^1H NMR (400 MHz, DMSO) δ 10.57 – 10.20 (m, 1H), 9.23 (s, 1H), 8.92 (s, 1H), 8.57 – 8.28 (m, 4H), 8.23 (s, 2H), 8.20 – 8.01 (m, 2H), 7.96 – 7.81 (m, 2H), 7.74 – 7.31 (m, 6H), 7.18 – 7.00 (m, 2H), 6.93 – 6.74 (m, 4H), 6.66 – 6.49 (m, 4H),

5.28 – 5.12 (m, 2H), 4.26 – 4.20 (m, 4H), 3.90 – 3.85 (m, 6H), 3.59 (s, 6H), 3.56 – 3.40 (m, 10H), 1.33 – 1.25 (m, 4H), 0.96 – 0.70 (m, 16H).

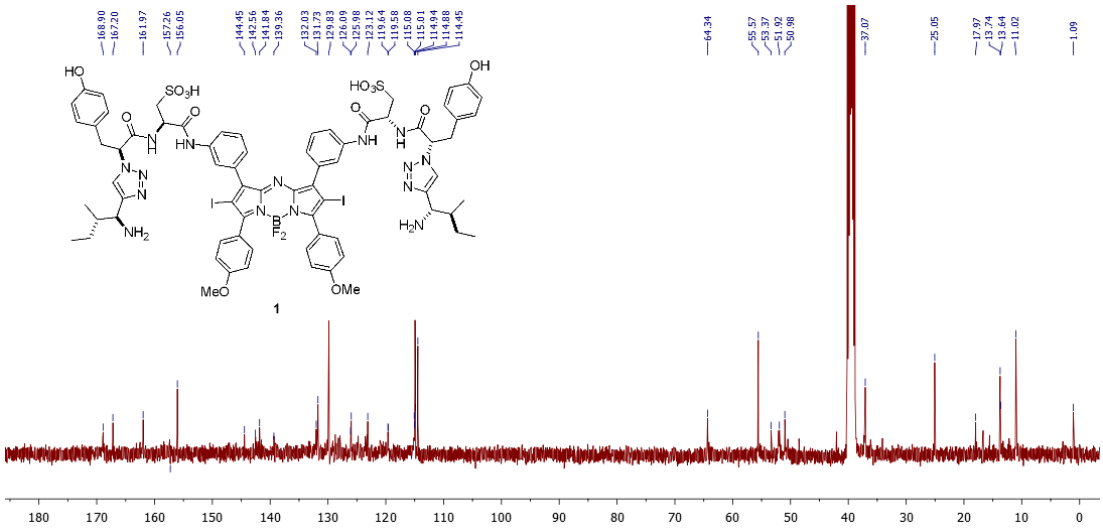

5

$C_{50}H_{52}BF_2I_2N_7O_{14}S_2$

^{1}H NMR (400 MHz, MeOD) δ 8.05 (s, 2H), 7.64 (d, J = 8.4 Hz, 4H), 7.54 – 7.28 (m, 8H), 7.00 (d, J = 8.7 Hz, 4H), 4.59 (s, 2H), 3.86 (s, 6H), 3.79 (dd, J = 17.2, 11.8 Hz, 2H), 3.66 (dd, J = 13.0, 6.5 Hz, 2H), 3.07 – 2.97 (m, 2H), 1.83 – 1.75 (m, 2H), 1.46 (s, 18H).

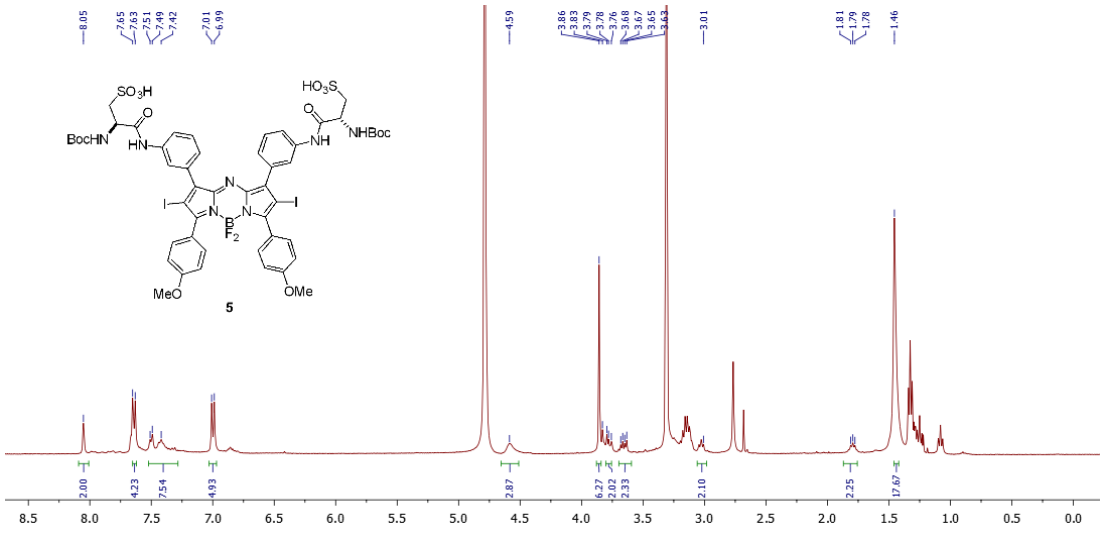

^{11}B NMR (128 MHz, DMSO) δ 0.20, -0.04, -0.27.

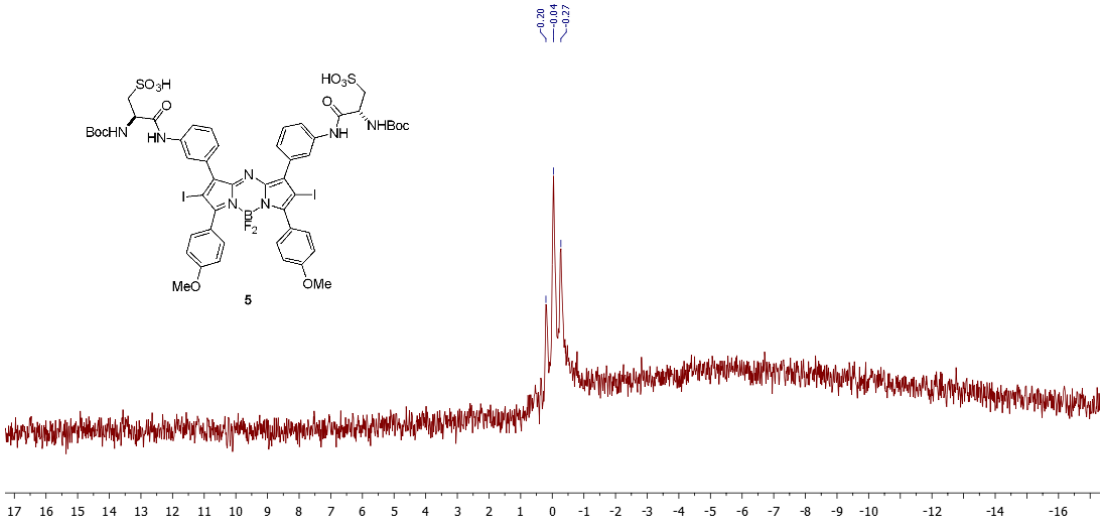

^{19}F NMR (376 MHz, DMSO) δ -130.38, -130.46, -130.54, -130.61.

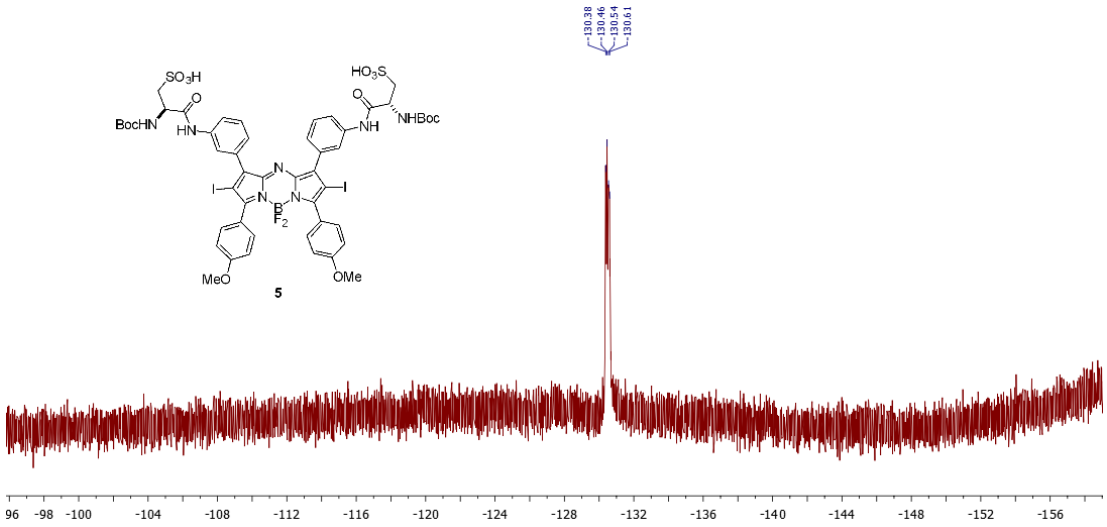

6

$C_{40}H_{36}BF_2I_2N_7O_{10}S_2$

^{1}H NMR (400 MHz, DMSO) δ 10.84 (s, 2H), 8.24 (s, 4H), 7.96 (s, 2H), 7.61 (d, J = 8.5 Hz, 4H), 7.49 – 7.38 (m, 4H), 7.07 (d, J = 8.8 Hz, 4H), 4.29 (s, 2H), 3.84 (s, 6H), 3.74 (dd, J = 11.3, 5.6 Hz, 1H), 3.60 (dd, J = 8.4, 4.5 Hz, 1H), 3.12 (dd, J = 9.4, 5.3 Hz, 1H), 2.94 – 2.88 (m, 1H).

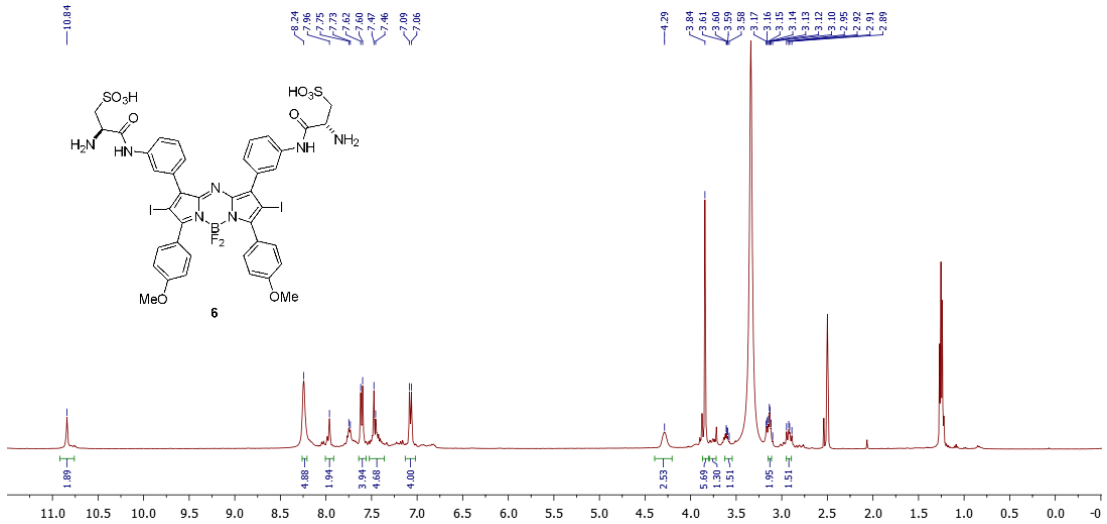

^{11}B NMR (128 MHz, DMSO) δ 0.19, -0.02, -0.25.

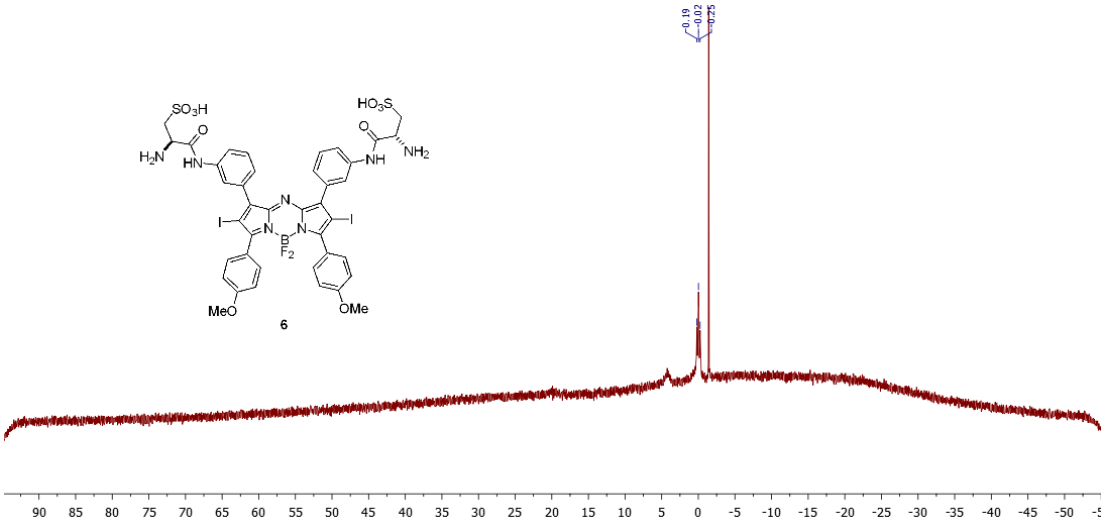

^{19}F NMR (376 MHz, DMSO) δ -130.38, -130.45, -130.58, -130.59.

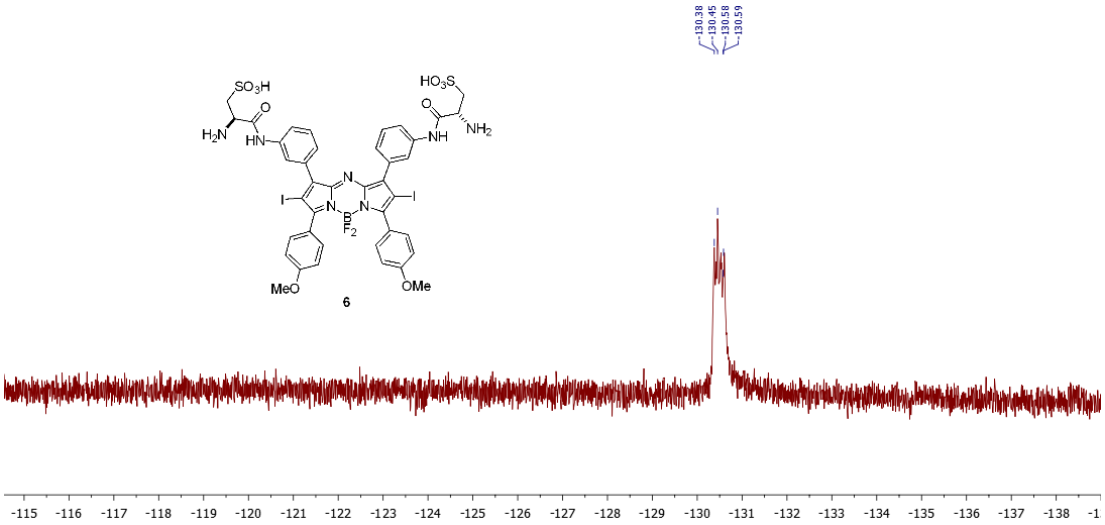

8

$C_{21}H_{30}N_4O_5$

^{1}H NMR (400 MHz, MeOD) δ 7.73 (s, 1H), 6.82 (d, J = 8.1 Hz, 2H), 6.56 (t, J = 5.6 Hz, 2H), 5.50 (dd, J = 10.4, 4.3 Hz, 1H), 4.58 (d, J = 5.7 Hz, 1H), 3.47 (dd, J

= 14.3, 4.6 Hz, 1H), 3.40 – 3.29 (m, 1H), 1.84 – 1.68 (m, 1H), 1.48 – 1.40 (m, 1H), 1.38 (s, 9H), 1.11 – 0.94 (m, 1H), 0.86 (t, J = 7.4 Hz, 3H), 0.72 (d, J = 6.8 Hz, 3H).

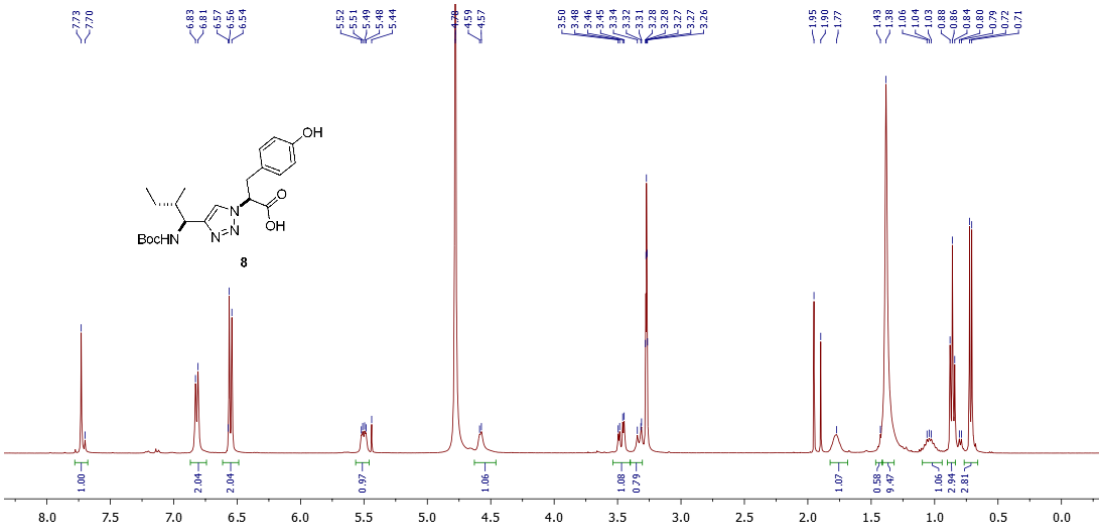

^{13}C NMR (101 MHz, MeOD) δ 175.16, 171.21, 157.59, 149.19, 131.01, 127.67, 124.00, 116.32, 80.33, 65.89, 53.08, 40.44, 38.45, 28.74, 26.28, 15.85, 11.58.

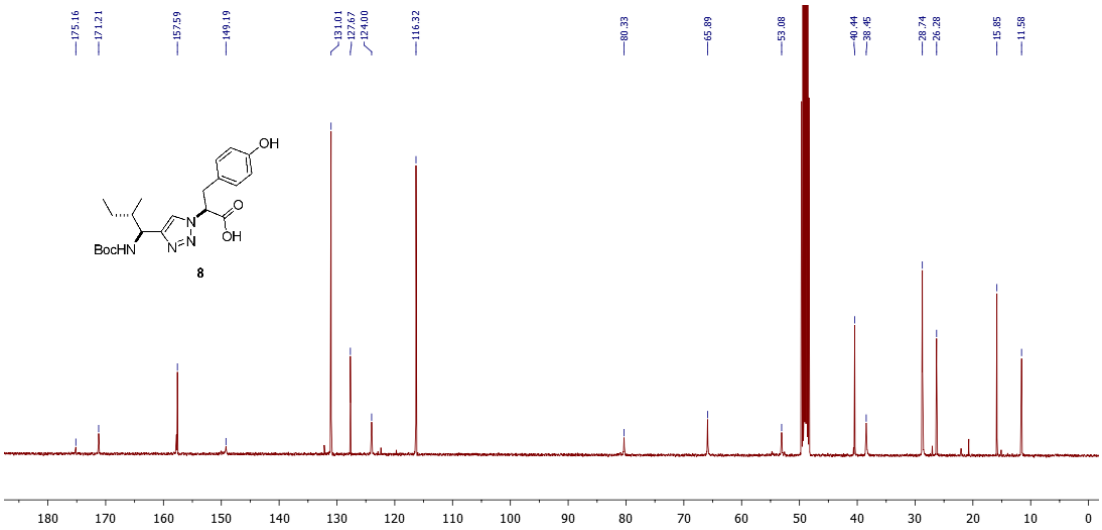

9

$C_{21}H_{30}N_4O_5$

^{1}H NMR (400 MHz, $CDCl_3$) δ 7.38 (s, 1H), 6.74 (d, J = 8.1 Hz, 2H), 6.69 – 6.56 (m, 2H), 5.23 – 4.90 (m, 2H), 3.74 (t, J = 6.6 Hz, 1H), 3.21 – 2.79 (m, 2H), 2.27 – 1.98 (m, 1H), 1.38 (s, 9H), 1.25 – 1.12 (m, 1H), 0.96 (d, J = 6.6 Hz, 3H), 0.92 – 0.87 (m, 1H), 0.87 – 0.71 (m, 3H).

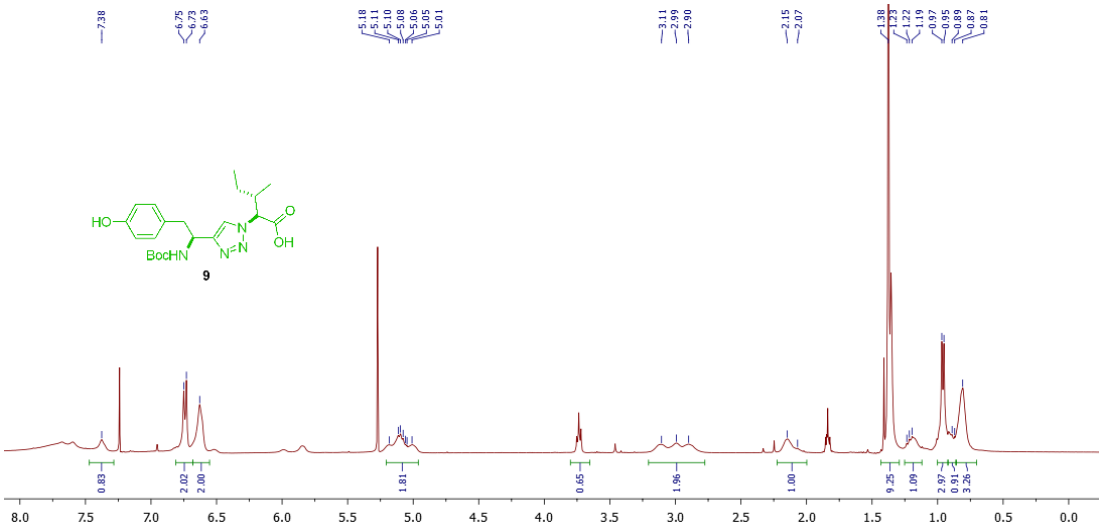

10

$C_{82}H_{92}BF_2I_2N_{15}O_{18}S_2$

^{1}H NMR (400 MHz, DMSO) δ 9.10 (s, 2H), 8.18 (s, 2H), 8.04 – 7.85 (m, 6H), 7.34 – 7.05 (m, 10H), 7.03 – 6.85 (m, 8H), 6.59 (d, J = 6.8 Hz, 4H), 5.29 – 5.06 (m, 2H), 3.88 (s, 6H), 3.66 – 3.53 (m, 4H), 3.14 – 3.07 (m, 4H), 3.07 – 2.93 (m, 8H), 1.26 (s, 9H), 1.24 (s, 9H), 0.99 (t, J = 7.2 Hz, 6H), 0.93 – 0.82 (m, 8H).

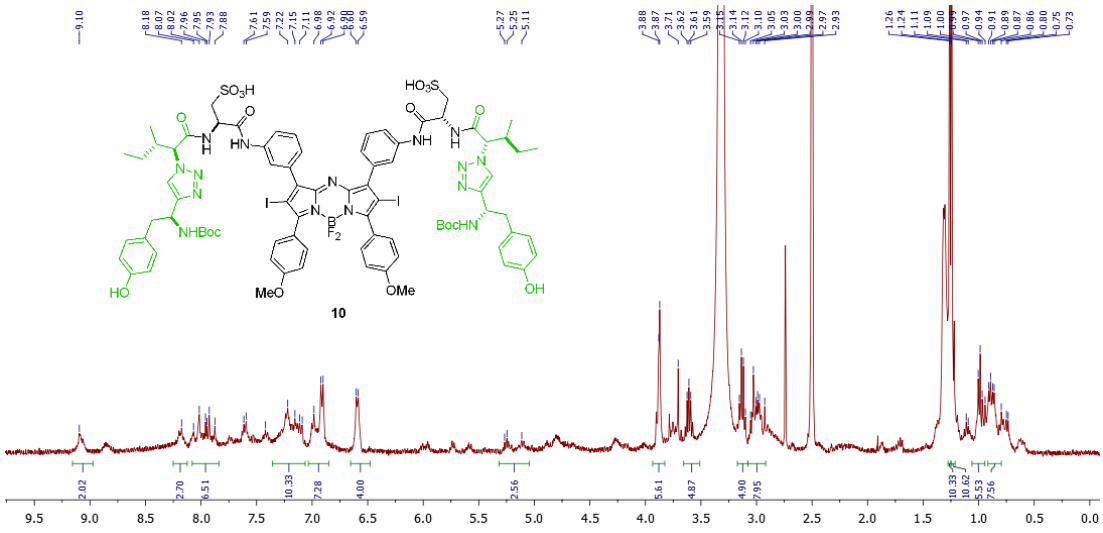

^{19}F NMR (376 MHz, DMSO) δ -131.19, -131.29, -131.40, -131.51.

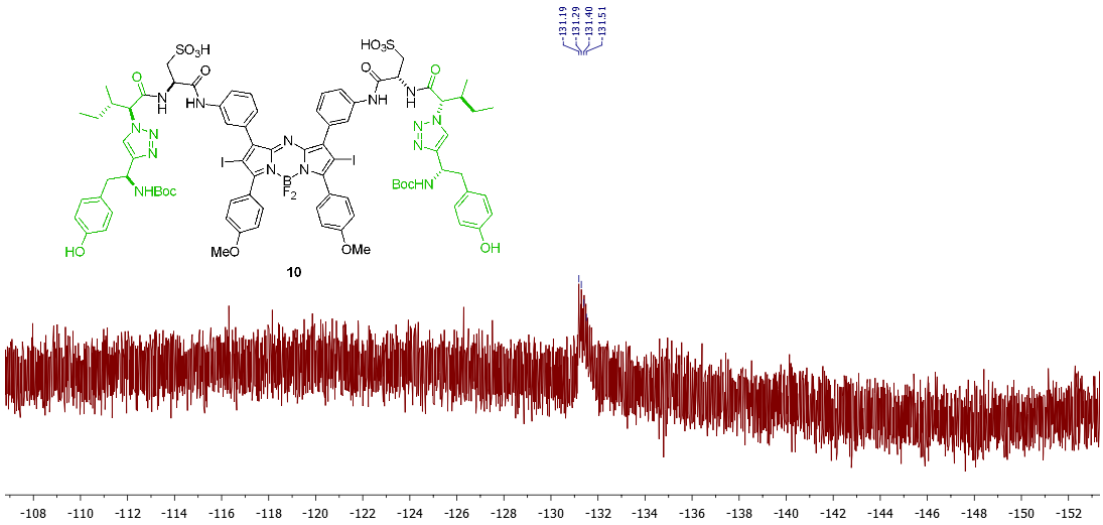

11

$C_{33}H_{39}N_3O_6$

^{1}H NMR (400 MHz, $CDCl_3$) δ 7.45 – 7.25 (m, 10H), 7.11 (d, J = 8.3 Hz, 2H), 6.90 (d, J = 8.4 Hz, 2H), 5.43 (d, J = 8.4 Hz, 1H), 5.14 (s, 2H), 5.06 (s, 2H), 4.78 (d, J

= 5.5 Hz, 1H), 3.57 – 3.39 (m, 3H), 3.38 – 3.16 (m, 3H), 3.05 – 2.81 (m, 4H), 1.45 (s, 9H).

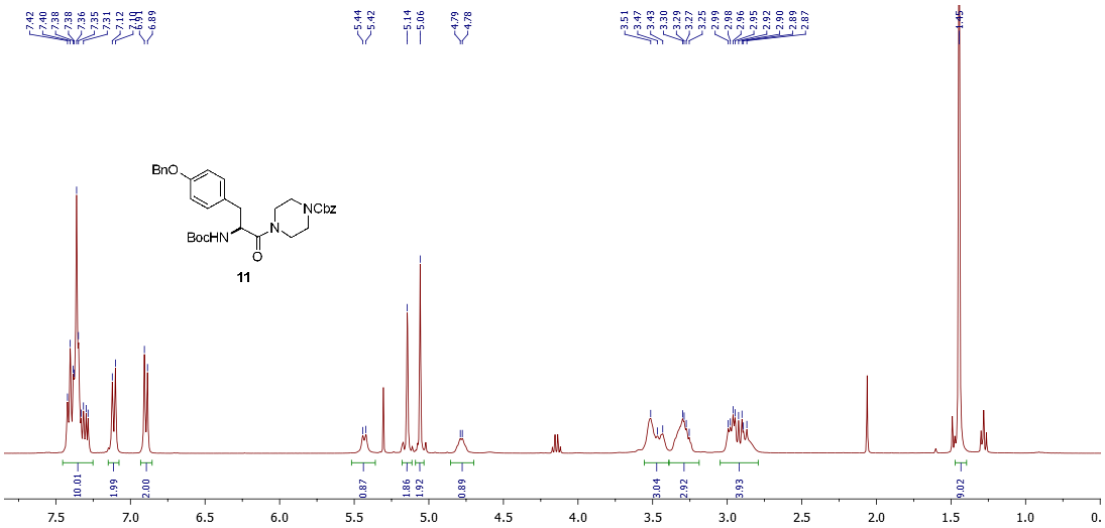

^{13}C NMR (101 MHz, $CDCl_3$) δ 170.77, 158.01, 155.08, 137.07, 136.49, 131.64, 130.65, 130.59, 129.67, 128.81, 128.72, 128.63, 128.37, 128.19, 128.10, 127.61, 127.49, 115.23, 80.03, 70.18, 67.63, 51.29, 45.43, 43.53, 41.84, 39.66, 28.51.

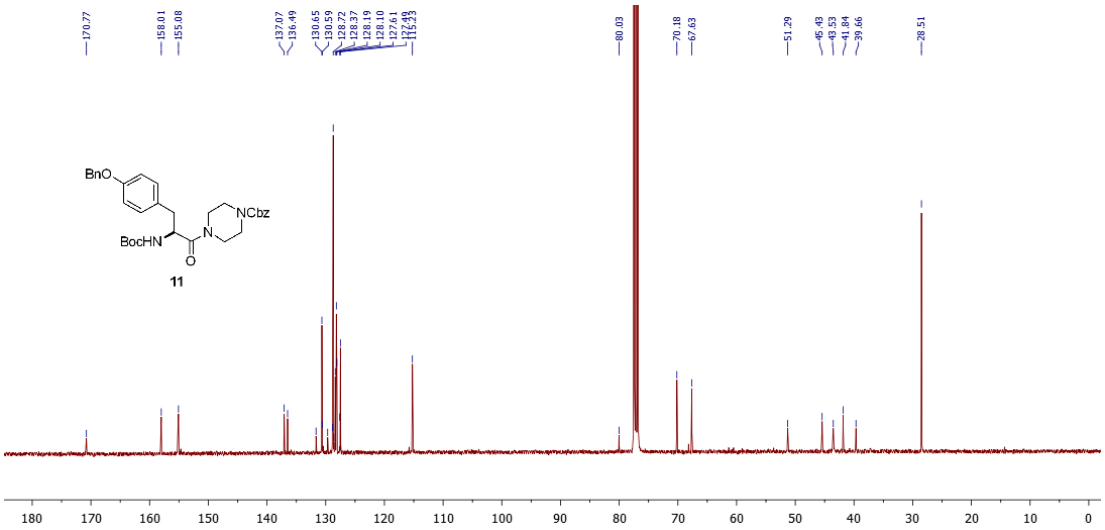

12

$C_{39}H_{50}N_4O_7$

^{1}H NMR (400 MHz, $CDCl_3$) δ 7.43 – 7.25 (m, 10H), 7.15 – 6.99 (m, 2H), 6.88 – 6.79 (m, 2H), 5.10 (d, J = 1.8 Hz, 2H), 5.06 – 5.02 (m, 1H), 5.01 (s, 2H), 3.96 (s, 1H), 3.54 – 3.32 (m, 3H), 3.27 (dt, J = 13.2, 8.1 Hz, 3H), 2.91 (ddd, J = 22.3, 13.2, 7.3 Hz, 4H), 1.85 (ddd, J = 9.5, 7.9, 5.1 Hz, 2H), 1.43 (s, 9H), 1.06 (ddd, J = 13.4, 9.5, 7.2 Hz, 1H), 0.97 – 0.81 (m, 6H).

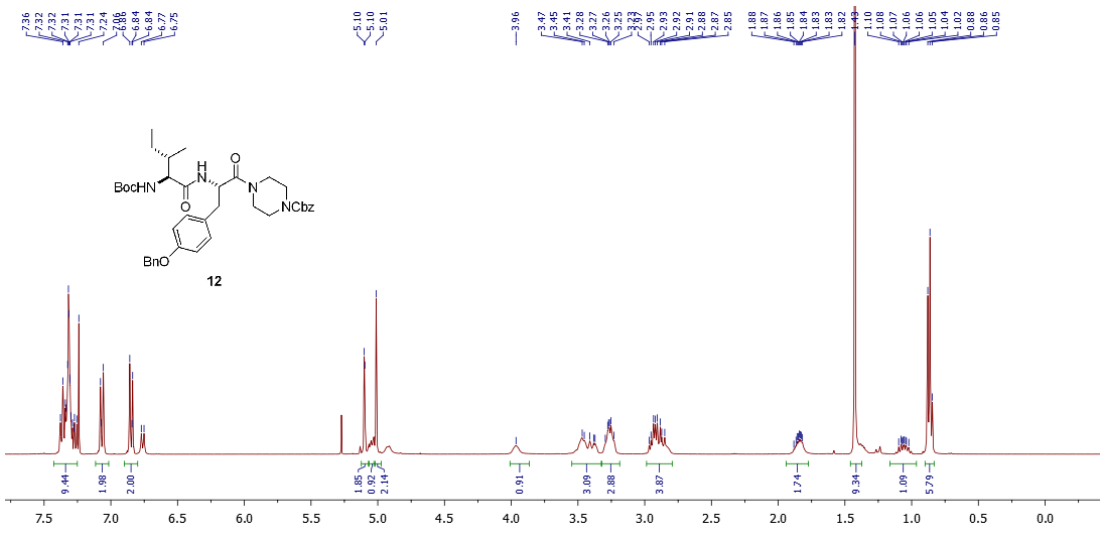

13

$C_{35}H_{40}N_4O_6$

^{1}H NMR (400 MHz, $CDCl_3$) δ 7.69 – 7.51 (m, 10H), 7.40 (d, J = 8.5 Hz, 2H), 7.14 (d, J = 8.6 Hz, 2H), 5.51 (s, 1H), 5.41 (s, 2H), 5.37 (dd, J = 10.3, 6.0 Hz, 1H), 5.26 (s, 2H), 4.11 (d, J = 3.7 Hz, 1H), 3.95 – 3.58 (m, 9H), 3.53 (dd, J = 14.3, 5.8 Hz, 1H), 2.09 – 1.95 (m, 1H), 1.39 – 1.28 (m, 2H), 1.16 – 1.05 (m, 6H).

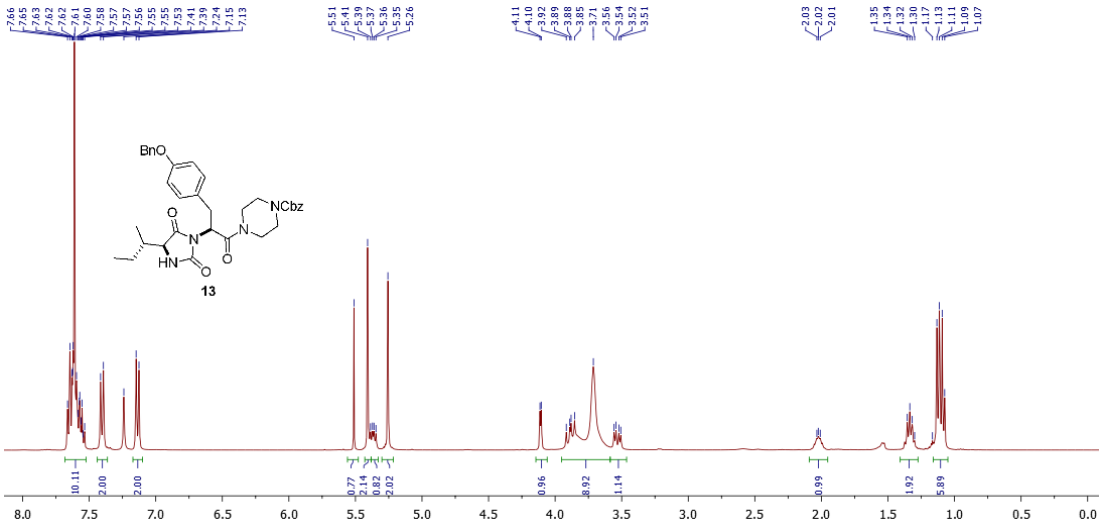

^{13}C NMR (101 MHz, $CDCl_3$) δ 173.18, 166.96, 157.74, 157.18, 154.90, 136.83, 136.20, 130.16, 128.72, 128.44, 128.42, 128.09, 127.87, 127.81, 127.30, 114.85, 69.84, 67.37, 61.49, 53.42, 52.23, 43.56, 36.72, 33.33, 23.28, 14.68, 11.39.

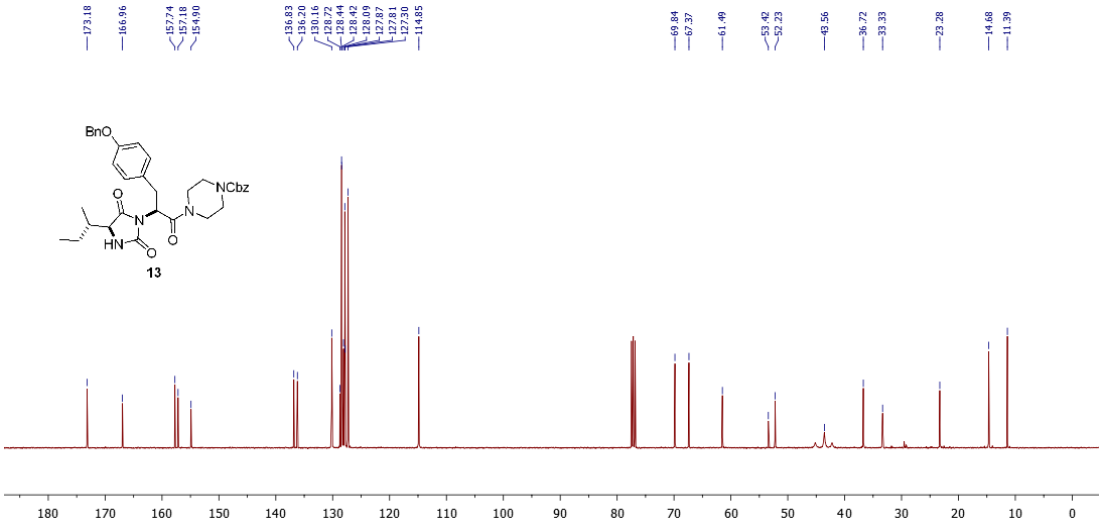

14

$C_{20}H_{28}N_4O_4$

^{1}H NMR (400 MHz, MeOD) δ 6.99 (d, J = 8.3 Hz, 2H), 6.63 (d, J = 8.3 Hz, 2H), 5.09 (dd, J = 10.7, 5.6 Hz, 1H), 3.83 (d, J = 3.7 Hz, 1H), 3.83 (d, J = 3.7 Hz, 1H), 3.58 – 3.35 (m, 5H), 3.29 – 3.23 (m, 1H), 3.11 (dd, J = 14.2, 5.6 Hz, 1H), 2.80 – 2.61 (m, 3H), 1.77 – 1.58 (m, 1H), 1.06 – 0.91 (m, 2H), 0.84 – 0.73 (m, 6H).

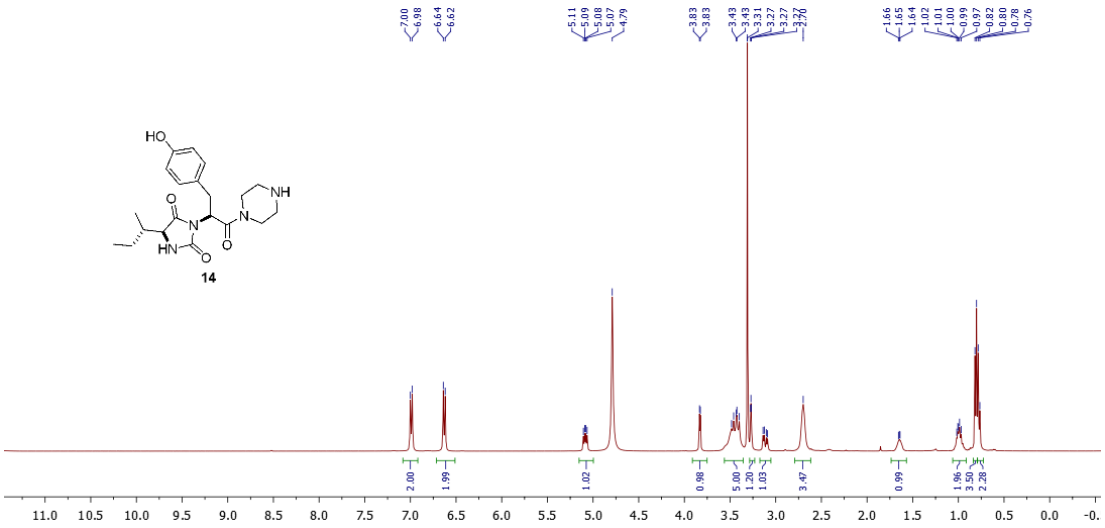

15

$C_{52}H_{70}N_{12}O_{11}$

^{1}H NMR (400 MHz, MeOD) δ 7.10 – 7.00 (m, 4H), 6.68 (dd, J = 8.5, 3.4 Hz, 4H), 5.17 (dd, J = 10.0, 6.2 Hz, 2H), 4.17 (d, J = 2.3 Hz, 2H), 3.90 (dd, J = 13.7, 3.5 Hz, 2H), 3.80 – 3.37 (m, 31H), 3.22 (ddd, J = 31.0, 14.3, 5.8 Hz, 2H), 2.83 (t, J = 2.3 Hz, 1H), 1.83 – 1.74 (m, 1H), 1.71 – 1.61 (m, 1H), 1.42 – 1.30 (m, 1H), 1.26 – 1.13 (m, 1H), 1.07 – 0.95 (m, 2H), 0.90 (t, J = 7.4 Hz, 3H), 0.82 (dd, J = 16.2, 7.3 Hz, 6H), 0.65 (d, J = 6.8 Hz, 3H).

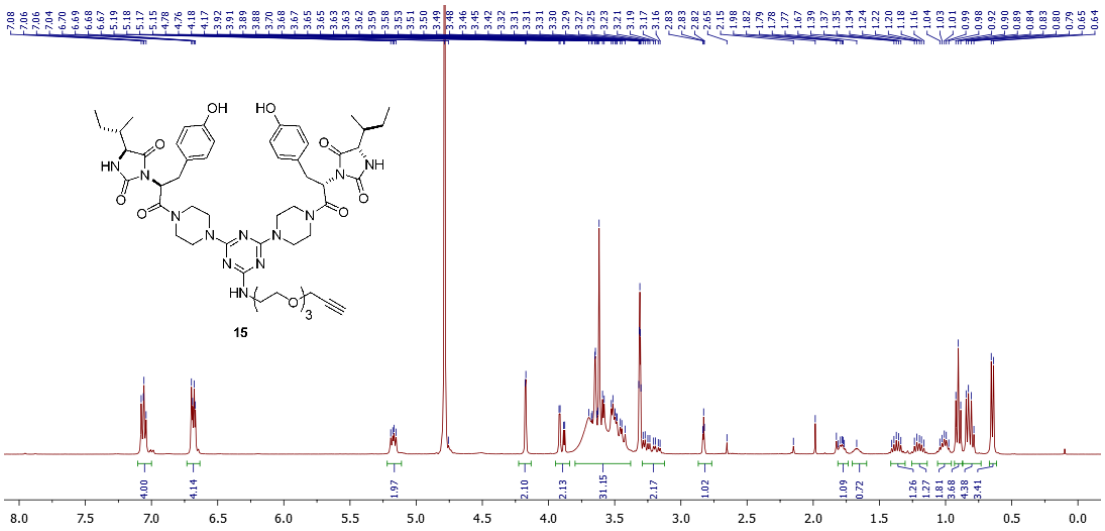

^{13}C NMR (101 MHz, MeOD) δ 175.89, 175.38, 169.37, 169.35, 167.66, 166.49, 159.07, 158.58, 157.47, 157.44, 131.50, 131.39, 128.79, 128.72, 116.32, 116.30, 80.69, 76.01, 71.57, 71.37, 71.26, 71.03, 70.12, 62.90, 61.63, 59.05, 54.29, 53.72, 46.65, 44.30, 43.93, 43.63, 41.37, 38.14, 37.84, 34.50, 34.37, 27.10, 24.57, 15.30, 13.60, 12.02, 11.89.

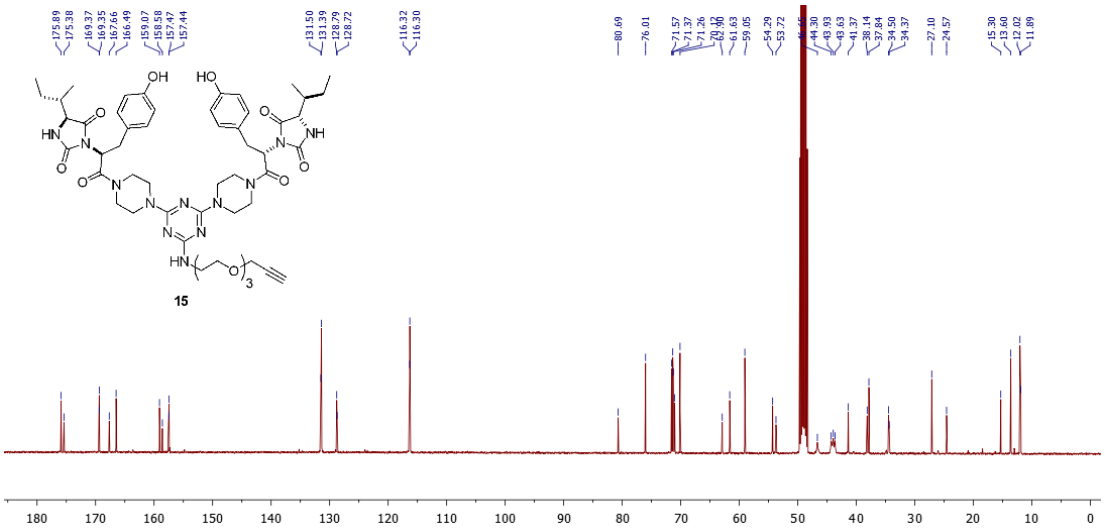

16

$C_{17}H_{24}N_2O_3$

^{1}H NMR (400 MHz, $CDCl_3$) δ 7.82 (d, J = 9.0 Hz, 2H), 6.80 (d, J = 9.0 Hz, 2H), 3.67 – 3.40 (m, 4H), 3.37 – 3.08 (m, 4H), 2.45 (s, 3H), 1.43 (s, 9H).

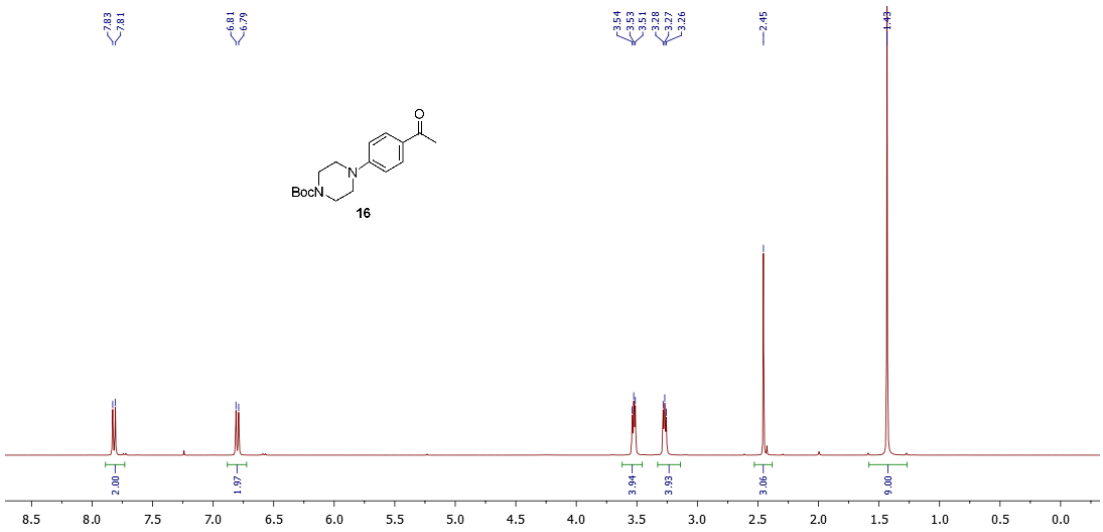

^{13}C NMR (101 MHz, $CDCl_3$) δ 196.55, 154.78, 154.12, 130.53, 128.25, 113.88, 80.29, 47.52, 28.55, 26.23.

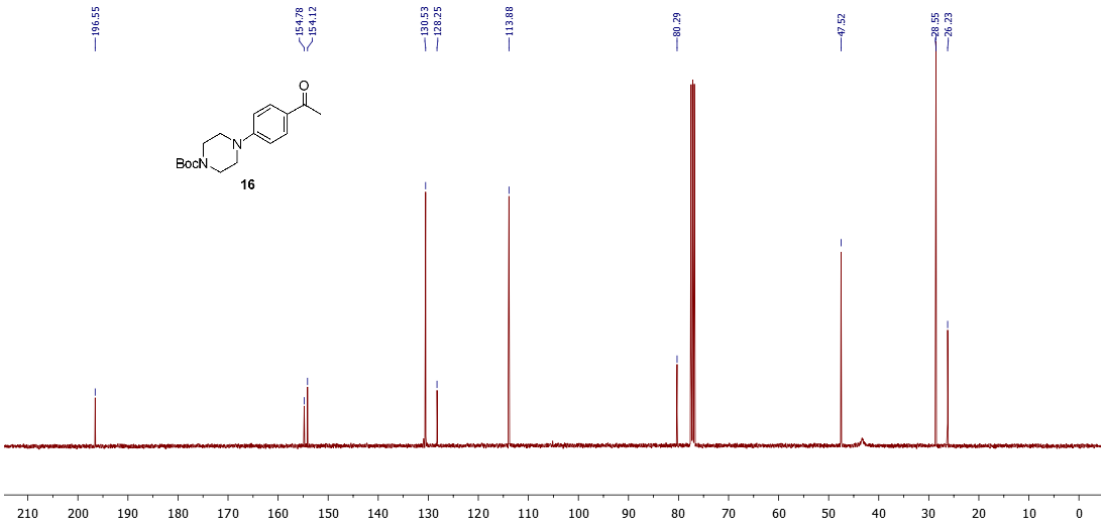

17

$C_{24}H_{27}BrN_2O_3$

^{1}H NMR (400 MHz, $CDCl_3$) δ 7.97 (d, J = 8.8 Hz, 2H), 7.69 (d, J = 15.6 Hz, 1H), 7.55 – 7.42 (m, 5H), 6.88 (d, J = 8.9 Hz, 2H), 3.65 – 3.49 (m, 4H), 3.42 – 3.27 (m, 4H), 1.47 (s, 9H).

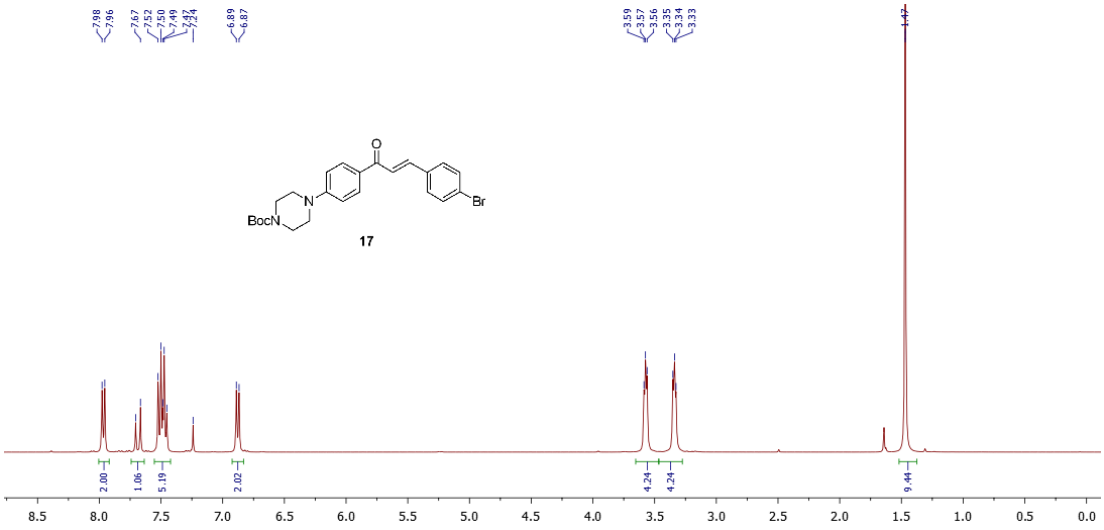

^{13}C NMR (101 MHz, $CDCl_3$) δ 187.82, 154.77, 154.12, 141.92, 134.40, 132.25, 130.85, 129.77, 128.62, 124.41, 122.70, 113.93, 80.31, 47.41, 28.55.

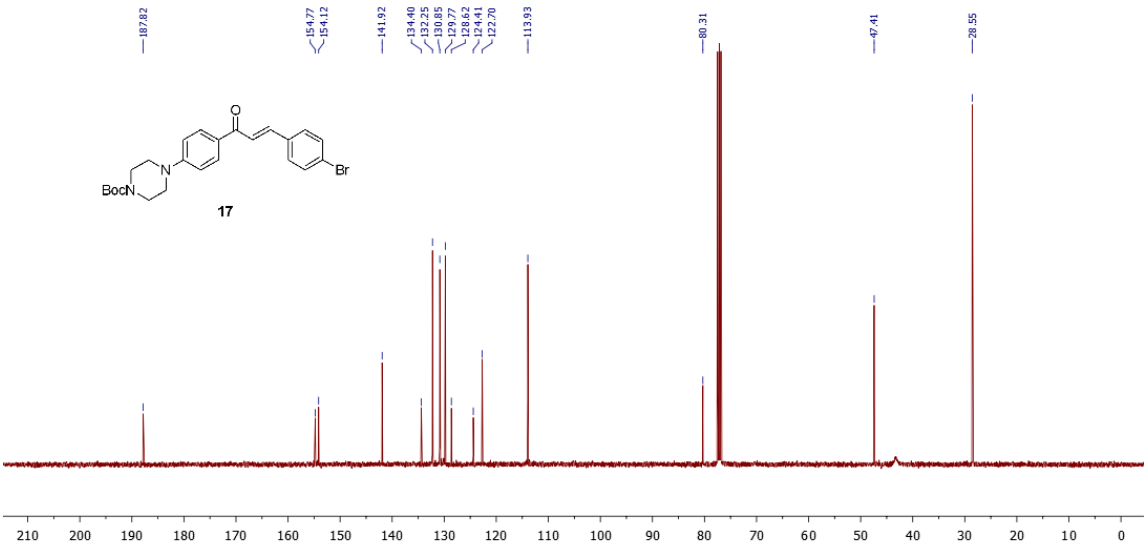

18

$C_{25}H_{30}BrN_3O_5$

^{1}H NMR (400 MHz, $CDCl_3$) δ 7.80 (d, J = 9.0 Hz, 2H), 7.42 (d, J = 8.4 Hz, 2H), 7.14 (d, J = 8.4 Hz, 2H), 6.81 (d, J = 9.0 Hz, 2H), 4.79 (dd, J = 12.6, 6.3 Hz, 1H), 4.62 (dd, J = 12.6, 8.3 Hz, 1H), 4.21 – 4.07 (m, 1H), 3.60 – 3.52 (m, 4H), 3.36 – 3.23 (m, 6H), 1.46 (s, 9H).

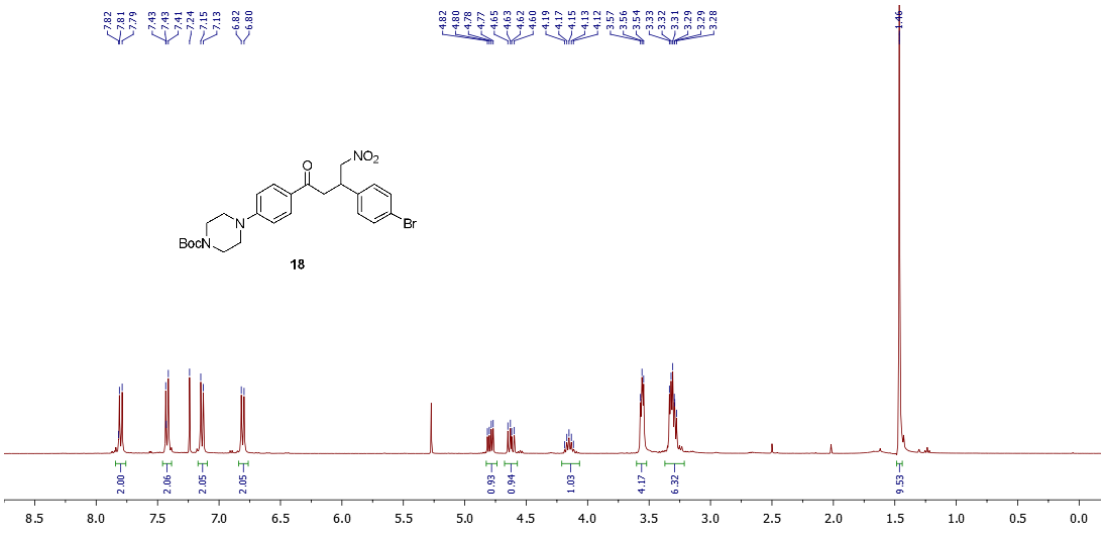

^{13}C NMR (101 MHz, $CDCl_3$) δ 194.57, 154.78, 154.38, 138.62, 132.28, 130.34, 129.37, 126.91, 121.84, 113.72, 80.40, 79.53, 47.26, 40.83, 39.22, 28.56.

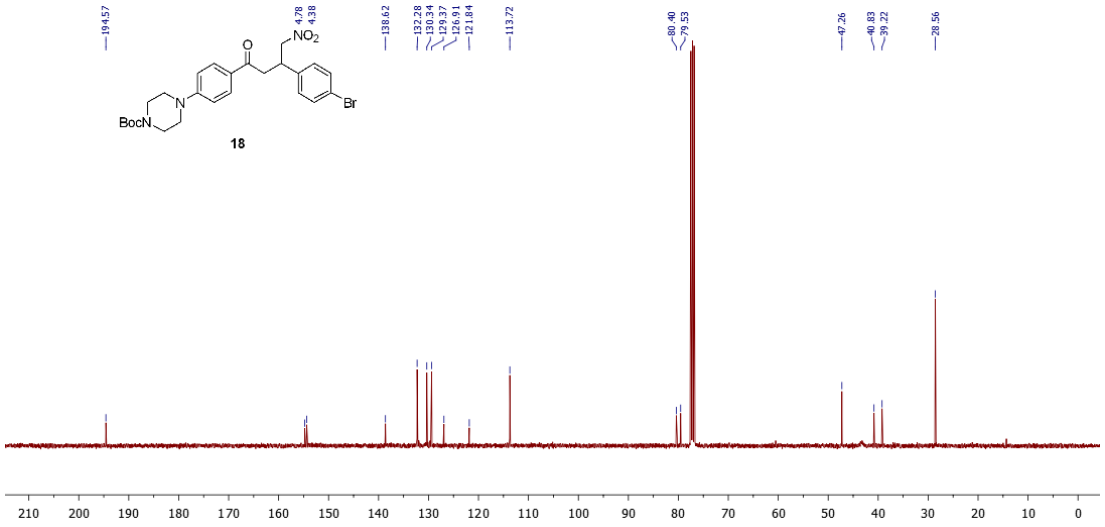

19

$C_{50}H_{53}Br_2N_7O_4$

^{1}H NMR (400 MHz, $CDCl_3$) δ 7.84 (d, J = 8.3 Hz, 4H), 7.74 (d, J = 8.5 Hz, 4H), 7.46 (d, J = 8.3 Hz, 4H), 7.01 (s, 2H), 6.94 (d, J = 8.5 Hz, 4H), 3.62 (s, 8H), 3.32 (s, 8H), 1.49 (s, 18H).

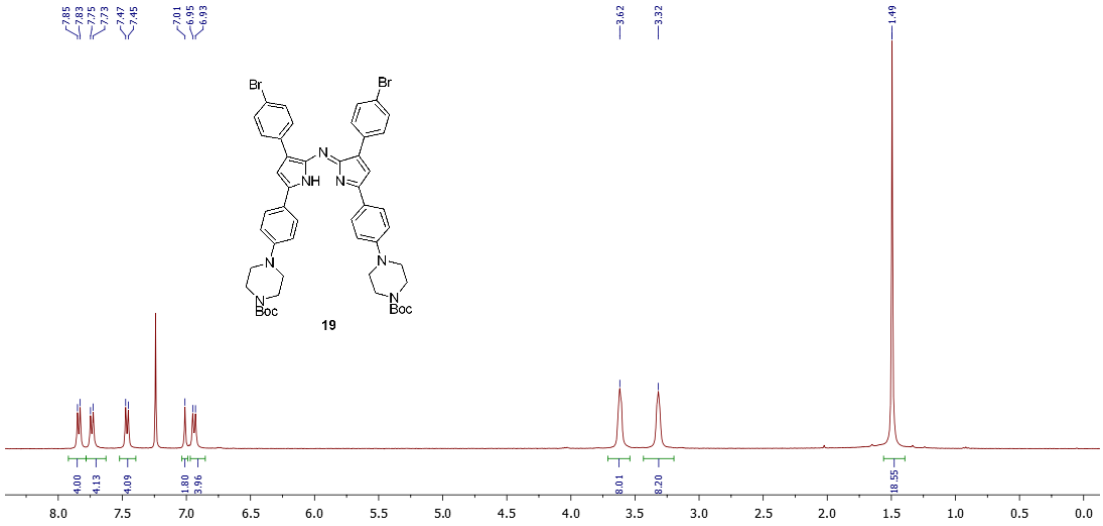

^{13}C NMR (101 MHz, $CDCl_3$) δ 154.86, 154.09, 152.22, 149.55, 140.30, 133.13, 131.43, 130.49, 128.10, 123.09, 122.04, 115.66, 114.35, 80.33, 53.55, 48.20, 28.62.

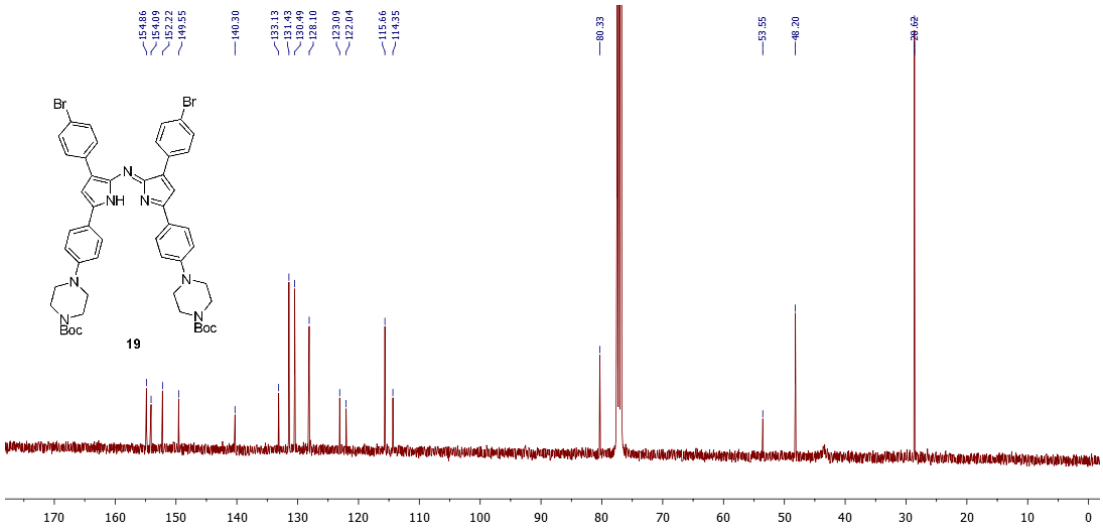

20

$C_{50}H_{52}BBr_2F_2N_7O_4$

^{1}H NMR (400 MHz, $CDCl_3$) δ 8.03 (d, J = 9.0 Hz, 4H), 7.83 (d, J = 8.6 Hz, 4H), 7.49 (d, J = 8.6 Hz, 4H), 6.97 (s, 2H), 6.86 (d, J = 9.1 Hz, 4H), 3.62 – 3.47 (m, 8H), 3.37 – 3.21 (m, 8H), 1.48 (s, 18H).

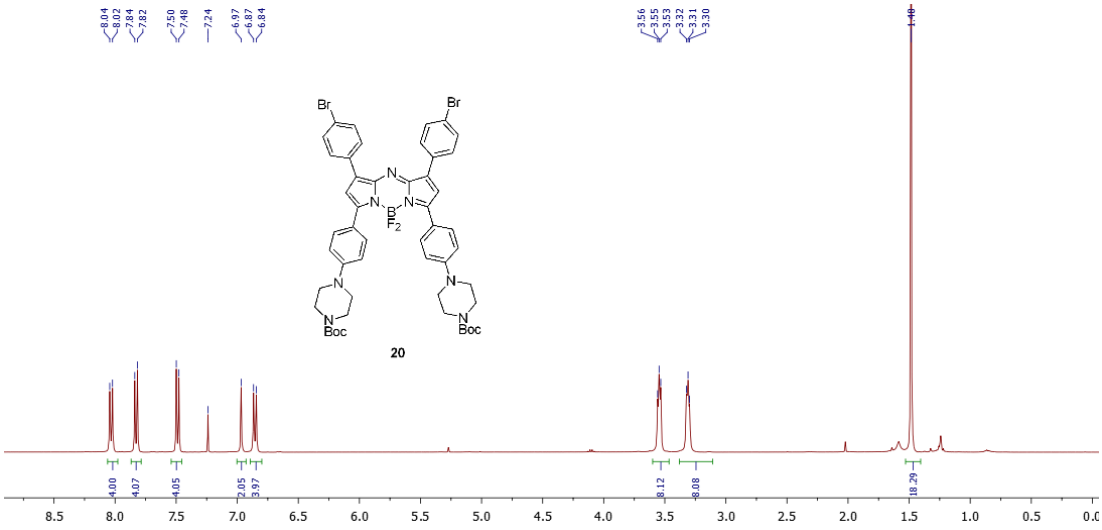

^{13}C NMR (101 MHz, $CDCl_3$) δ 156.79, 154.80, 152.30, 145.18, 140.23, 131.79, 131.74, 131.71, 130.55, 123.45, 121.54, 118.42, 114.47, 80.31, 47.36, 43.28, 28.58.

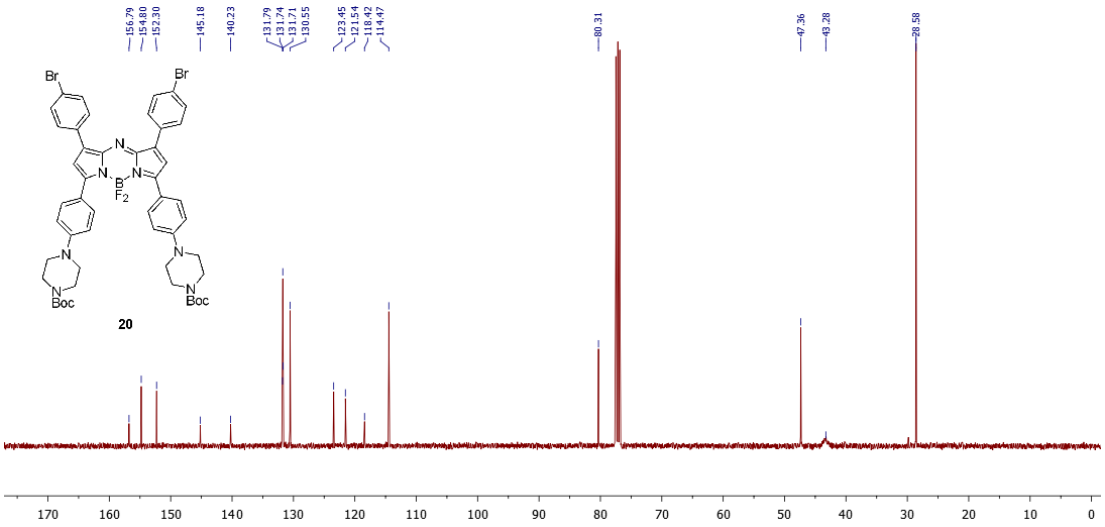

^{11}B NMR (128 MHz, $CDCl_3$) δ 1.35, 1.10, 0.85.

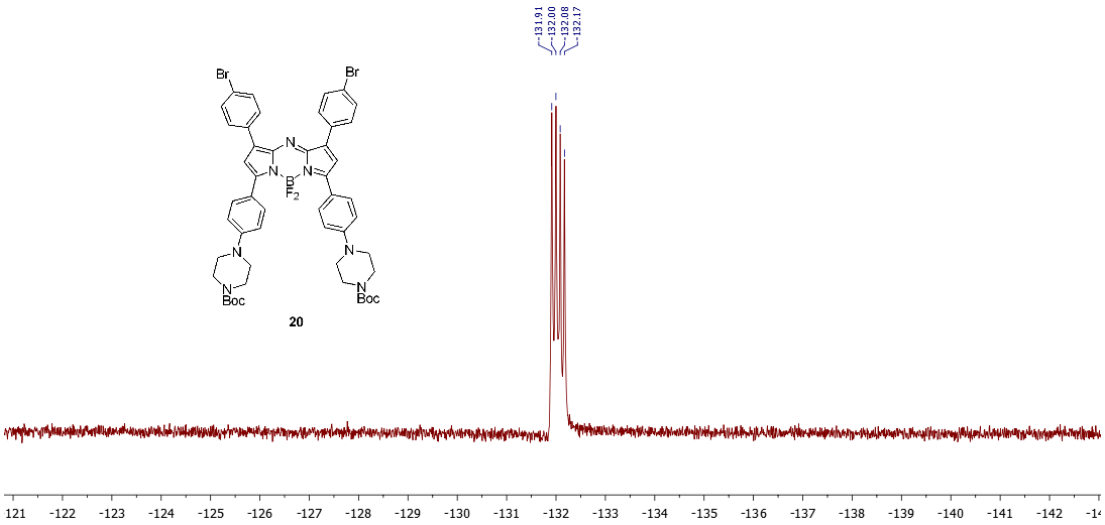

^{19}F NMR (376 MHz, $CDCl_3$) δ -131.91, -132.00, -132.08, -132.17.

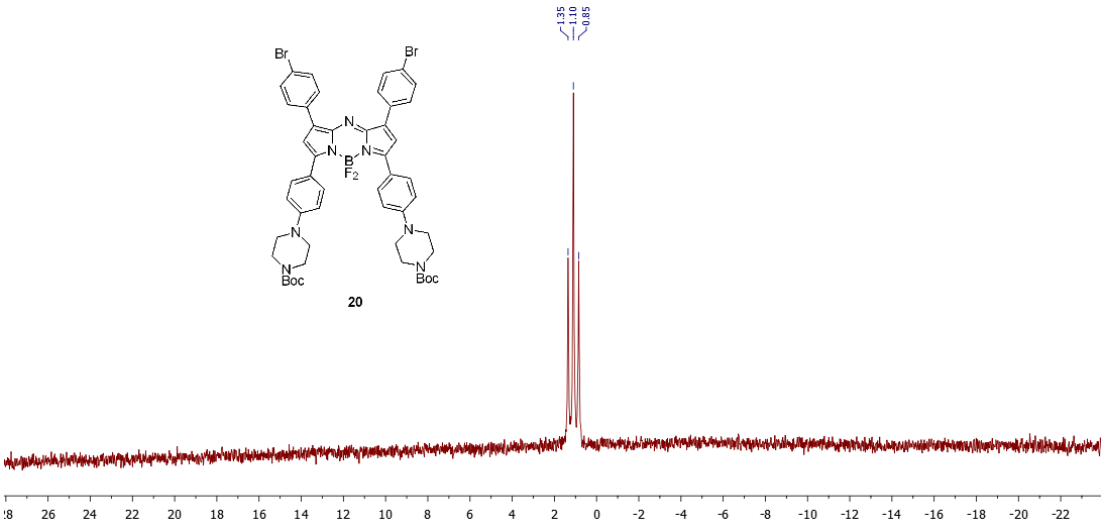

21

$C_{40}H_{36}BBr_2F_2N_7$

^{1}H NMR (400 MHz, DMSO) δ 9.29 (s, 4H), 8.17 (d, J = 8.8 Hz, 4H), 8.06 (d, J = 8.4 Hz, 4H), 7.72 (d, J = 8.5 Hz, 4H), 7.63 (s, 2H), 7.12 (d, J = 9.1 Hz, 4H), 3.70 (t, J = 9.1 Hz, 8H), 3.48 – 3.25 (m, 8H).

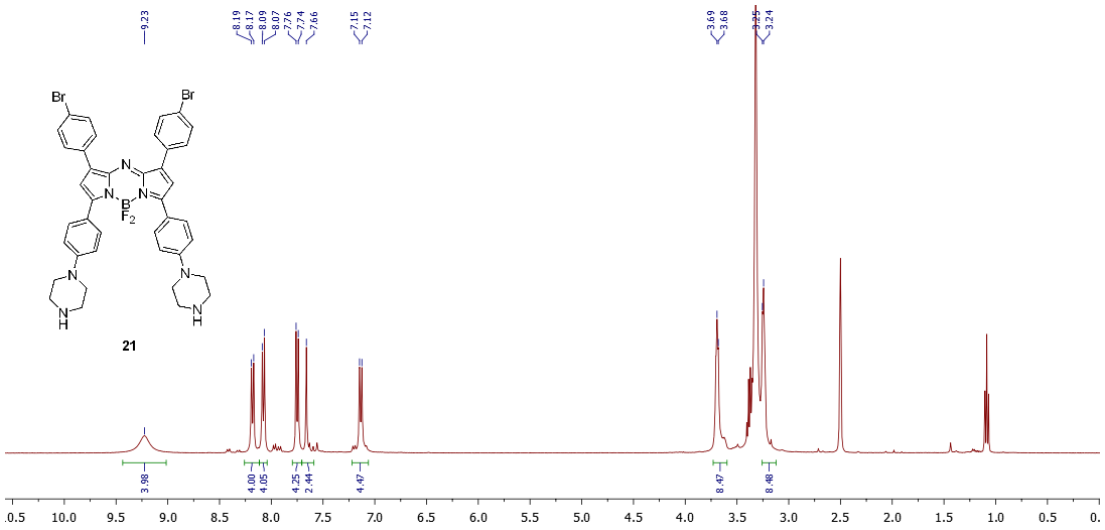

^{11}B NMR (128 MHz, DMSO) δ 1.31, 1.06, 0.80.

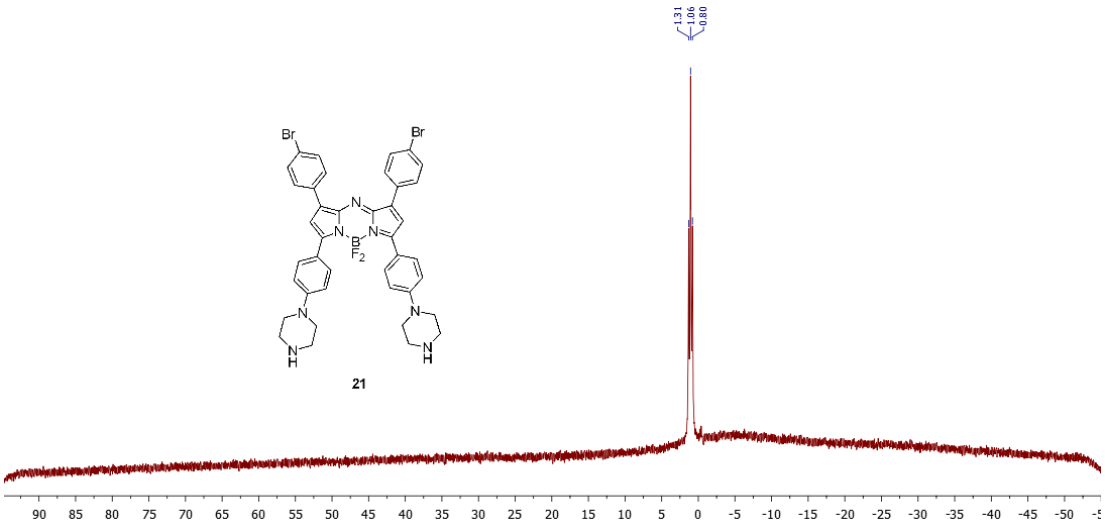

^{19}F NMR (376 MHz, DMSO) δ -130.67, -130.74, -130.83, -130.92.

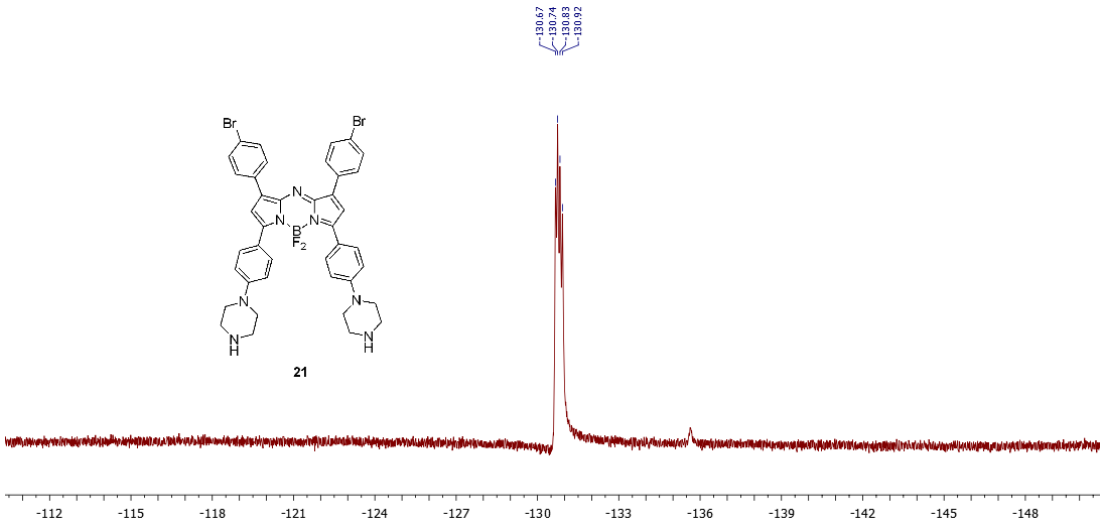

22

$C_{56}H_{62}BBr_2F_2N_9O_8S_2$

^{1}H NMR (400 MHz, MeOD) δ 8.09 (d, J = 8.9 Hz, 4H), 7.83 (d, J = 8.4 Hz, 4H), 7.44 (d, J = 8.4 Hz, 4H), 7.14 (s, 2H), 6.95 (d, J = 8.2 Hz, 4H), 5.14 – 4.97 (m,

2H), 4.02 – 3.87 (m, 4H), 3.80 – 3.73 (m, 4H), 3.62 – 3.55 (m, 2H), 3.53 – 3.35 (m, 8H), 3.11 – 3.02 (m, 2H), 1.46 (s, 18H).

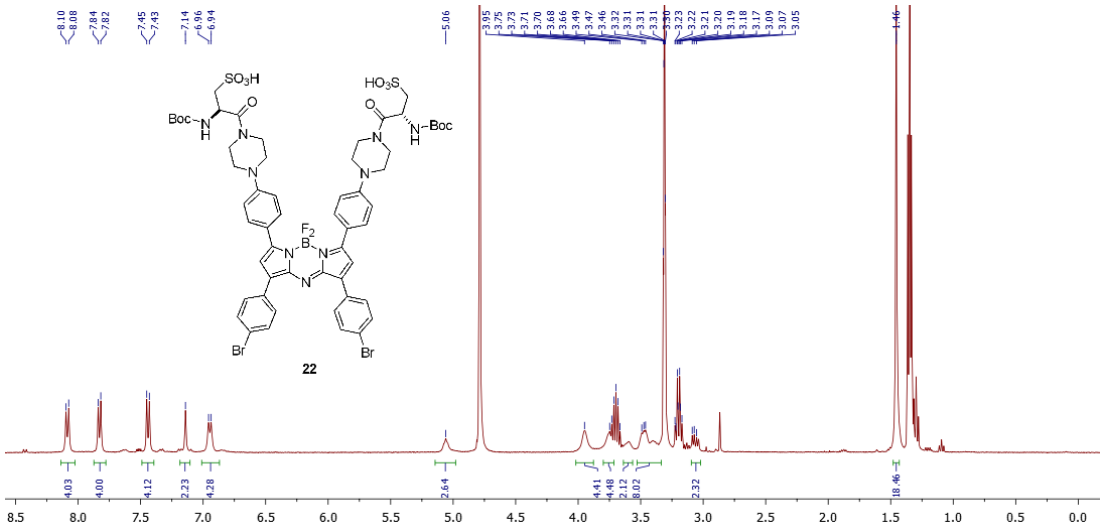

^{11}B NMR (128 MHz, MeOD) δ 1.10, 0.84, 0.59.

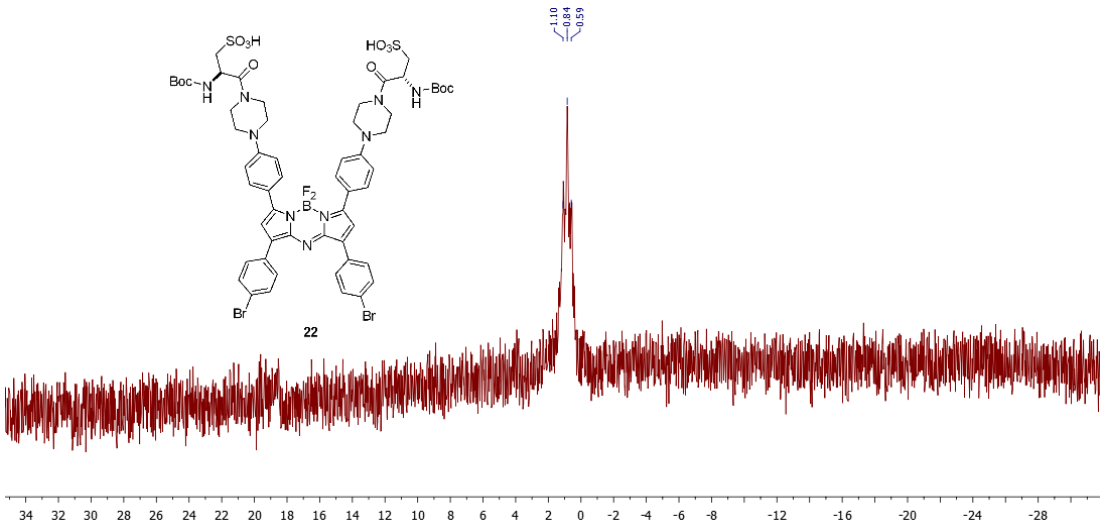

23

$C_{46}H_{46}BBr_2F_2N_9O_8S_2$

^{1}H NMR (400 MHz, DMSO) δ 8.17 (d, J = 9.0 Hz, 4H), 8.12 – 7.98 (m, 10H), 7.73 (d, J = 8.6 Hz, 4H), 7.64 (s, 2H), 7.11 (d, J = 9.1 Hz, 4H), 4.56 (d, J = 7.5 Hz, 2H), 3.79 – 3.48 (m, 16H), 2.98 (d, J = 14.4 Hz, 2H), 2.82 (dd, J = 14.3, 10.0 Hz, 2H).

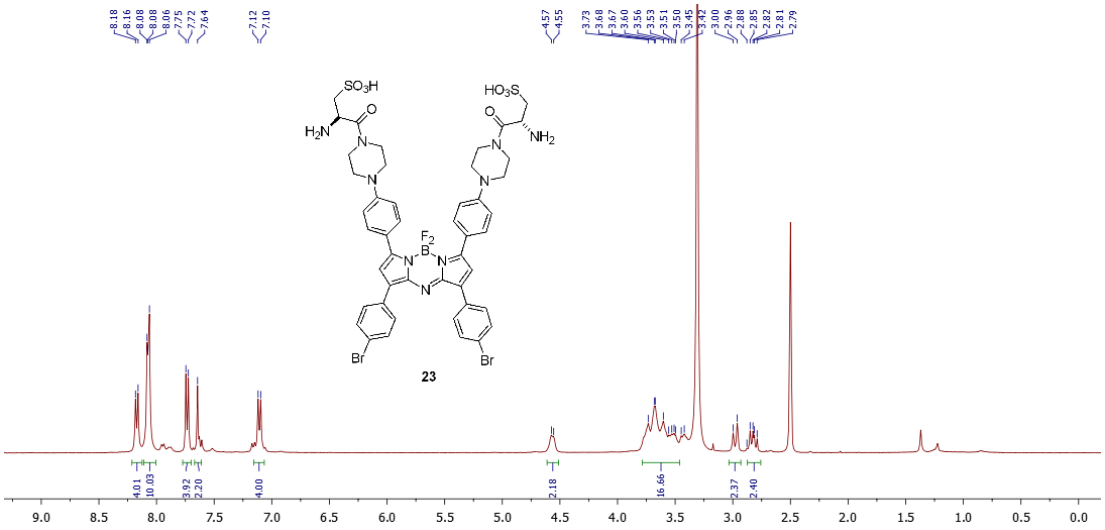

^{13}C NMR (101 MHz, DMSO) δ 165.87, 155.22, 151.69, 144.14, 138.37, 131.75, 131.59, 131.32, 131.16, 130.49, 122.59, 119.68, 119.33, 113.85, 49.72, 48.42, 46.07, 45.86, 44.11, 41.38.

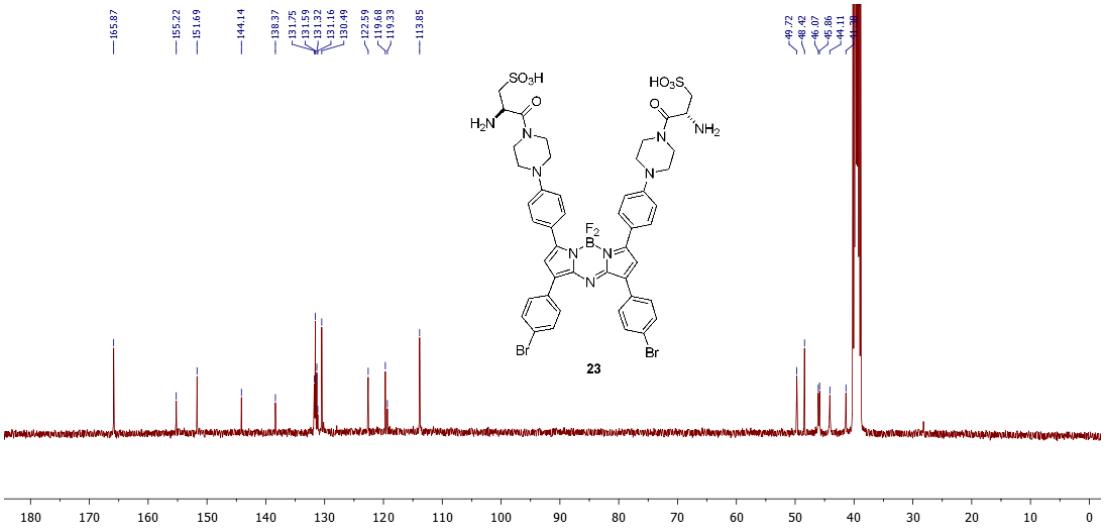

^{11}B NMR (128 MHz, DMSO) δ 1.37, 1.11, 0.85.

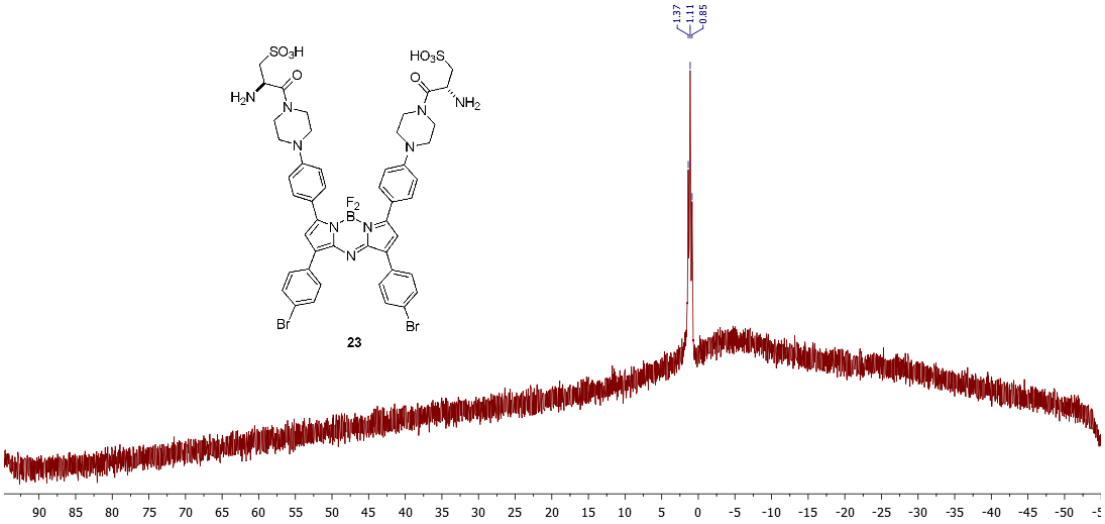

^{19}F NMR (376 MHz, DMSO) δ -130.69, -130.77, -130.86, -130.95.

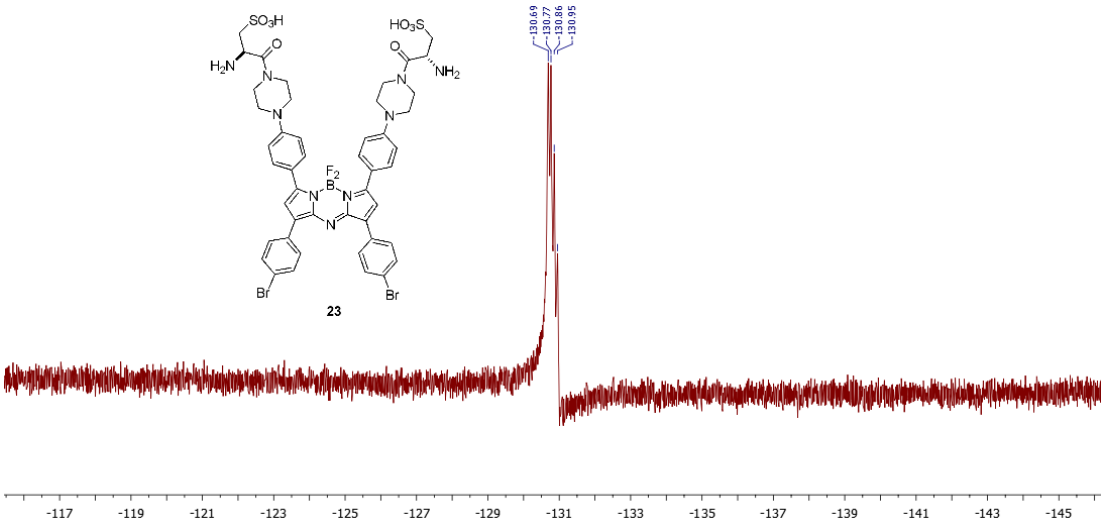

24

$C_{23}H_{30}N_2O_5$

^{1}H NMR (400 MHz, $CDCl_3$) δ 7.43 – 7.24 (m, 5H), 7.06 (d, J = 8.5 Hz, 2H), 6.87 (d, J = 8.6 Hz, 2H), 5.21 – 5.09 (m, 1H), 5.01 (s, 2H), 4.94 – 4.82 (m, 1H), 3.62

(s, 3H), 3.13 (s, 3H), 2.97 (dd, J = 13.6, 6.1 Hz, 1H), 2.81 (dd, J = 12.7, 6.5 Hz, 1H), 1.38 (s, 9H).

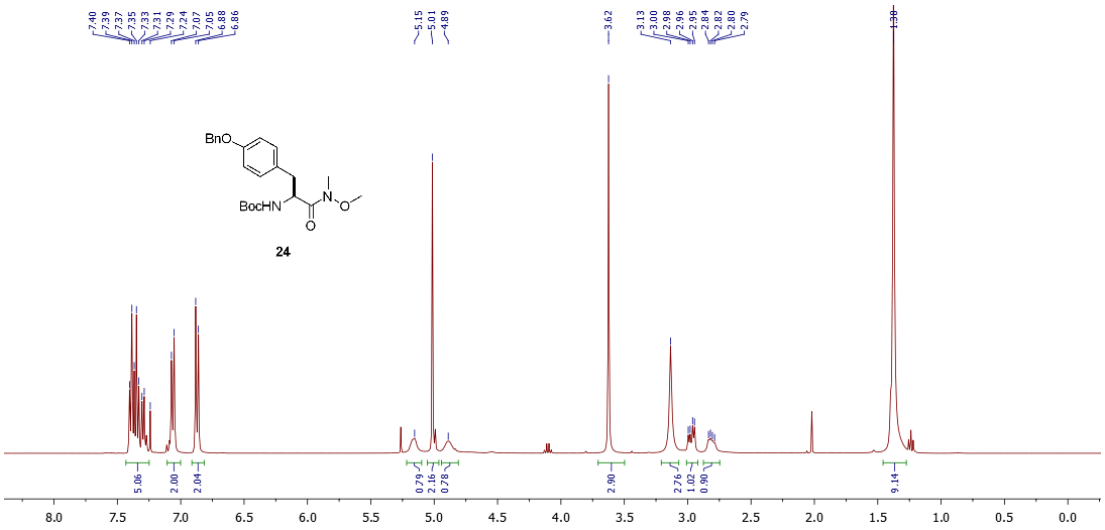

25

$C_{22}H_{25}NO_3$

^{1}H NMR (400 MHz, $CDCl_3$) δ 7.45 – 7.27 (m, 5H), 7.17 (d, J = 8.5 Hz, 2H), 6.91 (d, J = 8.6 Hz, 2H), 5.03 (s, 2H), 4.71 – 4.51 (m, 2H), 2.89 (qd, J = 13.5, 6.1 Hz, 2H), 2.26 (d, J = 2.0 Hz, 1H), 1.42 (s, 9H).

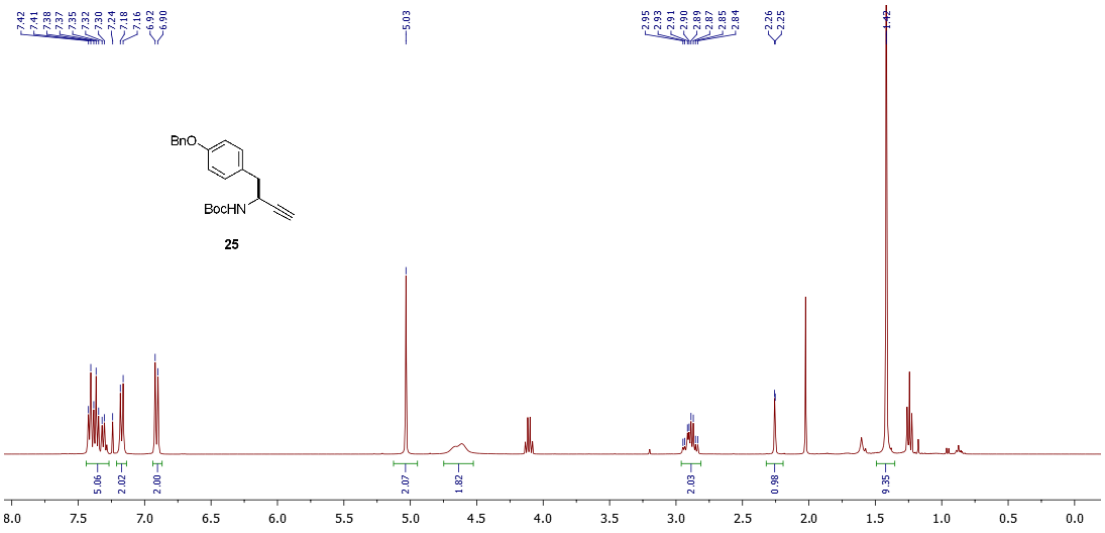

26

$C_{13}H_{17}N_3O_2$

^{1}H NMR (400 MHz, $CDCl_3$) δ 7.41 – 7.29 (m, 5H), 5.23 (d, J = 12.2 Hz, 1H), 5.18 (d, J = 12.2 Hz, 1H), 3.72 (d, J = 6.4 Hz, 1H), 2.03 – 1.88 (m, 1H), 1.48 (dtt, J = 15.0, 7.5, 3.8 Hz, 1H), 1.29 – 1.14 (m, 1H), 0.92 (d, J = 6.8 Hz, 3H), 0.86 (t, J = 7.4 Hz, 3H).

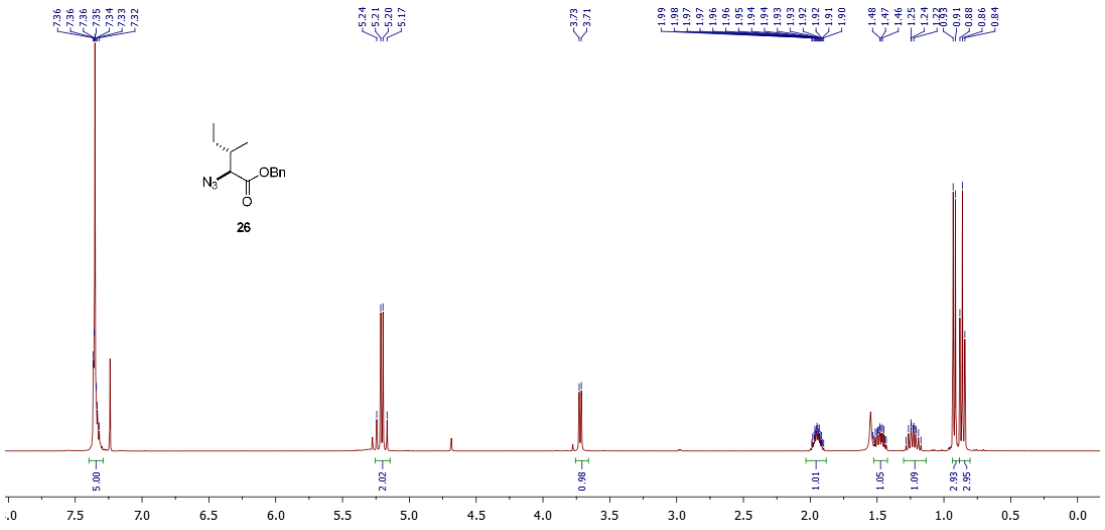

^{13}C NMR (101 MHz, $CDCl_3$) δ 170.22, 135.29, 128.80, 128.73, 128.64, 67.45, 67.37, 37.35, 25.18, 15.98, 11.24.

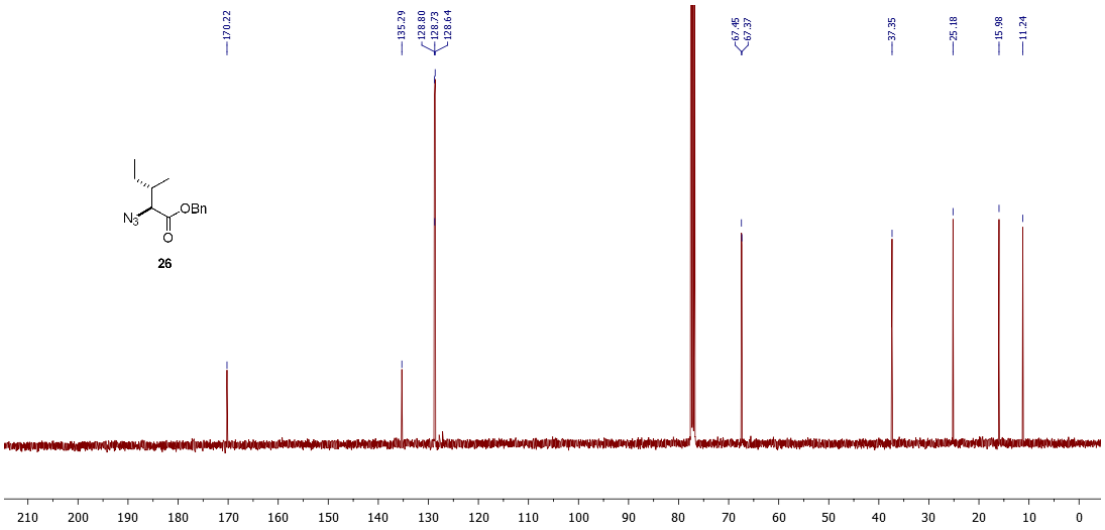

27

$C_{35}H_{42}N_4O_5$

^{1}H NMR (400 MHz, $CDCl_3$) δ 7.45 – 7.20 (m, 11H), 6.97 – 6.86 (m, 2H), 6.86 – 6.71 (m, 2H), 5.20 – 5.09 (m, 3H), 4.97 – 4.87 (m, 2H), 3.07 (ddd, J = 38.5, 31.4, 10.3 Hz, 2H), 2.20 – 1.94 (m, 1H), 1.39 (s, 9H), 1.15 – 1.05 (m, 1H), 0.87 (dd, J = 13.9, 6.8 Hz, 3H), 0.78 (t, J = 7.5 Hz, 3H).

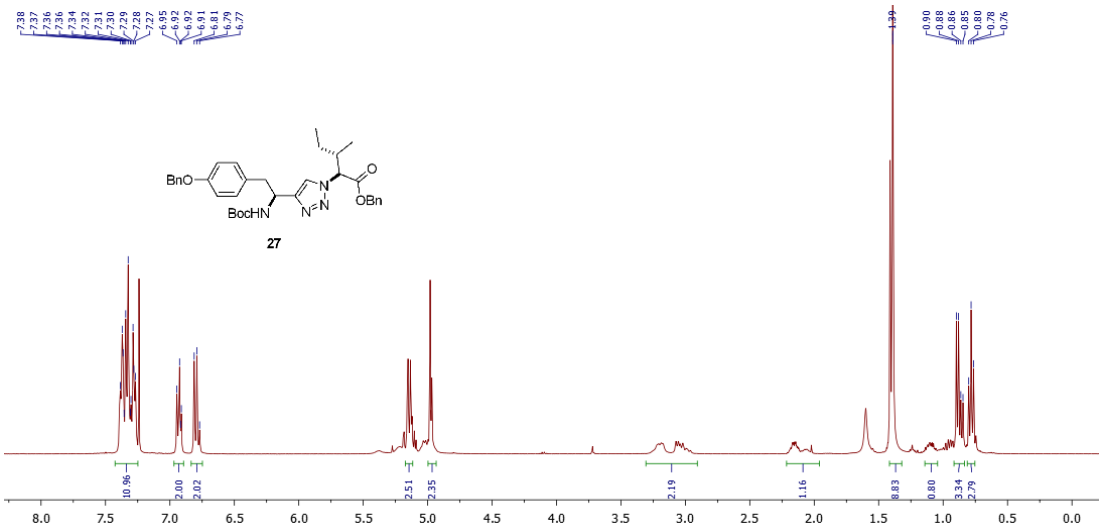

^{13}C NMR (101 MHz, $CDCl_3$) δ 168.51, 157.76, 155.27, 137.29, 134.86, 130.77, 128.88, 128.85, 128.69, 128.60, 128.06, 127.55, 70.19, 67.87, 41.02, 38.47, 28.50, 25.08, 15.53, 10.74.

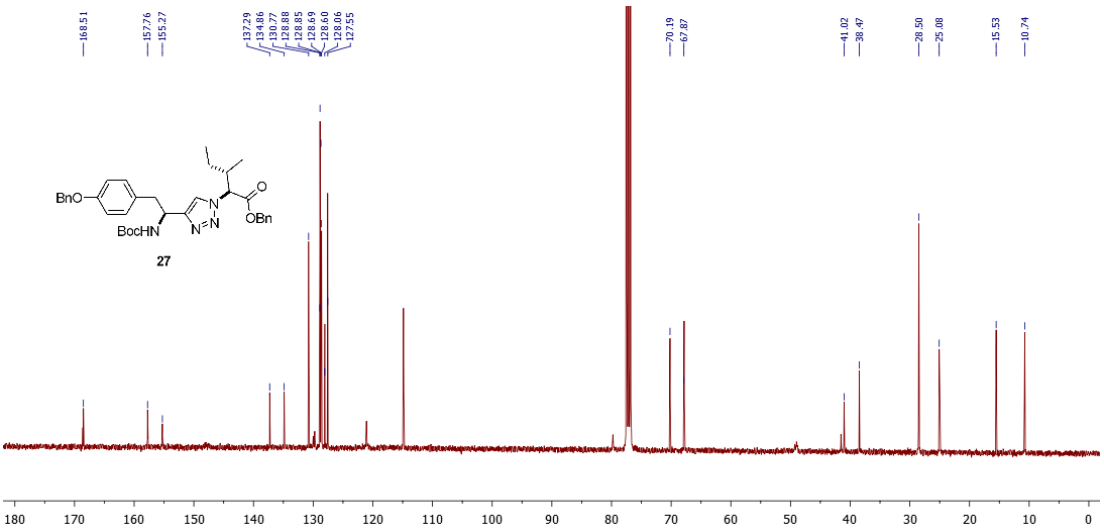

28

$C_{28}H_{31}NO_5$

^{1}H NMR (400 MHz, $CDCl_3$) δ 7.44 – 7.26 (m, 10H), 6.94 (d, J = 8.3 Hz, 2H), 6.82 (d, J = 8.5 Hz, 2H), 5.12 (q, J = 12.2 Hz, 2H), 5.01 (s, 2H), 4.96 (d, J = 7.1 Hz, 1H), 4.58 (d, J = 5.7 Hz, 1H), 3.07 – 2.93 (m, 2H), 1.41 (s, 9H).

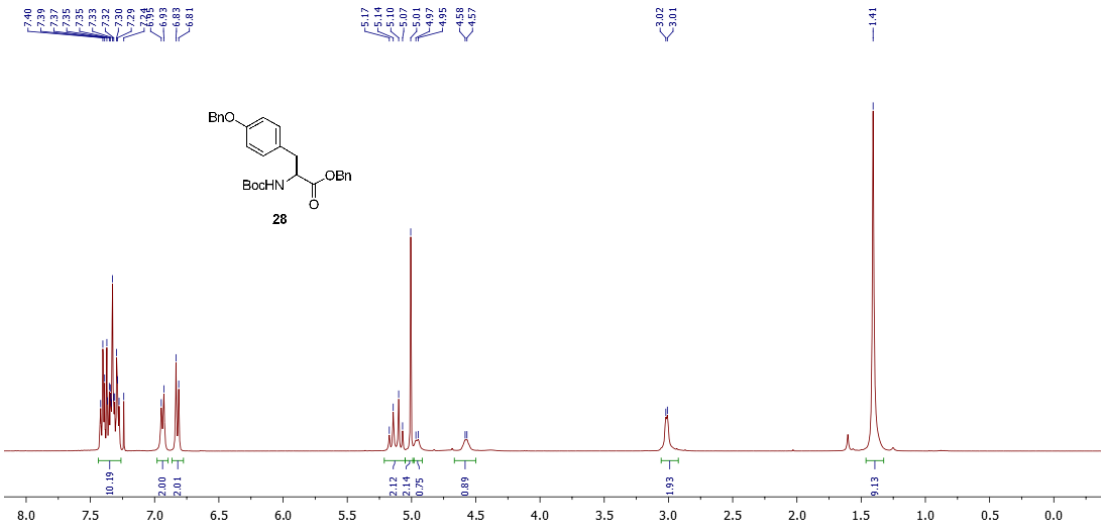

29

$C_{34}H_{42}N_2O_6$

^{1}H NMR (400 MHz, $CDCl_3$) δ 7.43 – 7.25 (m, 10H), 6.91 (d, J = 8.6 Hz, 2H), 6.80 (d, J = 8.6 Hz, 2H), 6.26 (d, J = 6.7 Hz, 1H), 5.14 (d, J = 12.1 Hz, 1H), 5.08 (d, J = 12.1 Hz, 1H), 4.99 (s, 3H), 4.86 (dd, J = 13.6, 5.9 Hz, 1H), 3.97 – 3.84 (m, 1H), 3.03 (d, J = 5.8 Hz, 2H), 1.86 – 1.74 (m, 1H), 1.42 (s, 9H), 1.11 – 0.99 (m, 1H), 0.90 – 0.79 (m, 6H).

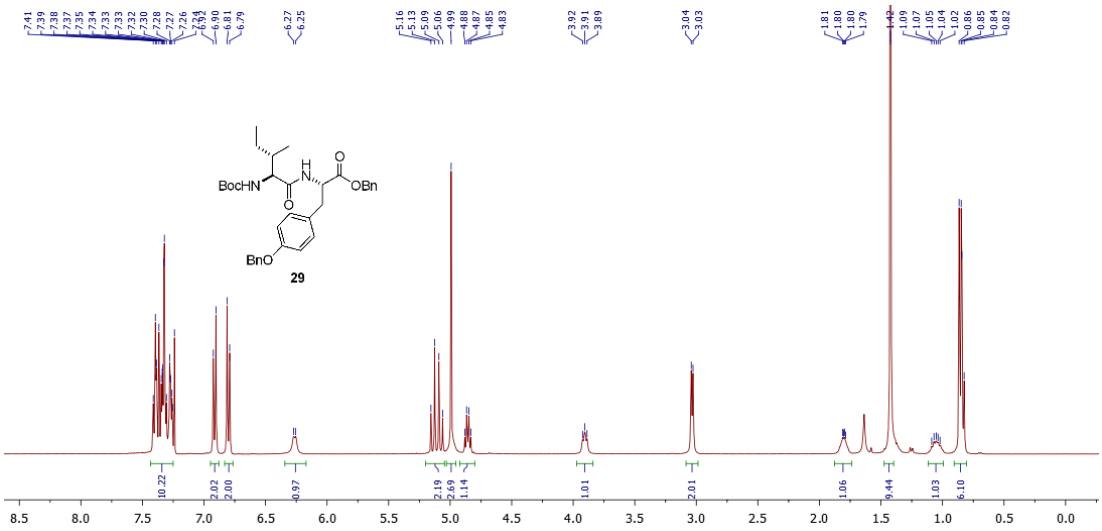

^{13}C NMR (101 MHz, $CDCl_3$) δ 171.26, 158.14, 137.18, 135.22, 130.52, 128.75, 128.73, 128.68, 128.11, 127.92, 127.61, 115.12, 79.72, 70.15, 67.38, 59.44, 53.37, 37.43, 37.31, 28.47, 24.87, 15.56, 11.55.

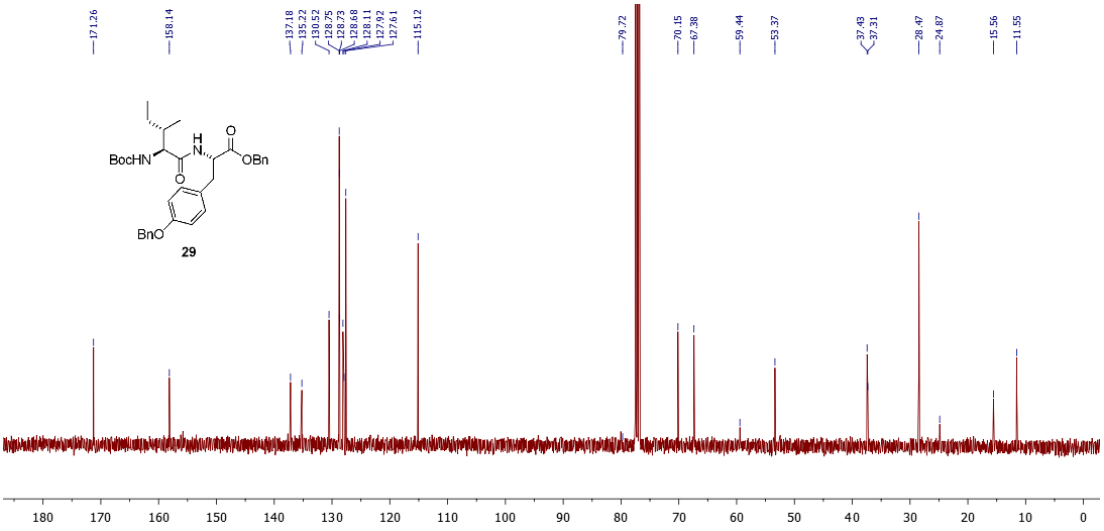

30

$C_{29}H_{34}N_2O_4$

^{1}H NMR (400 MHz, $CDCl_3$) δ 7.43 – 7.19 (m, 10H), 6.97 (d, J = 8.6 Hz, 2H), 6.80 (d, J = 8.6 Hz, 2H), 5.13 (d, J = 12.2 Hz, 1H), 5.06 (d, J = 12.0 Hz, 1H), 4.97 (s, 2H), 4.89 – 4.80 (m, 1H), 3.47 – 3.32 (m, 1H), 3.03 (dd, J = 6.3, 3.0 Hz, 2H), 2.15 (s, 2H), 1.95 – 1.79 (m, 1H), 1.29 – 1.15 (m, 1H), 1.09 – 0.95 (m, 1H), 0.87 (d, J = 6.9 Hz, 3H), 0.81 (t, J = 7.4 Hz, 3H).

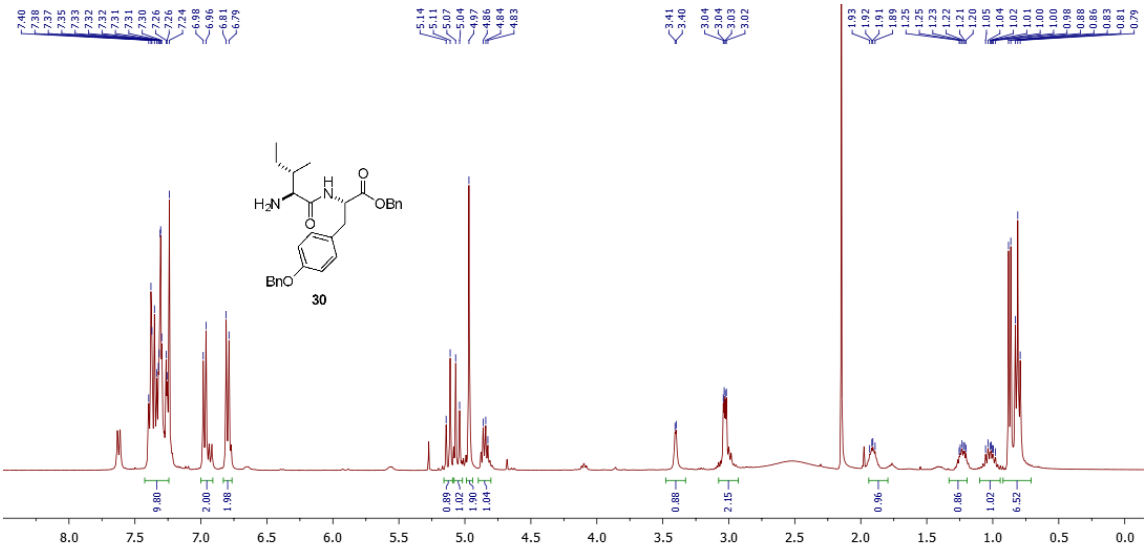

^{13}C NMR (101 MHz, $CDCl_3$) δ 171.74, 158.06, 137.20, 135.40, 130.48, 128.71, 128.62, 128.56, 128.36, 128.09, 127.60, 115.04, 70.14, 67.24, 59.62, 53.38, 37.76, 37.42, 31.03, 24.07, 15.78, 11.89.

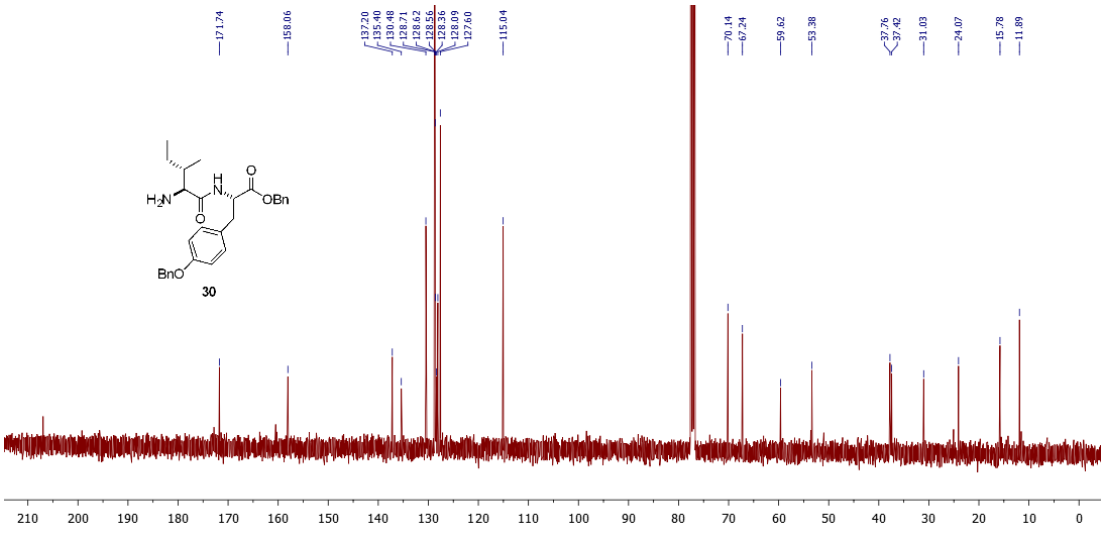

32

$C_{66}H_{68}BF_2N_{13}O_{14}S_2$

^{1}H NMR (400 MHz, DMSO) δ 10.26 (s, 2H), 8.63 – 8.49 (m, 2H), 8.20 (s, 2H), 8.16 (d, J = 8.7 Hz, 4H), 7.92 (d, J = 7.7 Hz, 2H), 7.67 (d, J = 7.9 Hz, 2H), 7.48 (ddd, J = 11.1, 8.3, 3.8 Hz, 2H), 7.37 (s, 2H), 7.20 (dd, J = 8.1, 5.6 Hz, 4H), 7.13 (d, J = 8.9 Hz, 4H), 6.87 (dd, J = 14.2, 8.4 Hz, 4H), 4.65 (dd, J = 12.6, 6.4 Hz, 2H), 4.15 (ddd, J = 24.8, 9.5, 4.4 Hz, 2H), 3.88 (s, 6H), 3.65 – 3.52 (m, 2H), 3.20 – 3.07 (m, 4H), 2.93 – 2.78 (m, 4H), 1.22 (s, 18H).

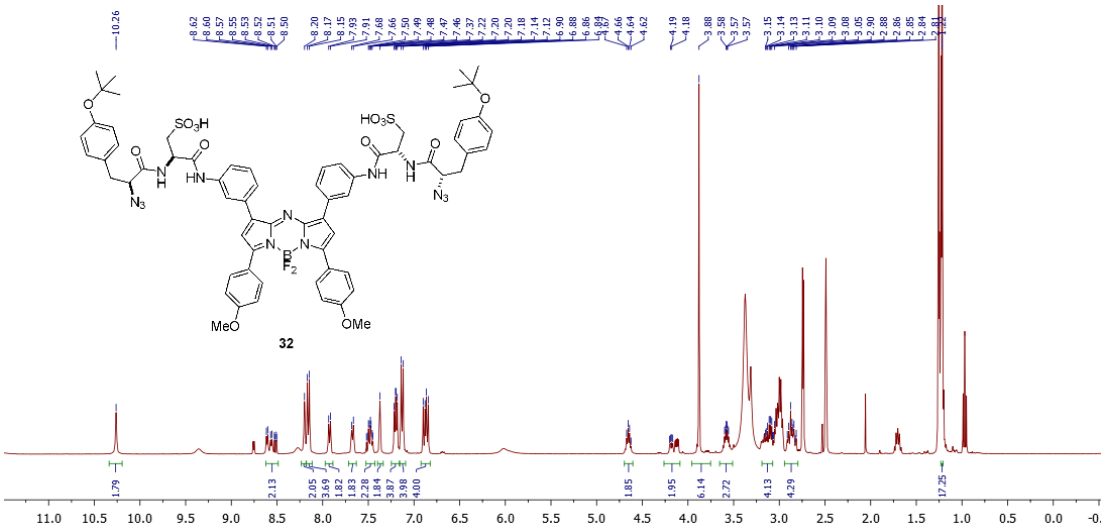

^{13}C NMR (101 MHz, MeOD) δ 170.44, 163.61, 159.01, 157.53, 155.59, 146.26, 139.55, 134.10, 133.06, 131.57, 131.11, 130.90, 130.08, 127.14, 125.40, 125.00, 122.81, 120.32, 116.48, 115.23, 79.59, 65.07, 56.06, 54.70, 44.13, 29.20, 27.22.

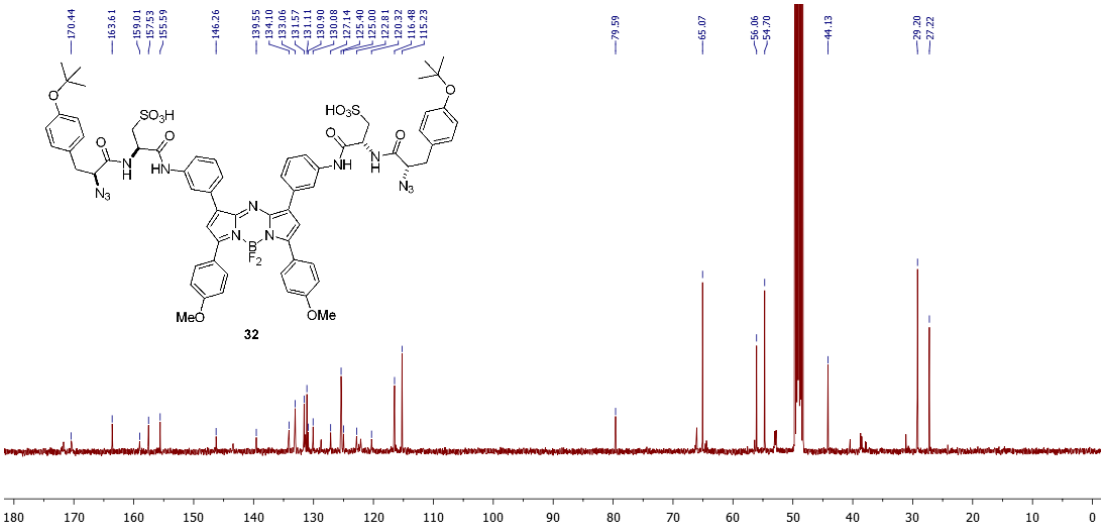

^{11}B NMR (128 MHz, DMSO) δ 1.14, 0.90, 0.64.

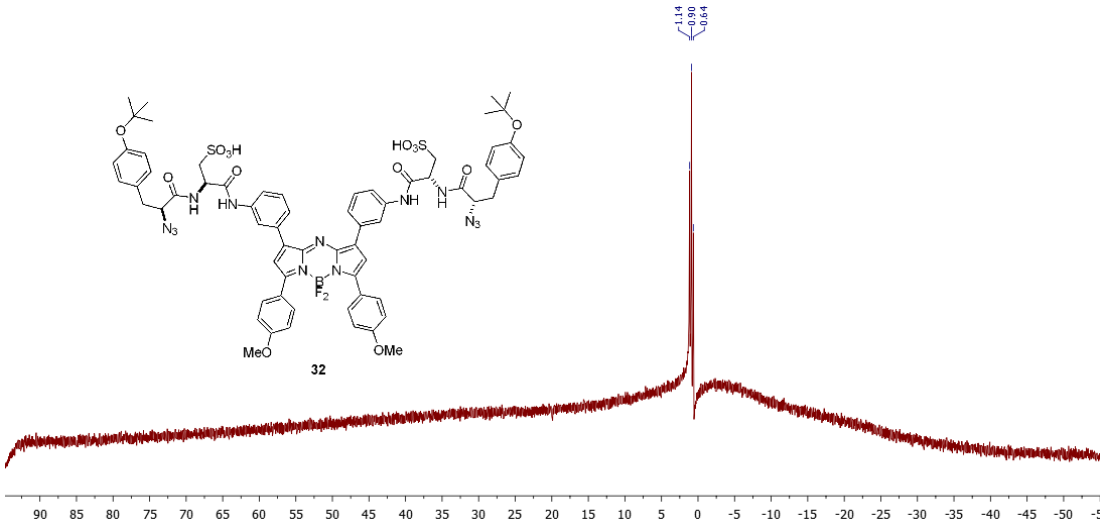

^{19}F NMR (376 MHz, DMSO) δ -130.33, -130.41, -130.50, -130.58.

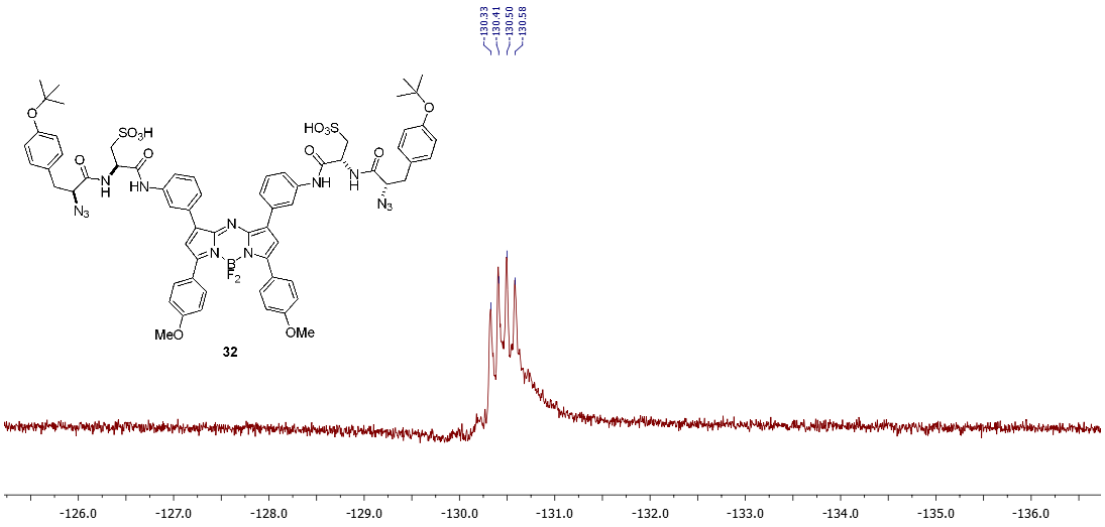

33

$C_{90}H_{110}BF_2N_{15}O_{18}S_2$

^{1}H NMR (400 MHz, DMSO) δ 8.20 – 8.13 (m, 4H), 8.10 (d, J = 9.2 Hz, 2H), 7.93 (d, J = 9.6 Hz, 2H), 7.66 (dd, J = 13.8, 7.9 Hz, 2H), 7.51 – 7.43 (m, 2H), 7.38 (s, 2H), 7.12 (t, J = 10.1 Hz, 4H), 7.01 (d, J = 8.3 Hz, 4H), 6.95 (d, J = 7.0 Hz, 2H),

6.71 (dd, J = 16.3, 8.4 Hz, 4H), 5.75 – 5.37 (m, 2H), 4.67 (dd, J = 36.5, 30.5 Hz, 4H), 3.88 (s, 6H), 3.14 – 2.92 (m, 8H), 2.89 (dd, J = 13.7, 6.6 Hz, 2H), 2.73 (t, J = 17.4 Hz, 4H), 1.70 (dd, J = 18.7, 11.2 Hz, 4H), 1.35 (s, 18H), 1.20 (s, 9H), 1.16 (s, 9H), 0.98 (t, J = 7.2 Hz, 4H), 0.78 (dd, J = 12.3, 7.3 Hz, 6H), 0.60 (t, J = 6.2 Hz, 6H).

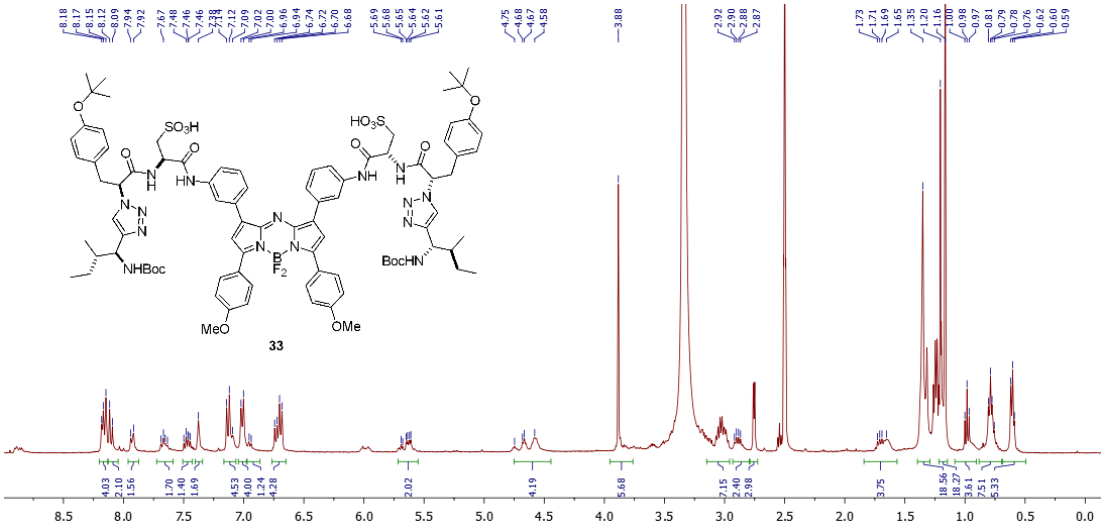

^{13}C NMR (101 MHz, DMSO) δ 168.94, 167.39, 167.32, 161.95, 157.40, 155.01, 153.66, 144.47, 139.45, 139.31, 132.04, 131.72, 130.79, 130.53, 129.40, 129.06, 124.78, 123.36, 123.17, 121.85, 120.91, 119.51, 114.44, 77.71, 77.57, 63.76, 55.54, 53.59, 42.23, 41.82, 28.40, 28.17, 18.03, 16.67, 14.98, 12.38, 11.17.

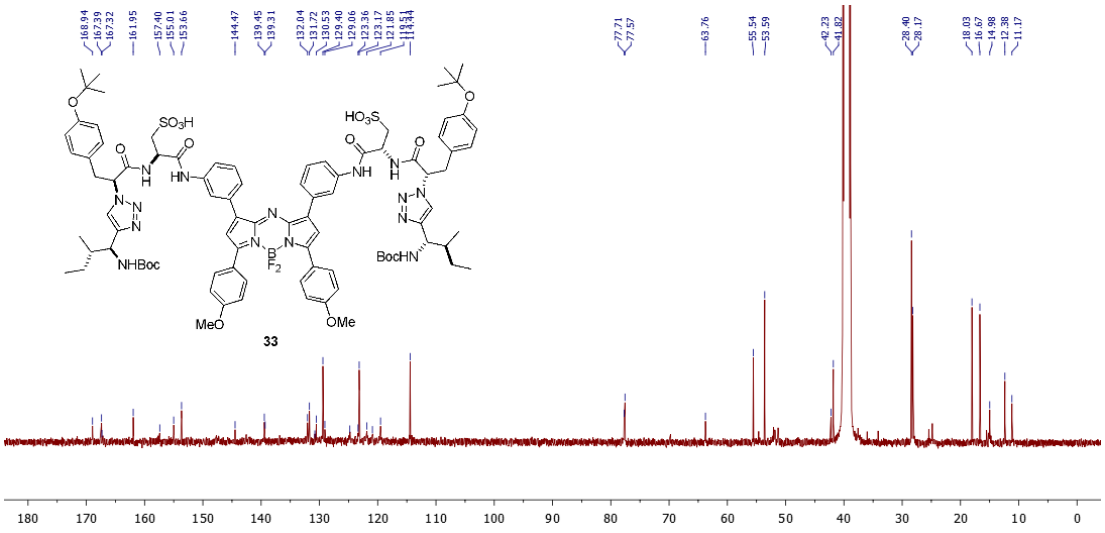

^{11}B NMR (128 MHz, MeOD) δ 1.14, 0.88, 0.63.

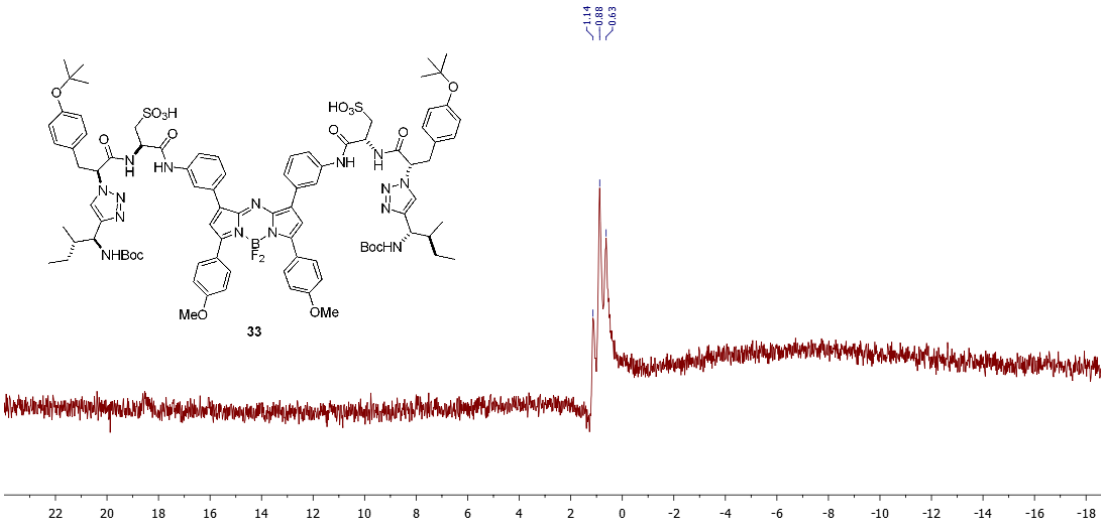

^{19}F NMR (376 MHz, DMSO) δ -130.33, -130.42, -130.50, -130.58.

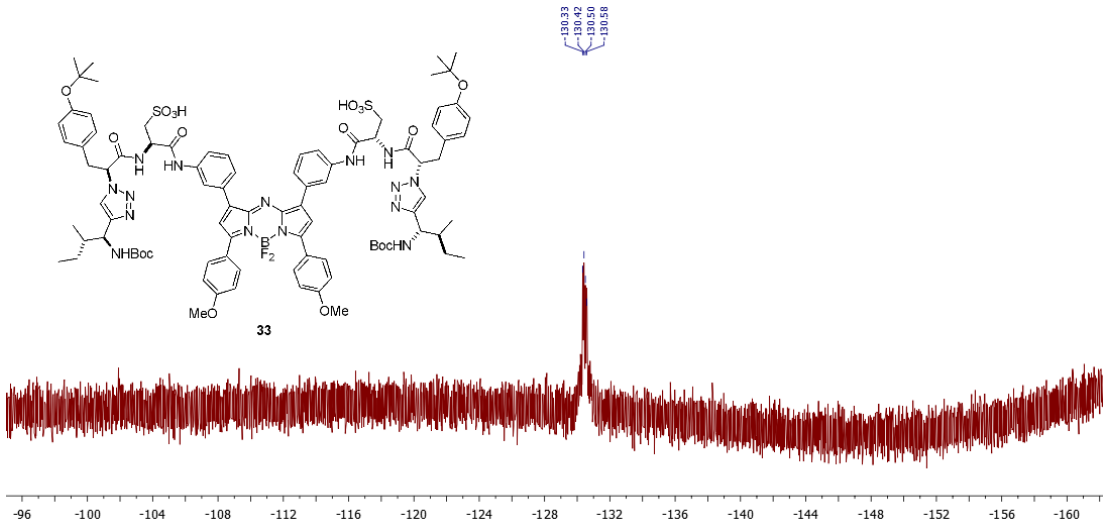
-130.33
-130.42
-130.50
-130.58
SO3H
HO3S
NHBoc
BocHN
MeO
OMe
33
-96
-100
-104
-108
-112
-116
-120
-124
-128
-132
-136
-140
-144
-148
-152
-156
-160

APPENDIX C

TRK TRANSFECTED CELLS GENERATION FOR OBOC LIBRARY SCREENING OF NOVEL TRK TARGETING LIGAND

C.1 Introduction

Tropomyosin receptor kinase (Trk) family plays an important role in signaling pathways related to cell proliferation and survival. Trk receptors are overexpressed in several different types of cancer and are strongly correlated with tumor progression and metastasis.[219-221] Non-specific synthetic Trk inhibitors are reported in literature that successfully reduced tumor growth.[222,223]

It would be beneficial to develop a unique binder to a specific Trk receptor for tumor treatment because it can potentially increase the therapeutic output and reduce the risk of side effect in chemotherapy. Preference of neurotrophin interactions on cell surface indicates the distinguishable extracellular domains among TrkA – C, making it possible to develop small organic molecules that selectively bind to one type of Trk receptor.

Cancer cellular membranes usually contain varied amounts of Trk receptors and other proteins, which poses a significant challenge in identifying a selective Trk ligand via a cell-based assay. Hence, it is desirable to overexpress a single Trk gene in a transfected cell line. Unfortunately, it is extremely hard to obtain commercial Trk transfected cells based on the same cell line, which is

ideal when comparing the ligand affinity to different Trk receptors. Thus, the aim of this project was to obtain uniform Trk transfected cells.

Several factors need to be considered when performing gene transfections. First, a proper host cell line is required for the transfected mammalian gene to be translated and folded correctly. Human embryonic kidney 293 (HEK293) and Chinese hamster ovary (CHO) cells are most typical for mammalian gene transfection. NIH3T3 and some other cell lines are also used as host cells in transfection.[224-227] Second, the design of the DNA plasmid or gene construct is crucial for gene expression that is generally beyond our knowledge. Luckily, Addgene has several plasmids deposited by Dr. Moses Chao's research group that showed Trk receptor expression in their previous work.[224] In their design, CMV and SV40 promoters were used to improve the expression efficiency of the inserted genes. Third, a proper method to perform the plasmid transfection into the host cells is important. In general, the plasmid can be transfected by chemical, physical or biological methods.[226,228,229] Phosphate precipitation and liposome complexation are the widely applied chemical methods and suitable for most of the cell types,[226,230] while electroporation is the most common physical way to introduce foreign gene.[231,232] Furthermore, a suitable way for selecting cell population with high transfected protein expression is another key factor to improve the transfection efficacy. Usually, a fluorescence tag or an antibiotic resistant selection marker is incorporated with the target gene, and either cell sorting (via flow cytometry) or

antibiotic pressure (in culture medium) is applied to remove the population with low transfection rate.[225,226]

In this chapter, the general protocol of Trk gene transfection and results are summarized for future reference.

C.2 Results and Discussion

C.2.1 Sequencing and quality check of the plasmids

Plasmids containing TrkA, B and C genes were extracted from single colonies of *E. coli*. and sequenced briefly to confirm the correct gene insert was obtained from Addgene (Figure C.1a). As a sample study, a list of primers was designed with primer-BLAST tool[233] in order to confirm the whole sequence of the inserted TrkC gene on pcDNA-TrkC plasmid (Table C-1).

Table C.1. Primers designed for pcDNA-TrkC plasmid.

forward primers

site	sequence	T_m (^oC)
768-788	ACGCAAATGGGCGGTAGGCGT	67.60
1302-1320	CCAGCATCAACATCACGGA	57.84
1752-1771	TGACTGTCCGAGAAGGAGAC	58.46
2318-2338	GACTTTGAGTCTGATGCGAGC	59.34
2750-2769	GTCTTCCTGGCTGAGTGCTA	59.10
3139-3159	CACCAGGAACTGCCTAGTTGG	60.61

Table C.1. Continued.

reverse primers

site	sequence	T_m (^oC)
3700-3683	TAGAAGGCACAGTCGAGG	55.56
3168-3149	AGGTTGGCTCCAACTAGGCA	61.13
2681-2661	ATGTGTCTGGCTTGTGGCAAT	60.82
2214-2194	TTGTTGTAGTGGGTGGGCTTG	60.75
1715-1695	ACTGACTGATGTTCATGCGGA	59.72
1172-1153	CATAGTCCAGCCAGACGCTT	59.82

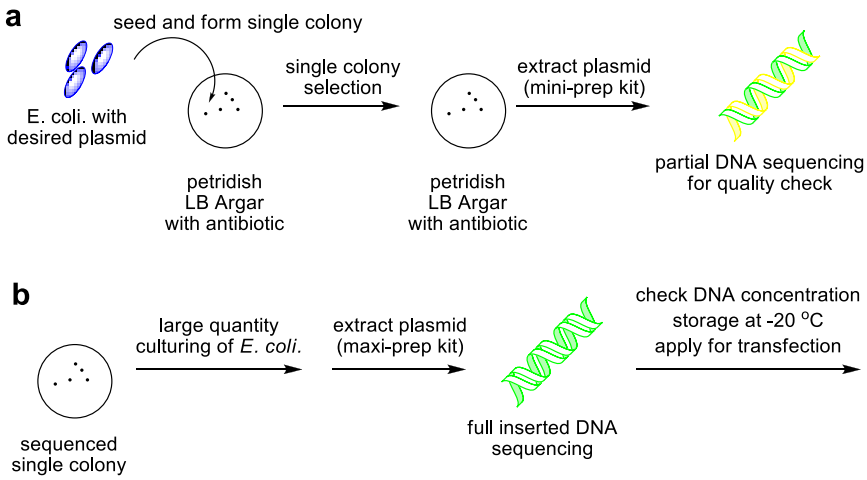

Figure C.1. General protocol to prepare DNA plasmid for mammalian cell transfection. Detailed plasmid extraction protocol can be obtained from Zymo Research website.

When designing the primers, several factors were taken into consideration. (i) Length of the primer was between 15 to 25 nucleotides. (ii) Estimated melting temperature (T_m) of the primer was 60 ± 5 ^oC {estimated by equation T_m (^oC) = 4(C + G) + 2(A + T), primer-BLAST also provide an estimate value listed in Table C.1}. (iii) No homo-dimer or hairpin structure was formed for a single primer; each primer was unique for the plasmid sequence region it was designed to bind to (no match with other positions on the whole plasmid). (iv) The distance between two primers on the same sequencing direction was less than 700 nucleotides. More detailed discussion has been presented in literature.[234]

C.2.2 TrkC plasmid transfection into mammalian cells

NIH3T3 and HEK 293 cell lines are well characterized in our group that it does not express notable amount of Trk receptors (via flow cytometry and western blots, as negative controls in Figure C.2). Thus it was applied as the parent cell line for the gene transfection. TrkC plasmids were transfected into NIH3T3 and HEK293 cells by using Lipofectamine 3000 transfection kit. 0.8 g/L G418 were added in the culture medium to eliminate the untransfected cells. Expression of TrkC protein was checked when the growth rate of the transfected cells recovered.

C.2.3 TrkC protein expression check after transfection

Western blotting result (Figure C.2a) provided positive feedback proving the TrkC proteins were expressed in the transfected NIH3T3 cells; yet further test with flow cytometry (Figure C.2b) showed negative respond (no difference among all four samples) indicating TrkC proteins were not correctly located on cellular membrane.

Similar protocols were applied to HEK293 cells, and obtained same results as mentioned above (Figure C.2c, d). A higher loading of pcDNA-TrkC plasmid resulted in an even lower expression of TrkC.

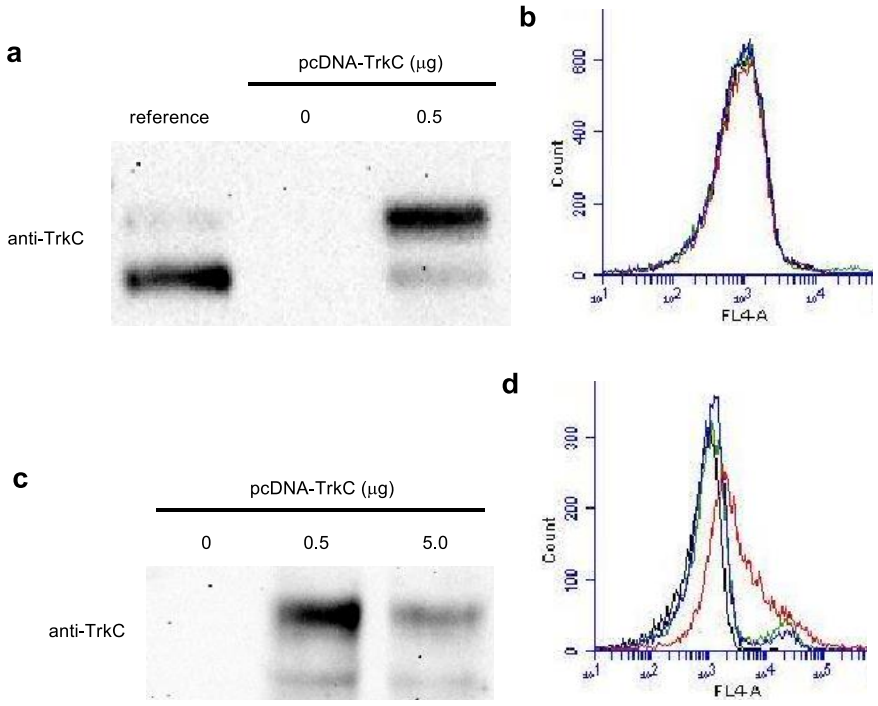

Figure C.2. TrkC protein expression confirmation after mammalian cell transfection. **a** Western blot (lysate of $TrkC^+$ cell was used as reference) and **b** flow cytometry result for pcDNA-TrkC transfected NIH3T3 cells. **c** Western blot and **d** flow cytometry result for pcDNA-TrkC transfected HEK293 cells. Red

lines in **b** and **d** represented transfected cells with anti-TrkC and corresponding 2nd antibody staining.

C.3 Conclusions

Correct Trk DNA plasmids were obtained from Addgene and successfully extracted from host *E. coli*. The extracted plasmids were also successfully transfected into mammalian cells (NIH3T3 and HEK293) and fully translated into corresponding proteins. But due to unknown reason, the Trk protein did not localize on cell surface that stopped its application in our research.

C.4 Experimental Methods

E. coli. samples with TrkA-RFP (Addgene® # 24093), pcDNA-TrkB (Addgene® #24088), and pcDNA-TrkC (Addgene® #24089) plasmids, which all contain CMV promoter and were encoded with antibiotic resistance genes (Kanamycin/Neomycin resistance for TrkA and Ampicillin/Neomycin resistance for TrkB and C), were obtained from Addgene (deposited by Dr. Moses Chao[224]).

C.4.1 Plasmid extraction and sequencing protocol

Before preparing larger amount of DNA plasmid for transfection in mammalian cells, the plasmid quality was tested. *E. coli*. with TrkA, B, or C plasmid were seeded on lysogeny broth (LB) argar plate with antibiotics and kept at 37 ^{o}C for growth for 12 h. Random single colonies were picked and further cultured on both LB argar gel and buffer to increase the number of copies

of plasmids. Each colonies were numbered and the colony on the gel were kept in 4 ^{o}C refrigerator while the *E. coli.* samples cultured in buffer were centrifuged down. Plasmids from each sample were extracted via a commercial kit (Zymo Research® #D4209). Two Primers (CMV-Forward, sequence: CGCAAATGGG-CGGTAGGCGTG; DsRed1-N, sequence: GTACTGGAACTGGGGGGACAG) at 5' and 3' end of the inserted genes were applied for a partial sequencing to confirm the correct gene was implanted into the plasmid we received. Most of the samples (sequenced by McLab) showed perfect alignment with the Trk genes logged within the gene databank as well as the references from Addgene. (Figure C.1a) One colony for each Trk gene was selected and cultured for larger amount of plasmids which was extracted by Zymo maxi-prep kit (Zymo Research® #D4202). Extracted pcDNA-TrkC plasmids were concentrated and confirmed DNA concentration as 2.1 mg/mL (concentration = A_{260} on a Take3® micro-volume plate with a path length of 0.5 mm).

C.4.2Trk plasmid transfection protocol

NIH3T3 cells are relative vulnerable for antibiotic G418 (killing curve shown in Figure C.3), as 0.8 mg/mL G418 in culture medium almost killed all cells after 6 d (medium refreshed every 3 d). Same concentration of G418 was applied to select out the proper transfected populations in NIH3T3 cells.

NIH3T3 cells were cultured with full culture medium (DMEM-F12 with 10% FBS) in a 24-well plate until reaching 80 – 90% confluence. TrkC plasmids (0.5

μg) were then transfected into NIH3T3 cells using Lipofectamine 3000 transfection kit (Life Technologies® #L3000-001). The transfected cells were then incubated with the plasmids for 48 h, and then detached and reseeded into a T25 tissue culture flask with 0.8 g/L antibiotic G418 in the full culture medium. The cells were kept under constant antibiotic pressure while culturing. Two weeks after transfection, growth rate of the transfected NIH3T3 cells recovered, and enough number of cells were harvested to check the TrkC protein expression.

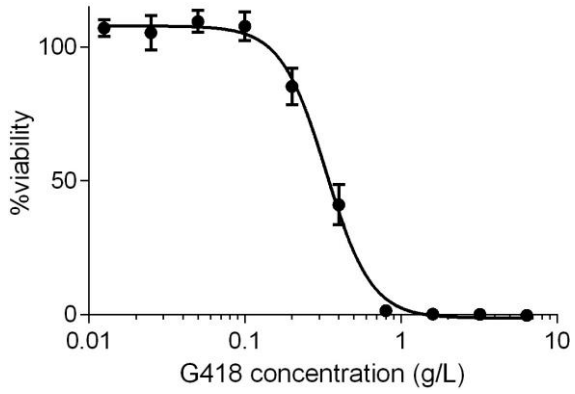

Figure C.3. Killing curve of NIH3T3 wild type cells with G418 after 6 d. Data was averaged from 8 independent parallel experiments. (n = 8, mean ± SD)

C.4.3 Western blotting protocol for checking TrkC expression after transfection

The pcDNA-TrkC transfected NIH3T3 cells were seeded on a T75 tissue culture flask and cultured in DMEM/F12 medium containing 0.8 g/L G418 till 80% confluency. After washing with cold PBS buffer twice, 1.0 mL RIPA lysis and extraction buffer (Thermo Scientific® #89900) containing 1% protease and

phosphatase inhibitor cocktail (Thermo Scientific® #78440) was added and kept on ice for 30 min. The mixture was scratched and transferred to a 1.5 mL Eppendorf tube. After centrifuging at 12500 x g at 4 ^{o}C for 20 min, the supernatant was collected as cell lysates. Total protein concentration was confirmed by BCA protein assay kit (Thermo Scientific® #23225), and 30 µg of protein was loaded into each lane of the 15% SDS-PAGE protein gel. After electrophoresis with 180 V for 70 min, the gel was washed and protein got transferred to a PVDF membrane (Thermo Scientific® #LC2005) and stained with primary anti-TrkC antibody (1:1000 dilution, Cell Signaling Technology® #3376S) followed by corresponding secondary antibody conjugated with Horseradish Peroxidase (HRP) (1:5000 dilution, Jackson ImmunoResearch® #111-035-144). Western blotting image was taken after treatment with blotting substrate (Thermo Scientific® #32106).

C.4.4 Flow cytometry protocol for checking TrkC expression after transfection

To check the TrkC protein expression level on cellular membrane, cultured transfected NIH3T3 cells were detached from the tissue culture flask with enzyme-free dissociation buffer (Thermo Scientific® #13151014). Cells were collected in each sample vial 1 – 4 (0.5 million each), and incubated with either blank control buffer or primary antibody (1 & 2 blank buffer, 3 anti-TrkB (Cell Signaling Technology® #4603), 4 anti-TrkC) 30 min. After washing with PBS buffer, either blank buffer or secondary antibody {vial 1 blank buffer, vials 2,

3 & 4 anti-rabbit IgG with red fluorescence label (Thermo Scientific® #A21245)} was used to resuspend cell pellets. Thorough washed and resuspended with PBS, the samples in vials 1 – 4 were analyzed with flow cytometer (gated with live cells, check fluorescence counts in FL4 red channel). If TrkC was detected on cell surface, sample vial 4 (in red) should present significantly stronger fluorescence signal, while all other vials emit low or none fluorescence.

APPENDIX D

SUPPORTING INFORMATION FOR CHAPTER II*

D.1 General Experimental Procedures

All reactions were carried out under an inert atmosphere (nitrogen, or argon where stated) with dry solvents under anhydrous conditions. Glassware for anhydrous reactions was dried in an oven at 140 ^{o}C for minimum 6 h prior to use. Dry solvents were obtained by passing the previously degassed solvents through activated alumina columns. Reagents were purchased at a high commercial quality (typically 97% or higher) and used without further purification, unless otherwise stated.

Flash chromatography was performed using silica gel (230 - 400 mesh). Analytical thin layer chromatography (TLC) was carried out on Silicycle® silica gel plates and visualized by UV, ninhydrin, *para*-methoxybenzaldehyde and/or potassium permanganate stains. A reversed phase column on preparation high performance liquid chromatography (prepHPLC) was also applied to purify compounds in 10 – 90% MeCN/water gradient with 0.1% trifluoroacetic acid over 20 minutes.

---

*Reprinted with permission from Jiang, Z.; Yang, Z.; Li, F.; Li, Z.; Fishkin, N.; Burgess, K., Targeted Maytansinoid Conjugate Improves Therapeutic Index for Metastatic Breast Cancer Cells. *Bioconjugate Chem.* **2018,** *29*, 2920-2926.

High field NMR spectra were recorded with Bruker Avance III at 400 MHz for ^{1}H, and 101 MHz for ^{13}C for all compounds except **1** and **2**. NMR spectra of **1** and **2** were taken with Bruker Avance 500 at 500 MHz for ^{1}H, and 126 MHz for ^{13}C. All spectra were calibrated using residual non-deuterated solvent as an internal reference ($CDCl_3$: ^{1}H NMR = 7.24, ^{13}C NMR = 77.0, MeOD-d_4: ^{1}H NMR = 3.30, ^{13}C NMR = 49.0, DMSO-d_6: ^{1}H NMR = 2.50, ^{13}C NMR = 39.5). The following abbreviations were used to explain the multiplicities: s = singlet, d = doublet, t = triplet, q = quartet, quint = quintet, dd = double doublet, dt = double triplet, dq = double quartet, m = multiplet, br = broad. Electrospray ionization mass spectrometry (ESI-MS) data were collected on triple-stage quadrupole instrument in a positive mode. All statistical analyses were carried out by GraphPad Prism® 6.0 Software. Results are represented as means ± SD.

Cell Culture. Hs578t (ATCC®) and MCF-7 cells were cultured on 75 cm^2 tissue culture flasks in Dulbecco's Modified Eagle Medium/nutrient mixture F-12 Ham (DMEM/F12, Millipore Sigma) supplement with 10% fetal bovine serum (FBS). NIH3T3-TrkC cells, NIH3T3 cells transfected with tropomyosin receptor kinase C (TrkC), were cultured on 75 cm^2 tissue culture flasks in DMEM/F12 supplement with 10% FBS including 0.4 g/L G418 (GIBCO®). 4T1 cells were cultured on 75 cm^2 tissue culture flasks in RPMI-1640 medium (ATCC®) with 10% FBS. All cells were cultured in a humidified incubator at 37 °C with 5% CO_2 and 95% air.

D.2 Compound Synthesis and Characterization

*D.2.1 Preparation and Characterization of Compound **B***

Compounds **C**, **D** and **E** were prepared following the protocol previously described.[41,81] Compound **B** was first published by our group.[3] Briefly, compound **C** (2.4 equiv.) and **E** (1.0 equiv.) were dissolved in DMSO (0.02 M), K_2CO_3 (5.0 equiv.) was then added to the reaction mixture, and stirred at room temperature for 36 h. Product was purified via reversed phase column on prepHPLC, with 25 – 35% yield.

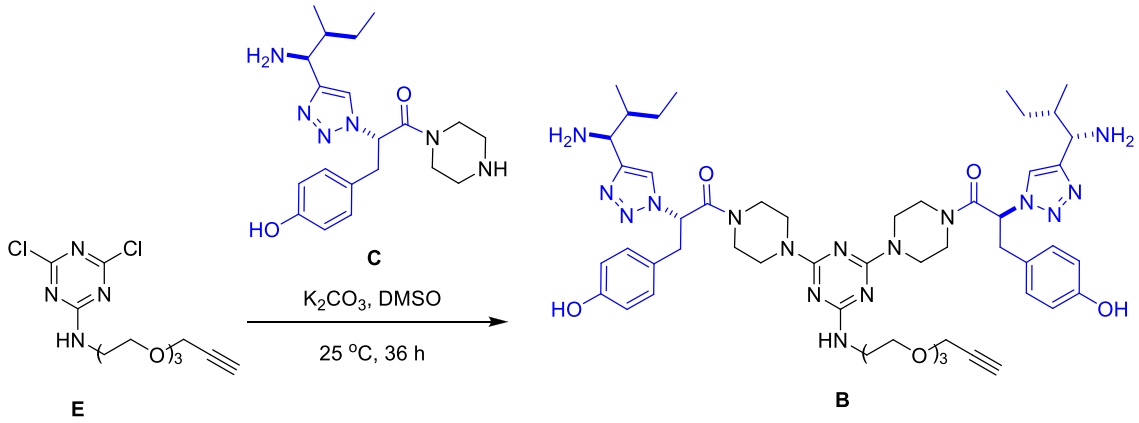

Scheme D.1. Synthesis of targeting moiety **B**. Reprinted with permission from [217].

B (IY-IY-TEG)

$C_{52}H_{74}N_{16}O_7$

^{1}H NMR (400 MHz, DMSO-d_6) δ 8.28 (s, 2H), 6.99 (d, 4H), 6.61 (d, 4H), 6.16 (s, 2H), 4.38 (s, 2H), 4.13 (s, 2H), 3.49 – 3.00 (m, 31H), 2.54 (s, 2H), 1.91 (s, 2H), 1.33 (d, 2H), 1.05 – 0.94 (m, 2H), 0.93 – 0.84 (m, 6H), 0.75 (d, 6H);

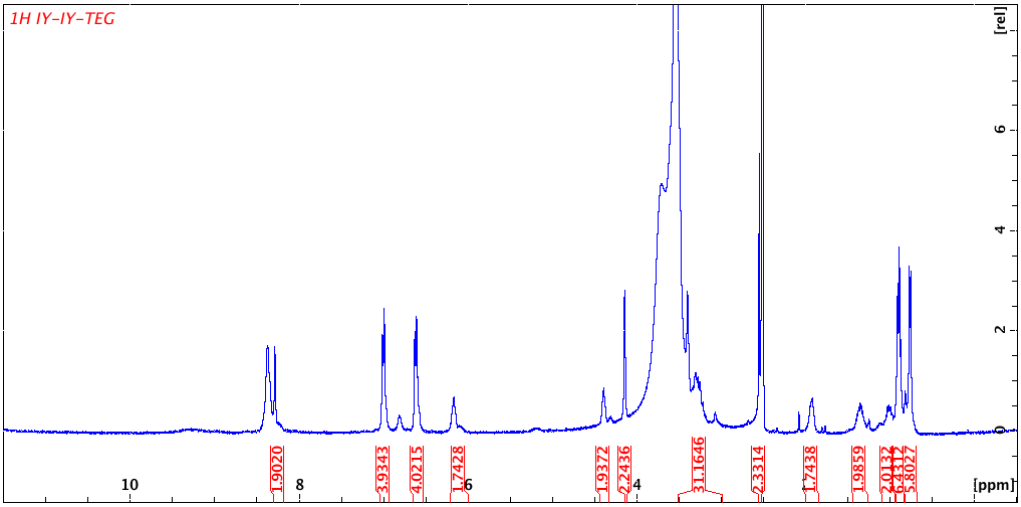

^{13}C NMR (101 MHz, DMSO-d_6) δ 165.86, 158.14, 157.80, 156.27, 141.51, 130.23, 125.37, 123.47, 115.03, 80.28, 77.00, 69.70, 69.46, 68.94, 68.48, 60.28, 57.45, 50.68, 44.94, 42.55, 42.19, 40.43, 37.16, 25.09, 23.94, 13.63, 11.07.

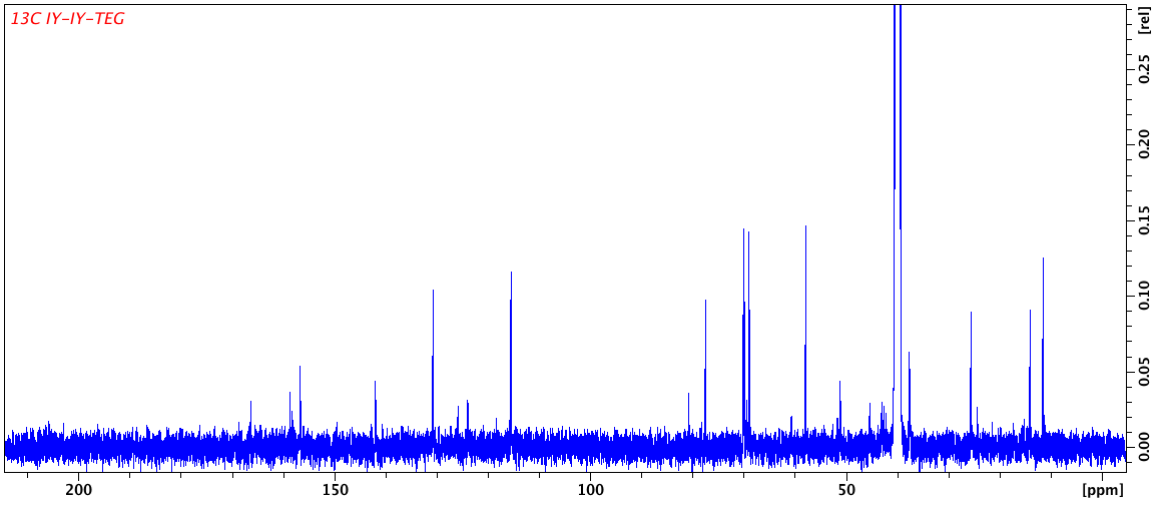

*D.2.2 Synthesis and Characterization of Targeted and Non-targeted Maytansinoid **DM4** Conjugates (**3**, **4**, **1**, **5**, **2**)*

Preparation of 4,6-dichloro-N-(2-(pyridin-2-yldisulfanyl)ethyl)-1,3,5-triazin-2-amine (3)

2-(pyridin-2-yldisulfanyl)ethanamine (336 mg, 2.0 mmol), Cyanuric chloride (369 mg, 2.0 mmol) were dissolved in 20 mL 1,4-dioxane. K_2CO_3 (552 mg, 4.0 mmol) was added to reaction mixture and stirred at room temperature for 12 h. Solvent was removed in vacuum, and compound was used without further purification.

Synthesis of (S,S,2S,2'S)-1,1'-(4,4'-(6-(2-(pyridin-2-ldisulfanyl)ethylamino)-1,3,5-triazine-2,4-diyl)bis(piperazine-4,1-diyl))bis(2-(4-((1S,2S)-1-amino-2-methylbutyl)-1H-1,2,3-triazol-1-yl)-3-(4-hydroxyphenyl)propan-1-one) (4)

Compound **3** (334 mg, 1.0 mmol) and **C** (773 mg, 2.0 mmol) were dissolved in 10 mL DMSO. K_2CO_3 (1.38 g, 10.0 mmol) was added to reaction mixture and stirred at room temperature for 24 h. Solvent was removed in vacuum, compound was purified via flash chromatography on Biotage® Isolera purification system with 10 g reversed phase silica gels column (200 – 400 mesh). Column was flushed at 12 mL/min, 10% water / 90% MeCN for 1 column volume (1 CV), then changed to 100% MeCN gradually in 10 CV, followed by MeCN wash in 2 CV. Fractions containing **4** were collected, and solvent was removed on lyophilizer (349 mg, 0.34 mmol, 34% yield).

4

$C_{50}H_{67}N_{17}O_4S_2$

^{1}H NMR (400 MHz, MeOD-d_4) δ 8.41 (d, 1H), 7.99 (s, 2H), 7.80 (d, 1H), 7.73 (t, 1H), 7.17 (t, 1H), 6.99 (d, 4H), 6.67 (d, 4H), 6.04 (t, 2H), 3.96 (d, 2H), 3.34-3.70 (m, 22H), 2.95 (t, 2H), 1.74 (m, 2H), 1.42 (m, 2H), 1.06 (m, 2H), 0.90 (t, 6H), 0.81 (d, 6H);

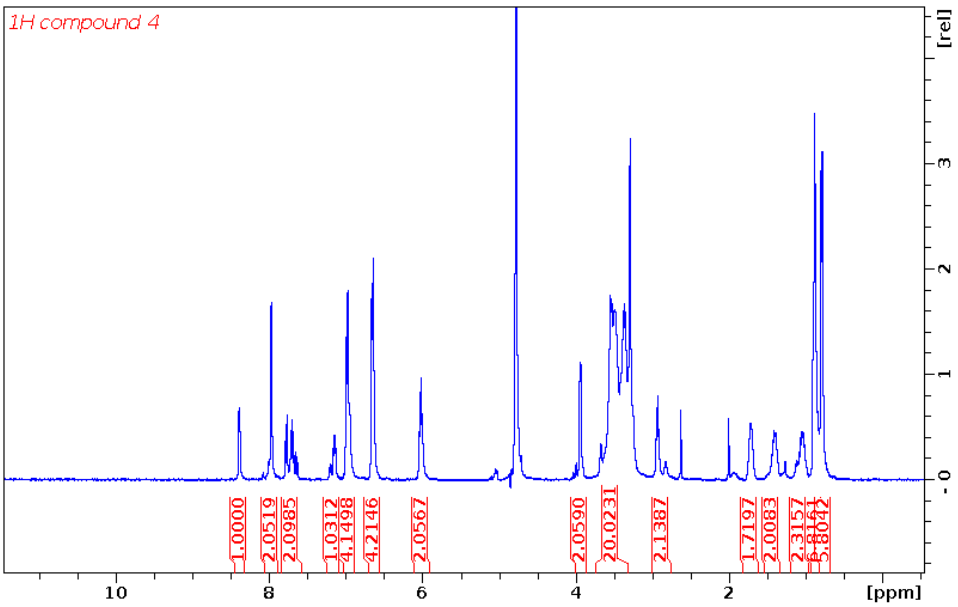

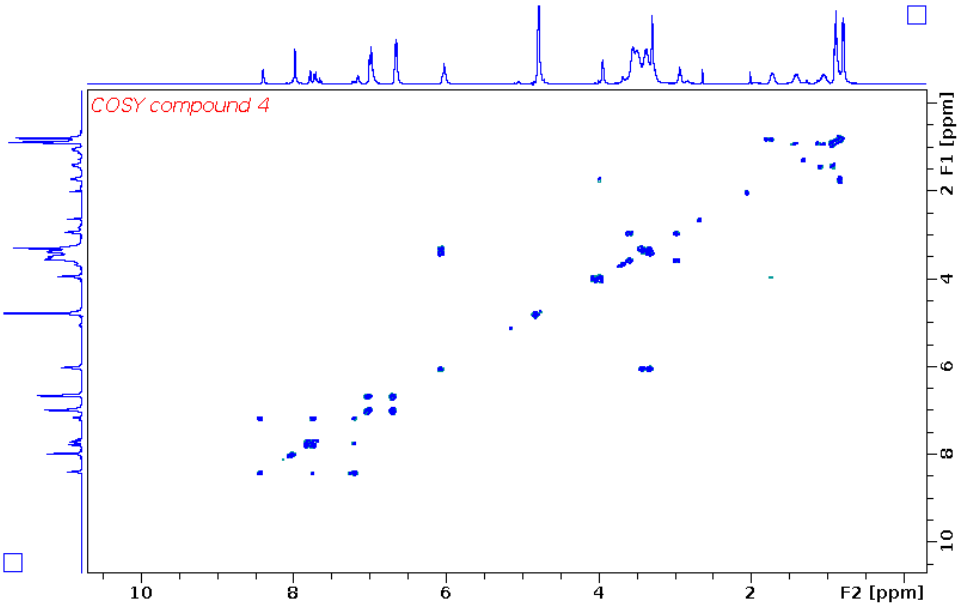

^{13}C NMR (101 MHz, MeOD-d_4) δ 168.15, 167.44, 166.29, 161.52, 157.95, 151.50, 150.49, 139.01, 131.57, 127.14, 122.85, 122.29, 121.25, 116.55, 74.32, 61.98, 53.78, 46.79, 44.01, 43.63, 42.22, 39.08, 26.47, 15.26, 11.91.

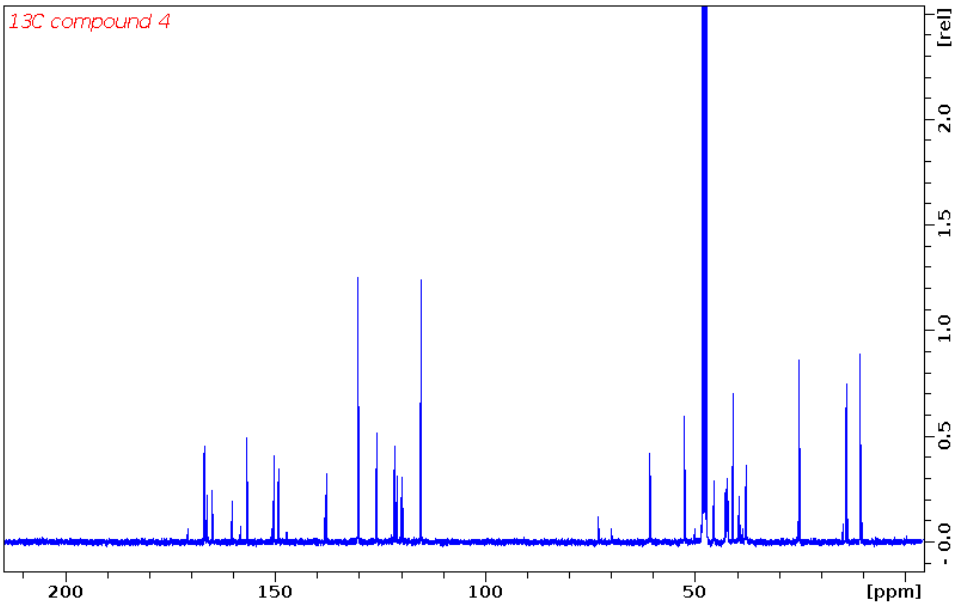

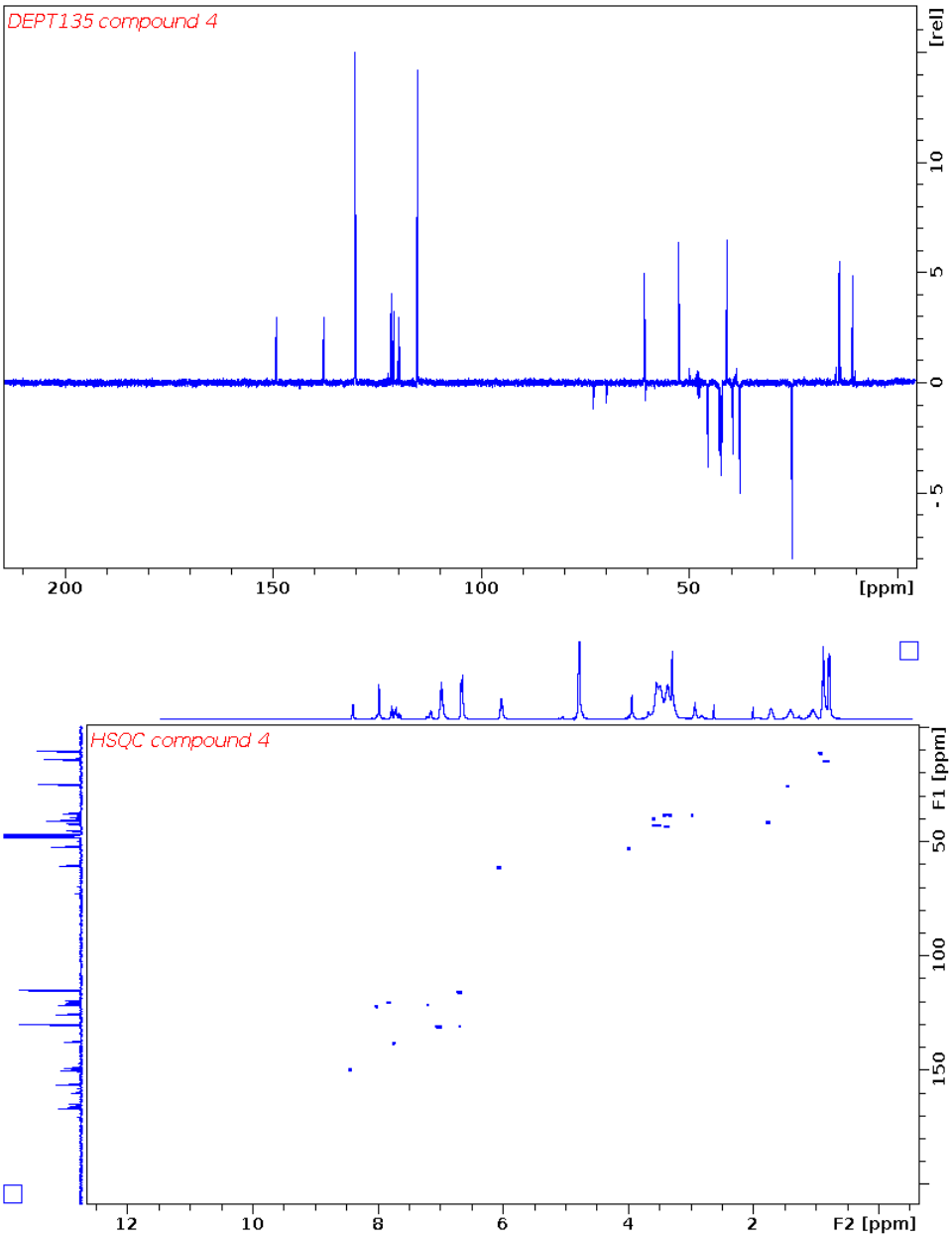

HRMS (ESI) m/z calculated for $C_{50}H_{68}N_{17}O_4S_2^+$ 1034.5076; found $(M+H)^+$ 1034.5063

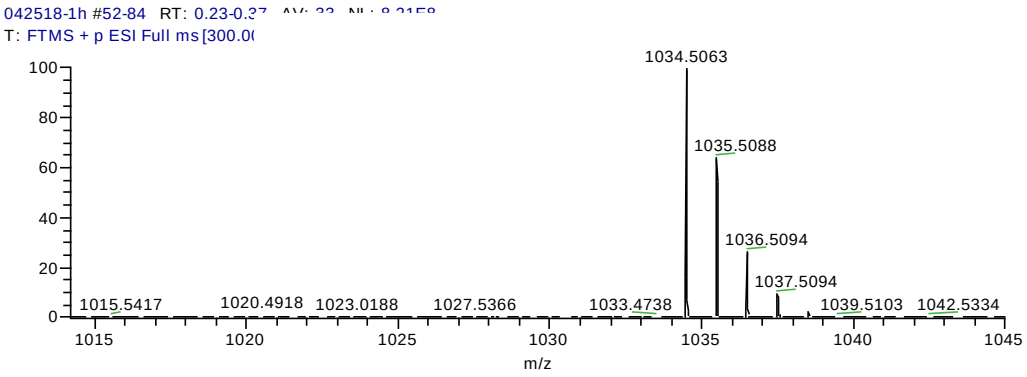

Characterization of maytansinoid DM4

DM4

$C_{38}H_{54}ClN_3O_{10}S$

^{1}H NMR (400 MHz, $CDCl_3$) δ 6.82 (s, 1H), 6.73 (d, 1H), 6.66 (s, 1H), 6.42 (dd, 1H), 6.20 (s, 1H), 5.68 (dd, 1H), 5.42 (q, 1H), 4.79 (d, 1H), 4.27 (t, 1H), 3.98 (s, 3H), 3.64 (d, 1H), 3.50 (d, 1H), 3.35 (s, 3H), 3.28 (s, 1H), 3.23 (s, 3H), 3.11 (d, 1H), 3.03 (d, 1H), 2.88 (s, 3H), 2.67 – 2.39 (m, 3H), 2.18 (d, 1H), 2.03 – 1.75 (m, 2H), 1.64 (s, 3H), 1.52 – 1.39 (m, 2H), 1.33 (d, 6H), 1.29 (d, 6H), 1.21 (d, 1H), 0.80 (s, 3H);

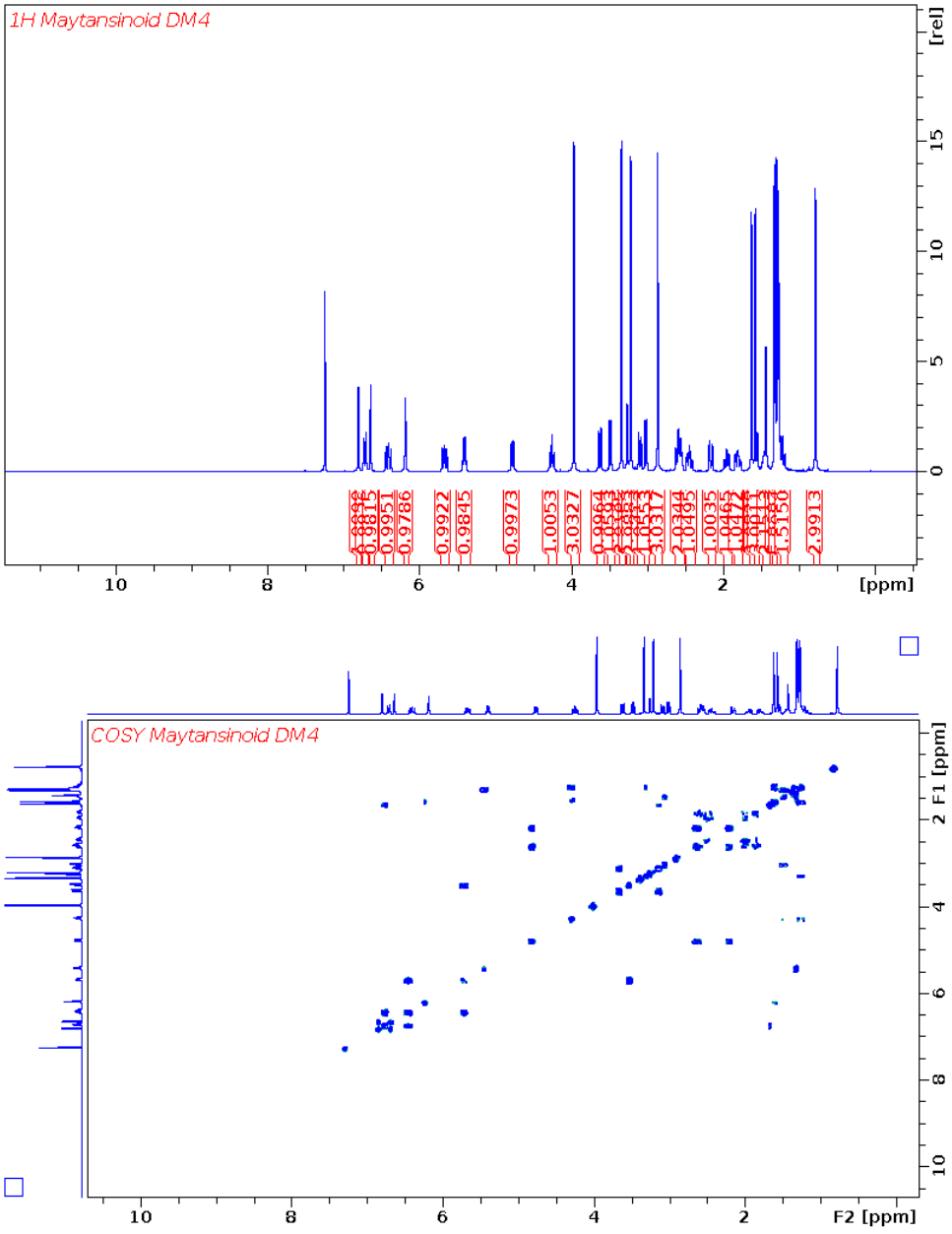

^{13}C NMR (101 MHz, $CDCl_3$) δ 172.38, 171.06, 168.85, 156.13, 152.27, 142.42, 141.07, 139.22, 133.44, 127.87, 125.61, 122.36, 119.05, 113.26, 88.66, 81.06, 78.29, 74.26, 67.33, 60.10, 56.75, 52.49, 46.78, 44.14, 41.35, 39.04, 36.31, 35.67, 33.37, 32.68, 32.54, 30.95, 30.10, 15.60, 14.70, 13.43, 12.30.

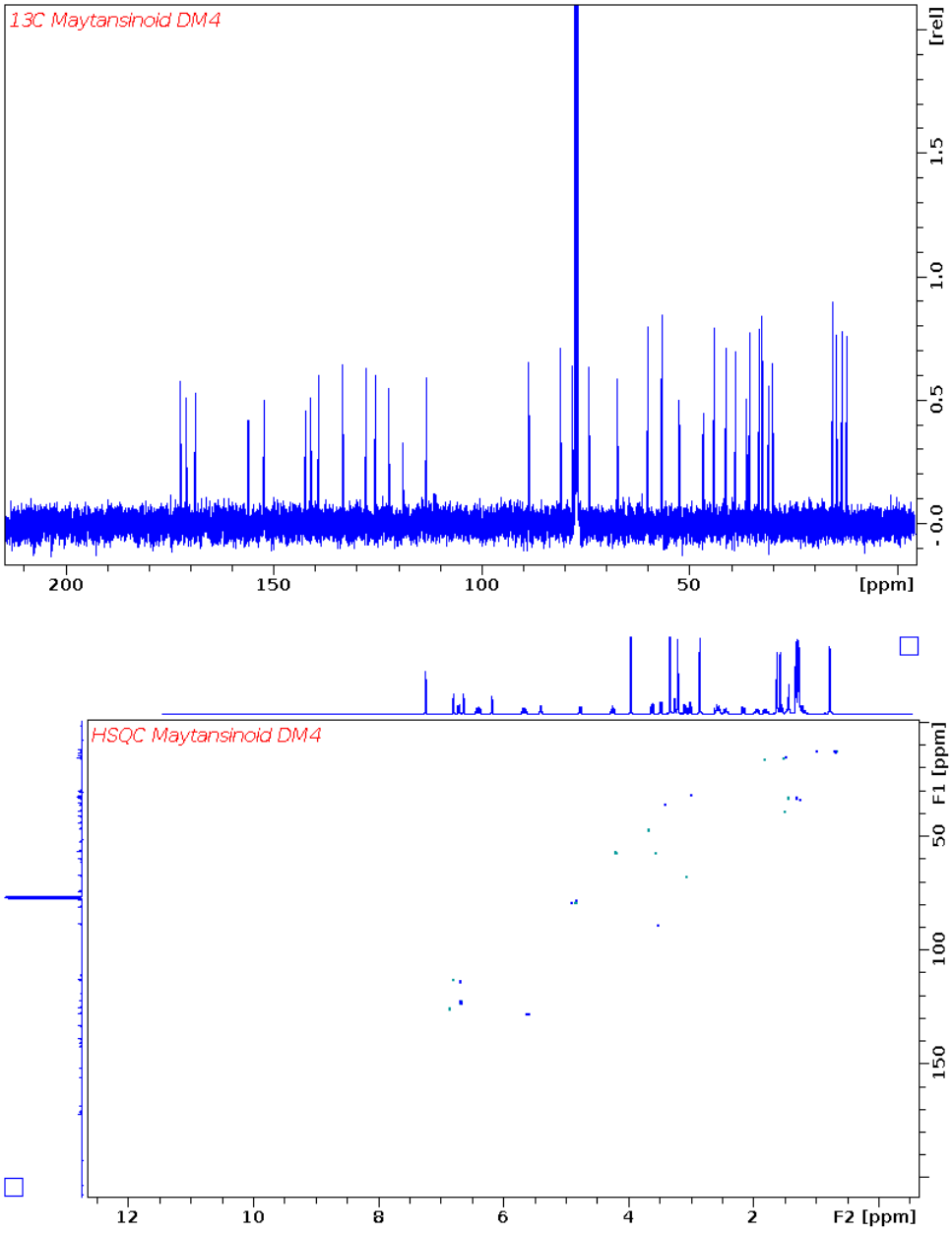

Synthesis of targeted DM4 maytansinoid conjugate 1

Compound **4** (8.3 mg, 0.008 mmol) and maytansinoid **DM4** (9.3 mg, 0.012 mmol) were dissolved in 0.5 mL DMF, and stirred at room temperature for 12 h. **1** was purified via prepHPLC (8.0 mg, 0.0047mmol, 59% yield).

1 (IY-DM4)

$C_{83}H_{116}ClN_{19}O_{14}S_2$

^{1}H NMR (500 MHz, MeOD-d_4) δ 8.22 (s, 2H), 7.07 (d, 4H), 6.71 (d, 4H), 6.67 (d, 2H), 6.59 (m, 1H), 6.19 (t, 2H), 5.69 (dd, 1H), 5.46 (d, 1H), 4.66 (dd, 1H), 4.45 (d, 2H), 4.19 (m, 1H), 3.93 (s, 3H), 3.79 – 3.42 (m, 20H), 3.39 – 3.34 (m, 5H), 3.25 – 3.15 (m, 4H), 2.94 (d, 1H), 2.84 (s, 3H), 2.82 – 2.63 (m, 4H), 2.59 – 2.38 (m, 2H), 2.15 (dd, 1H), 2.07 – 1.89 (m, 5H), 1.67 (s, 3H), 1.58 – 1.43 (m, 5H), 1.32 – 1.27 (m, 6H), 1.27 – 1.20 (m, 6H), 1.19 – 1.10 (m, 2H), 1.05 (d, 1H), 0.99 (t, 6H), 0.90 (d, 6H), 0.85 (s, 3H);

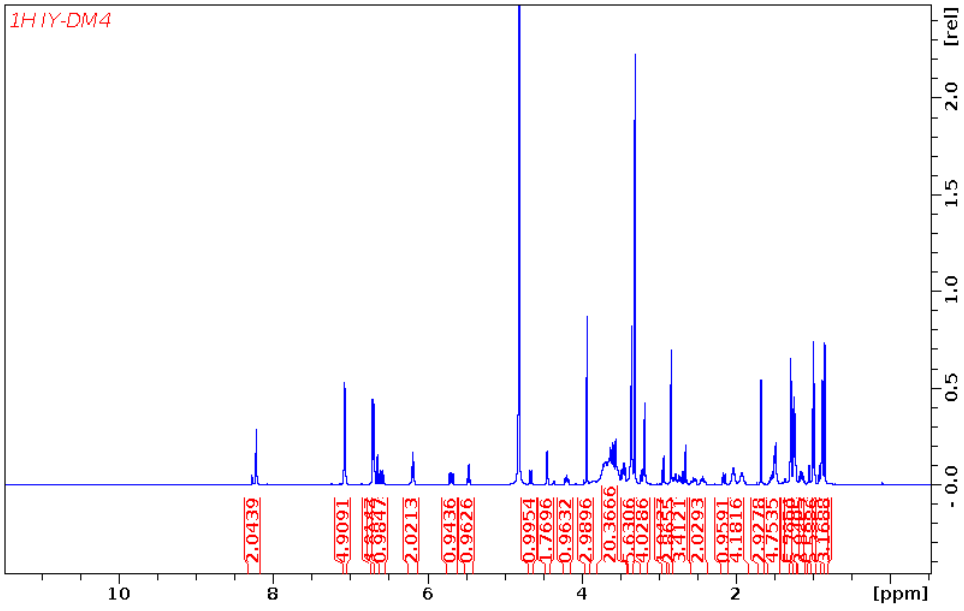

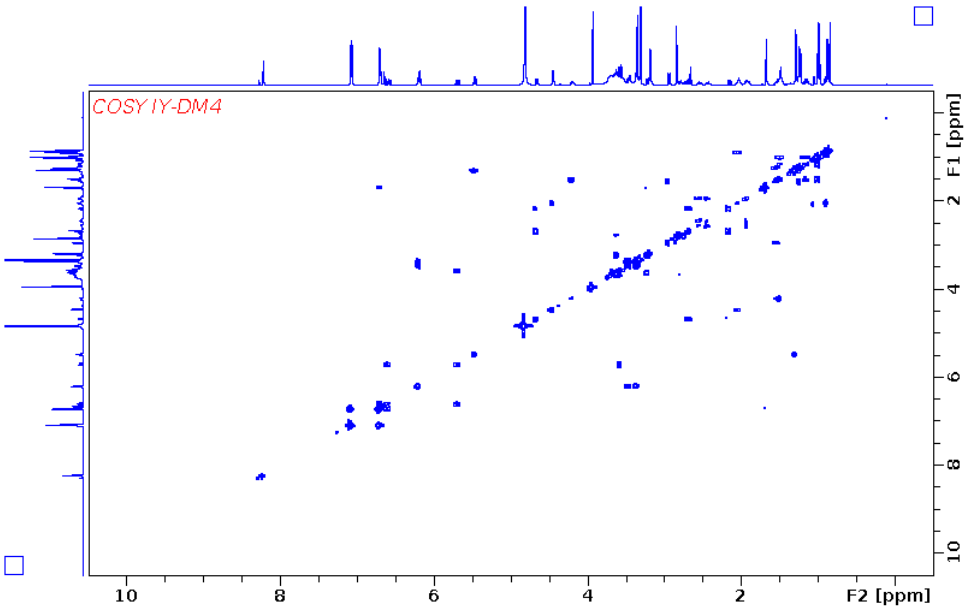

^{13}C NMR (126 MHz, MeOD-d_4) δ 174.33, 172.30, 171.27, 168.38, 162.69, 162.41, 158.12, 157.60, 155.28, 143.17, 142.90, 140.39, 134.50, 131.63, 129.70, 126.76, 126.72, 124.65, 123.18, 119.38, 119.11, 116.64, 115.12, 89.84, 81.74, 79.50, 75.71, 68.86, 61.95, 61.38, 57.31, 56.97, 53.82, 52.99, 51.29, 47.31, 44.50, 44.26, 40.58, 40.12, 39.67, 39.13, 37.87, 37.16, 36.56, 33.51, 31.17, 30.50, 28.81, 27.33, 26.67, 15.64, 14.74, 14.46, 13.65, 12.58, 11.46.

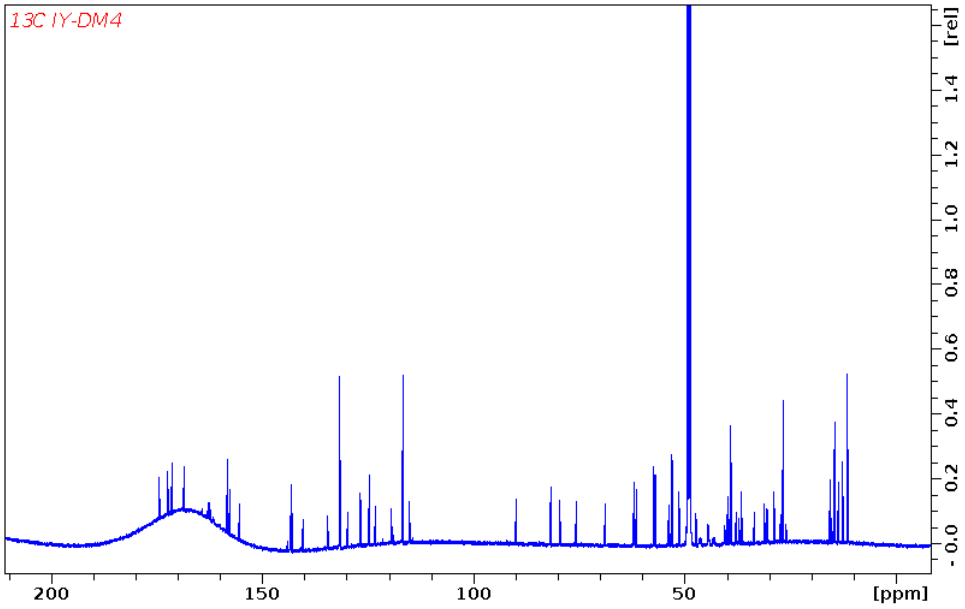
13C IY-DM4
[rel]
1.4
1.2
1.0
0.8
0.6
0.4
0.2
-0.0
200
150
100
50
[ppm]

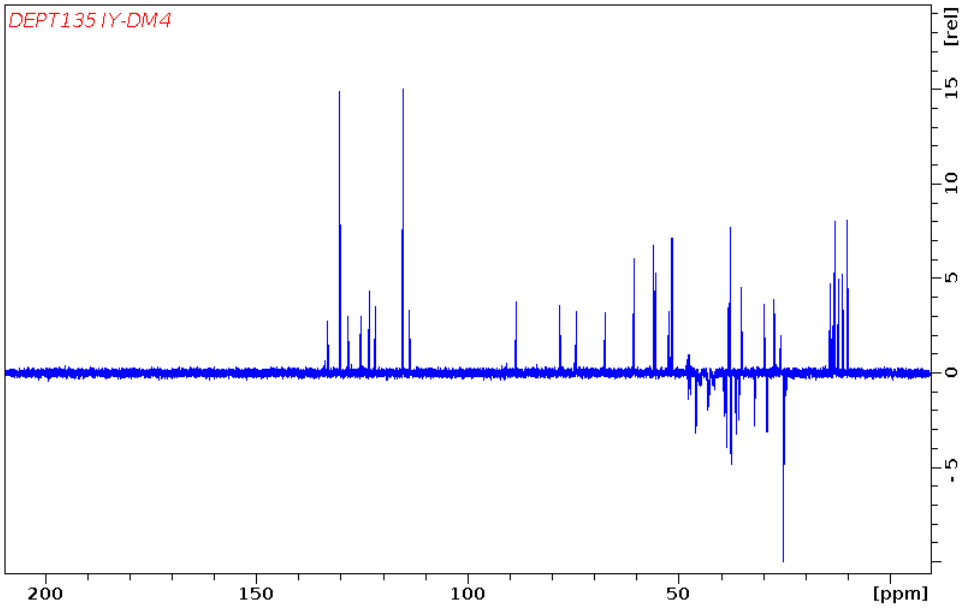
DEPT135 IY-DM4
[rel]
15
10
5
0
-5
200
150
100
50
[ppm]

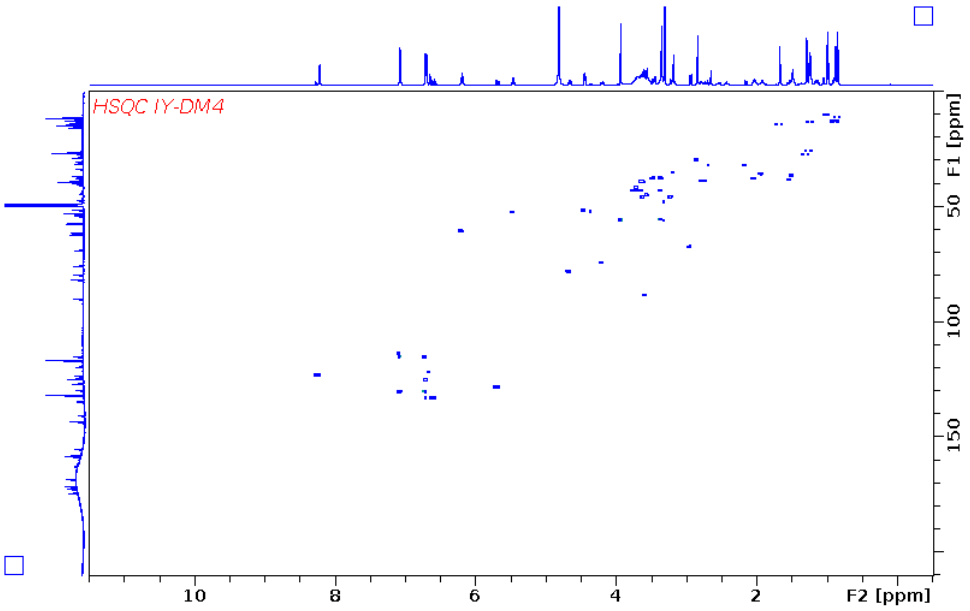

HRMS (ESI) m/z calculated for $C_{83}H_{118}ClN_{19}O_{14}S_2^{2+}$ 851.9113; found $(M+2H)^{2+}$ 851.9129

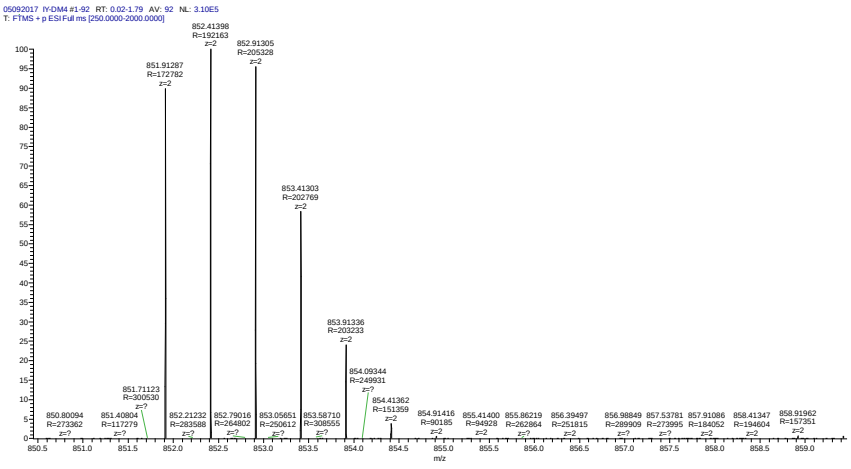

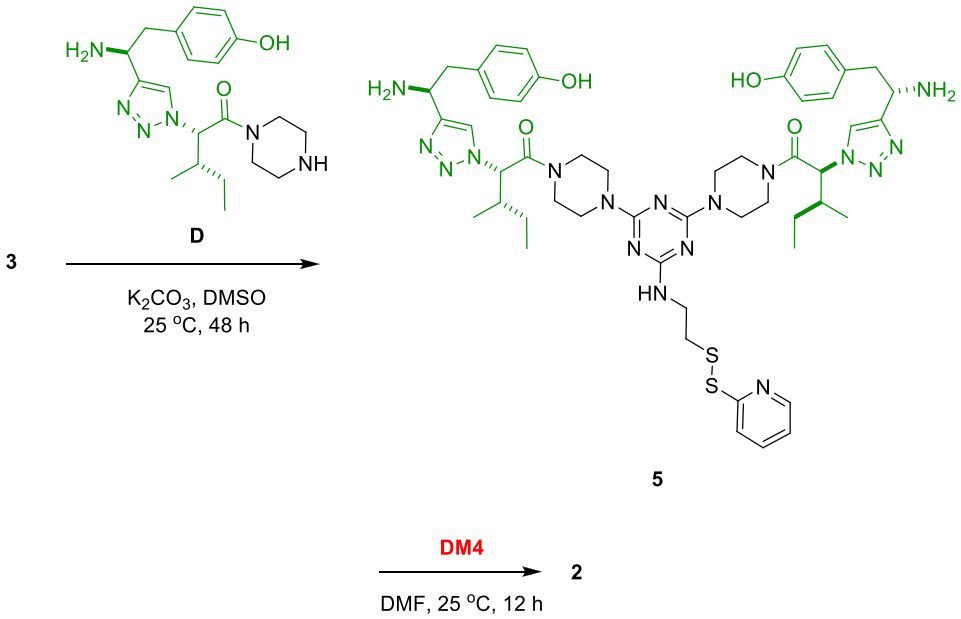

Scheme D.2. Synthesis of non-targeted DM4 maytansinoid conjugate **2**. Reprinted with permission from [217].

Synthesis of (S,2S,2'S,3S,3'S)-1,1'-(4,4'-(6-(2-(pyridin-2-yldisulfanyl) ethylamino) -1,3,5-triazine-2,4-diyl) bis (piperazine-4,1-diyl)) bis (2-(4-((S)-1-amino-2-(4-hydroxyphenyl)ethyl)-1H-1,2,3-triazol-1-yl)-3-methylpentan-1-one) (5)

Compounds **3** (30 mg, 0.09 mmol) and **D** (69.6 mg, 0.18 mmol) were dissolved in 1.0 mL DMSO. K_2CO_3 (124 mg, 0.9 mmol) was added to reaction mixture and stirred at room temperature for 48 h. Solvent was removed in vacuum, compound was purified through reversed phase column on prepHPLC (10.0 mg, 0.01 mmol, 11% yield).

5

$C_{50}H_{67}N_{17}O_4S_2$

^{1}H NMR (400 MHz, MeOD-d_4) δ 8.45 (s, 1H), 7.96 (s, 2H), 7.85 (d, 1H), 7.80 (d, 1H), 7.22 (br, 1H), 6.93 (d, 4H), 6.63 (d, 4H), 5.66 (d, 2H), 4.76 – 4.66 (m, 2H), 4.09 – 3.41 (m, 18H), 3.29 – 3.10 (m, 4H), 3.02 (m, 2H), 2.36 (br, 2H), 1.01 (m, 10H), 0.85 (d, 6H);

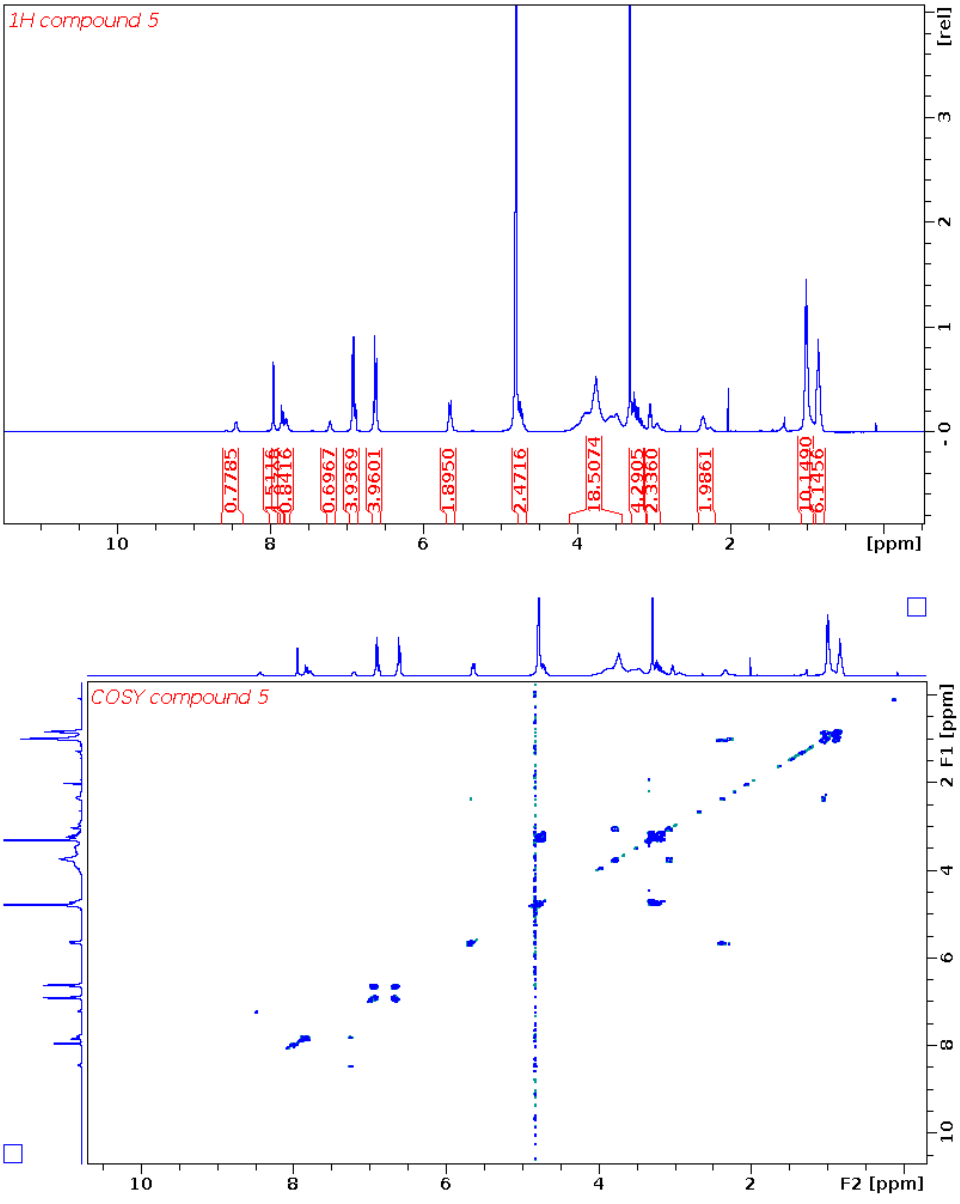

^{13}C NMR (101 MHz, MeOD-d_4) δ 168.09, 161.25, 157.86, 150.55, 144.71, 139.18, 131.48, 131.43, 126.91, 126.85, 124.04, 122.48, 121.22, 116.58, 64.96, 50.02, 45.05, 44.46, 43.17, 40.87, 39.49, 39.08, 25.49, 15.69, 10.93.

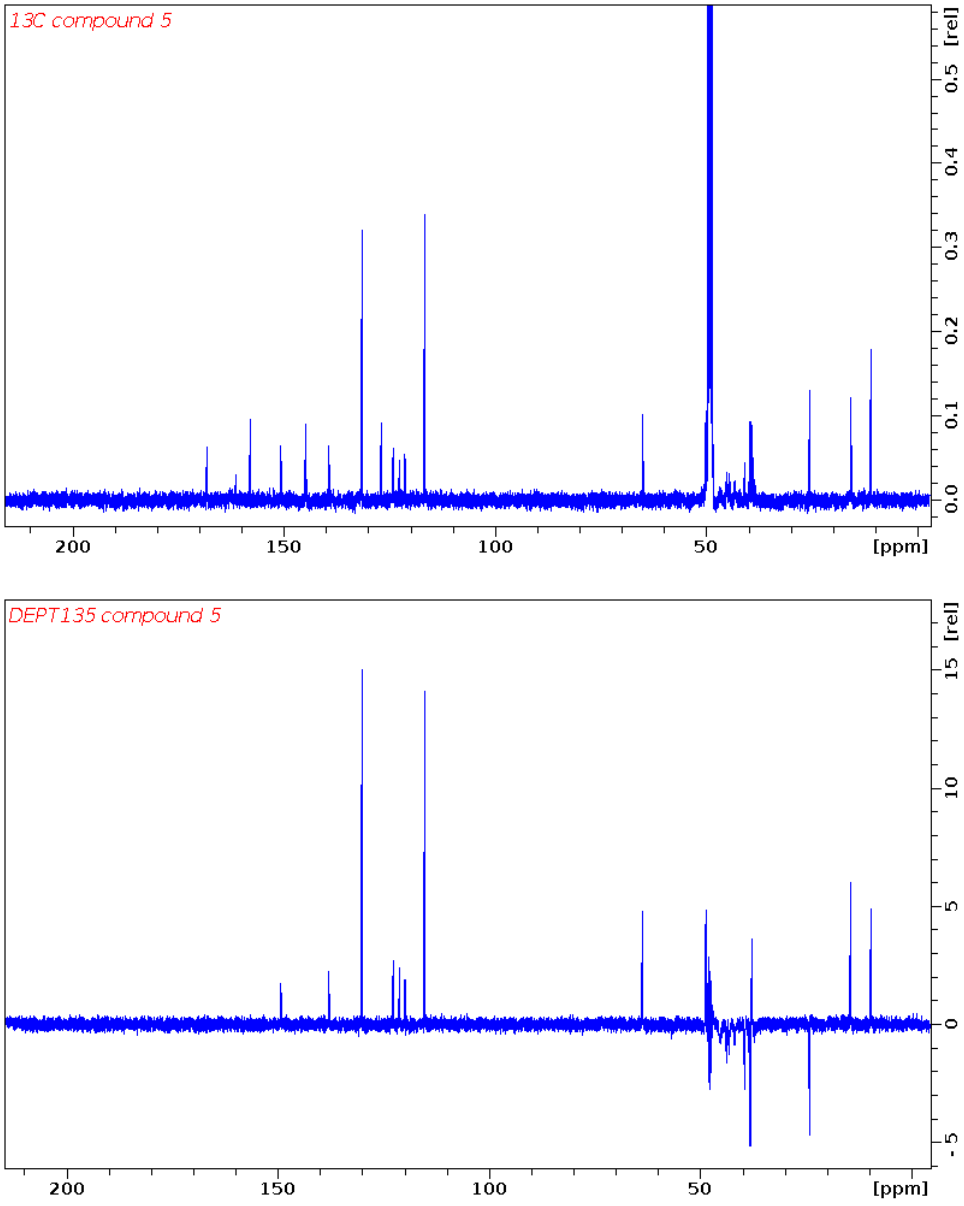

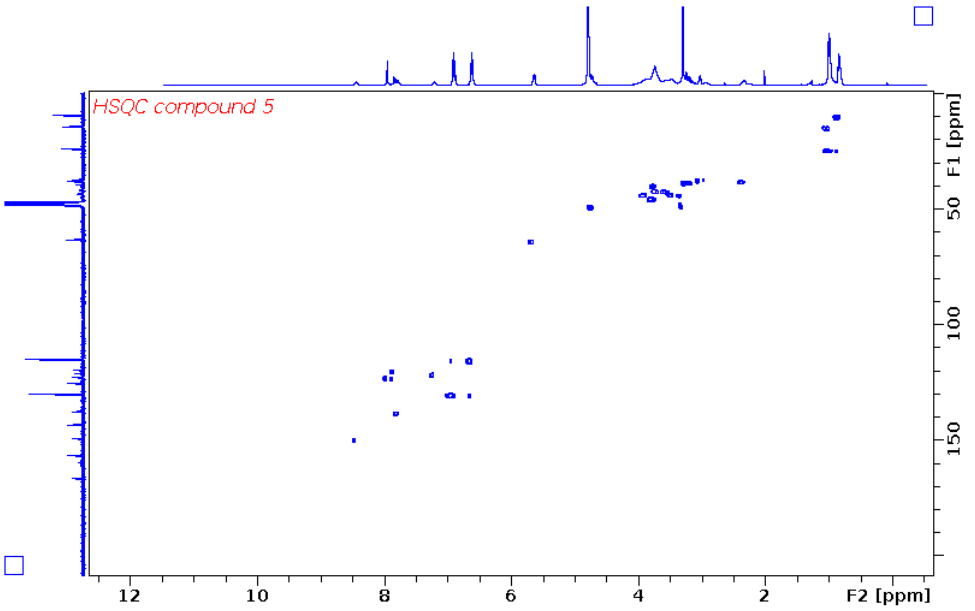

HRMS (ESI) m/z calculated for $C_{50}H_{68}N_{17}O_4S_2^+$ 1034.5076; found $(M+H)^+$ 1034.5067

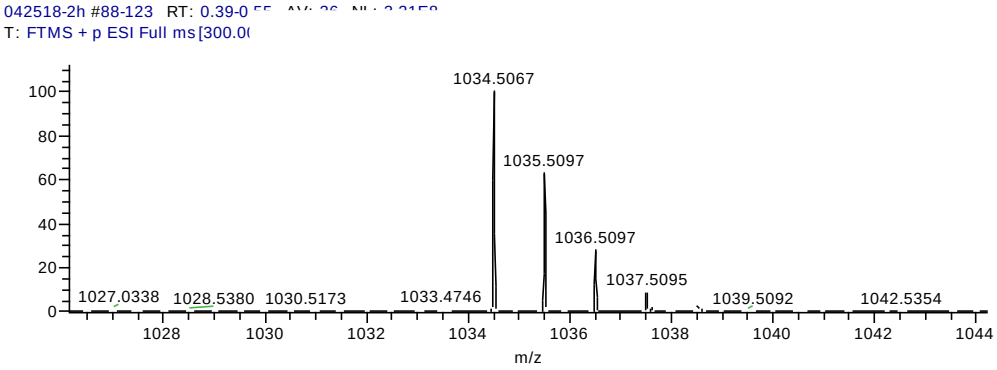

Synthesis of non-targeted DM4 maytansinoid conjugate 2

5 (9.8 mg, 0.0095 mmol) and maytansinoid **DM4** (9.1 mg, 0.0117 mmol) were dissolved in 0.5 mL DMF, and stirred at room temperature for 12 h. **2** was purified through reversed phase column on prepHPLC (6.2 mg, 0.0036mmol, 38% yield).

2 (YI-DM4)

$C_{83}H_{116}ClN_{19}O_{14}S_2$

^{1}H NMR (500 MHz, MeOD-d_4) δ 7.97 (s, 2H), 7.08 (d, 2H), 6.92 (m, 4H), 6.72 – 6.55 (m, 7H), 5.69 (m, 3H), 5.46 (dd, 1H), 4.74 (dd, 1H), 4.66 (d, 2H), 4.30 – 4.13 (m, 2H), 4.07 – 3.49 (m, 20H), 3.37 (s, 3H), 3.29 – 3.10 (m, 8H), 2.96 – 2.71 (m, 7H), 2.66 (t, 2H), 2.60 – 2.30 (m, 5H), 2.14 (d, 1H), 1.93 (m, 2H), 1.68 (s, 3H), 1.58 – 1.46 (m, 3H), 1.35 – 1.18 (m, 12H), 1.05 – 0.90 (m, 9H), 0.88 – 0.80 (m, 8H);

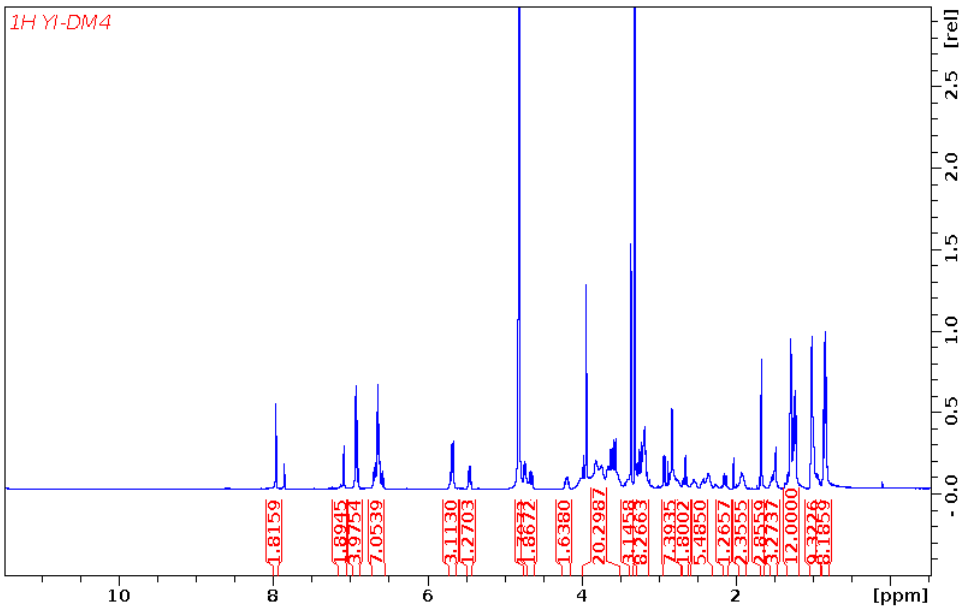

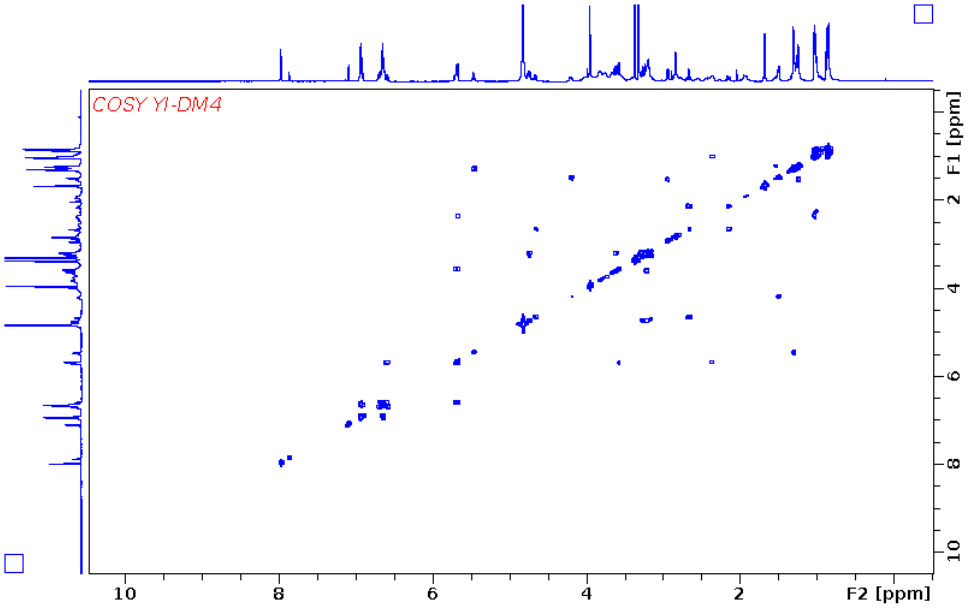

^{13}C NMR (126 MHz, MeOD-d_4) δ 174.35, 172.29, 171.25, 168.11, 157.88, 157.60, 155.27, 144.73, 143.20, 142.90, 140.38, 134.49, 131.50, 131.45, 129.70, 126.84, 126.71, 124.02, 123.17, 119.37, 116.59, 116.55, 115.12, 89.84, 81.74, 79.49, 75.70, 68.83, 64.95, 61.37, 57.31, 56.97, 53.82, 51.32, 50.03, 47.29, 45.07, 40.64, 39.81, 39.66, 39.53, 39.07, 37.87, 37.19, 36.56, 33.49, 31.17, 30.51, 28.75, 27.40, 25.48, 15.71, 15.62, 14.74, 13.66, 12.57, 10.95.

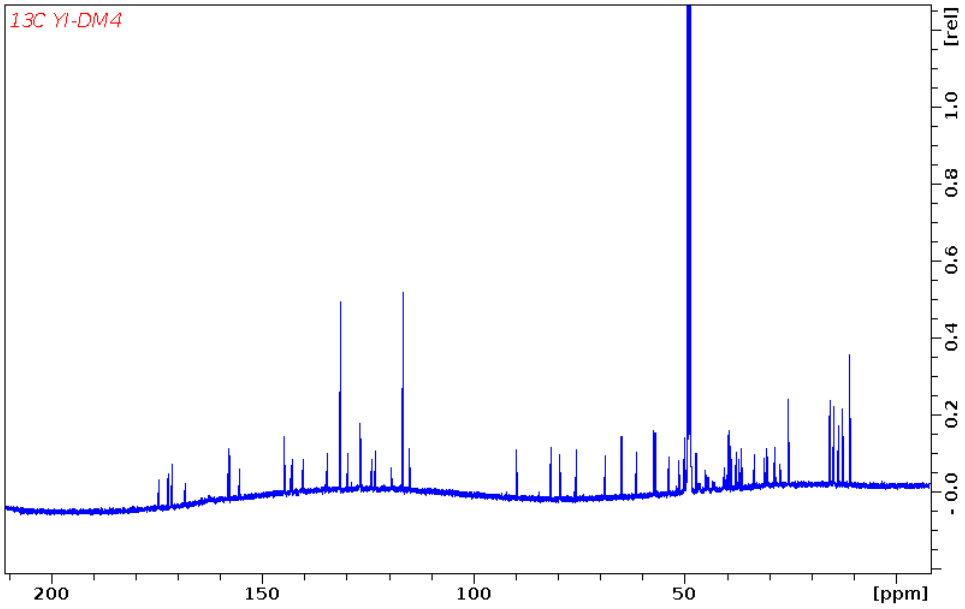
13C YI-DM4
[rel]
1.0
0.8
0.6
0.4
0.2
- 0.0
200
150
100
50
[ppm]

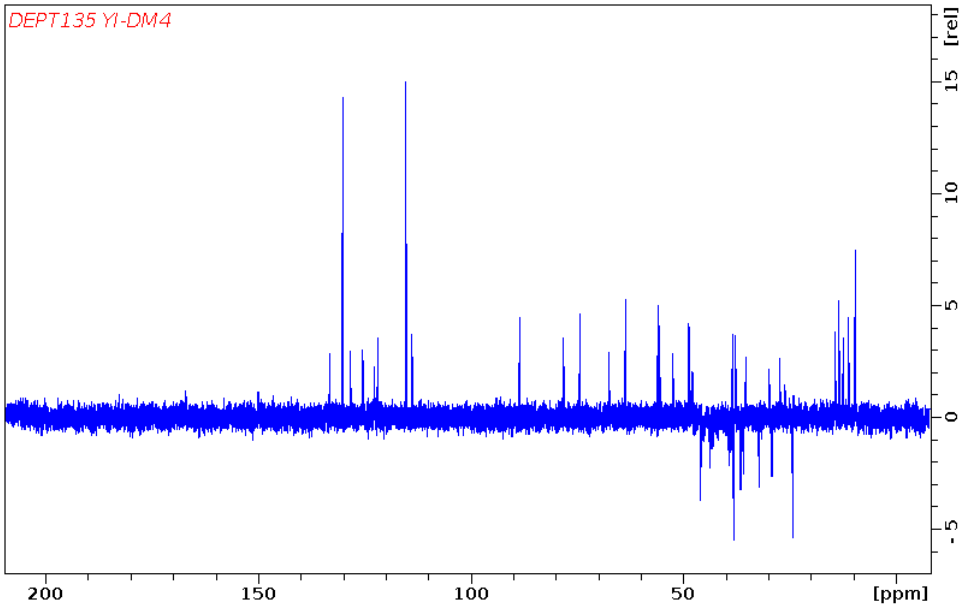
DEPT135 YI-DM4
[rel]
15
10
5
0
- 5
200
150
100
50
[ppm]

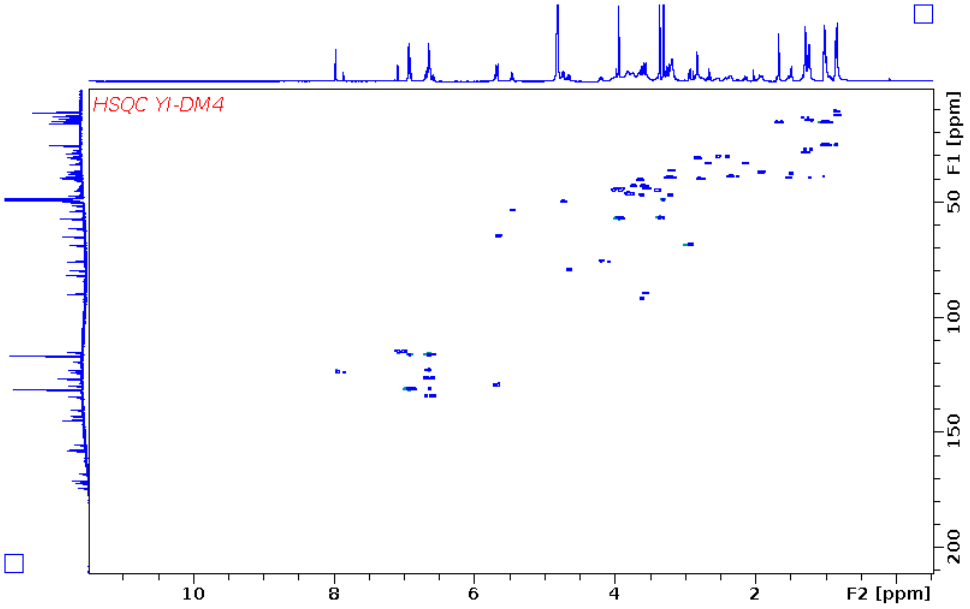

HRMS (ESI) m/z calculated for $C_{83}H_{118}ClN_{19}O_{14}S_2^{2+}$ 851.9113; found $(M+2H)^{2+}$ 851.9100

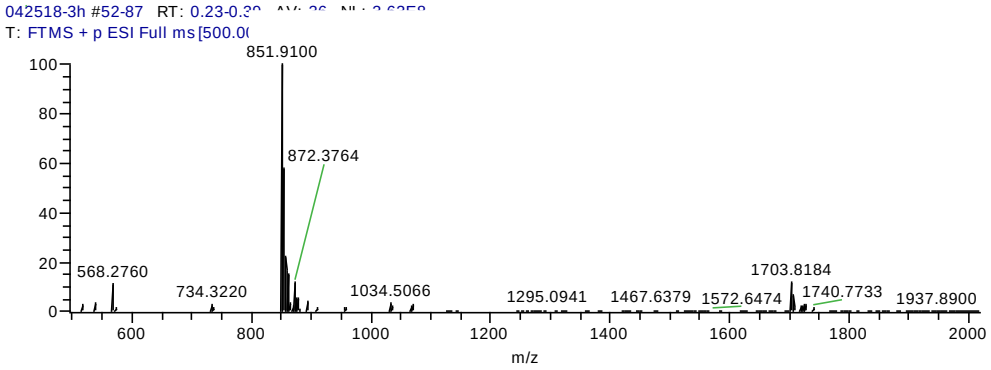

*D.2.3 1D NMR Spectra Comparison between **DM4** and Compound **1***

Stacking 1D NMR spectra of **DM4** and **1** shows no significant chemical shifts for most protons or carbons from DM4, newly appeared peaks in **1** come from the targeting moiety in **4**. (Figure D.1) Thus the core structure of **DM4** is not disrupted during the disulfide exchange.

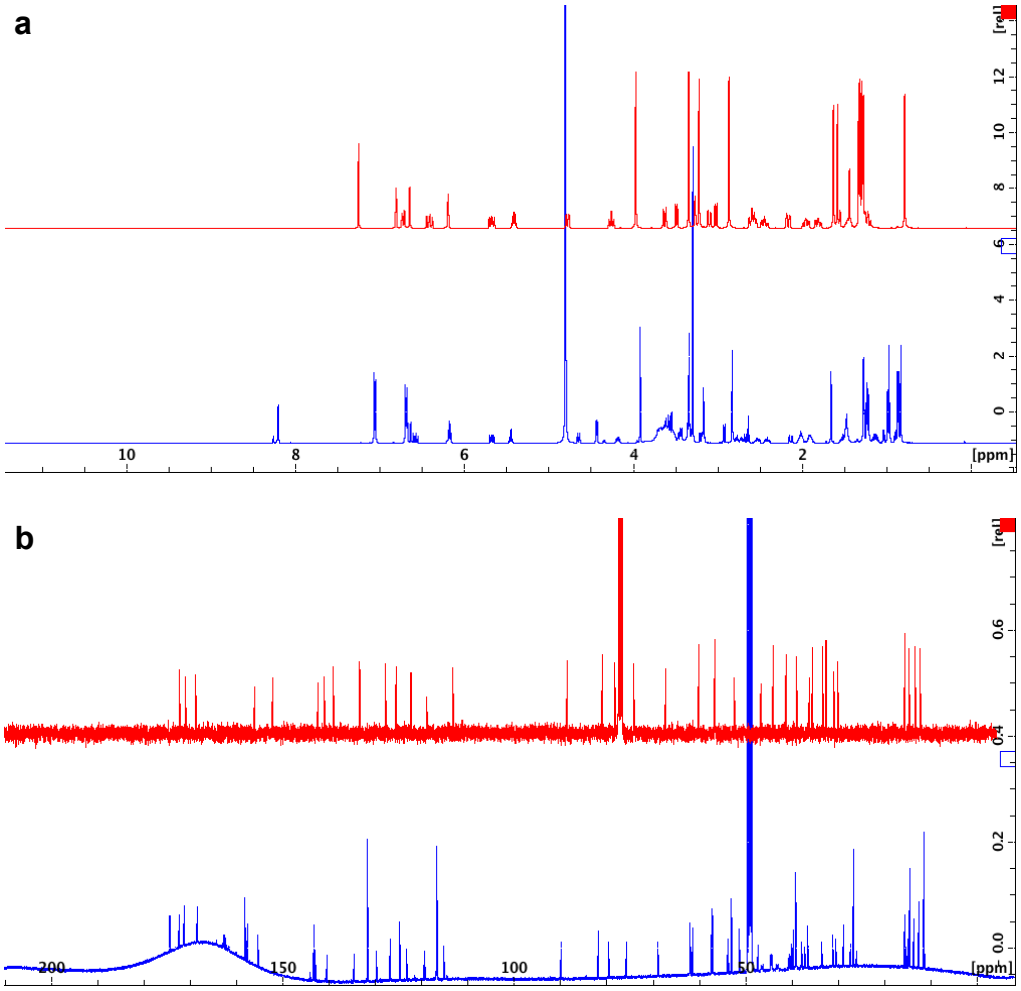

Figure D.1. Comparison of NMR spectra of **DM4** (red) and **1** (blue). **a** ^{1}H NMR. **b** ^{13}C NMR. Reprinted with permission from [217].

D.3 Compound Property Check

D.3.1 Cell-based Assay for Dissociation Constant Measurement

Dissociation constant of our TrkC targeting moiety was determined via a cell-based assay.[85] NIH3T3-TrkC cells were seeded in 24-well plate with 2 x 10^4 cells/well and incubated overnight. For total binding test, culture medium in each well were replaced with 250 µL DMEM/F12 containing 1% BSA and

incubated for 2 h. Fluorescent probe **A** was dissolved in DMEM/F12 containing 1% BSA with various concentrations, 250 μL was added to each well to make final concentrations from 0 to 300 nM (as shown in Figure II.2). For non-specific binding test, medium containing 200x concentrations of **B** (relative to **A** to be added in each well) was applied for the first 2 h incubation.

After 1 h incubation, the medium was removed and cells were washed carefully twice with 500 μL PBS containing 0.5% Cremophor EL. Then washing buffer was replaced by 500 μL 1% SDS aqueous solutions, fluorescence intensity (Ex/Em 485/528 nm) was scanned with BioTek® Synergy H4 hybrid microplate reader. Results were analyzed with GraphPad Prism® 6.0 software using one site-total and non-specific binding model.

D.3.2 Protocol for Solubility Measurement

Compound solubility was measured by UV absorbance following the literature.[88,209] Briefly, stock solution (50 mM) of **1** was prepared in DMSO. Then various concentrations (0 – 500 μM, Figure II.3a) were prepared in pH 7.40 PBS with 9% ethanol, 1% DMSO and 0.5% CrEL on 24-well plate (500 μL per concentration). The plate was shaken on a horizontal orbital shaker in dark for 6 h at room temperature, and kept steady overnight for equilibrium. Then the plate was centrifuged at 600x g for 10 min. 3 x 100 μL supernatant was transferred into 96-well UV transparent plate (Corning® 96 Well Clear Flat Bottom UV-

Transparent Microplate) and read compound absorbance at 254 nm against blank using microplate reader (BioTek® Synergy H4).

D.3.3 Determination of Conjugate Stability

Compound **1** was prepared as 20 μM stock in pH 7.40 PBS, or DMEM/F12 with 10% FBS, containing 0.5% CrEL, and kept at 37 ^{o}C. Boc-L-tyrosine was prepared as 6 mM separate stock in pH 7.40 PBS, kept at 4 ^{o}C, and used as internal standard for analytical HPLC trace analysis. 300 μL solution of **1** and 100 μL solution of Boc-L-tyrosine were taken out from stock and mixed after certain time of incubation (0 – 196 h). Mixed samples were injected to analytical HPLC column (0.75 mL/min flow rate, 10% MeCN / 90% water to 95% MeCN / 5% water gradient with 0.1% trifluoroacetic acid in 20 min), and traces of absorbance at 254 nm were collected (Figure D.2a, b; retention time 9.5 min for Boc-L-tyrosine, 12.4 min for **1**). Area under curves for **1** was normalized and plotted in GraphPad Prism® 6.0 software.

Conjugate stability in mouse serum is tested in a similar way. **1** was prepared as 20 μM stock in mouse serum:PBS (1:1, pH 7.40), containing 0.5% CrEL, and kept at 37 ^{o}C. Boc-L-tyrosine was prepared as 3 mM separate stock in pH 7.40 PBS, kept at 4 ^{o}C, and used as internal standard for analytical HPLC trace analysis. 40 μL solution of **1** and 10 μL solution of **Boc**-L-**tyrosine** were taken out from stock and mixed after certain time of incubation (0 – 24 h). Mixed samples were injected to analytical HPLC column (0.75 mL/min flow rate, 10%

MeCN / 90% water to 95% MeCN / 5% water gradient with 0.1% trifluoroacetic acid in 20 min), and traces of absorbance at 254 nm were collected (Figure D.2c. retention time 8.6 min for **Boc**-L-**tyrosine**, 13.3 min for **1**).

Based on the HPLC-UV traces, there was no other significant peak except the internal standard (Boc-Tyrosine) and conjugate **1** even after 24 h of incubation, which means the conjugate was relatively stable, and free **DM4** is not released at detectable level (Figure D.2). Previous studies also indicated that hindered disulfide bond was resistant to thiol exchange reactions.[61]

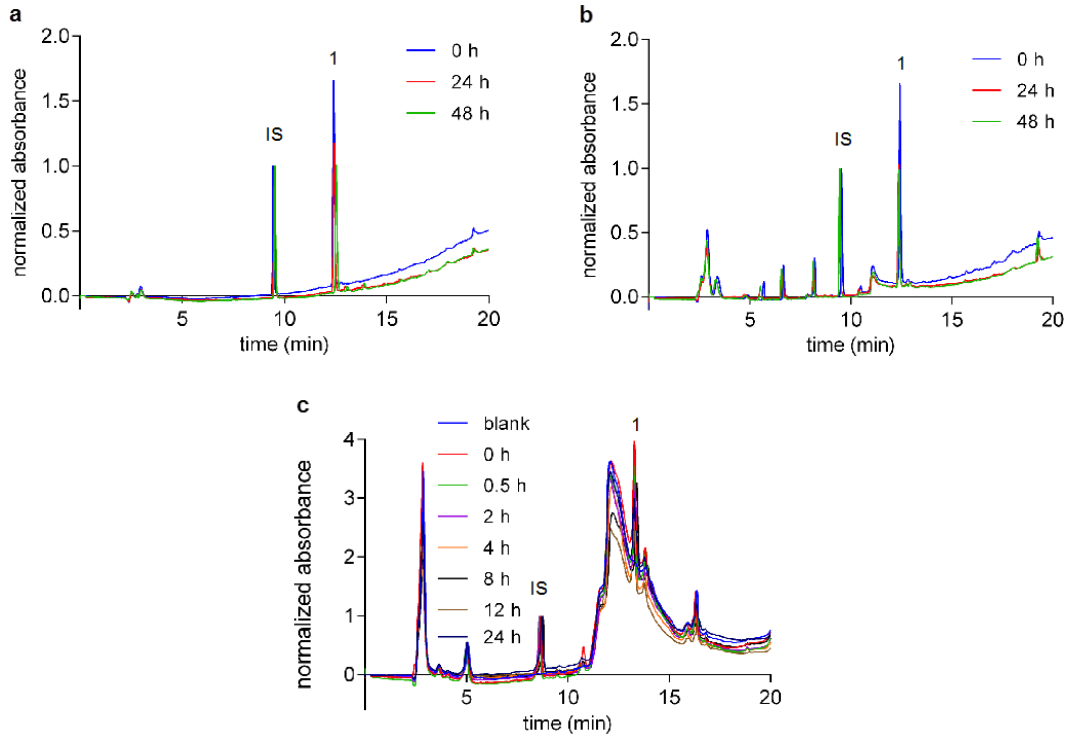

Figure D.2. Normalized HPLC traces for conjugate **1** stability in **a** PBS, **b** DMEM with 10% FBS, **c** mouse serum:PBS (1:1) (IS: internal standard Boc-L-tyrosine, **1**: conjugate **1**). Reprinted with permission from [217].

D.4 Biological Studies

D.4.1 TrkC Expression Confirmation of Cells involved

Western Blots were applied to check TrkC expression level on Hs578t and MCF-7 cells.

Cell lysates were prepared from cells cultured in a 75 cm^2 tissue culture flask by adding 1 mL of RIPA buffer (Thermo Scientific® #89901) with 1% protease inhibitor cocktail (Thermo Scientific® #78440). After 30 min incubation on ice, the mixtures were transferred to 1.5 mL Eppendorf tube and spin down at 14,000X g for 20 min at 4 ^oC. Supernatant was transferred out carefully as lysates, and the protein concentration was measured out by BCA protein assay kit (Thermo Scientific® #23227).

20 µg of each cell lysate was loaded onto 10% SDS-PAGE protein gels, and added 180V/80mA electric current for 75 min to separate the proteins in the lysate. Separated proteins were then transferred to PVDF membrane (Invitrogen® #LC2005), blocked with blocking buffer in PBS (Thermo Scientific® #37515) for 1 h, and incubated with anti-TrkC rabbit mAb (Cell Signaling Technology® #3376) overnight at 4 ^oC. After thorough wash with tris-buffered saline (TBS) containing 0.05% Tween 20, the membrane was incubated with 1:5000 dilution of goat anti-rabbit IgG secondary antibody with HRP tag (Invitrogen® #31460), and imaged after reacting with ECL western blotting substrate (Thermo Scientific® #32106).

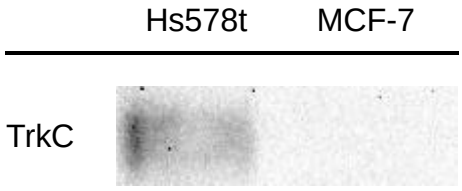

Figure D.3. Western Blot imaging result with anti-TrkC mAb on Hs578t and MCF-7. Reprinted with permission from [217].

The Western Blotting result clearly showed that TrkC protein is expressed in Hs578t ($TrkC^+$) cells but not MCF-7 ($TrkC^-$) cells, which is consistent with other studies.[75 76]

Immunohistochemistry staining using anti-TrkC rabbit mAb (Cell Signaling Technology® #3376) demonstrated TrkC overexpression in 4T1 tumor tissue. Previous studies also reported that 4T1 tumor overexpresses TrkC, and TrkC plays an essential role in breast tumor growth and metastasis.[75]

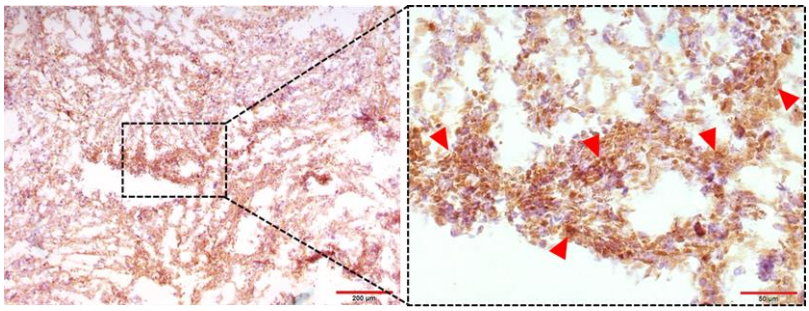

Figure D.4. Immunohistochemistry staining of 4T1 tumor using anti-TrkC antibody. Reprinted with permission from [217].

D.4.2 In vitro Cytotoxicity Assay

Hs578t ($TrkC^+$) or MCF-7 ($TrkC^-$) cells were seeded on 96-well plates as 5000 cells/well (50 µL) and incubated in the incubator overnight. Various concentrations of **DM4**, **1** and **2** were prepared in 50 µL protein-free hybridoma medium (PFHM II) and added to cells to make final concentrations from 0.03 nM to 10 µM. All plates were incubated for 72 h, and cell viability was tested with AlamarBlue assay (Invitrogen). Briefly, in a well containing 100 µL medium, 10 µL of AlamarBlue reagent was added, and incubated for 2 h. Fluorescence intensity (Ex/Em 560/590 nm) was measured on a microplate reader (BioTek® Synergy H4). Results are processed through GraphPad Prism® 6.0 software.

Cytotoxicities (IC_{50}) of all compounds are listed as:

With Hs578t cells ($TrkC^+$): **DM4**, 1.10 ± 0.11 nM; **1**, 28.1 ± 1.9 nM; **2**, 23.0 ± 2.5 nM.

With MCF-7 cells ($TrkC^-$): **DM4**, 1.86 ± 0.63 nM; **1**, 137 ± 14 nM; **2**, 50.2 ± 6.6 nM.

Cellular therapeutic indexes were calculated based on the following equation:

cellular therapeutic index = IC_{50} with $TrkC^-$ cells / IC_{50} with Trk^+ cells

Cytotoxicity of conjugate **1** against 4T1 cells was tested with the same protocol (Figure D.5).

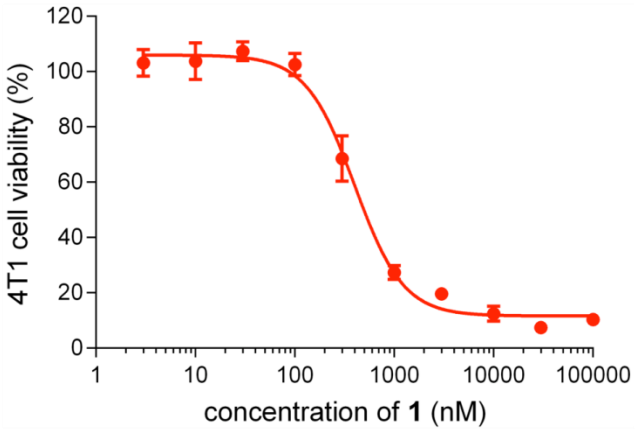

Figure D.5. Cytotoxicity of conjugate **1** on 4T1 cells. IC_{50} = 401 ± 38 nM. Reprinted with permission from [217].

D.4.3 In vivo therapeutic study

Breast tumor model was created by inoculating 4T1 cells on BALB/c mouse (Charles River®). Briefly, 4T1 cells were cultured under recommended condition of DMEM media supplemented with 10% FBS at 37 ^{o}C and 5% CO_2. Upon reaching ~70% confluence, cells were harvested and mixed with 10 mg/mL Corning® Matrigel® matrix, and then inoculated into BALB/c mice at total number of 1 x 10^6 cells per mouse. 10 days was waited after tumor implantation to allow tumor growth reach to 2~3 mm (long side). To start therapy, tumor-implanted mice were randomly assigned into two study groups with 5 mice per group. For therapy group, 30 nmol **1** in 100 µL solution cocktail (5% DMSO, 5% Cremophor EL surfactant, and 90% PBS) was intravenously injected into mouse every other day for seven shots. Similarly, **2** was injected as control group. Specifically, compounds were firstly dissolved into DMSO, then diluted into

CrEL-contained PBS to yield 30 nmol per 100 μL solution for each shot of i.v. injection. From the start of therapy, tumor size was measured as length of short side and long side, and weight of mouse was monitored on a daily basis until the end of study. Tumor size was calculated by the formula of (short side)^2 x (long side)/2. The study was ended after three-week therapy by scarifying the mice as described in animal protocol. Lastly, 4T1 tumors were harvested and *ex vivo* measured of the size. All animal experiments were performed under approved protocols in compliance with the guidelines established by the Institutional Animal Care and Use Committee (IACUC) of the Houston Methodist Research Institute.

APPENDIX E

SUPPORTING INFORMATION OF CHAPTER III

E.1 General Experimental Procedures

General reaction and purification methods are the same as Appendix D.

High field NMR spectra were recorded with Bruker Avance III at 400 MHz for ^{1}H, and 101 MHz for ^{13}C for all compounds except for compound **5**. NMR spectra of **5** were taken with Bruker Avance 500 at 500 MHz for ^{1}H, and 126 MHz for ^{13}C.

Electrospray ionization mass spectrometry (ESI-MS) data were collected on triple-stage quadrupole instrument in a positive mode. Paper spray mass spectrometry data were obtained with LTQ XL mass spectrometer (Thermo Scientific®, San Jose, CA). Instrumental conditions used for the positive-mode mass spectrometry is specified as following: paper spray voltage: 3.5 kV; heated-capillary temperature: 275 °C; heated-capillary voltage: 33 V; tube lens voltage: 65 V. Both the full-scan and tandem mass spectra were acquired, and the corresponding m/z values confirmed the structure of each species. The qualitative filter paper (VWR® #8310-026) was cut into an isosceles triangle shape with 10 mm height and 5 mm base. A copper clip was employed as both the paper holder and the spray voltage conductor. The distance from the paper tip to the mass spectrometer inlet was kept to be 5 mm.

Cell Culture. U87 cells were cultured on 75 cm^2 tissue culture flasks in Dulbecco's Modified Eagle Medium/nutrient mixture F-12 Ham (DMEM/F12, Millipore Sigma) supplement with 10% fetal bovine serum (FBS). All cells were cultured in a humidified incubator at 37 °C with 5% CO2 and 95% air.

E.2 Compound Synthesis and Characterization

*E.2.1 Preparation and Characterization of Compound **F***

Compound **F** was prepared via the protocol previous published.[108] Briefly, 2-(1H-Benzotriazole-1-yl)-1,1,3,3-tetramethylaminium tetrafluoroborate (TBTU, 1.2 g, 1.2 equiv.) and compound **H**[108] (1.1 g, 3.0 mmol, 1.0 equiv.) were dissolved in *N,N*-dimethylformamide (DMF, 0.3 M) in an ice bath, gemcitabine hydrochloride (0.90 g, 3.0 mmol, 1.0 equiv.) and *N,N*-diisopropylethylamine ($^{i}Pr_2NEt$, 1.1 mL, 2.0 equiv.) were then added to the reaction mixture, and stirred at room temperature for 18 h. Product was purified via flash chromatography (2 – 5% MeOH in CH2Cl2) with 63% yield (1.1 g). Protecting group of the thiol in the product (0.59 g, 1.0 mmol) was then removed under acidic conditions in 1:3 (v/v) trifluoroacetic acid (TFA):CH2Cl2 (0.2 M) on ice for 1 h, with triethylsilane (Et3SiH, 0.39 mL, 2.4 equiv.) as scavenger. After removing solvents, reaction was washed with diethyl ether 5 mL X 2 to get compound **F** (0.36 g as 1.0 equiv. TFA salt, 80% yield).

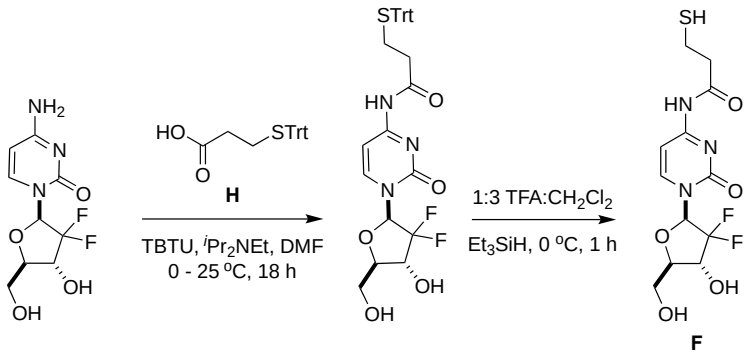

Scheme E.1. Synthesis of gemcitabine derivative **F**.

F

$C_{12}H_{15}F_2N_3O_5S$

^{1}H NMR (400 MHz, MeOD) δ 8.17 (d, J = 7.9 Hz, 1H), 6.28 (t, J = 8.1 Hz, 1H), 6.16 (d, J = 7.9 Hz, 1H), 5.50 (dt, J = 13.5, 6.9 Hz, 1H), 4.27 (dd, J = 6.7, 3.1 Hz, 1H), 3.95 (d, J = 11.1 Hz, 1H), 3.80 (dd, J = 12.8, 3.2 Hz, 1H), 2.85 – 2.72 (m, 4H).

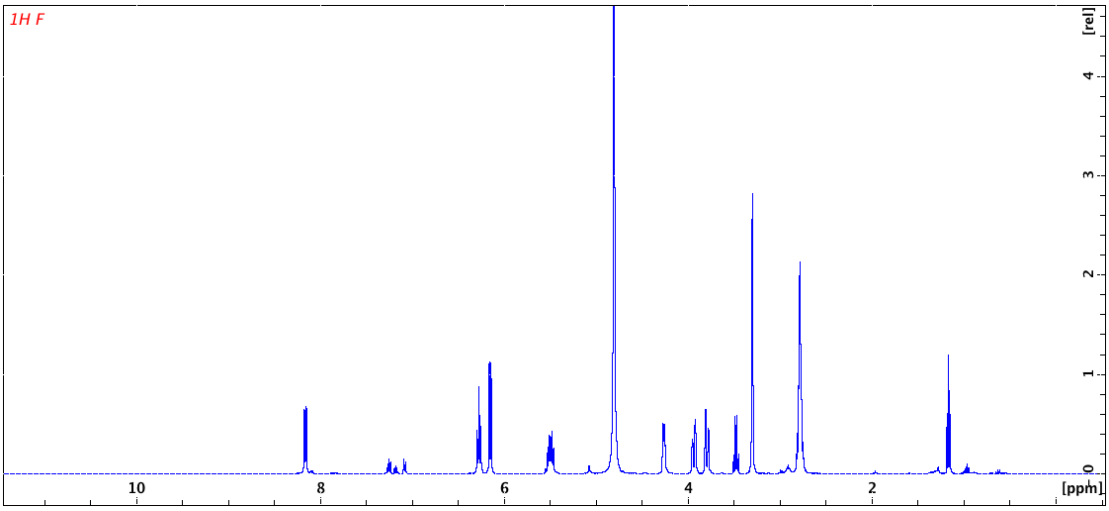

^{13}C NMR (101 MHz, MeOD) δ 171.66, 145.40, 130.47, 129.25, 127.29, 122.73, 95.82, 81.80, 71.07 (dd, J = 31.8, 16.8 Hz), 60.57, 38.94, 20.00.

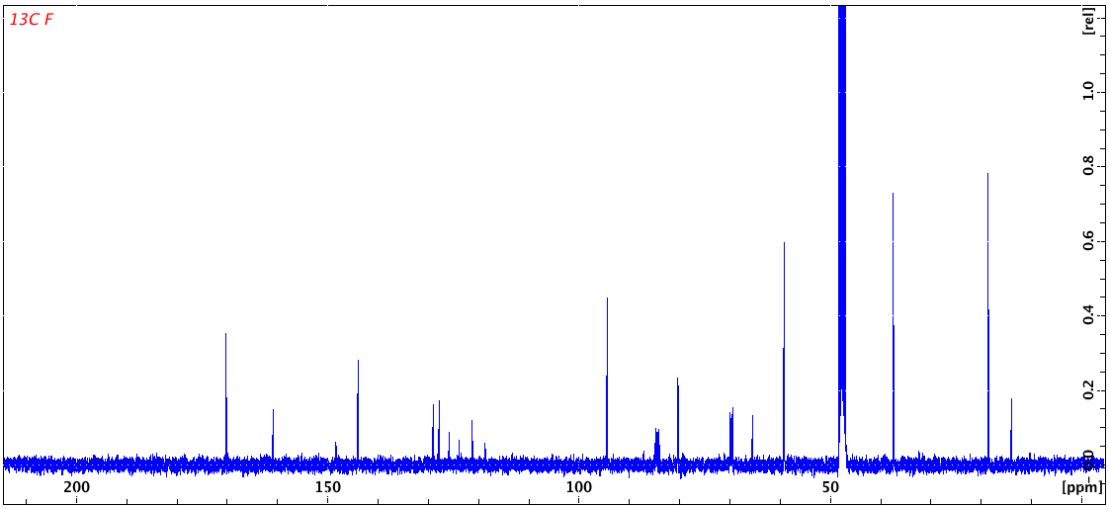

162.29, 85.88 (dd, J = 40.0, 22.0 Hz) from TFA, 66.87, 15.41 from Et_2O.

*E.2.2 Synthesis and Characterization of Targeted (**1a** – **d**), Control Cyanine-Gemcitabine Conjugates (**2a**, **b**, **d**) and Compound **3** – **5***

Synthesis of 1a – d

Compounds **B** (Sigma Aldrich® #543292) and **D** (abcr GmbH® #AB332015) were commercially available, and compounds **A** and **C** were prepared by the protocol previously described.[235] As shown in Scheme III.1, equal equiv. of compound **F** and representative free heptamethine dye **A** – **D** were dissolved in DMF (0.06 M), followed by 2.0 equiv. of triethylamine (Et_3N) and stirred at 25 °C for 6 h. Solvent was removed in vacuum, and compound was purified via prepHPLC and lyophilized to get **1a** – **d** (30 – 40% yield).

1a

$C_{54}H_{66}ClF_2N_5O_9S$

^{1}H NMR (400 MHz, DMSO) δ 8.66 (s, 2H), 8.24 (d, *J* = 7.6 Hz, 1H), 7.56 (d, *J* = 7.4 Hz, 2H), 7.46 – 7.37 (m, 6H), 7.30 – 7.20 (m, 3H), 6.34 – 6.23 (m, 1H), 6.19 – 6.08 (m, 1H), 4.23 – 4.10 (m, 6H), 3.95 – 3.85 (m, 1H), 3.85 – 3.71 (m, 1H), 3.71 – 3.59 (m, 1H), 3.10 – 3.02 (m, 2H), 2.78 (t, *J* = 6.5 Hz, 2H), 2.70 – 2.59 (m, 4H), 2.30 (t, *J* = 7.3 Hz, 1H), 2.21 (t, *J* = 7.3 Hz, 4H), 1.92 – 1.80 (m, 2H), 1.77 – 1.51 (m, 22H), 1.46 – 1.35 (m, 4H).

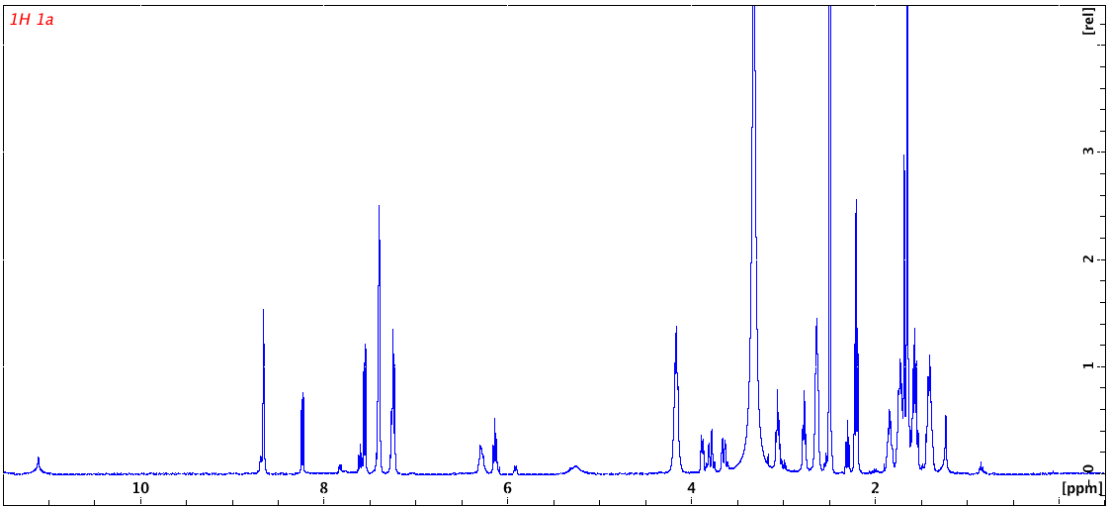

^{13}C NMR (101 MHz, DMSO) δ 174.22, 171.69, 171.64, 162.65, 154.87, 154.01, 144.53, 142.13, 140.83, 132.92, 128.51, 124.80, 122.34, 111.16, 95.93, 94.56, 81.09, 58.87, 58.78, 48.70, 43.48, 36.70, 33.45, 33.05, 31.72, 27.41, 27.36, 27.33, 26.58, 25.66, 24.12, 24.06, 20.37.

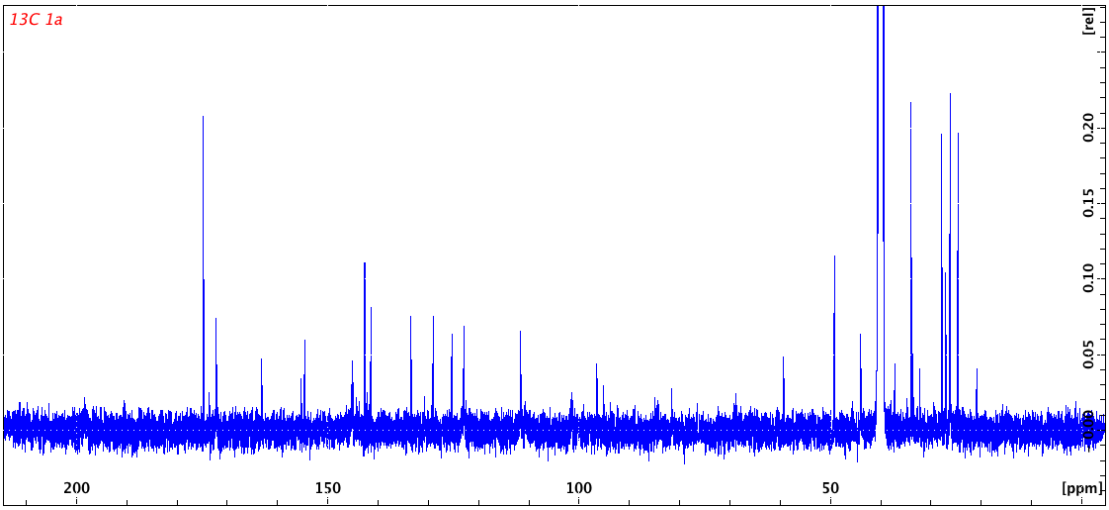

Measured M^+ ($C_{54}H_{66}F_2N_5O_9S^+$) (m/z): 998.4531 Calculated M^+: 998.4544 (1.3 ppm).

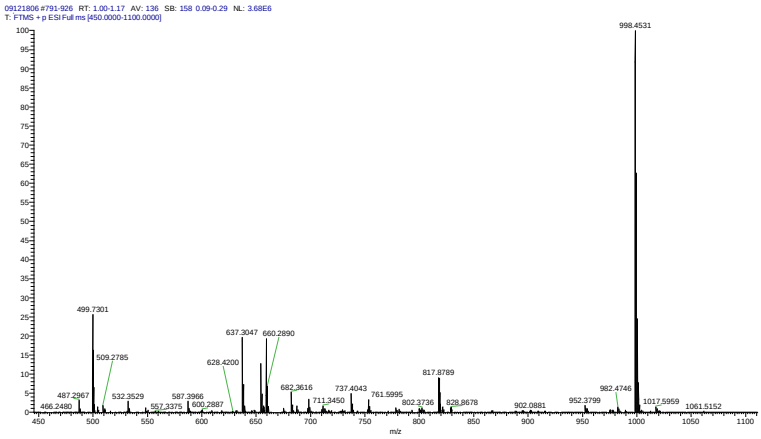

1b

$C_{50}H_{62}ClF_2N_5O_{11}S_3$

^{1}H NMR (400 MHz, DMSO) δ 9.99 (s, 1H), 8.99 (s, 1H), 8.74 – 8.62 (m, 2H), 8.26 (d, *J* = 7.6 Hz, 1H), 8.16 (d, *J* = 7.9 Hz, 1H), 7.72 – 7.61 (m, 1H), 7.57 (dd, *J* = 15.2, 7.3 Hz, 2H), 7.47 – 7.35 (m, 3H), 7.32 – 7.20 (m, 2H), 6.34 (dd, *J* =

14.2, 6.2 Hz, 2H), 6.26 (d, *J* = 7.9 Hz, 1H), 6.18 – 6.03 (m, 1H), 4.27 – 4.12 (m, 5H), 3.96 – 3.85 (m, 1H), 3.80 (d, *J* = 12.7 Hz, 1H), 3.65 (dd, *J* = 12.8, 3.3 Hz, 1H), 3.17 (s, 1H), 3.08 (t, *J* = 6.4 Hz, 1H), 2.99 (t, *J* = 6.8 Hz, 1H), 2.78 (t, *J* = 6.5 Hz, 1H), 2.72 – 2.52 (m, 8H), 1.89 – 1.71 (m, 12H), 1.71 – 1.55 (m, 12H).

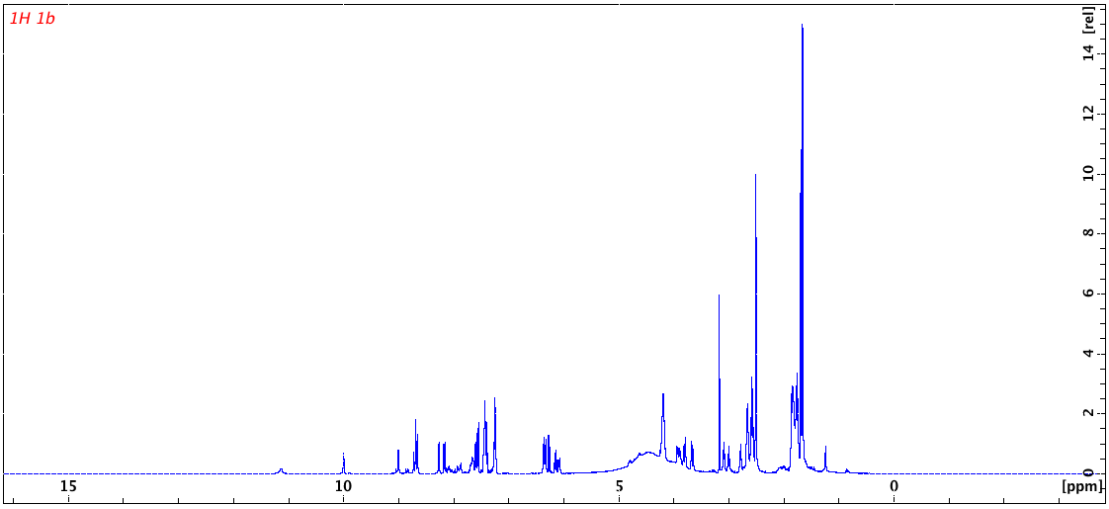

^{13}C NMR (101 MHz, DMSO) δ 172.22, 171.72, 171.65, 162.66, 159.27, 154.89, 154.00, 146.77, 144.78, 142.18, 140.91, 140.85, 133.09, 128.51, 124.74, 122.28, 111.29, 101.32, 95.99, 94.76, 58.78, 58.71, 50.68, 48.74, 48.71, 48.56, 43.58, 27.42, 25.97, 25.75, 22.38.

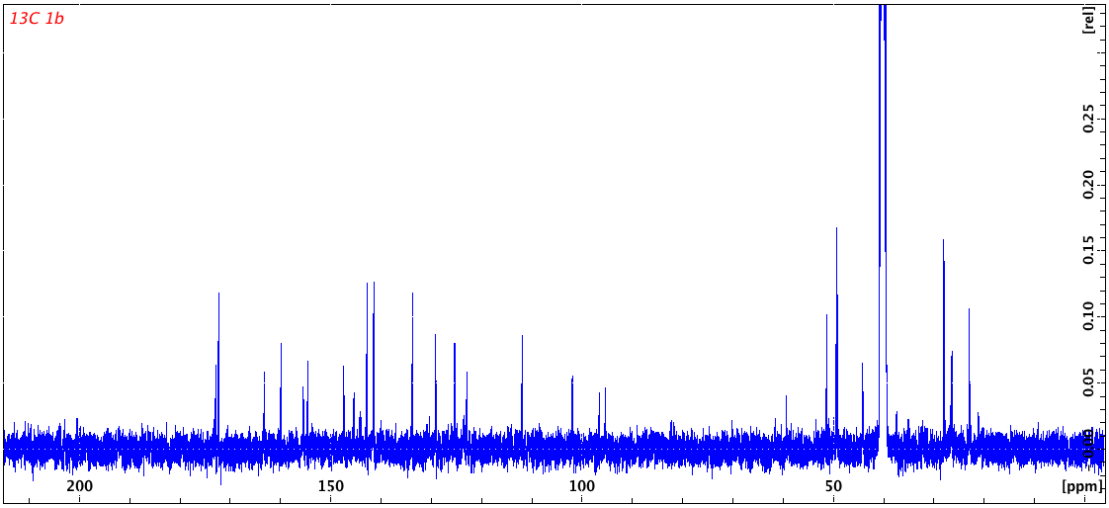

Measured M^+ ($C_{50}H_{62}F_2N_5O_{11}S_3^+$) (m/z): 1042.3564 Calculated M^+: 1042.3571 (0.7 ppm).

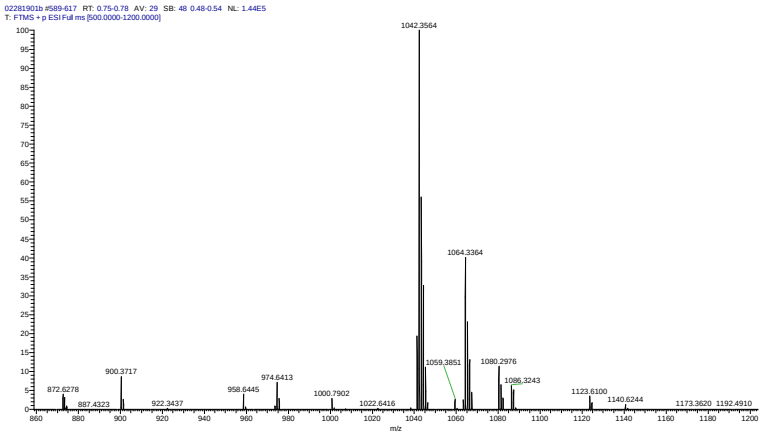

1c

$C_{52}H_{64}ClF_2N_5O_{10}S_2$

^{1}H NMR (400 MHz, DMSO) δ 8.70 (d, *J* = 14.2 Hz, 1H), 8.63 (d, *J* = 14.0 Hz, 1H), 8.24 (d, *J* = 7.6 Hz, 1H), 7.55 (dd, *J* = 10.2, 7.6 Hz, 2H), 7.49 – 7.33 (m, 5H), 7.29 – 7.20 (m, 4H), 6.38 (d, *J* = 14.3 Hz, 1H), 6.25 (d, *J* = 14.1 Hz, 1H), 6.14 (t,

J = 7.5 Hz, 1H), 4.25 – 4.10 (m, 5H), 3.91 – 3.86 (m, 1H), 3.80 (d, *J* = 11.4 Hz, 2H), 3.67 (d, *J* = 3.5 Hz, 1H), 3.64 (d, *J* = 3.5 Hz, 1H), 3.08 (t, *J* = 6.5 Hz, 2H), 2.78 (t, *J* = 6.5 Hz, 2H), 2.70 – 2.60 (m, 4H), 2.54 (d, *J* = 7.2 Hz, 2H), 2.21 (t, *J* = 7.3 Hz, 2H), 2.06 (s, 1H), 1.90 – 1.79 (m, 4H), 1.79 – 1.68 (m, 4H), 1.67 – 1.62 (m, 12H), 1.62 – 1.53 (m, 2H), 1.45 – 1.35 (m, 2H).

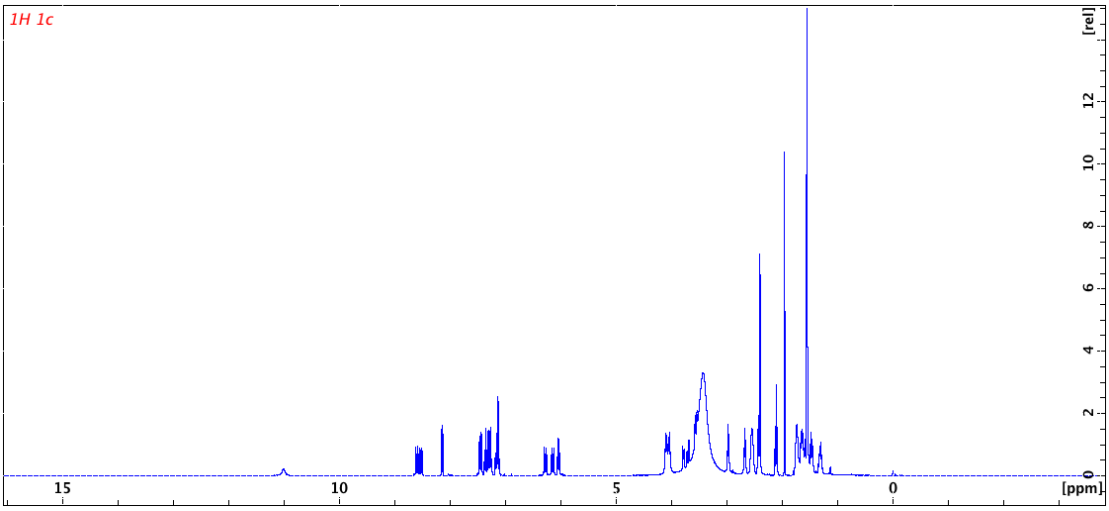

^{13}C NMR (101 MHz, DMSO) δ 174.31, 172.32, 171.71, 171.12, 162.73, 154.94, 154.11, 145.28, 144.86, 144.07, 142.27, 142.10, 141.01, 140.75, 133.52, 132.69, 128.61, 128.52, 125.47, 125.06, 124.57, 122.90, 122.34, 118.01, 117.22, 111.53, 110.96, 101.87, 100.75, 96.05, 81.14, 68.45, 58.83, 50.65, 48.92, 48.60, 43.80, 43.38, 36.83, 33.51, 31.77, 27.54, 27.49, 27.42, 27.37, 26.57, 26.05, 25.79, 25.71, 24.18, 22.49, 20.47.

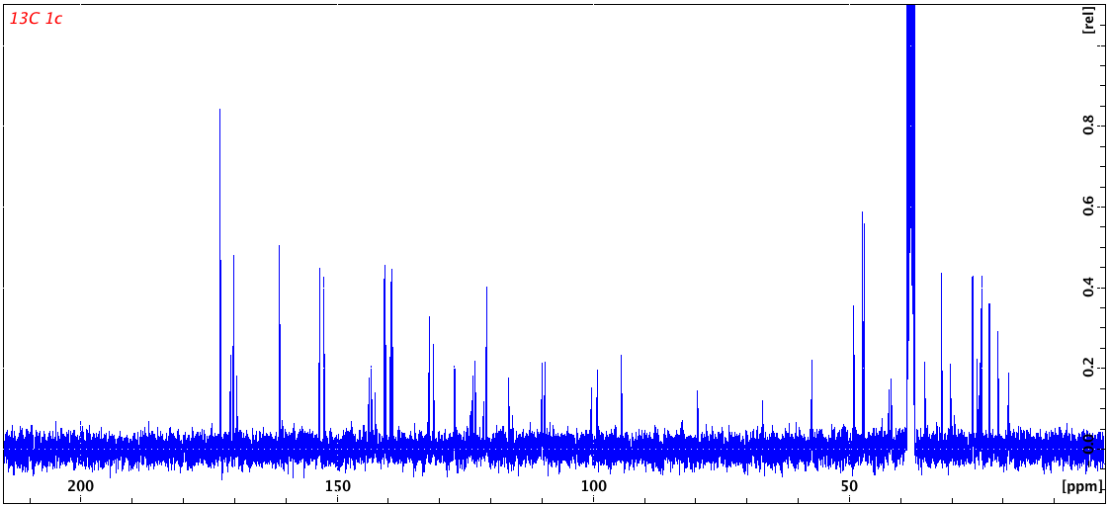

Measured M^+ ($C_{52}H_{64}F_2N_5O_{10}S_2^+$) (m/z): 1020.4040 Calculated M^+: 1020.4057 (1.7 ppm).

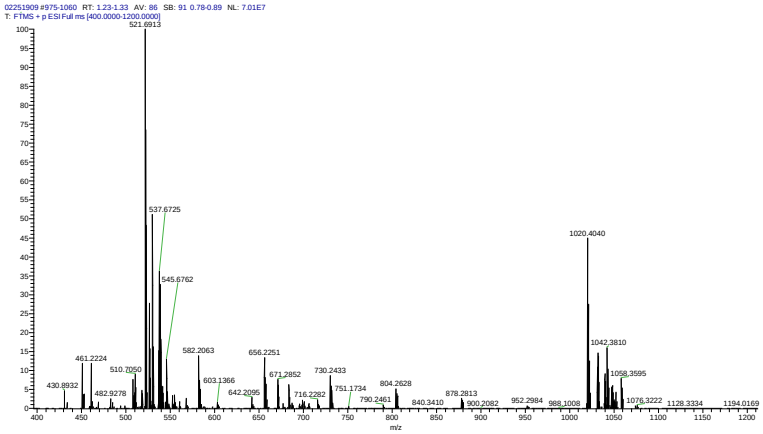

1d

$C_{48}H_{58}ClF_2N_5O_5S$

^{1}H NMR (400 MHz, DMSO) δ 8.71 – 8.63 (m, 2H), 8.24 (d, *J* = 7.6 Hz, 1H), 7.57 (d, *J* = 7.4 Hz, 2H), 7.47 – 7.37 (m, 4H), 7.31 – 7.20 (m, 3H), 6.39 – 6.25 (m, 2H), 6.14 (t, *J* = 7.5 Hz, 1H), 4.24 – 4.10 (m, 6H), 3.94 – 3.60 (m, 4H), 3.07 (t, *J* = 6.6

Hz, 2H), 2.77 (t, *J* = 6.5 Hz, 2H), 2.64 (t, *J* = 5.6 Hz, 4H), 1.89 – 1.60 (m, 19H), 1.00 – 0.92 (m, 6H).

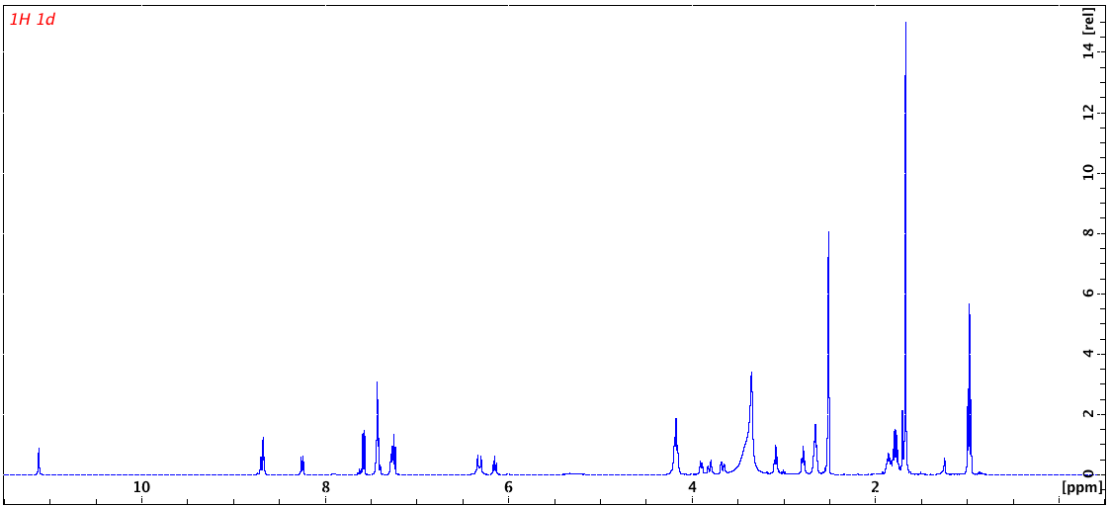

^{13}C NMR (101 MHz, DMSO) δ 171.91, 171.88, 171.62, 162.65, 154.83, 154.01, 144.83, 144.59, 142.27, 140.80, 132.93, 128.49, 124.78, 122.83, 122.34, 111.24, 101.24, 95.91, 81.12, 68.44, 58.78, 48.74, 44.93, 36.70, 31.63, 27.46, 27.40, 25.73, 20.36, 11.05.

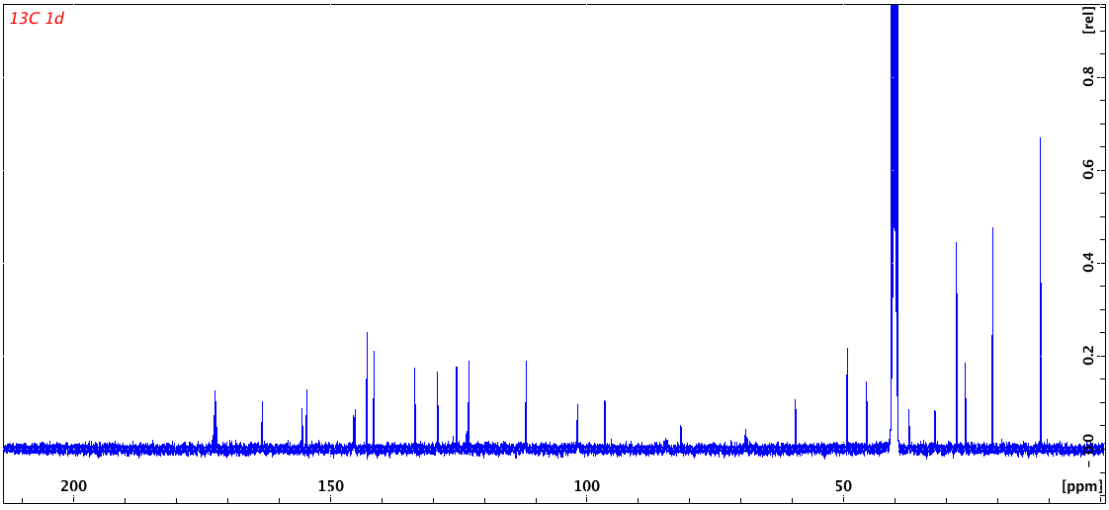

Measured M^+ ($C_{48}H_{58}F_2N_5O_5S^+$) (m/z): 854.4091 Calculated M^+: 854.4121 (3.5 ppm).

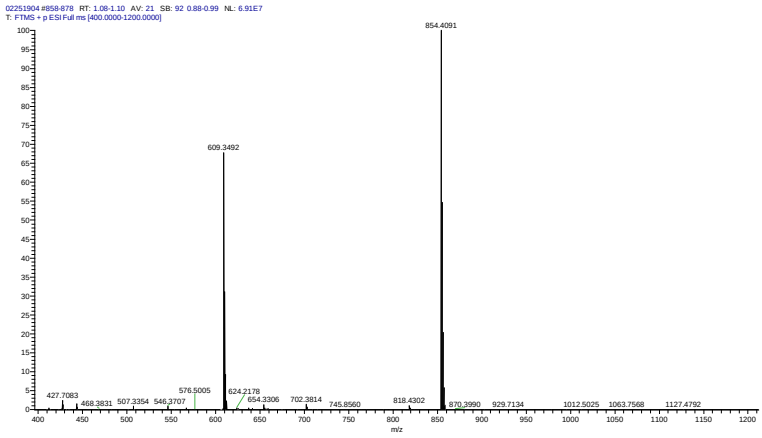

Synthesis of 2a, b, d

Compounds **2** were prepared in the same way as for compounds **1** described above (Scheme E.2). Briefly, TBTU (3.86 g, 1.2 equiv.) and compound **H** (3.49 g, 1.0 equiv.) were dissolved in DMF (0.3 M) in an ice bath, 2'-deoxycytidine (**2dC**, 2.27 g, 10.0 mmol, 1.0 equiv.) and $^{i}Pr_2NEt$ (2.10 mL, 1.2 equiv.) were then added to the reaction mixture, and stirred at room temperature for 18 h. Product compound **3** was purified via flash chromatography (2 – 4% MeOH in CH_2Cl_2) with 22% yield (1.20 g). Protecting group of the thiol in **3** was then removed under acidic conditions in 1:3 (v/v) TFA:CH_2Cl_2 (0.2 M) on ice for 1 h, with Et_3SiH (2.4 equiv.) as scavenger. After removing solvents, reaction was washed with diethyl ether 5 mL X 2 to get compound **4** (quantitative).

Then equal equiv. of compound **4** and representative free heptamethine dye **A**, **B** or **D** were dissolved in DMF (0.06 M), followed by 2.0 equiv. of Et_3N

and stirred at 25 °C for 6 h. Solvent was removed in vacuum, and compound was purified via prepHPLC and lyophilized to get **2a**, **b** or **d** (30 – 40% yield).

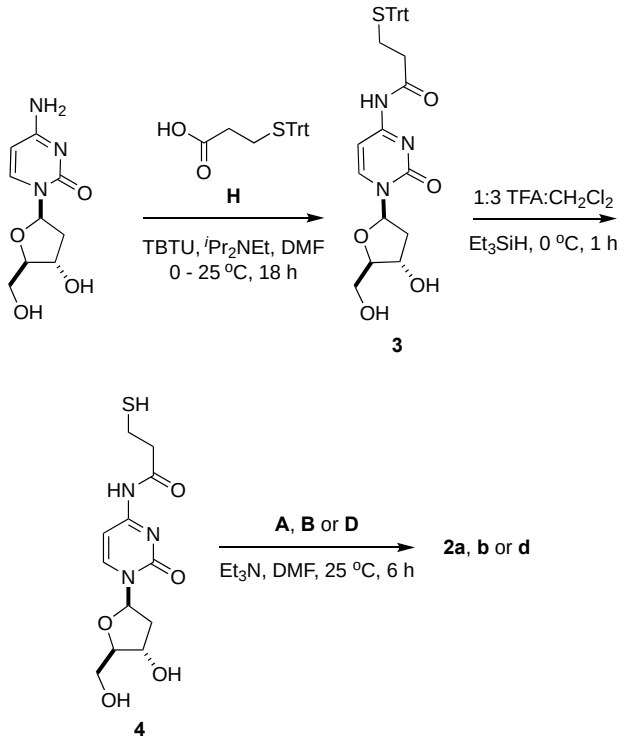

Scheme E.2. Synthesis of control compounds **2**.

3

$C_{31}H_{31}N_3O_5S$

^{1}H NMR (400 MHz, DMSO) δ 8.31 (d, *J* = 7.4 Hz, 1H), 7.40 – 7.28 (m, 12H), 7.28 – 7.21 (m, 3H), 7.15 (d, *J* = 7.5 Hz, 1H), 6.10 (t, *J* = 6.3 Hz, 1H), 5.20 (d, *J* = 15.2 Hz, 1H), 5.05 – 4.96 (m, 1H), 4.27 – 4.15 (m, 1H), 4.09 – 3.96 (m, 1H), 3.86 (q, *J* = 3.7 Hz, 1H), 3.66 – 3.50 (m, 2H), 3.28 (d, *J* = 9.5 Hz, 1H), 2.38 – 2.23 (m, 3H), 2.09 – 1.95 (m, 2H).

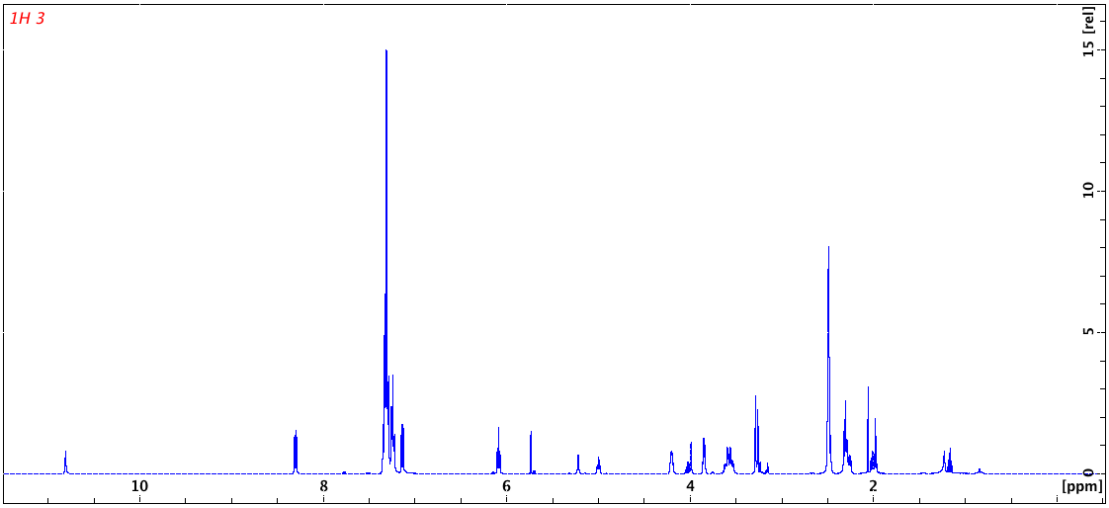

^{13}C NMR (101 MHz, DMSO) δ 171.68, 161.89, 154.31, 145.01, 144.29, 129.01, 127.98, 126.69, 95.13, 87.79, 86.12, 69.78, 66.13, 60.79, 40.79, 35.18, 26.50.

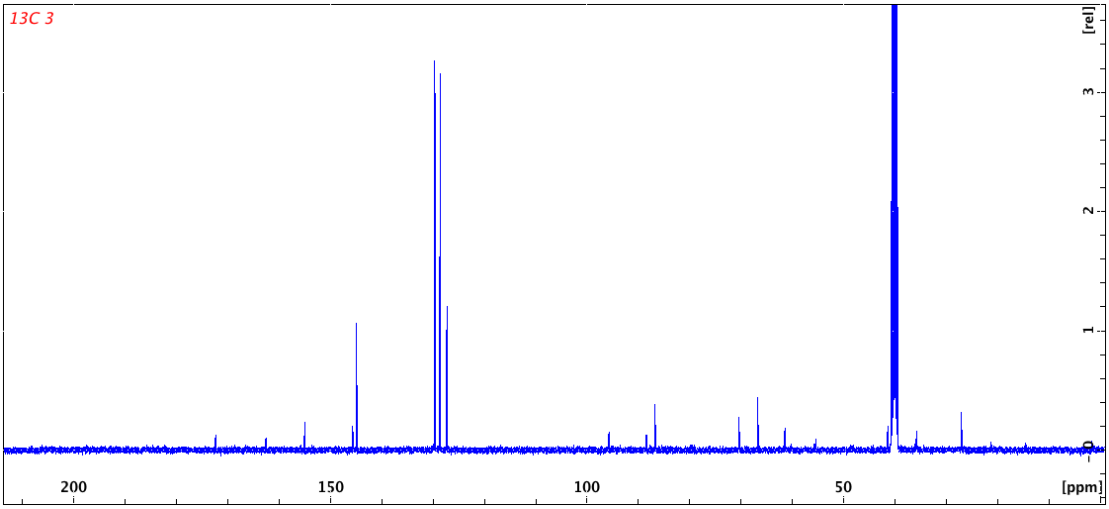

4

$C_{12}H_{17}N_3O_5S$

^{1}H NMR (400 MHz, DMSO) δ 8.33 (d, *J* = 7.4 Hz, 1H), 7.84 (d, *J* = 7.0 Hz, 1H), 7.20 (d, *J* = 7.4 Hz, 1H), 7.09 (d, *J* = 7.0 Hz, 1H), 6.10 (t, *J* = 6.2 Hz, 1H), 4.31 –

4.15 (m, 1H), 3.86 (d, *J* = 3.5 Hz, 1H), 3.59 (qd, *J* = 11.9, 3.8 Hz, 2H), 2.86 – 2.62 (m, 5H), 2.38 (m, 1H), 2.34 – 2.22 (m, 1H), 2.08 – 1.90 (m, 1H).

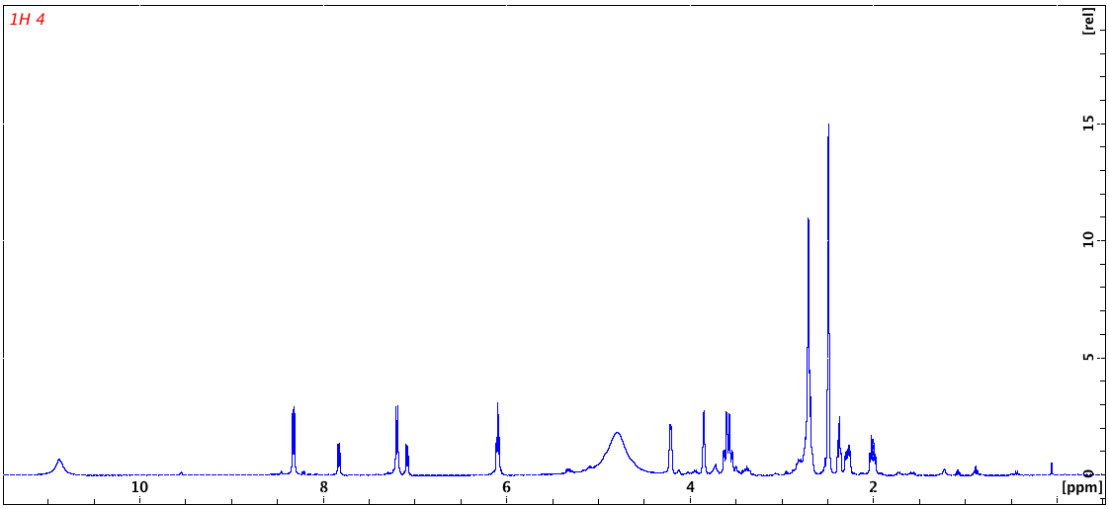

^{13}C NMR (101 MHz, DMSO) δ 172.01, 162.04, 154.30, 145.04, 95.25, 87.89, 86.15, 69.89, 60.91, 40.86, 40.35, 18.90.

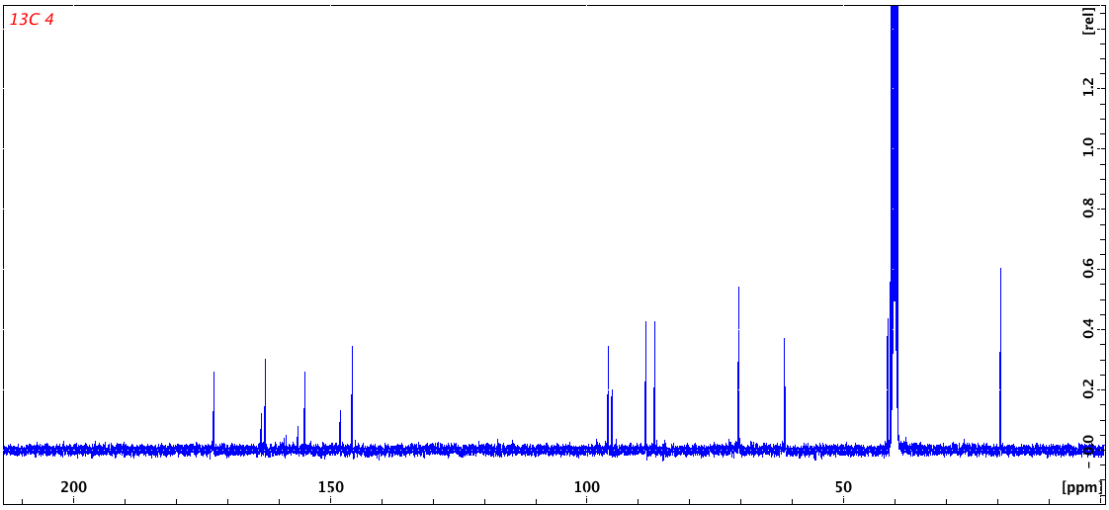

Measured M+H (m/z): 316.0963 Calculated M+H: 316.0962 (0.3 ppm).

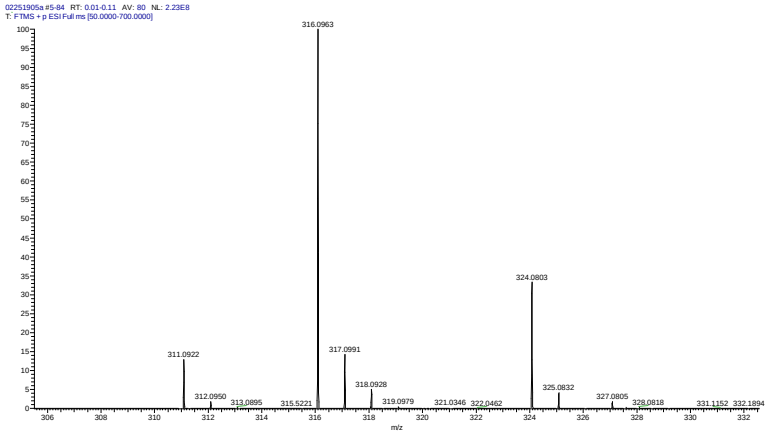

2a

$C_{54}H_{68}ClN_5O_9S$

^{1}H NMR (400 MHz, DMSO) δ 8.67 (d, *J* = 14.0 Hz, 2H), 8.37 (d, *J* = 7.5 Hz, 1H), 7.57 (d, *J* = 7.4 Hz, 2H), 7.46 – 7.36 (m, 5H), 7.31 – 7.21 (m, 2H), 7.18 (d, *J* = 7.5 Hz, 1H), 6.29 (d, *J* = 14.2 Hz, 2H), 6.07 (t, *J* = 6.3 Hz, 1H), 4.27 – 4.10 (m, 5H), 3.90 – 3.82 (m, 1H), 3.58 (qd, *J* = 12.0, 3.8 Hz, 1H), 3.06 (t, *J* = 6.4 Hz, 2H), 2.76 (t, *J* = 6.2 Hz, 2H), 2.69 – 2.59 (m, 4H), 2.31 – 2.15 (m, 5H), 1.99 – 1.80 (m, 3H), 1.78 – 1.35 (m, 28H), 1.27 – 1.18 (m, 1H).

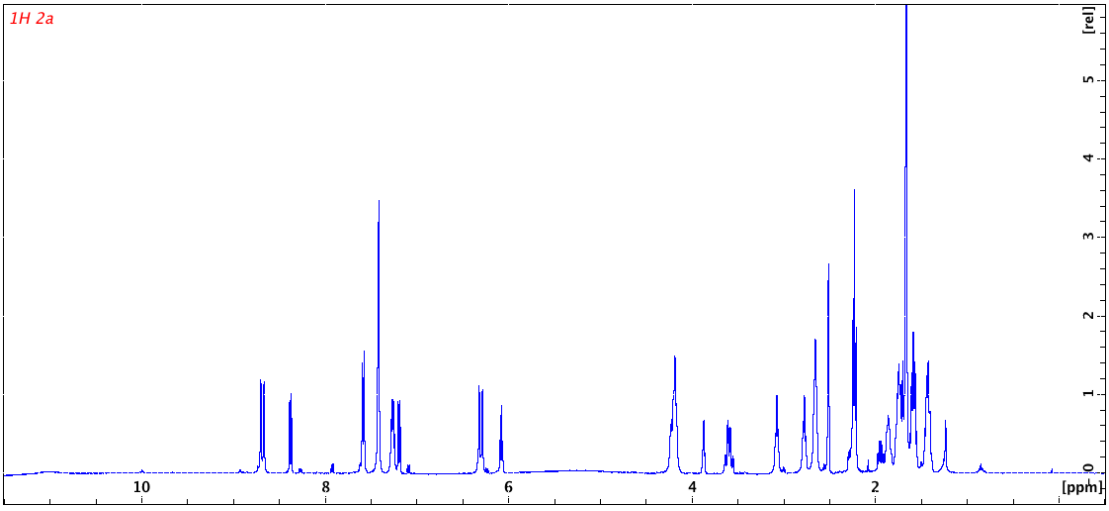

^{13}C NMR (101 MHz, DMSO) δ 174.20, 171.74, 171.43, 161.93, 154.85, 154.09, 145.18, 144.62, 142.13, 140.85, 133.01, 128.51, 124.79, 122.37, 111.18, 101.23, 95.34, 87.99, 86.20, 69.92, 60.87, 48.75, 43.51, 40.89, 36.63, 33.51, 31.84, 27.42, 26.60, 25.73, 25.68, 24.15, 20.40.

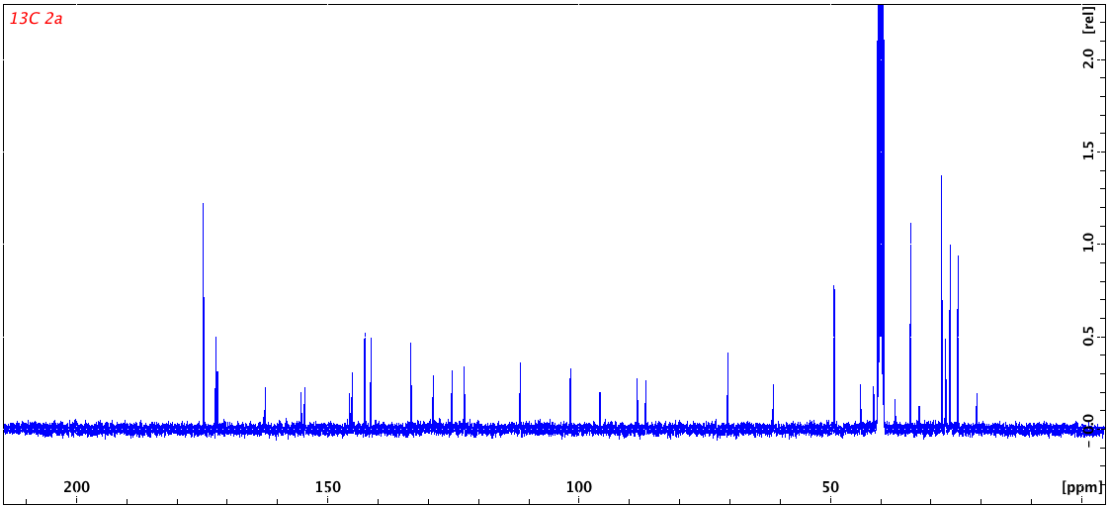

Measured M^+ ($C_{54}H_{68}N_5O_9S^+$) (m/z): 962.4721 Calculated M^+: 962.4732 (1.1 ppm).

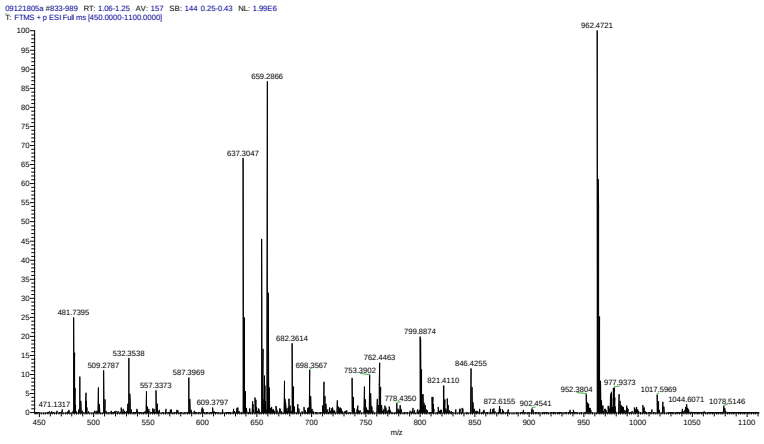

2b

$C_{50}H_{64}ClN_5O_{11}S_3$

^{1}H NMR (400 MHz, DMSO) δ 9.73 – 9.54 (m, 1H), 8.89 – 8.67 (m, 4H), 8.23 (d, *J* = 7.9 Hz, 1H), 8.11 – 7.75 (m, 3H), 7.70 – 7.55 (m, 3H), 7.49 – 7.36 (m, 3H), 7.25 (t, *J* = 7.3 Hz, 2H), 6.35 (d, *J* = 14.2 Hz, 1H), 6.16 (d, *J* = 7.9 Hz, 1H), 6.10 – 5.98 (m, 1H), 4.29 – 4.13 (m, 4H), 3.85 (q, *J* = 3.4 Hz, 1H), 3.59 (dd, *J* = 9.5, 3.6 Hz, 1H), 2.99 (t, *J* = 6.8 Hz, 1H), 2.70 – 2.62 (m, 4H), 2.60 – 2.51 (m, 6H), 2.28 – 2.02 (m, 3H), 1.90 – 1.63 (m, 24H).

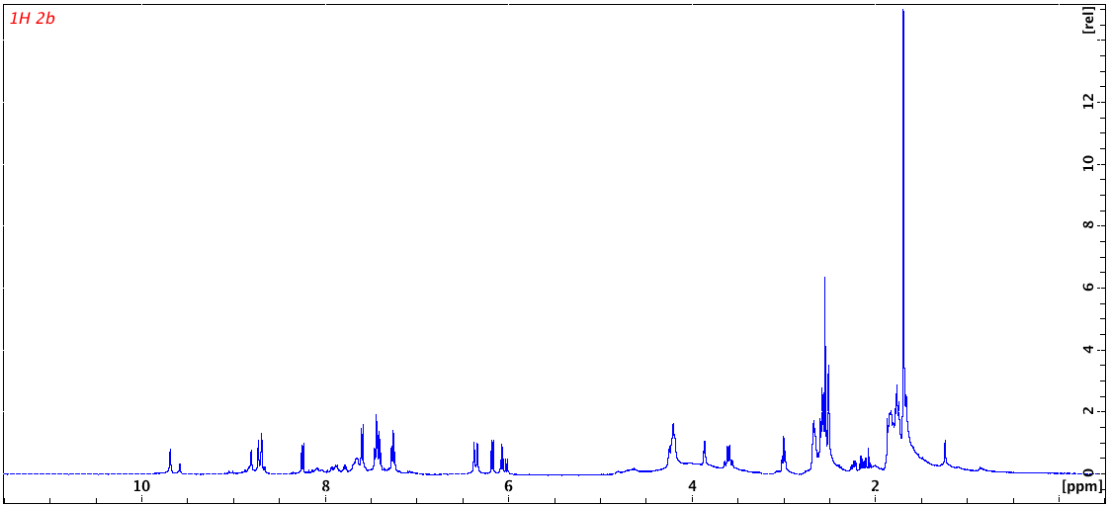

^{13}C NMR (101 MHz, DMSO) δ 172.22, 171.73, 159.23, 154.82, 147.59, 146.87, 144.77, 144.41, 142.20, 140.90, 133.11, 128.51, 124.75, 122.34, 111.29, 101.39, 99.49, 93.75, 88.05, 85.82, 69.74, 60.74, 50.71, 48.74, 43.57, 40.43, 34.48, 27.43, 26.01, 25.70, 22.41.

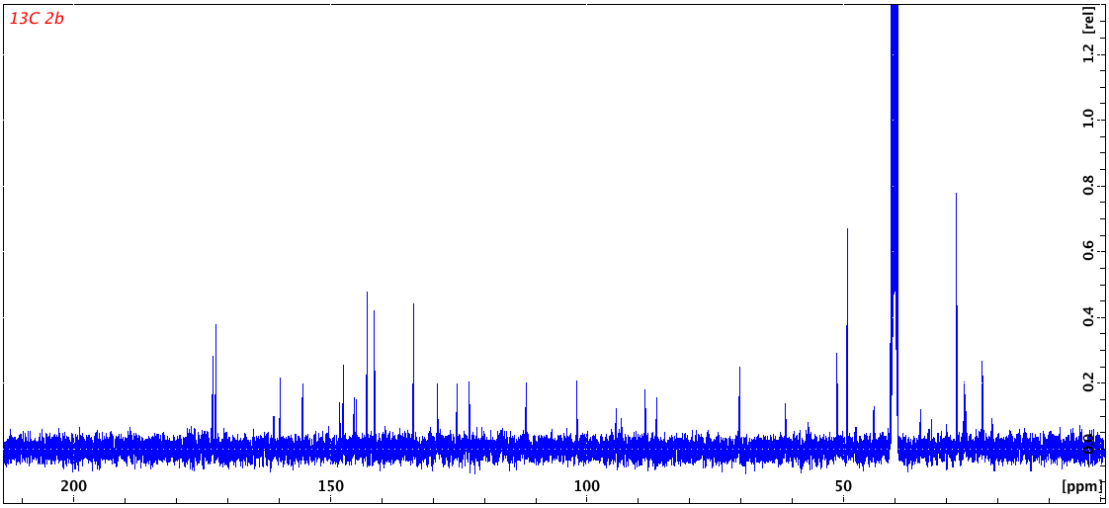

Measured M^+ ($C_{50}H_{64}N_5O_{11}S_3^+$) 1006.3757 (m/z): Calculated M^+: 1006.3759 (0.2 ppm).

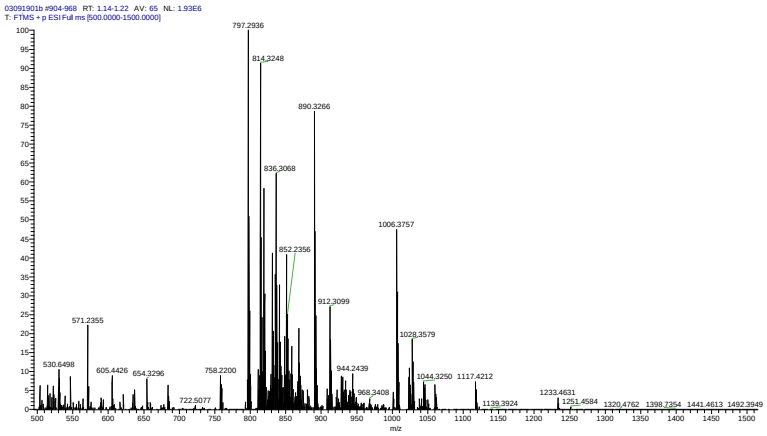

2d

$C_{48}H_{60}ClN_5O_5S$

^{1}H NMR (400 MHz, DMSO) δ 8.98 (d, *J* = 16.3 Hz, 1H), 8.74 – 8.66 (m, 2H), 8.26 (d, *J* = 7.8 Hz, 1H), 7.73 – 7.66 (m, 1H), 7.60 (d, *J* = 7.4 Hz, 2H), 7.47 – 7.37 (m, 4H), 7.29 – 7.22 (m, 1H), 6.39 – 6.27 (m, 1H), 6.23 (d, *J* = 7.8 Hz, 1H),

6.07 (dd, *J* = 13.7, 6.9 Hz, 1H), 4.29 – 4.12 (m, 5H), 3.85 (dd, *J* = 7.1, 3.5 Hz, 1H), 3.59 (ddd, *J* = 21.8, 12.0, 3.7 Hz, 2H), 3.03 – 2.94 (m, 2H), 2.69 – 2.60 (m, 3H), 2.58 – 2.51 (m, 2H), 2.31 – 2.09 (m, 2H), 2.08 (s, 2H), 1.89 – 1.72 (m, 8H), 1.70 – 1.64 (m, 12H), 1.08 – 1.02 (m, 1H), 0.99 – 0.93 (m, 5H).

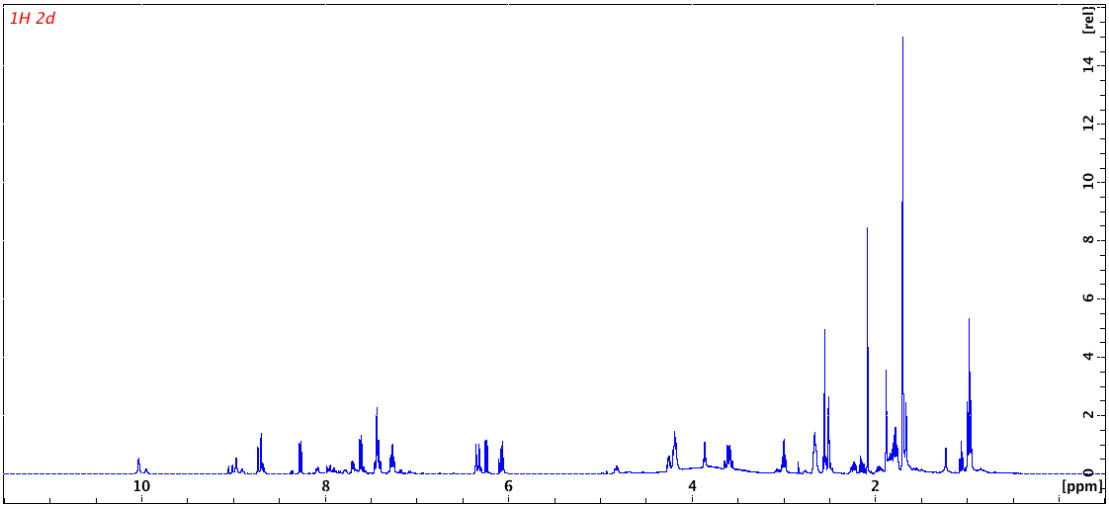

^{13}C NMR (101 MHz, DMSO) δ 172.18, 171.99, 159.55, 154.82, 147.33, 146.69, 144.70, 142.30, 140.88, 132.94, 128.50, 124.80, 122.41, 111.28, 101.34, 93.69, 88.07, 85.82, 69.70, 60.68, 52.61, 48.80, 44.97, 34.49, 32.35, 30.63, 27.45, 25.79, 20.40, 11.09.

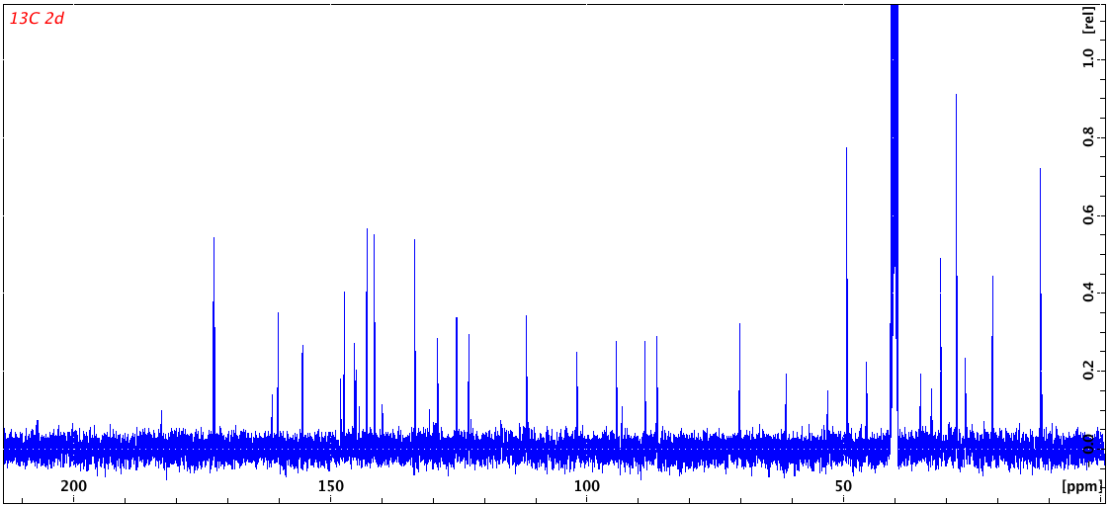

Measured M^+ ($C_{48}H_{60}N_5O_5S^+$) (m/z): 818.4293 Calculated M^+: 818.4310 (2.1 ppm).

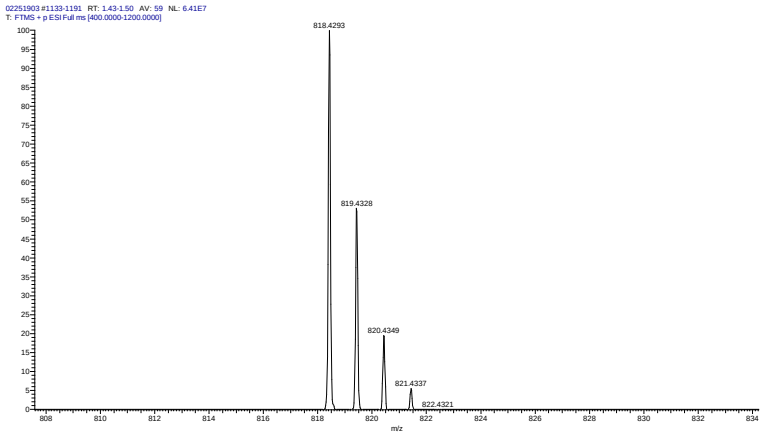

Preparation of 5

2.0 equiv. of 3-mercaptopropionic acid and 1.0 equiv. of heptamethine dye **A** were dissolved in DMF (0.1 M), followed by 3.0 equiv. of Et_3N and stirred at 25 °C for 6 h. Solvent was removed in vacuum, and compound was purified via prepHPLC and lyophilized to get **5** (4.0 mg, 20% yield).

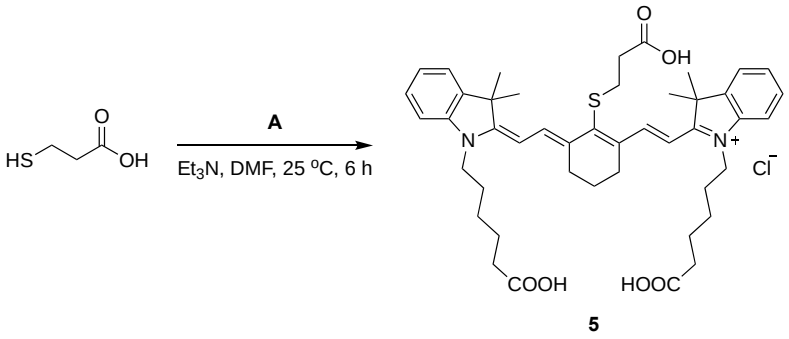

Scheme E.3. Synthesis of compound **5**.

5

$C_{45}H_{57}ClN_2O_6S$

^{1}H NMR (500 MHz, DMSO) δ 8.71 (d, *J* = 14.1 Hz, 2H), 7.60 (d, *J* = 7.3 Hz, 2H), 7.45 – 7.38 (m, 4H), 7.29 – 7.23 (m, 2H), 6.30 (d, *J* = 14.2 Hz, 2H), 4.18 (t, *J* = 7.2 Hz, 4H), 2.99 (t, *J* = 6.9 Hz, 2H), 2.64 (t, *J* = 5.9 Hz, 4H), 2.55 – 2.51 (m, 2H), 2.24 – 2.13 (m, 4H), 1.88 – 1.80 (m, 2H), 1.77 – 1.71 (m, 4H), 1.70 (s, 12H), 1.62 – 1.53 (m, 5H), 1.45 – 1.34 (m, 4H), 1.25 (s, 2H).

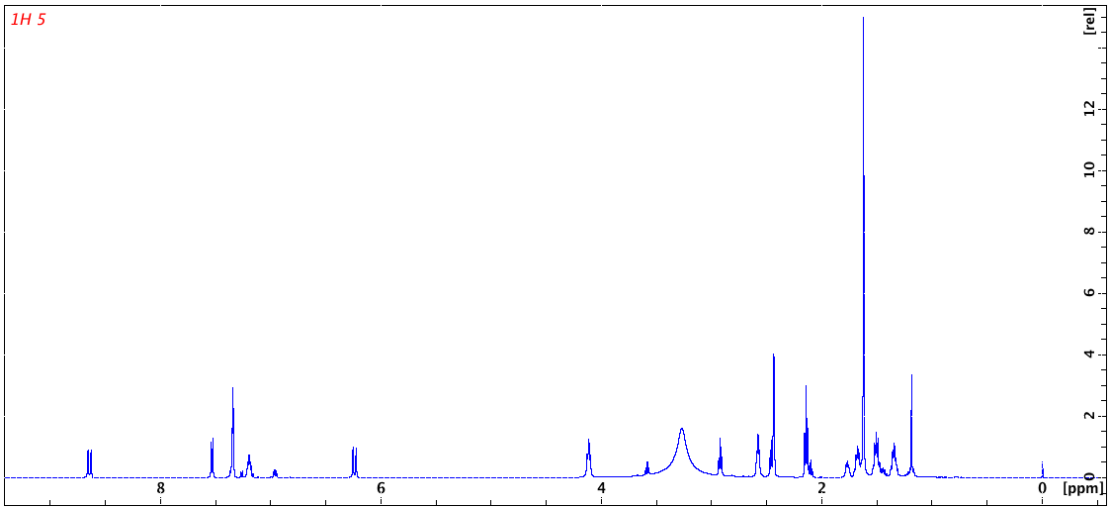

^{13}C NMR (126 MHz, DMSO) δ 174.29, 172.33, 171.86, 154.94, 144.75, 142.18, 141.58, 140.92, 135.35, 132.99, 128.55, 124.84, 122.44, 111.21, 101.29, 48.80, 43.50, 43.29, 33.52, 27.41, 26.64, 25.70, 24.18, 20.49.

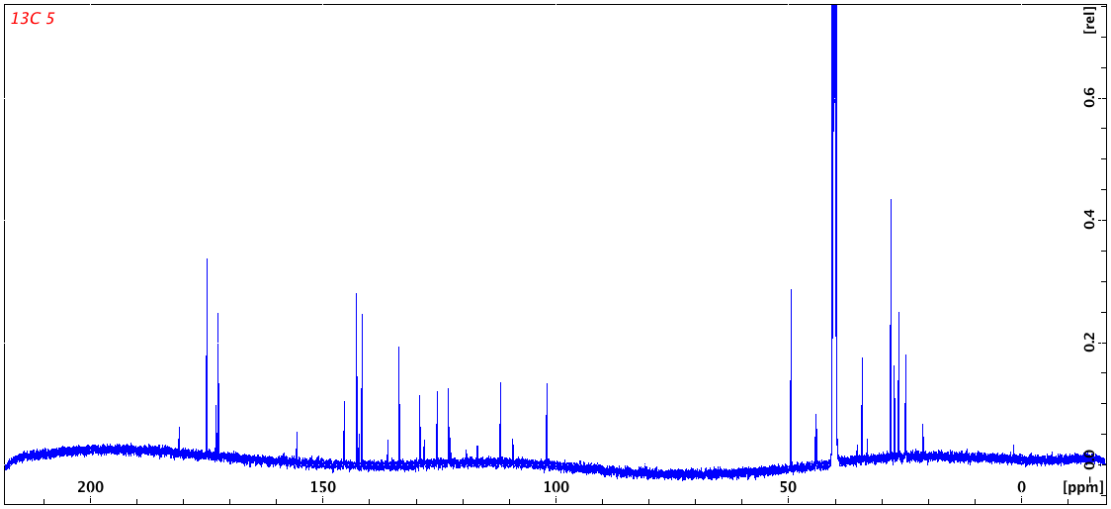

Measured M^+ ($C_{45}H_{57}N_2O_6S^+$) (m/z): 753.3922 Calculated M^+: 753.3932 (1.3 ppm).

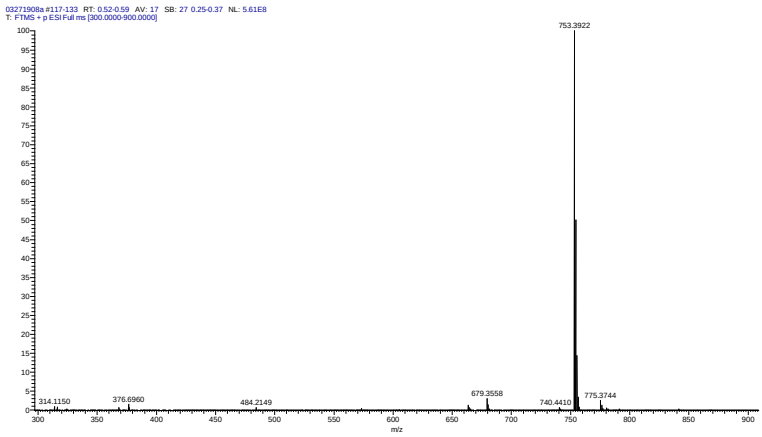

E.3. Compound properties *in vitro*

*E.3.1 Photo-physical Properties of Compounds **1***

Compounds **1** were solubilized as DMSO stock solutions before diluting to 1 μM in PBS buffer. Absorbance and fluorescence spectrum of each compound were measured at the same concentration first (Figure E.1a). Absorbance spectrum was taken with Cary 100 Bio UV-Visible Spectrophotometer (absorbance region 500 – 900 nm, blank solvent as baseline), and fluorescence spectrum was taken by Cary Eclipse Fluorescence Spectrophotometer (excited with 750 nm light and emission region 780 – 900 nm, blank solvent as baseline). Extinction coefficient (ε) of compounds **1** were calculated based on Lambert-Beer's Law (Table E.1).

Table E.1. Photo-physical properties of compounds **1a** – **d**.

	$\varepsilon(cm^{-1}M^{-1})$	Ex/Em (nm)	$\Phi(ex_{750})$	brightness
1a	1.62×10^5	799/817	0.071	1.15×10^4
1b	1.56×10^5	795/816	0.076	1.19×10^4
1c	1.99×10^5	798/817	0.078	1.55×10^4
1d	1.75×10^5	795/811	0.098	1.72×10^4

Different concentrations of each compound were then prepared with A_{750} lies in the range between 0.01 and 0.1 (X axis in Figure E.1b), and corresponding fluorescence spectrum was taken with area under curve calculated (Y axis in Figure E.1b). Fluorescence quantum yield (Φ, in Table E.1)

of each compound was then calculated based on the equation shown in Figure E.1.[236] Brightness of each conjugate equals $\varepsilon \times \Phi$.

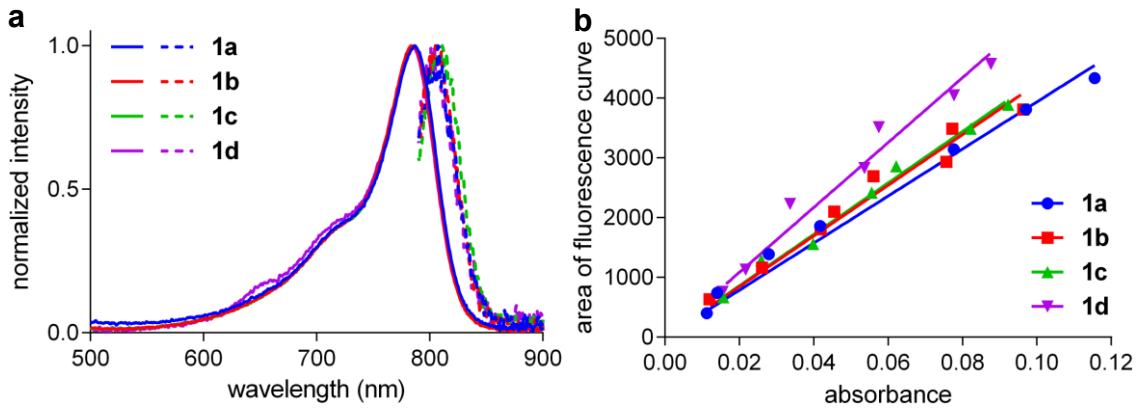

Figure E.1. Photo-physical properties of compounds **1a** – **d**. **a** UV-vis (solid lines) and fluorescence (dashed lines) spectrum of each compound. **b** plot of area of fluorescence curve vs. absorbance for calculation of fluorescence quantum yield of each compound, slope k_x = 39389 (**1a**), 42405 (**1b**), 43045 (**1c**), 54309 (**1d**). Indocyanine Green (ICG) was applied as standard, with Φ_s = 0.17. $\Phi_x = \Phi_s \times \frac{k_x}{k_s} \times \frac{\eta_x^2}{\eta_s^2}$

*E.3.2 Subcellular Localization of Conjugates **1** and free dyes **A** – **D***

U87 cells were seeded in a 4-well imaging chamber (Thermo Scientific® #155383) as 10,000 per well, and incubated at 37 °C overnight. 20 μM of the test compound (conjugates **1** or free dyes **A** – **D**) were prepared in FluoroBrite DMEM medium (Thermo Scientific® #A1896701) and added to the imaging chamber after removing original culture medium and incubated at 37 °C for 45 min. Medium was removed and cells were washed with Hank's Balanced Salt Solution (HBSS) buffer twice. Then cells were incubated with either

LysoTracker (1:10,000 dilution, Invitrogen® #L5726) or MitoTracker (1:15,000 dilution, Invitrogen® #M5714) for 15 min at 37 °C before HBSS wash. 0.5 mL FluoroBrite DMEM medium was then added to imaging chamber followed by 1 drop of NucBlue Live Cell Stain ReadyProbes reagent (Invitrogen® #R37605). 5 min after incubation, medium was removed and washed with HBSS buffer once, and fresh FluoroBrite DMEM medium was added.

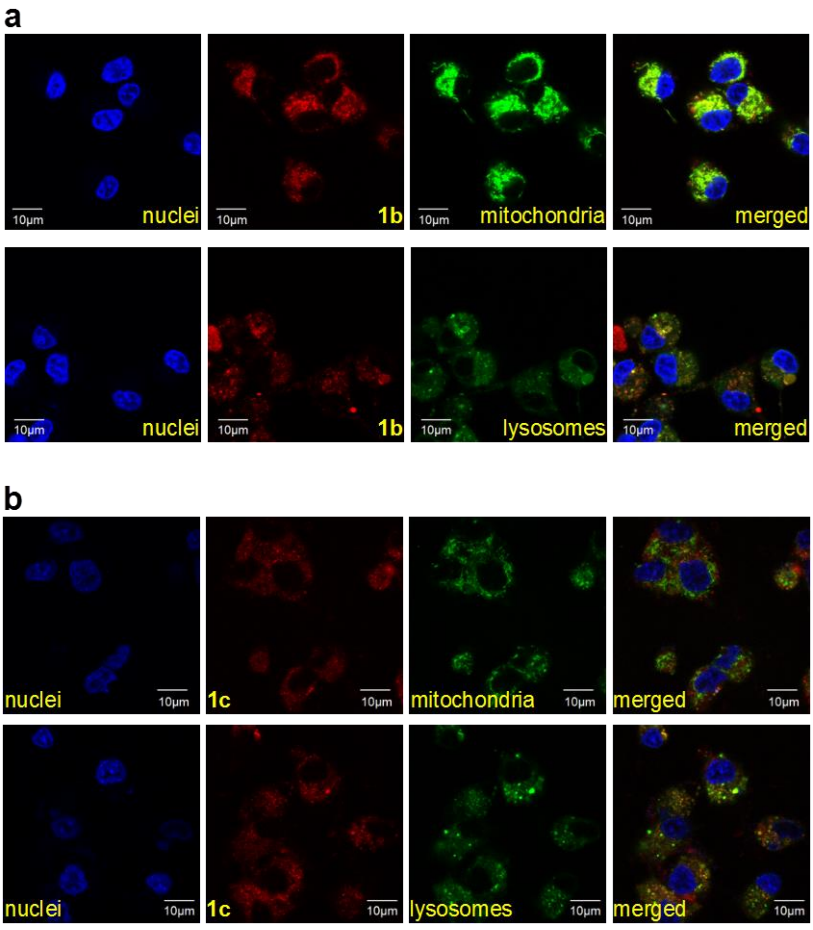

Figure E.2. Subcellular localization in U87 cells of compounds **1b** – **d**. PCC value between red (**1**) and green (organelle stain) fluorescence were shown as "mitochondria (R_m)" and "lysosomes (R_l)". **a 1b** was localized in both mitochondria (0.80) and lysosomes (0.51); **b 1c** was localized in lysosomes

(0.40), but not mitochondria (0.17); **c 1d** was localized in both mitochondria (0.79) and lysosomes (0.73).

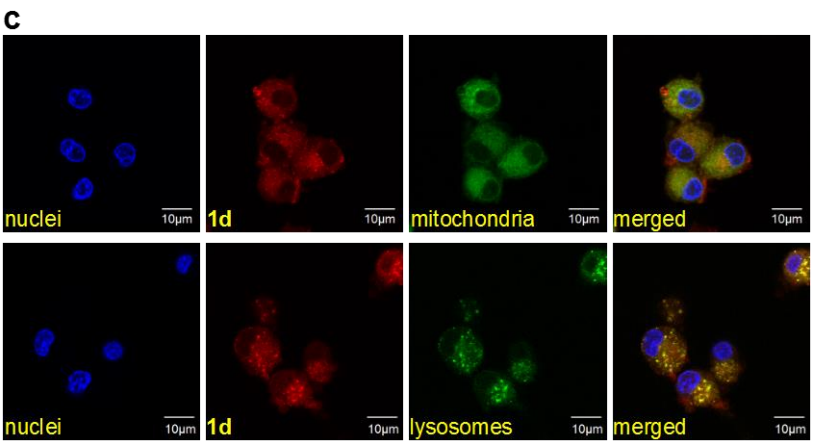

Figure E.2. Continued.

All images were taken by a confocal fluorescence microscope (Olympus® FV-1000) with 60X (water immerse, NA 1.20) objective, excitation laser applied: 405 nm for nuclei stain, 488 nm for Lyso- or Mito-tracker, 633 nm for tested near infrared dye or conjugate in the Microscopy and Imaging Center at Texas A & M University. Pearson's correlation coefficient (PCC) was used to quantify colocalization of the tested fluorescent compound and stained organelle.[237,238] PCC for the region of interest in each set of image was calculated by the Coloc 2 plug-in in Fiji software.

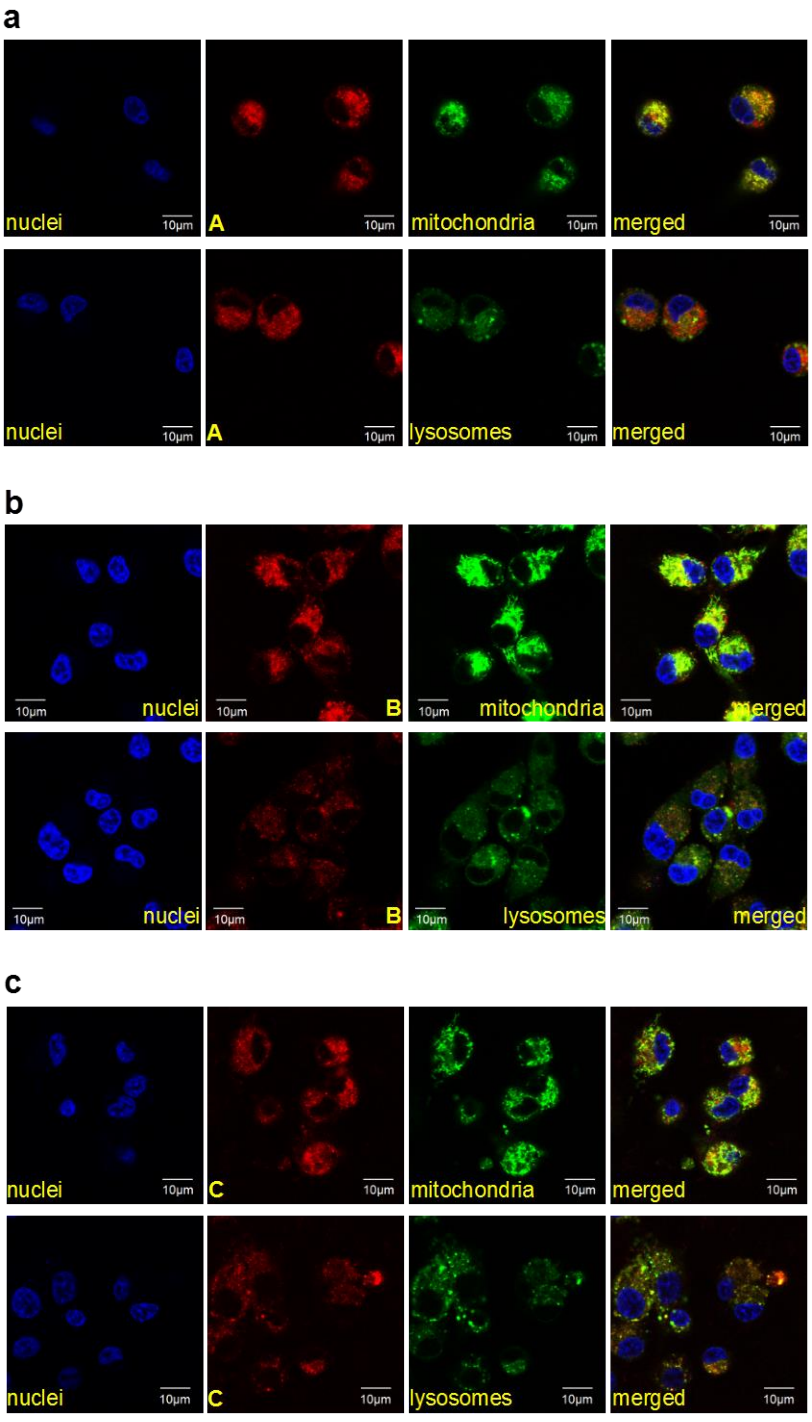

Figure E.3. Subcellular localization in U87 cells of compounds **A** – **D**. **a A** was localized in both mitochondria (0.83) and lysosomes (0.53); **b B** was localized in both mitochondria (0.74) and lysosomes (0.50); **c C** was localized in both

mitochondria (0.75) and lysosomes (0.52); **d D** was localized in both mitochondria (0.69) and lysosomes (0.62).

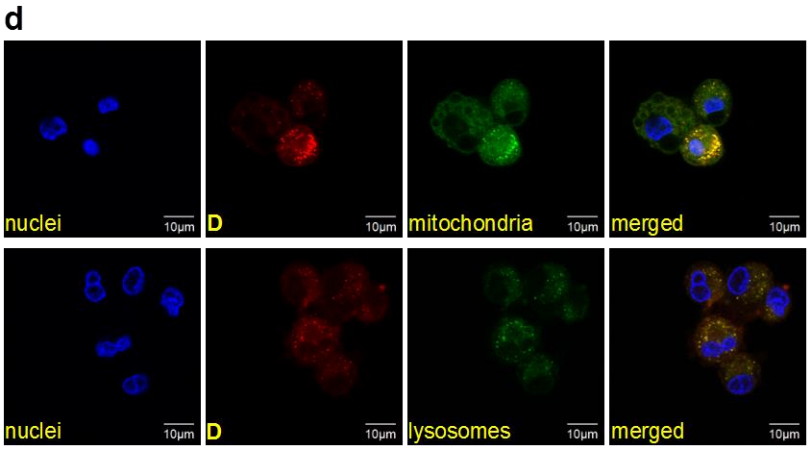

Figure E.3. Continued.

*E.3.3 Determination of Conjugate **1a** Stability*

U87 cell lysate as well as tumor homogenate were prepared to check the conjugate **1a** stability. ~2 g of U87 tumor tissue from a mouse model was cut into small pieces and incubated with 2 mL RIPA buffer (Thermo Scientific® #89901) on ice for 15 min before blended. Blended mixture was then centrifuged down and supernatant was taken out and filtered through a 0.2 μm mesh filter as the tumor homogenate. To generate U87 cell lysate, U87 cells were cultured in a 75 cm^2 tissue culture flask to 80% confluency. After removing culture medium, cells were washed with 8 mL cold PBS buffer twice and then incubated with 1 mL RIPA buffer on ice for 25 min. Mixtures were scratched and transferred into a 1.5 mL Eppendorf tube and centrifuged down (12,500 x g, 4 °C,

20 min) to collet supernatant as cell lysate. **1a** was prepared as 50 μM in U87 tumor homogenate or cell lysate and incubated at 37 °C, for up to 72 h. At designed incubation time, 5 μL samples were injected to analytical C4 HPLC column (0.50 mL/min flow rate, 5% MeCN / 95% water to 90% MeCN / 10% water gradient with 0.1% TFA in 15 min), and traces of absorbance at 780 nm were collected (Figure E.4). Area under curves for **1a** was normalized and plotted in GraphPad Prism® 6.0 software (Figure III.2).

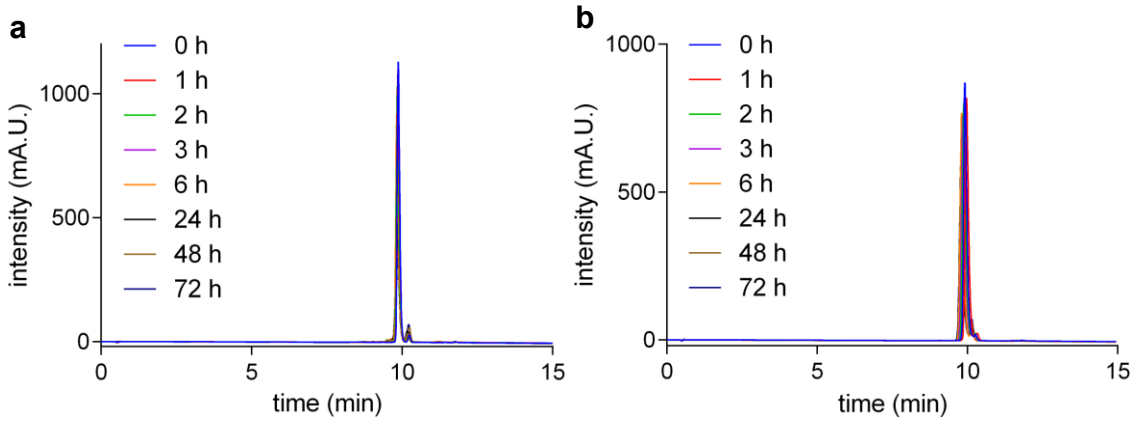

Figure E.4. Absorbance traces of conjugate **1a** in different solutions on analytical HPLC. **a** U87 tumor homogenate; **b** U87 cell lysate.

Stability of **1a** in mouse serum was also tested in the same way by solubilizing **1a** in commercial mouse serum and checked traces of absorbance at 780 nm (Figure E.5a). Conjugate **1a** was metabolized generating a new compound with longer retention time. When Protease and Phosphatase Inhibitor Cocktail (Thermo Scientific® #78440) were premixed with serum (10%

in serum), metabolism of **1a** was inhibited; incubating **1a** in serum at low temperature also inhibited the metabolism (Figure E.5b, c).

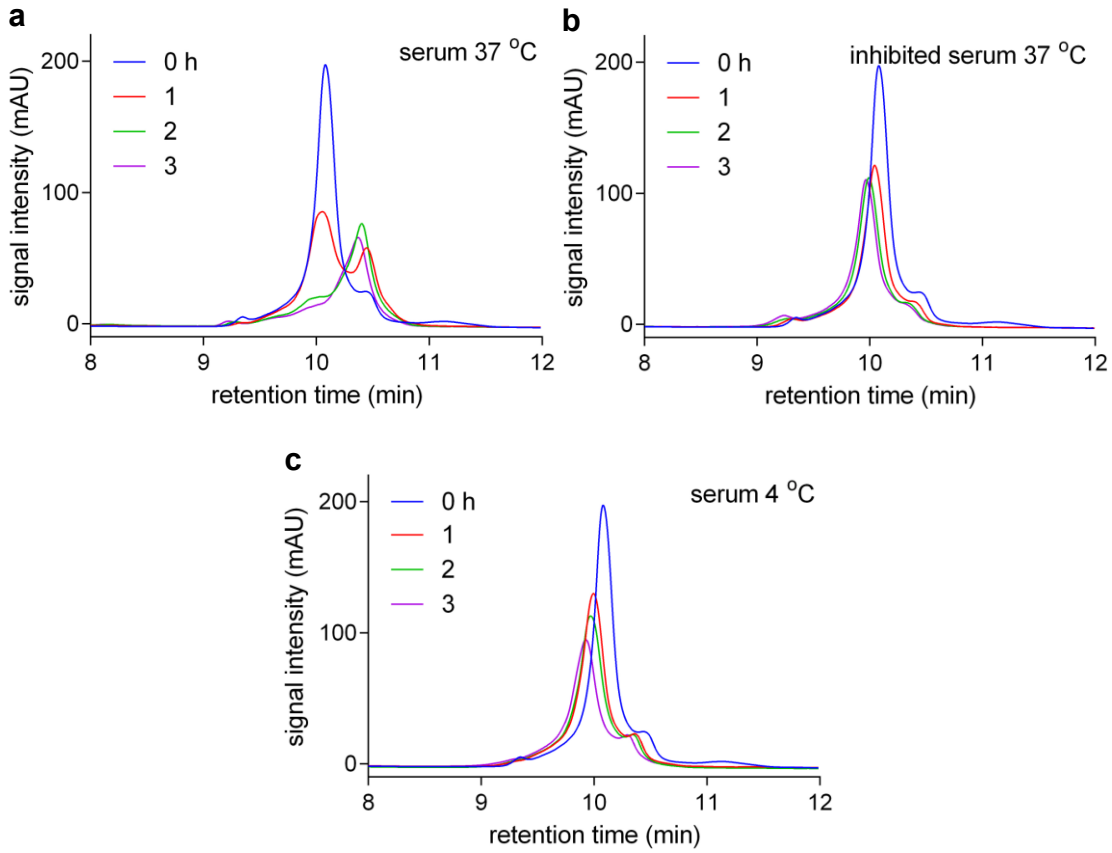

Figure E.5. Conjugate stability of **1a** in mouse serum. **a** conjugate **1a** was metabolized to a new compound in ~3 h (re-presentation of Figure III.2b); **b** protease and phosphatase inhibitor cocktail (10% in serum), and **c** low temperature prohibited the metabolism of **1a**.

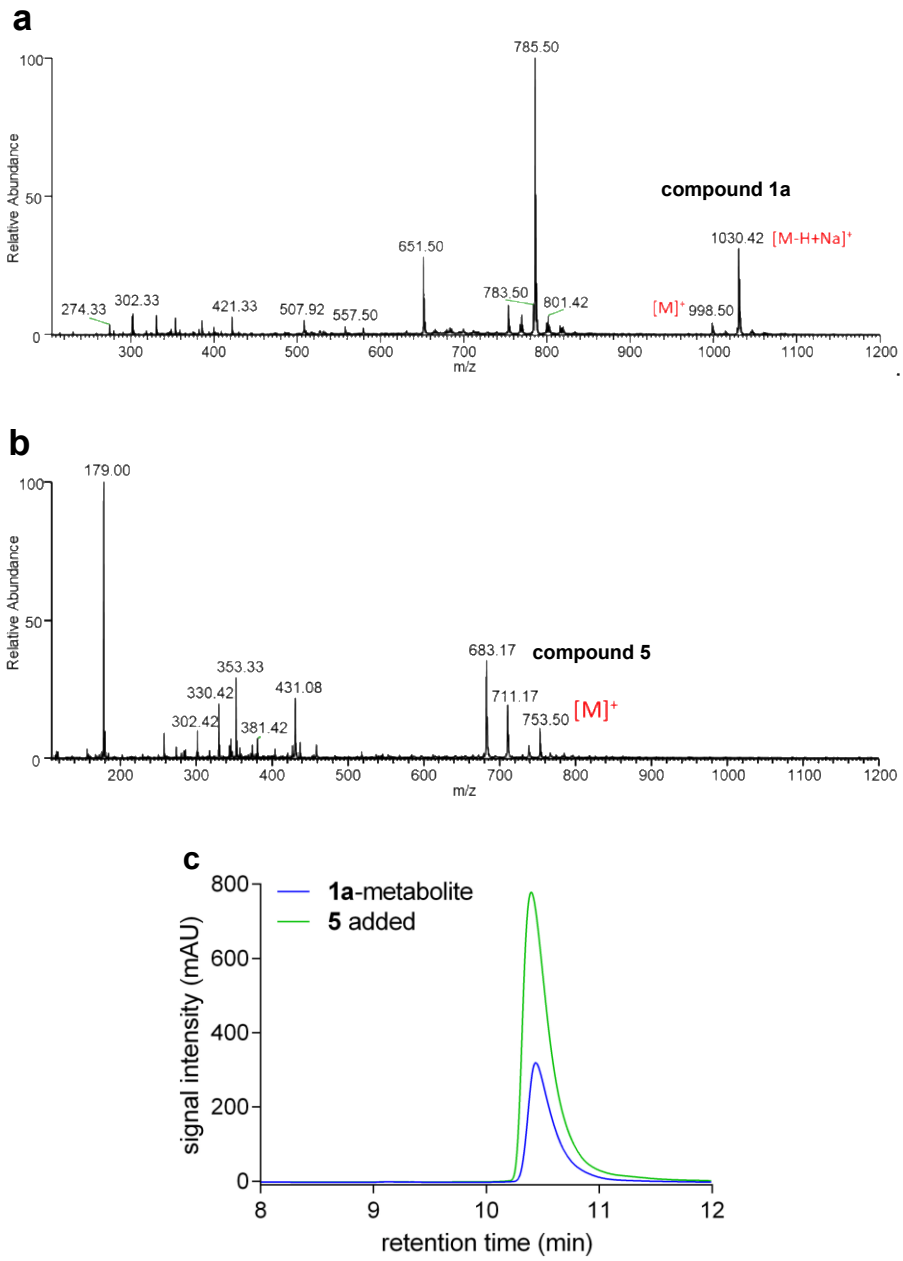

Figure E.6. Paper spray mass spectrometric and HPLC analysis of metabolic product of **1a** in mouse serum. **a** mass spectrum of compound **1a** (calculated M^+ = 998.45) as standard; **b** mass spectrum of **1a**-metabolite in mouse serum, compound **5** (calculated M^+ = 753.39) was possibly the key product; **c** adding equivalent amount of compound **5** into **1a**-metabolite in mouse serum resulted in an analytical HPLC trace with a single peak at higher intensity, which indicates **5** was the **1a**-metabolite in serum.

E.3.4 In vitro Cytotoxicity Tests

U87 cells were seeded on 96-well plates as 5000 cells/well (50 µL) and incubated in the incubator overnight. Various concentrations of gemcitabine, its derivative **F**, conjugates **1**, **2** as well as free heptamethine dyes **A** – **D** were prepared in 50 µL protein-free hybridoma medium (PFHM II) and added to cells to make final concentrations from 0.001 to 10 µM. All plates were incubated for 72 h, and cell viability was tested with AlamarBlue assay (Invitrogen). Briefly, in a well containing 100 µL medium, 10 µL of AlamarBlue reagent was added, and incubated for 2 h. Fluorescence intensity (Ex/Em 560/590 nm) was measured on a microplate reader (BioTek® Synergy H4). Results are processed through GraphPad Prism® 6.0 software. Cytotoxicity of dye **D** was also observed in other's work.[239]

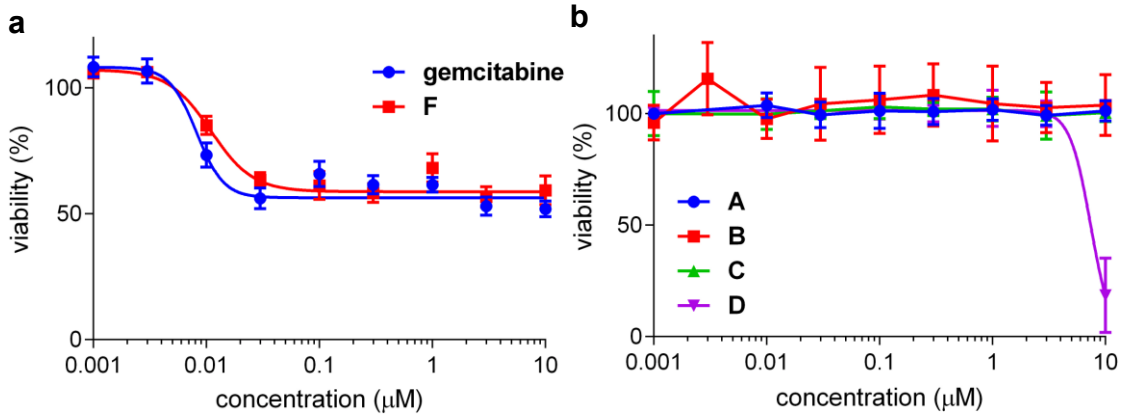

Figure E.7. Compounds cytotoxicity comparison. **a** gemcitabine and its derivative **F**; **b** free heptamethine dyes **A** – **D**.

IC_{50} values of each compound are listed as: gemcitabine, 8.2 ± 1.7; **F**, 11.0 ± 1.4; **1a**, 20.9 ± 5.0; **1b**, 20.7 ± 3.2; **D**, 7.1 ± 1.7 nM; IC_{50} of **1d** is ambiguous.

E.4 *In vivo* Tumor Model Studies

E.4.1 In vivo Imaging for conjugate localization

Mice were anesthetized with isoflurane and then imaged for fluorescence or luminescence on an IVIS Spectrum (*in vivo* imaging system; Perkin Elmer®). For luminescence imaging, mice were subcutaneously injected with *D*-luciferin (15 mg/mL, Perkin Elmer® #122796) in µL at 10x the mouse weight. During imaging mice remained anesthetized by isoflurane. Fluorescence was measured by radiant efficiency and luminescence was measured by counts. Red Fluorescence Protein (RFP) from the U87 cells was captured at an excitation wavelength of 570 nm and an emission wavelength of 620 nm. The near IR dye fluorescence was capture at an excitation wavelength of 745 nm and an emission wavelength of 840 nm. Images were captured and data were analyzed using Living Image Software (Perkin Elmer®).

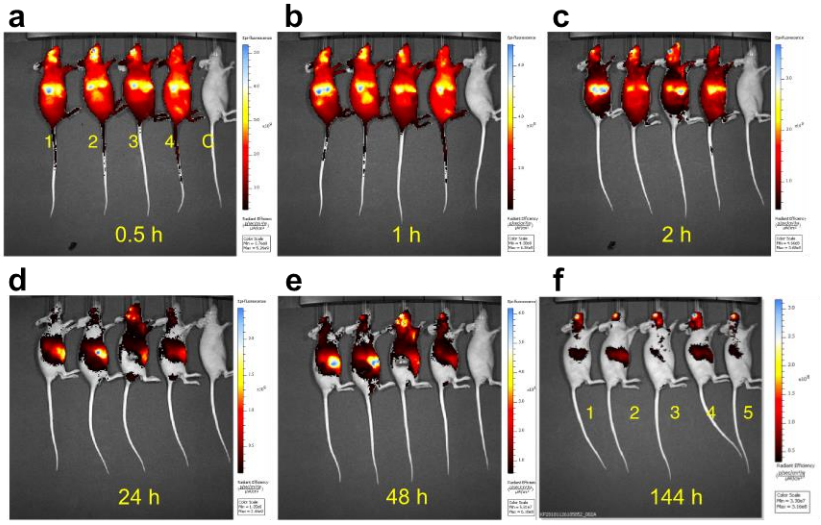

Figure E.8. Fluorescence imaging of **1a** can be detected up to 6 days after intravenous injection (before normalization). **a** – **e** Fluorescence of **1a**-injected mice after intravenous injection (mice 1 – 4) compared to an uninjected control (mouse C). **f** Fluorescence of **1a**-injected mice (mice 1 – 5). Fluorescence is normalized to an uninjected control mouse (not shown).

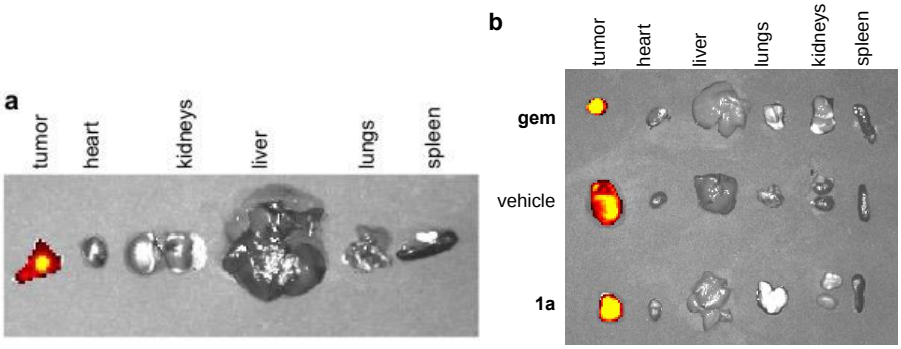

Figure E.9. 1a localizes to tumors. **a** RFP signal from a GBM subcutaneous tumor 2 h post intravenous injection of **1a**. **b** RFP signal from GBM subcutaneous tumors 2 d after intravenous injection of **gem**, vehicle, or **1a**. **c** Fluorescence of **1a** in 3 different tumor-bearing mice 2 d after intravenous injection. Compound **1a** remained in the blood and localized to the intestines, tumor, liver, and kidneys.

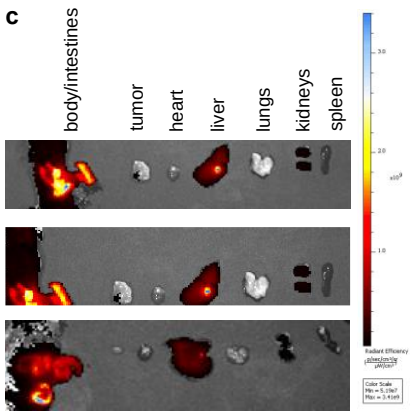

Figure E.9. Continued.

E.4.2 In vivo therapeutic study

Seven-week-old Foxn1 nu females were ordered from Jackson Lab. U87-RFP-LUC cells (5 x 10^5) were injected subcutaneously into the right flank of the mice. Four days later (day 4) intravenous injections of the drugs and vehicle were administered through retro orbital injections. The mice were injected again 4 days later (day 8), and the injections were subsequently administered once weekly. Compounds were administered at a concentration of 10 mg/kg for 5 weeks. Tumor growth was monitored by luminescence and fluorescence (RFP; 570 – 620 nm) imaging and drug clearance/localization of **1a** was monitored by the fluorescence imaging (745 – 840 nm).

A cocktail vehicle (2% DMSO, 9% ethanol, 9% BSA in PBS buffer) was applied to solubilize **1a** and **gem** for retro orbital injections. Compound **1a** was prepared as 3 mM solution and **gem** was prepared as 10 mM solution. Volume

(< 100 μL) of each compound administered was calculated based on the body weight of each mouse to deliver 10 mg/kg dose.

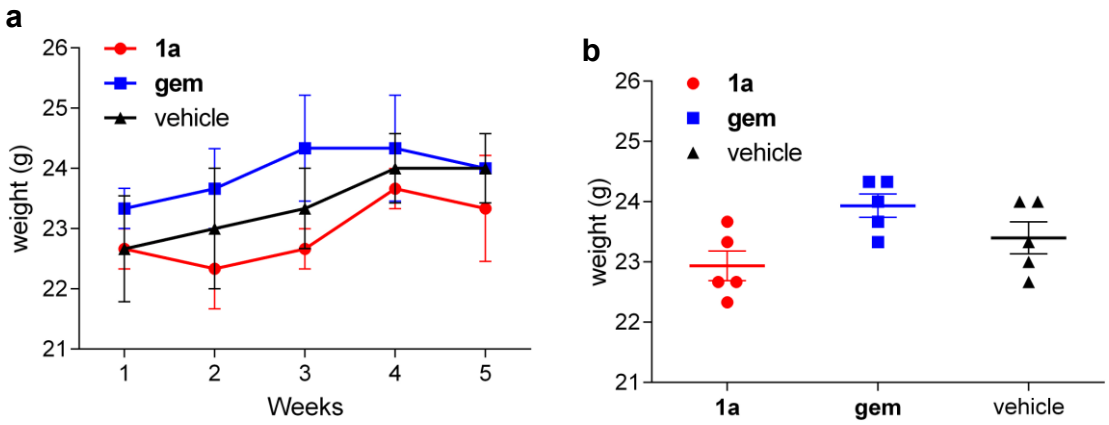

Figure E.10. Mouse weights show no significant reduction between treatments and control. **a** Average of mouse weights in grams by treatment group over five weeks with SEM (n = 3). Two-way ANOVA with Bonferroni posttest shows no statistically significant differences between groups. **b** Average of mouse weights in grams by treatment group with SEM. Points represent average mouse weight by week within a treatment group (n = 3). Two-way ANOVA with Bonferroni posttest shows no statistically significant differences between groups.

All animal experiments were performed under approved protocols in compliance with the guidelines established by the Institutional Animal Care and Use Committee (IACUC).